Summary of the Bulletin of the International Seismological Centre

2010

July – December

Volume 47 Issue 7-12

www.isc.ac.uk

isc-mirror.iris.washington.edu

ISSN 2309-236X

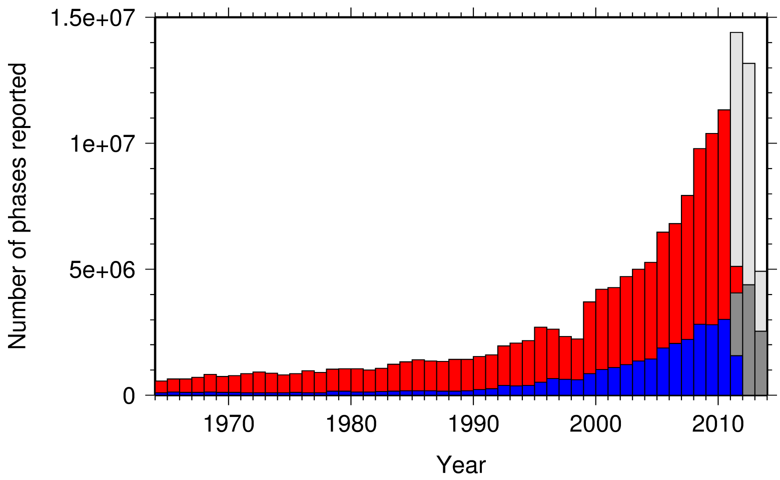

The number of phases (red) and number of amplitudes (blue) collected by the ISC for events each year since 1964. The data in grey covers the current period where data are still being collected before the ISC review takes place and are accurate at the time of publication. See Section 8.3.

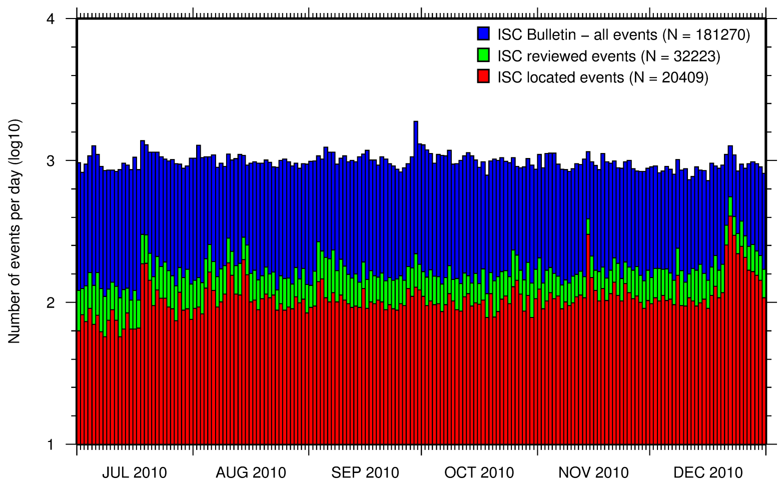

The number of events within the Bulletin for the current summary period. The vertical scale is logarithmic. See Section 9.1.

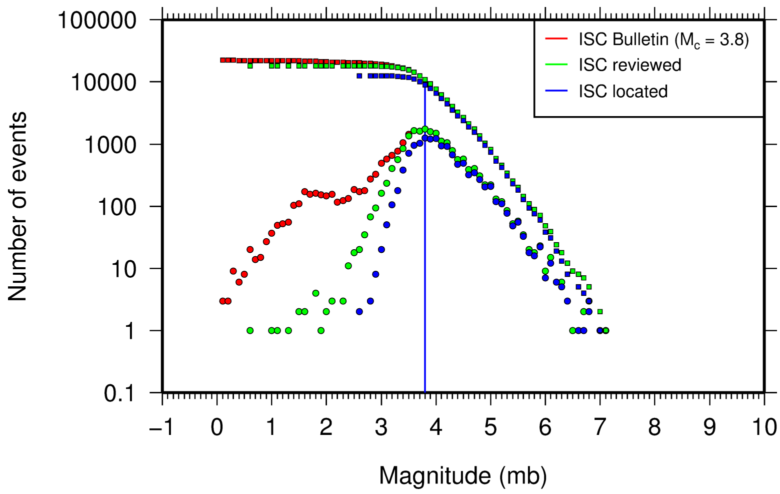

Frequency and cumulative frequency magnitude distribution for all events in the ISC Bulletin, ISC reviewed events and events located by the ISC. The magnitude of completeness (M_C) is shown for the ISC Bulletin. Note: only events with values of m_b are represented in the figure. See Section 9.4.

Contents

1 Preface **1**

2 The International Seismological Centre **2**

2.1 The ISC Mandate 2

2.2 Member Institutions of the ISC 3

2.3 Sponsoring Organisations 9

2.4 Data Contributing Agencies 9

2.5 ISC Staff 17

3 Availability of the ISC Bulletin **22**

4 Citing the International Seismological Centre **23**

5 Operational Procedures of Contributing Agencies **25**

5.1 Seismic Network and Routine Data Processing -Japan Meteorological Agency- 25

5.1.1 Overview 25

5.1.2 Types of networks 27

5.1.3 Data sharing with other organizations 30

5.1.4 Data processing 31

5.1.5 Data availability 37

5.1.6 History of the seismic network 38

5.1.7 Acknowledgements 39

5.1.8 References 40

5.1.9 Appendix: Instrumental seismic intensity 41

6 Summary of Seismicity, July - December 2010 **43**

7 Notable event **48**

7.1 The Canterbury, New Zealand Earthquake Sequence I: The M_w 7.1 Darfield Earthquake of 3 September 2010 and Aftershock Sequence 48

7.1.1 Introduction 48

7.1.2 Mainshock Source Properties 50

7.1.3 Aftershock Sequence 55

7.1.4 Stress Studies and Aftershock Forecasts 58

7.1.5 Discussion 61

7.1.6 Conclusions 61
7.1.7 Acknowledgements 62
7.1.8 References 62

8 Statistics of Collected Data **66**
8.1 Introduction 66
8.2 Summary of Agency Reports to the ISC 66
8.3 Arrival Observations 71
8.4 Hypocentres Collected 78
8.5 Collection of Network Magnitude Data 80
8.6 Moment Tensor Solutions 85
8.7 Timing of Data Collection 88

9 Overview of the ISC Bulletin **90**
9.1 Events 90
9.2 Seismic Phases and Travel-Time Residuals 99
9.3 Seismic Wave Amplitudes and Periods 105
9.4 Completeness of the ISC Bulletin 107
9.5 Magnitude Comparisons 108

10 The Leading Data Contributors **113**
10.1 The Largest Data Contributors 113
10.2 Contributors Reporting the Most Valuable Parameters 115
10.3 The Most Consistent and Punctual Contributors 121

11 Appendix **122**

12 Glossary of ISC Terminology **142**

13 Acknowledgements **146**

References **147**

International Seismological Centre

1

Preface

Dear Colleague,

This is the second and concluding 2010 issue of the Summary of the Bulletin of the ISC. The Bulletin remains the most fundamental reason for the ISC continued operations. This issue covers the period of July-December 2010.

This publication presents a description of the ISC data available on the attached DVD-ROM and from the ISC website. It contains information on the ISC, its Members, Sponsors and Data providers. It offers analysis of the data contributed to the ISC by many seismological agencies worldwide as well as analysis of the data in the ISC Bulletin itself. This somewhat smaller issue misses some of the standard information on routine procedures usually published in the first issue of each year.

From this issue onwards, we shall also publish invited articles describing the history, current status and operational procedures at those networks that contribute data to the ISC. By tradition that goes back to Prof. John Milne, we decided to start with Japan and asked the Japan Meteorological Agency (JMA) to take the lead.

This issue also contains an invited article on the notable September 2010 Darfield earthquake and related aftershock sequence.

We hope that you find this relatively new publication useful in your work. If your home-institution or company is unable, for one reason or another, to support the long-term international operations of the ISC in full by becoming a Member, then, please, consider subscribing to this publication by contacting us at admin@isc.ac.uk.

With kind regards to our Data Contributors, Members, Sponsors and users,

Dr Dmitry A. Storchak
Director
International Seismological Centre (ISC)

2

The International Seismological Centre

2.1 The ISC Mandate

The International Seismological Centre (ISC) was set up in 1964 with the assistance of UNESCO as a successor to the International Seismological Summary (ISS) to carry forward the pioneering work of Prof. John Milne, Sir Harold Jeffreys and other British scientists in collecting, archiving and processing seismic station and network bulletins and preparing and distributing the definitive summary of world seismicity.

Under the umbrella of the International Association of Seismology and Physics of the Earth Interior (IASPEI/IUGG), the ISC has played an important role in setting international standards such as the International Seismic Bulletin Format (ISF), the IASPEI Standard Seismic Phase List (SSPL) and both the old and New IASPEI Manual of the Seismological Observatory Practice (NMSOP-2) (www.iaspei.org/projects/NMSOP.html).

The ISC has contributed to scientific research and prominent scientists such as John Hodgson, Eugine Herrin, Hal Thirlaway, Jack Oliver, Anton Hales, Ola Dahlman, Shigeji Suehiro, Nadia Kondorskaya, Vit Karnik, Stephan Müller, David Denham, Bob Engdahl, Adam Dziewonski, John Woodhouse and Guy Masters all considered it an important duty to serve on the ISC Executive Committee and the Governing Council.

The current mission of the ISC is to maintain:

- the ISC **Bulletin** – the longest continuous definitive summary of World seismicity (collaborating with 130 seismic networks and data centres around the world). (www.isc.ac.uk/iscbulletin/)
- the **International** Seismographic Station Registry (**IR**, jointly with the World Data Center for Seismology, Denver). (www.isc.ac.uk/registries/)
- the IASPEI Reference Event List (Ground Truth, **GT**, jointly with IASPEI). (www.isc.ac.uk/gtevents/)

These are fundamentally important tasks. Bulletin data produced, archived and distributed by the ISC for almost 50 years is the definitive source of such information and are used by thousands of seismologists worldwide for seismic hazard estimation, for tectonic studies and for regional and global imaging of the Earth's structure. Key information in global tomographic imaging is derived from the analysis of ISC data. The ISC Bulletin served as a major source of data for such well known products as the ak135 global 1-D velocity model and the EHB (*Engdahl et al.*, 1998) and Centennial (*Engdahl and Villaseñor*, 2002) catalogues. It presents an important quality-control benchmark for the Comprehensive Test Ban Treaty Organization (CTBTO). Hypocentre parameters from the ISC Bulletin are used by the Data

Management Center of the Incorporated Research Institutions for Seismology (IRIS DMC) to serve event oriented user requests for waveform data. The ISC-GEM Bulletin is a cornerstone of the ISC-GEM Global Instrumental Reference Earthquake Catalogue for Global Earthquake risk Model (GEM).

The ISC relational database currently holds approximately 90 Gb of unique data. The ISC Bulletin contains over 5 million seismic events: earthquakes, chemical and nuclear explosions, mine blasts and mining induced events. As many as 1.5 million of them are regional and teleseismically recorded events that have been reviewed by the ISC analysts. The ISC Bulletin contains approximately 150 million individual seismic station readings of arrival times, amplitudes, periods, SNR, slowness and azimuth, reported by approximately 17,000 seismic stations currently registered in the IR. As many as 6,000 stations have contributed to the ISC Bulletin in recent years. This number includes the numerous sites of the USArray. The IASPEI GT List currently contains 7802 events for which latitude, longitude and depth of origin are known with high confidence (to 5 km or better) and seismic signals were recorded at regional and/or teleseismic distances.

2.2 Member Institutions of the ISC

Article IV(a-b) of the ISC Working Statutes stipulates that any national academy, agency, scientific institution or other non-profit organisation may become a Member of the ISC on payment to the ISC of a sum equal to at least one unit of subscription and the nomination of a voting representative to serve on the ISC's governing body. Membership shall be effective for one year from the date of receipt at the ISC of the annual contribution of the Member and is thereafter renewable for periods of one year.

The ISC is currently supported with funding from its 61 Member Institutions and a four-year Grant Award EAR-0949072 from the US National Science Foundation.

Figures 2.1 and 2.2 show major sectors to which the ISC Member Institutions belong and proportional financial contributions that each of these sectors make towards the ISC's annual budget.

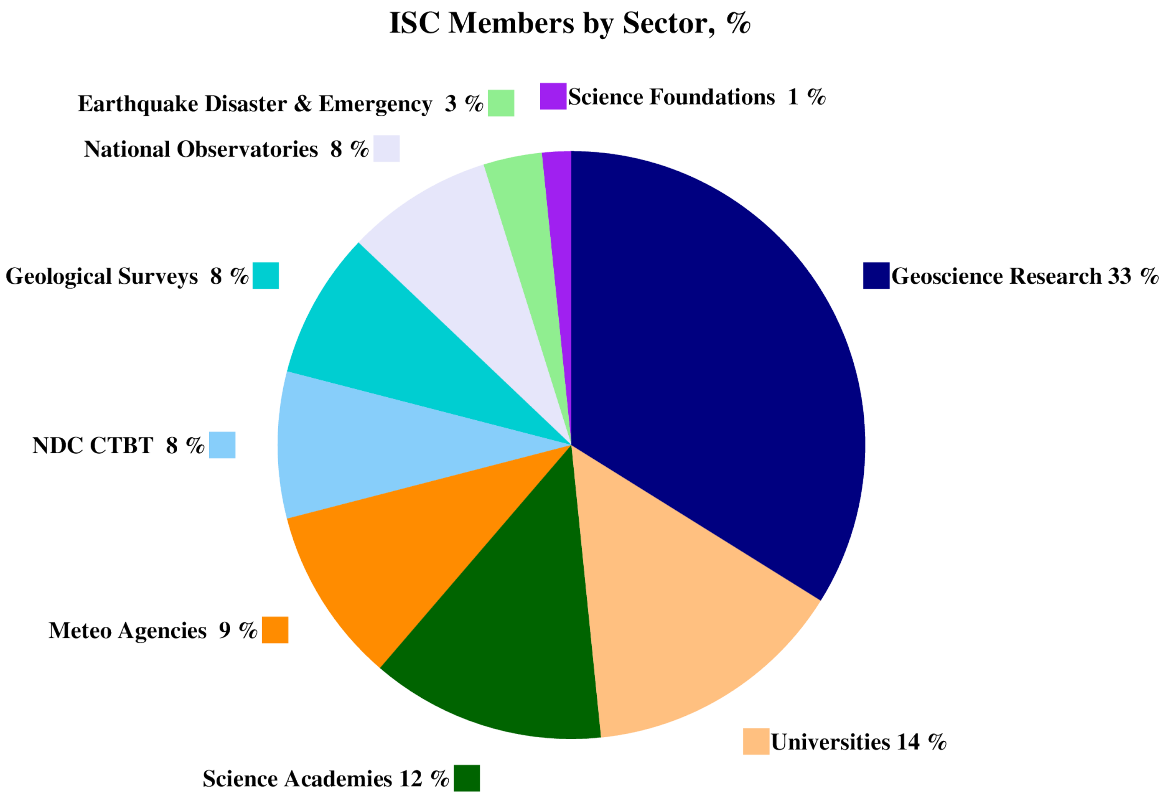

Figure 2.1: Distribution of the ISC Member Institutions by sector in year 2012 as a percentage of total number of Members.

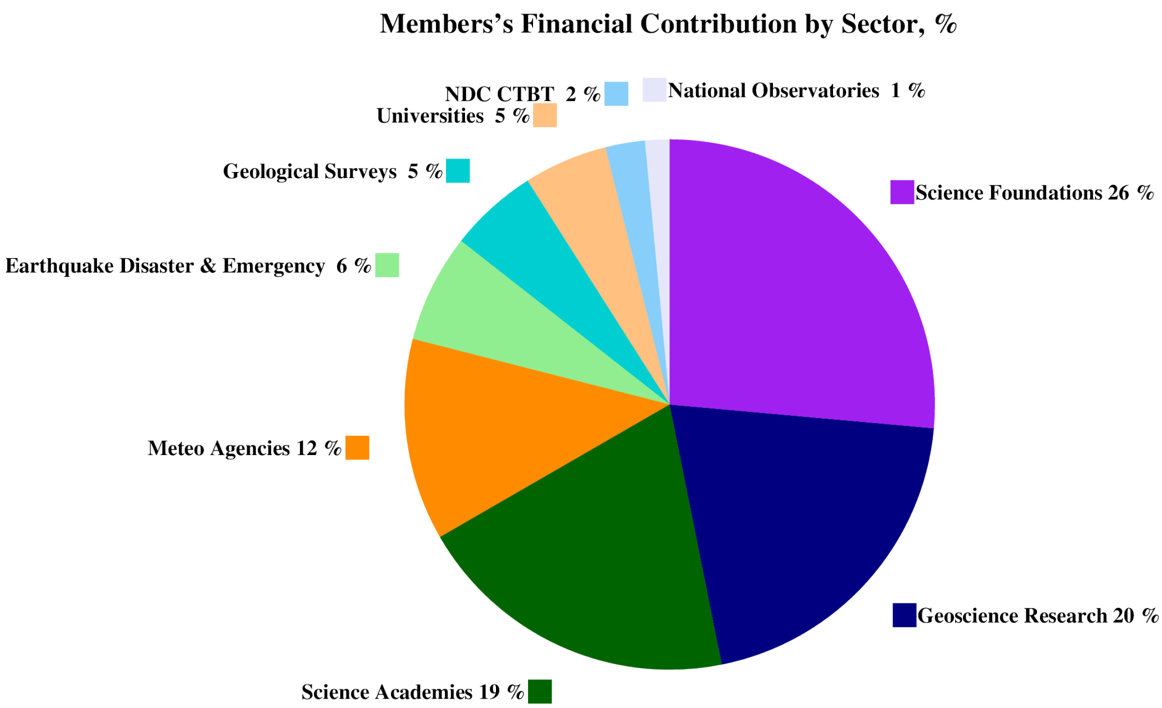

Figure 2.2: Distribution of Member's financial contributions to the ISC by sector in year 2012 as a percentage of total annual Member contributions.

There follows a list of all current Member Institutions with a category (1 through 9) assigned according to the ISC Working Statutes. Each category relates to the number of membership units contributed.

Centre de Recherche en Astronomie, Astrophysique et Géophysique (CRAAG)
Algeria
www.craag.dz
Category: 1

Instituto Nacional de Prevención Sísmica (INPRES)
Argentina
www.inpres.gov.ar
Category: 1

Seismology Research Centre
Australia
www.seis.com.au
Category: 1

Geoscience Australia
Australia
www.ga.gov.au
Category: 3

The University of Melbourne
Australia
www.unimelb.edu.au
Category: 1

Bundesministerium für Wissenschaft und Forschung
Austria
www.bmbwk.gv.at
Category: 2

Centre of Geophysical Monitoring (CGM) of the National Academy of Sciences of Belarus
Belarus
www.cgm.org.by
Category: 1

Observatoire Royal de Belgique
Belgium
www.astro.oma.be
Category: 1

The Geological Survey of Canada
Canada
gsc.nrcan.gc.ca
Category: 4

China Earthquake Administration
China
www.gov.cn
Category: 5

Institute of Earth Sciences, Academia Sinica
Chinese Taipei
www.earth.sinica.edu.tw
Category: 1

Geological Survey Department
Cyprus
www.moa.gov.cy
Category: 1

Academy of Sciences of the Czech Republic
Czech Republic
www.cas.cz
Category: 2

Geological Survey of Denmark and Greenland - GEUS
Denmark
www.geus.dk
Category: 2

National Research Institute for Astronomy and Geophysics (NRIAG), Cairo
Egypt
www.nriag.sci.eg
Category: 1

The University of Helsinki
Finland
www.helsinki.fi
Category: 2

Laboratoire de Détection et de Géophysique/CEA
France
www-dase.cea.fr
Category: 2

Institute National des Sciences de l'Univers
France
www.insu.cnrs.fr
Category: 4

Bundesanstalt für Geowissenschaften und Rohstoffe
Germany
www.bgr.bund.de
Category: 4

GeoForschungsZentrum Potsdam
Germany
www.gfz-potsdam.de
Category: 2

The Seismological Institute, National Observatory of Athens
Greece
www.noa.gr
Category: 1

The Hungarian Academy of Sciences
Hungary
www.mta.hu
Category: 1

The Icelandic Meteorological Office
Iceland
www.vedur.is
Category: 1

India Meteorological Department
India
www.imd.ernet.in
Category: 4

Iraqi Seismic Network
Iraq
www.imos-tm.com
Category: 1

Dublin Institute for Advanced Studies
Ireland
www.dias.ie
Category: 1

Soreq Nuclear Research Centre (SNRC)
Israel
www.soreq.gov.il
Category: 1

The Geophysical Institute of Israel
Israel
www.gii.co.il
Category: 1

Istituto Nazionale di Geofisica e Vulcanologia
Italy
www.ingv.it
Category: 3

Istituto Nazionale di Oceanografia e di Geofisica Sperimentale
Italy
www.ogs.trieste.it
Category: 1

University of the West Indies
Jamaica
www.mona.uwi.edu
Category: 1

Japan Agency for Marine-Earth Science and Technology (JAMSTEC)
Japan
www.jamstec.go.jp
Category: 3

Earthquake Research Institute, University of Tokyo
Japan
www.eri.u-tokyo.ac.jp
Category: 3

The Japan Meteorological Agency (JMA)
Japan
www.jma.go.jp
Category: 5

Natural Resources Authority, Amman
Jordan
www.nra.gov.jo
Category: 1

Institute of Geophysics, National University of Mexico
Mexico
www.igeofcu.unam.mx
Category: 1

The Royal Netherlands Meteorological Institute
Netherlands
www.knmi.nl
Category: 2

Institute of Geological and Nuclear Sciences
New Zealand
www.gns.cri.nz
Category: 3

Stiftelsen NORSAR
Norway
www.norsar.no
Category: 2

The University of Bergen
Norway
www.uib.no
Category: 2

Institute of Geophysics, Polish Academy of Sciences
Poland
www.igf.edu.pl
Category: 1

The Institute for Meteorology
Portugal
www.meteo.pt
Category: 2

Red Sísmica de Puerto Rico
Puerto Rico
redsismica.uprm.edu
Category: 1

Korean Meterological Administration
Republic of Korea
www.kma.go.kr
Category: 1

National Institute for Earth Physics
Romania
www.infp.ro
Category: 1

Russian Academy of Sciences
Russia
www.ras.ru
Category: 5

Environmental Agency of Slovenia
Slovenia
www.arso.gov.si
Category: 1

Council for Geoscience
South Africa
www.geoscience.org.za
Category: 1

Instituto Geográfico Nacional
Spain
www.ign.es
Category: 3

National Defence Research Establishment
Sweden
www.foi.se
Category: 1

Uppsala Universitet
Sweden
www.uu.se
Category: 2

The Swiss Academy of Sciences
Switzerland
www.scnat.ch
Category: 2

University of the West Indies
Trinidad and Tobago
sta.uwi.edu
Category: 1

Kandilli Observatory and Earthquake Research Institute
Turkey
www.koeri.boun.edu.tr
Category: 1

Disaster and Emergency Management Presidency
Turkey
www.deprem.gov.tr
Category: 2

The Royal Society of London
United Kingdom
www.royalsociety.org
Category: 6

British Geological Survey
United Kingdom
www.bgs.ac.uk
Category: 2

AWE Blacknest
United Kingdom
www.blacknest.gov.uk
Category: 1

The National Science Foundation of the United States. (Grant No. EAR-0949072)
U.S.A.
www.nsf.gov
Category: 9

University of Texas at Austin
U.S.A.
www.utexas.edu
Category: 1

National Earthquake Information Center, U.S. Geological Survey
U.S.A.
www.neic.usgs.gov
Category: 2

Incorporated Research Institutions for Seismology
U.S.A.
www.iris.edu
Category: 1

In addition the ISC is currently in receipt of grants from the International Data Centre (IDC) of the Preparatory Commission of the Comprehensive Test Ban Treaty Organization (CTBTO) and the Global Earthquake risk Model Foundation (GEM).

2.3 Sponsoring Organisations

Article IV(c) of the ISC Working Statutes stipulates any commercial organisation with an interest in the objectives and/or output of the ISC may become an Associate Member of the ISC on payment of an Associate membership fee, but without entitlement to representation with a vote on the ISC's governing body.

REF TEK A DIVISION OF TRIMBLE www.reftek.com

REF TEK, a division of Trimble, designs and manufactures application specific, high-performance, battery-operated, field-portable geophysical data acquisition devices for the global market. With over 35 years of experience, REF TEK provides customers with complete turnkey solutions that include high resolution recorders, broadband sensors, state-of-the-art communications (V-SAT, GPRS, etc), installation, training, and continued customer support. Over 7,000 REF TEK instruments are currently being used globally for multiple applications. From portable earthquake monitoring to telemetry earthquake monitoring, earthquake aftershock recording to structural monitoring and more, REF TEK equipment is suitable for a wide variety of application needs.

2.4 Data Contributing Agencies

In addition to its Members and Sponsors, the ISC owes its existence and successful long-term operations to its 126 seismic bulletin data contributors. These include government agencies responsible for national seismic networks, geoscience research institutions, geological surveys, meteorological agencies, universities, national data centres for monitoring the CTBT and individual observatories. There would be no ISC Bulletin available without the regular stream of data that are unselfishly and generously contributed to the ISC on a free basis.

The Institute of Seismology, Academy of Sciences of Albania
Albania
TIR

Centre de Recherche en Astronomie, Astrophysique et Geophysique
Algeria
CRAAG

Universidad Nacional de La Plata
Argentina
LPA

Instituto Nacional de Prevención Sísmica
Argentina
SJA

National Survey of Seismic Protection
Armenia
NSSP

Geoscience Australia
Australia
AUST

Österreichischer Geophysikalischer Dienst
Austria
VIE

International Data Centre, CTBTO
Austria
IDC

Republic Center of Seismic Survey
Azerbaijan
AZER

Centre of Geophysical Monitoring
Belarus
BELR

Royal Observatory of Belgium
Belgium
UCC

Instituto Astronomico e Geofísico
Brazil
VAO

Geophysical Institute, Bulgarian Academy of Sciences
Bulgaria
SOF

Canadian Hazards Information Service, Natural Resources Canada
Canada
OTT

Departamento de Geofísica, Universidad de Chile
Chile
GUC

China Earthquake Networks Center
China
BJI

Institute of Earth Sciences, Academia Sinica
Chinese Taipei
ASIES

Observatorio Vulcanológico y Sismológico de Costa Rica
Costa Rica
HDC

Central American Seismic Center
Costa Rica
CASC

Seismological Survey of the Republic of Croatia
Croatia
ZAG

Servicio Sismológico Nacional Cubano
Cuba
SSNC

Cyprus Geological Survey Department
Cyprus
NIC

Geophysical Institute, Academy of Sciences of the Czech Republic
Czech Republic
PRU

West Bohemia Seismic Network
Czech Republic
WBNET

Geological Survey of Denmark and Greenland
Denmark
DNK

Observatoire Geophysique d'Arta
Djibouti
ARO

Servicio Nacional de Sismología y Vulcanología
Ecuador
IGQ

National Research Institute of Astronomy and Geophysics
Egypt
HLW

University of Addis Ababa
Ethiopia
AAE

Institute of Seismology, University of Helsinki
Finland
HEL

Centre Sismologique Euro-Mediterraneen
France
CSEM

Institut de Physique du Globe
France
STR

Laboratoire de Détection et de Géophysique/CEA
France
LDG

Laboratoire de Géophysique/CEA
French Polynesia
PPT

Seismological Observatory Skopje
FYR Macedonia
SKO

Seismic Monitoring Centre of Georgia
Georgia
TIF

Geophysikalisches Observatorium Collm
Germany
CLL

Bundesanstalt für Geowissenschaften und Rohstoffe
Germany
BGR

Seismological Observatory Berggießhübel, TU Bergakademie Freiberg
Germany
BRG

Alfred Wegener Institute for Polar and Marine Research
Germany
AWI

National Observatory of Athens
Greece
ATH

Department of Geophysics, Aristotle University of Thessaloniki
Greece
THE

Hong Kong Observatory
Hong Kong
HKC

Geodetic and Geophysical Research Institute
Hungary
BUD

Icelandic Meteorological Office
Iceland
REY

India Meteorological Department
India
NDI

National Geophysical Research Institute
India
HYB

Badan Meteorologi, Klimatologi dan Geofisika
Indonesia
DJA

Tehran University
Iran
TEH

International Institute of Earthquake Engineering and Seismology (IIEES)
Iran
THR

Iraqi Meteorological and Seismology Organisation
Iraq
ISN

Dublin Institute for Advanced Studies
Ireland
DIAS

The Geophysical Institute of Israel
Israel
GII

Osservatorio Geofisico Sperimentale
Italy
TRI

Istituto Nazionale di Geofisica e Vulcanologia
Italy
ROM

Station Géophysique de Lamto
Ivory Coast
LIC

Jamaica Seismic Network
Jamaica
JSN

National Research Institute for Earth Science and Disaster Prevention
Japan
NIED

Japan Meteorological Agency
Japan
JMA

The Matsushiro Seismological Observatory
Japan
MAT

National Institute of Polar Research
Japan
SYO

Jordan Seismological Observatory
Jordan
JSO

National Nuclear Center
Kazakhstan
NNC

Kyrgyz Seismic Network
Kyrgyzstan
KNET

Institute of Seismology, Academy of Sciences of Kyrgyz Republic
Kyrgyzstan
KRNET

National Council for Scientific Research
Lebanon
GRAL

Geological Survey of Lithuania
Lithuania
LIT

Malaysian Meteorological Service
Malaysia
KLM

Instituto de Geofísica de la UNAM
Mexico
MEX

Red Sismica del Noroeste de Mexico (RESOM)
Mexico
ECX

Institute of Geophysics and Geology
Moldova
MOLD

Department of Mines and Geology, Ministry of Industry of Nepal
Nepal
DMN

IRD Centre de Nouméa
New Caledonia
NOU

University of Bergen
Norway
BER

Sultan Qaboos University
Oman
OMAN

Philippine Institute of Volcanology and Seismology
Philippines
MAN

Institute of Geophysics, Polish Academy of Sciences
Poland
WAR

Seismological Institute of Montenegro
Montenegro
PDG

Koninklijk Nederlands Meteorologisch Instituut
Netherlands
DBN

Institute of Geological and Nuclear Sciences
New Zealand
WEL

Stiftelsen NORSAR
Norway
NAO

Micro Seismic Studies Programme, PINSTECH
Pakistan
MSSP

Manila Observatory
Philippines
QCP

Instituto Português do Mar e da Atmosfera, I.P.
Portugal
INMG

Sistema de Vigilância Sismológica dos Açores
Portugal
SVSA

Instituto Geofisico do Infante Dom Luiz
Portugal
IGIL

Korea Meteorological Administration
Republic of Korea
KMA

National Institute for Earth Physics
Romania
BUC

Kamchatkan Experimental and Methodical Seismological Department
Russia
KRSC

Altai-Sayan Seismological Centre, GS SB RAS
Russia
ASRS

Geophysical Survey of Russian Academy of Sciences
Russia
MOS

Kola Regional Seismic Centre, GS RAS
Russia
KOLA

Yakutiya Regional Seismological Center, GS SB RAS
Russia
YARS

Sakhalin Experimental and Methodological Seismological Expedition, GS RAS
Russia
SKHL

Baykal Regional Seismological Centre, GS SB RAS
Russia
BYKL

North Eastern Regional Seismological Centre, GS RAS
Russia
NERS

Saudi Geological Survey
Saudi Arabia
SGS

Seismological Survey of Serbia
Serbia
BEO

Geophysical Institute, Slovak Academy of Sciences
Slovakia
BRA

Environmental Agency of the Republic of Slovenia
Slovenia
LJU

Ministry of Mines, Energy and Rural Electrification
Solomon Islands
HNR

Council for Geoscience
South Africa
PRE

Instituto Geográfico Nacional
Spain
MDD

University of Uppsala
Sweden
UPP

Swiss Seismological Sevice (SED)
Switzerland
ZUR

National Syrian Seismological Center
Syria
NSSC

Thai Meteorological Department
Thailand
BKK

University of the West Indies
Trinidad and Tobago
TRN

Disaster and Emergency Management Presidency
Turkey
DDA

Kandilli Observatory and Research Institute
Turkey
ISK

Subbotin Institute of Geophysics, National Academy of Sciences
Ukraine
SIGU

Dubai Seismic Network
United Arab Emirates
DSN

British Geological Survey
United Kingdom
BGS

United States Geological Survey
U.S.A.
USGS

IRIS Data Management Center
U.S.A.
IRIS

IASPEI Working Group on Reference Events
U.S.A.
IASPEI

Red Sísmica de Puerto Rico
U.S.A.
RSPR

Pacific Northwest Seismic Network
U.S.A.
PNSN

The Global CMT Project
U.S.A.
GCMT

National Earthquake Information Center
U.S.A.
NEIC

Scripps Institution of Oceanography
U.S.A.
SIO

Fundación Venezolana de Investigaciones Sismológicas
Venezuela
FUNV

National Center for Scientific Research
Vietnam
PLV

Yemen National Seismological Center
Yemen
DHMR

Goetz Observatory
Zimbabwe
BUL

CWB
Chinese Taipei
TAP

2.5 ISC Staff

Listed below are the staff (and their country of origin) who were employed at the ISC at the time of this ISC Bulletin Summary.

- Dmitry Storchak
- Director
- Russia/United Kingdom

- Maureen Aspinwall
- Administration Officer
- United Kingdom

- James Harris
- System and Database Administrator
- United Kingdom

- John Eve
- Data Collection Officer
- United Kingdom

- Emily Delahaye
- Seismologist/Lead Analyst
- Canada

- Elizabeth Robertson
- Seismologist/Analyst
- New Zealand

- Blessing Shumba
- Seismologist/Analyst
- Zimbabwe

- Rosemary Wylie
- Analyst
- United Kingdom

- Ivana Jukić
- Seismologist/Analyst
- Croatia

- István Bondár
- Senior Seismologist
- Hungary

- Wayne Richardson
- Senior Seismologist
- New Zealand

- Domenico Di Giacomo
- Seismologist
- Italy

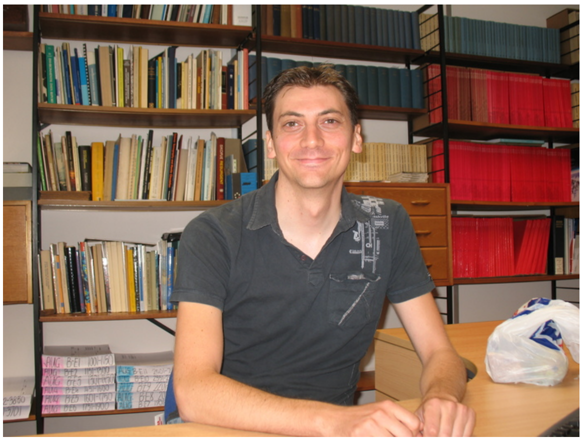

- Przemek Ozgo
- Junior System Administrator
- Poland

- Rebecca Verney
- Historical Data Entry Officer / Trainee Analyst
- United Kingdom

- Natalia Safronova
- Historical Data Entry Officer
- Russia

- Sepideh Rastin
- Developer
- Iran

3

Availability of the ISC Bulletin

The ISC Bulletin is available from the following sources:

- Web searches
  The entire ISC Bulletin is available directly from the ISC website via a number of searches.
  (www.isc.ac.uk/iscbulletin/search)
  (isc-mirror.iris.washington.edu/iscbulletin/search)

  - Bulletin search - provides the most verbose output of the ISC Bulletin in ISF or QuakeML.
  - Event catalogue - only outputs the prime hypocentre for each event, producing a simple list of events, locations and magnitudes.
  - Arrivals - search for arrivals in the ISC Bulletin. Users can search for specific phases for selected stations and events.

- CD-ROMs/DVD-ROMs

  CDs/DVDs can be ordered from the ISC for any published volume (one per year), or for all back issues of the Bulletin (not including the latest volume). The data discs contain the Bulletin as a PDF, in IASPEI Seismic Format (ISF), and in Fixed Format Bulletin (FFB) format. An event catalogue is also included, together with the International Registry of seismic station codes.

- FTP site

  The ISC Bulletin is also available to download from the ISC ftp site, which contains the Bulletin in PDF, ISF and FFB formats. (ftp://www.isc.ac.uk)
  (ftp://isc-mirror.iris.washington.edu)

Mirror service

A mirror of the ISC database, website and ftp site is available at IRIS DMC (isc-mirror.iris.washington.edu), which benefits from their high-speed internet connection, providing an alternative method of accessing the ISC Bulletin.

4

Citing the International Seismological Centre

Data from the ISC should always be cited. This includes use by academic or commercial organisations, as well as individuals. A citation should show how the data were retrieved and may be in one of these suggested forms:

Data retrieved from the ISC web site:

- International Seismological Centre, On-line Bulletin, http://www.isc.ac.uk, Internatl. Seis. Cent., Thatcham, United Kingdom, 2010.

Data transcribed from the IASPEI reference event bulletin:

- International Seismological Centre, Reference Event Bulletin, http://www.isc.ac.uk, Internatl. Seis. Cent., Thatcham, United Kingdom, 2010.

Data transcribed from the EHB bulletin:

- International Seismological Centre, EHB Bulletin, http://www.isc.ac.uk, Internatl. Seis. Cent., Thatcham, United Kingdom, 2010.

Data copied from ISC CD-ROMs/DVD-ROMs:

- International Seismological Centre, Bulletin Disks 1-9 [CD-ROM], Internatl. Seis. Cent., Thatcham, United Kingdom, 2010.

Data transcribed from the printed Bulletin:

- International Seismological Centre, Bull. Internatl. Seis. Cent., 36(1), Thatcham, United Kingdom, 2010.

The ISC is named as a valid data centre for citations within American Geophysical Union (AGU) publications. As such, please follow the AGU guidelines when referencing ISC data in one of their journals. The ISC may be cited as both the institutional author of the Bulletin and the source from which the data were retrieved.

BibTex entry example:

```
@manual{ISCcitation2010,
author = "International Seismological Centre",
```

title = "On-line Bulletin",
organization = "Int. Seis. Cent.",
note = "http://www.isc.ac.uk",
address = "Thatcham, United Kingdom",
year = "2010"
}

5

Operational Procedures of Contributing Agencies

5.1 Seismic Network and Routine Data Processing -Japan Meteorological Agency-

Doi, Keiji
Seismology and Volcanology Department
Japan Meteorological Agency
Tokyo
Japan

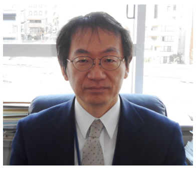

5.1.1 Overview

Japan and its vicinity is one of the most seismically active regions in the world, and the Japanese people have long suffered from damage by strong ground motions caused by earthquakes as well as from tsunamis. They experienced damaging earthquakes such as the Nobi earthquake in 1891, the Meiji-Sanriku earthquake in 1896, the Kanto earthquake in 1923, the Kobe earthquake in 1995[1] and the Tohoku earthquake in 2011[2], each of which caused more than 5,000 casualties, and many lives and properties have been lost in other events.

In order to study the earthquakes and mitigate disasters caused by them, contemporary seismic observations began late in the 19th century. It was also understood that a prompt warning/information system for earthquakes and tsunamis would be an important tool to reduce casualties. In this regard, Japan Meteorological Agency (JMA), as one of the responsible governmental organizations, has developed seismic observation networks that are designed for the prompt issuance of earthquake and tsunami warnings to notify as early as possible the regions likely to be affected by strong motions and tsunamis causing damage. JMA additionally plays an important role in providing countries in the northwest Pacific region with detailed forecast information on tsunamis in the area, acting as the Northwest Pacific Tsunami Advisory Center.

JMA also has the responsibility for maintaining a national earthquake catalogue covering the Japanese islands and their vicinity down to 700 km in depth (Figure 5.1). The data archive contains information on earthquake locations as well as phase arrival-time data and focal mechanisms. There are several other seismic networks in Japan developed by other institutions, including research universities for academic purposes and local governments for disaster mitigation purposes. JMA retrieves and uses all the available data from these other networks for a better understanding of the seismicity.

The seismic network of JMA is described here, along with JMA data processing and analysis.

[1] JMA officially named the Kobe earthquake as "the 1995 Southern Hyogo Prefecture Earthquake."
[2] JMA officially named the Tohoku earthquake as "the 2011 off the Pacific Coast of Tohoku Earthquake."

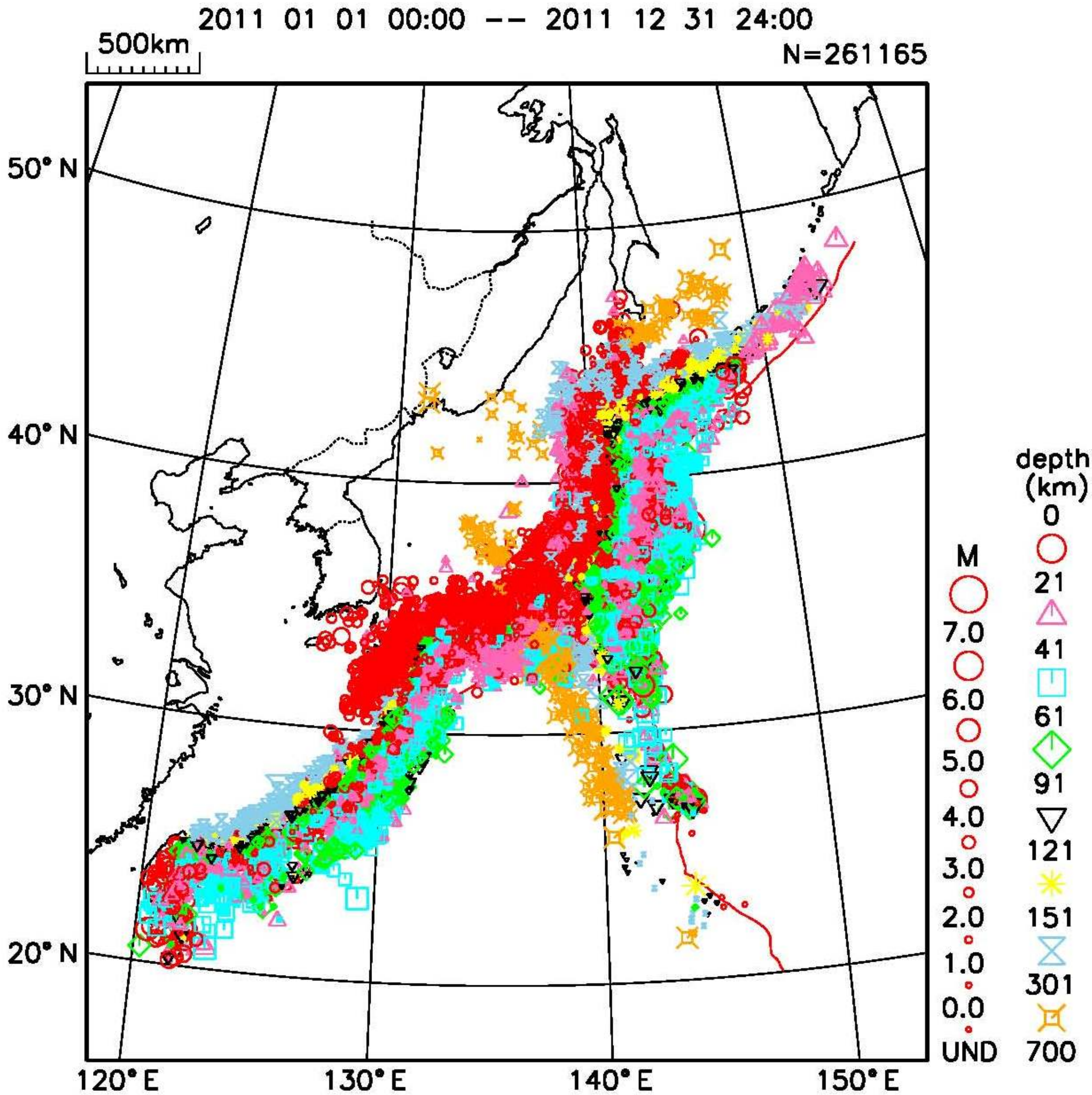

Figure 5.1: Earthquake distribution in 2011. The map shows the JMA coverage area for monitoring seismicity.

5.1.2 Types of networks

JMA operates several sub-networks, with combinations of accelerometers, velocity meters and broadband seismometers, for various purposes as described in the following.

i) The seismic network for Earthquake and Tsunami Early Warnings

One of the most important missions for JMA is to monitor earthquake activity so as to provide earthquake and tsunami early warnings in a timely manner to notify those who are likely to be affected by strong motions and tsunamis to take appropriate action and avoid danger. JMA operates a seismic network, consisting of accelerometers, velocity meters and ocean-bottom seismometers, designed for the prompt issuance of earthquake and tsunami early warnings.

Accelerometers - Multi-function seismic stations

There are about 280 accelerometers installed (Figure 5.2), each equipped with an on-site processor that is capable of determining automatically the seismic phase arrival-times and amplitudes, as well as estimates for the azimuth of the earthquake epicenter and the focal distance: these results are used as input data for the Earthquake Early Warning process (Kamigaichi *et al.*, 2009; Doi, 2011). They are also capable of estimating seismic intensity (see below). This type of station is referred to as a "multi-function seismic station" because it provides not only waveform data with 100 Hz sampling but also the several other types of analyzed outputs mentioned. The data and estimates are transmitted on a real-time basis through dedicated terrestrial telephone lines to the JMA Headquarters in Tokyo and to the Osaka Regional Headquarters. JMA has upgraded these stations by installing satellite-link communication equipment as a backup for the case of landline network interruption, by setting up emergency battery power supplies to cover a period of up to 72 hours in the event of a long-term electricity blackout.

Velocity meters

About 240 of the multi-function seismic stations also have velocity meters to detect small earthquakes. Waveform data with 100 Hz sampling from these velocity meters are transmitted on a real-time basis through dedicated terrestrial telephone lines to the JMA Headquarters in Tokyo and to the Osaka Regional Headquarters.

Ocean-bottom seismometers

JMA operates three sets of wired ocean-bottom seismometers, each of which has three-to-five velocity meters. One of the sets has five accelerometers in the same cells as the velocity meters. They are included in the accelerometer network for earthquake and tsunami early warning operation. Waveform data with 100 Hz sampling are transmitted on a real-time basis through dedicated terrestrial telephone lines to the JMA Headquarters in Tokyo and to the Osaka Regional Headquarters.

ii) The network of broadband stations

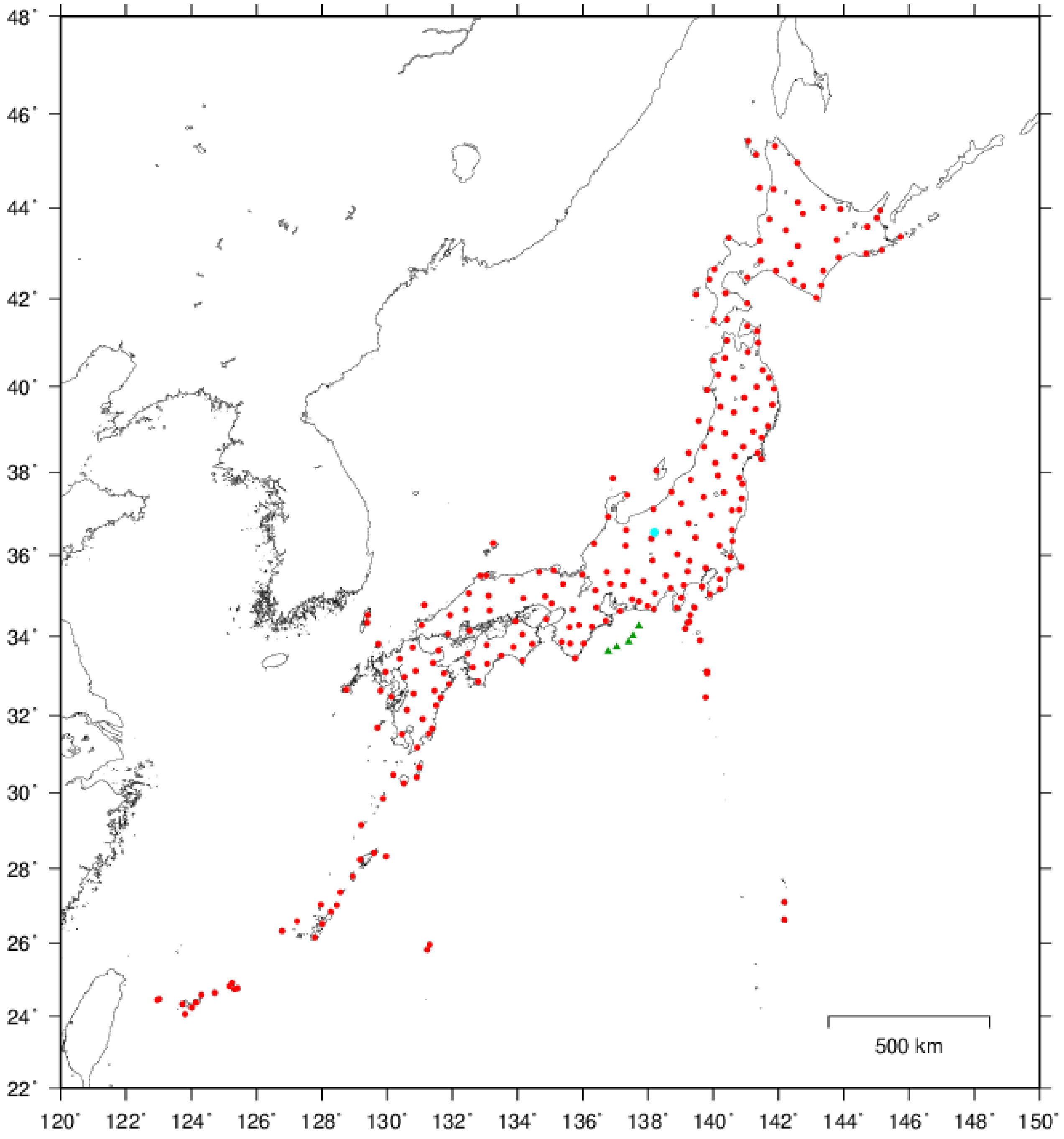

Figure 5.2: *The JMA seismic network of accelerometers.*

JMA operates 20 broadband stations with STS-2 seismometers (Figure 5.3). Waveform data with 20 Hz sampling are transmitted on a real-time basis through dedicated phone lines to the JMA Headquarters in Tokyo and to the Osaka Regional Headquarters. The broadband data are used not only for centroid moment tensor (CMT) solutions for earthquakes but also for evaluating the moment magnitude as an update for the earlier magnitude estimation of an earthquake in the tsunami forecast operation.

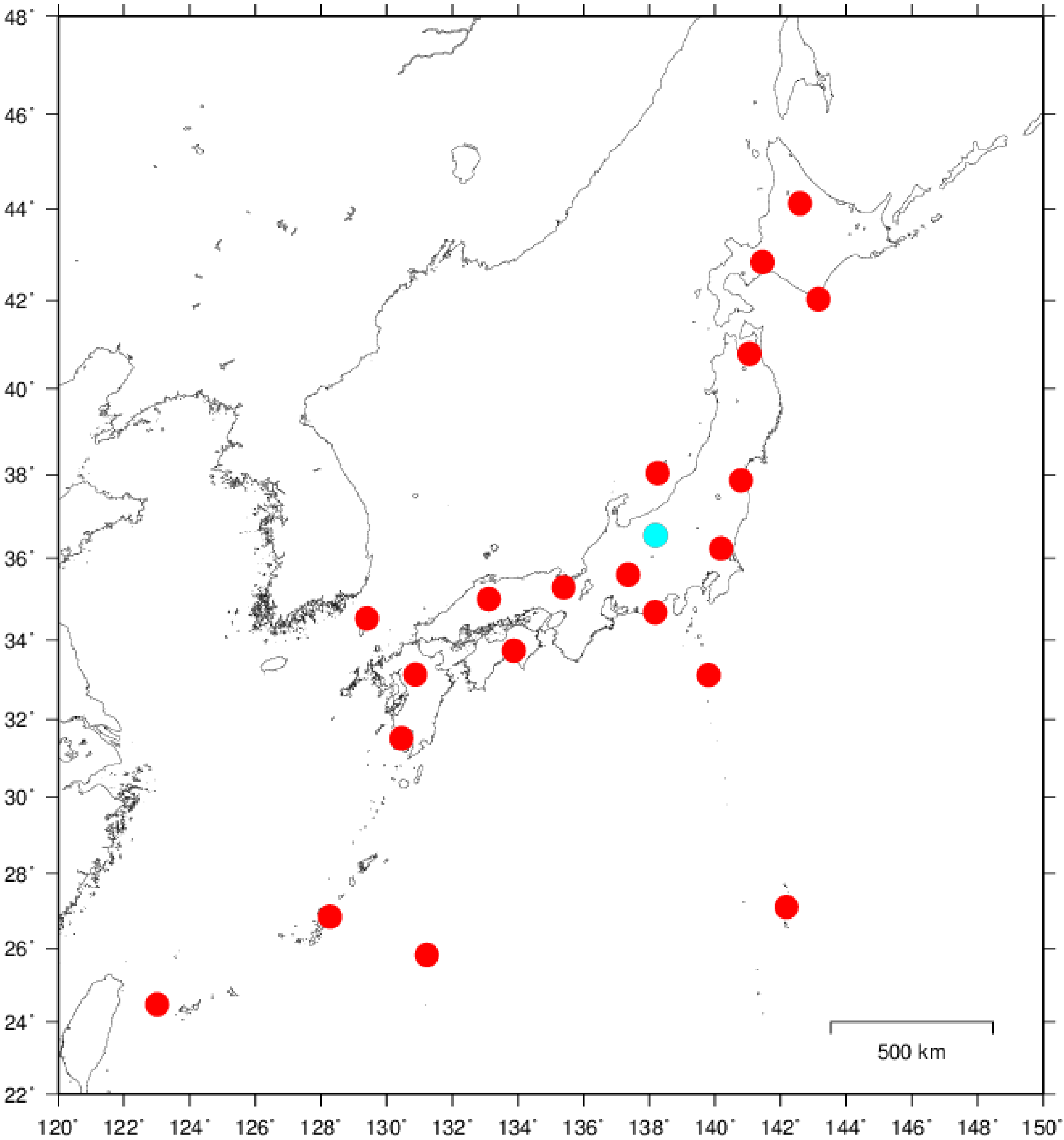

Figure 5.3: *Distribution of JMA broadband stations (STS-2). The blue circle shows a location of Matsushiro Observatory.*

iii) Matsushiro Seismic Array System (MSAS)

The MSAS consists of eight seismic stations arranged in a circle, the diameter of which is about 10 km, and the data processing units at Matsushiro Observatory (Figure 5.3). The advantage of seismic array observation is such that:

(1) It is possible to reduce the signal degradation from background noise, using the beam-forming technique in which individual channels are delayed and summed appropriately to enhance a signal and cancel the noise.

(2) The arrival direction and apparent velocity of the seismic signals can be determined from arrival-time differences at array elements used in forming the array beam to observe the best signal.

The system is mainly used for teleseismic event analysis and for locating small seismic swarms in the vicinity of the array.

iv) The network for seismic intensity measurement

Seismic intensity is key information in Japan, not only for emergency operation organizations but also for residents and visitors, for knowing how severe the strong ground-motion occurrence is and how wide-spread the damaging area is. The responsible agencies can then judge the necessity, urgency, and priority of search and rescue operations from the seismic intensity distribution following an earthquake occurrence.

JMA has developed an instrumental seismic intensity meter that is capable of measuring seismic intensity automatically from measurements of accelerations of ground motions, taking into account the amplitudes and frequencies (see Appendix 5.1.9). These seismic intensity values better represent human perceptions of the motions and the behaviours of furniture or buildings than single measures of PGA (peak ground acceleration) or PGV (peak ground velocity). It is thus possible to know, within a few minutes after the earthquake occurrence, the distribution of strong motions and the likely regions suffering damage.

JMA operates about 660 seismic intensity measurement stations nationwide (Figure 5.4), monitoring the damaging impact for densely populated cities and towns. Multi-function seismic stations also form part of the seismic intensity station network. Seismic intensity values are transmitted on a real-time basis through dedicated phone lines to the JMA Headquarters in Tokyo and to the Osaka Regional Headquarters. For backup resilience, half of the stations are equipped with a satellite communication capability using the geostationary meteorological satellite operated by JMA.

5.1.3 Data sharing with other organizations

There are other seismic networks in Japan that are maintained by universities and research institutes for their academic purposes. Several universities in Japan have co-operated and developed a regional seismic network, consisting of around 300 velocity-type seismometers and several accelerometers. The National Institute for Earth Science and Disaster Prevention (NIED) has also developed their nationwide network called “Hi-net” to monitor small earthquakes since 1997 and a broadband station network called

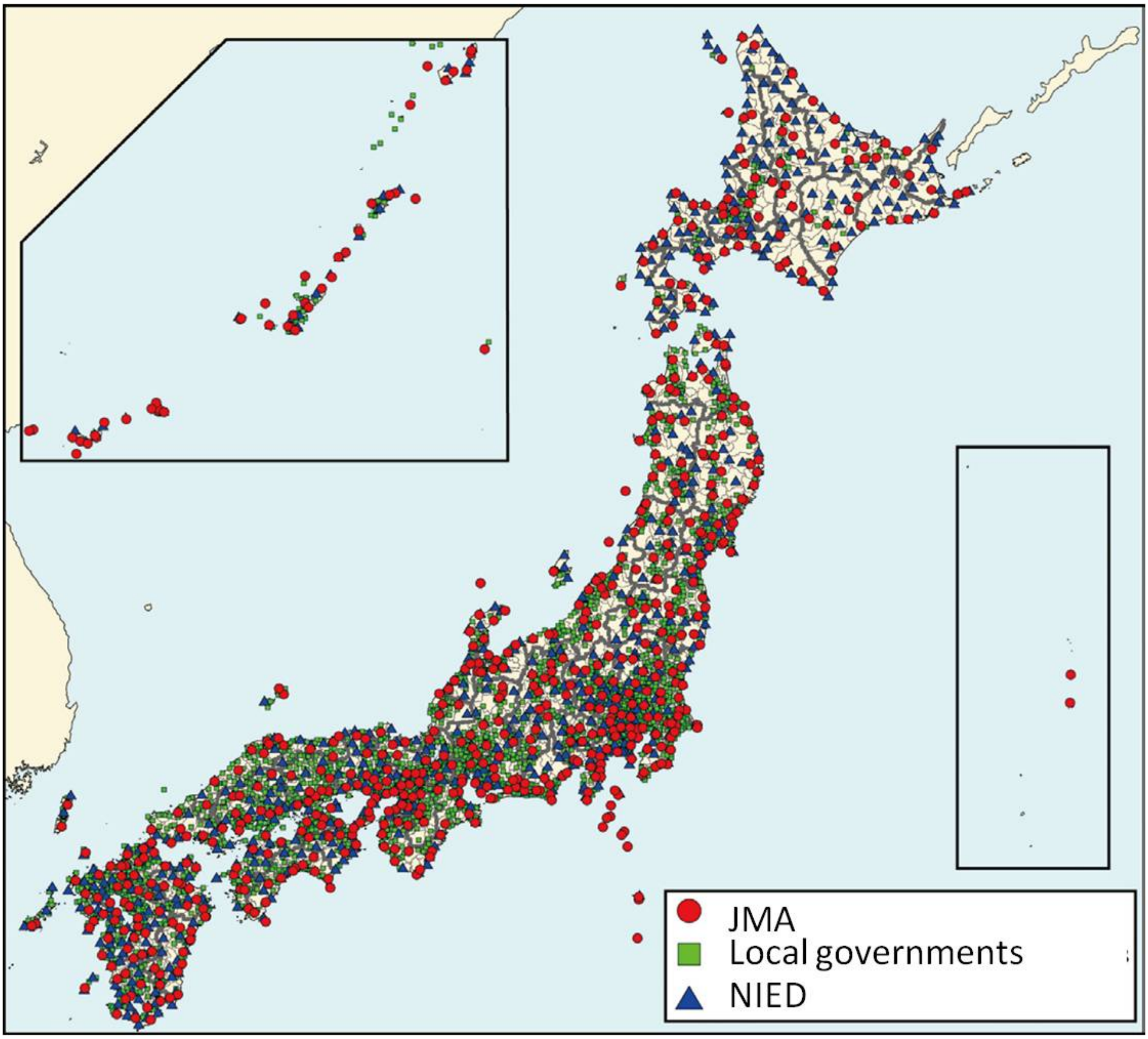

Figure 5.4: *Distribution of seismic intensity measurement stations.*

"F-net" since 1994. There are also some additional regional seismic stations maintained by other research institutes and local government authorities. Data from these stations (Figure 5.5) are shared among the network owners, and JMA uses all of the available data to improve the estimations of earthquake locations. The results are archived in the earthquake catalogue and are useful for evaluating seismic hazard.

NIED and local government authorities also operate as many as 3,700 seismic intensity measurement stations (Figure 5.4). The intensity values processed at each of these stations are disseminated to JMA on a real-time basis, and are then merged into JMA's own compilation for a prompt issuance of seismic intensity information. No waveform data from these stations are retrieved in real time.

5.1.4 Data processing

i) Emergency operation - Automatic processing of earthquake early warnings and fast

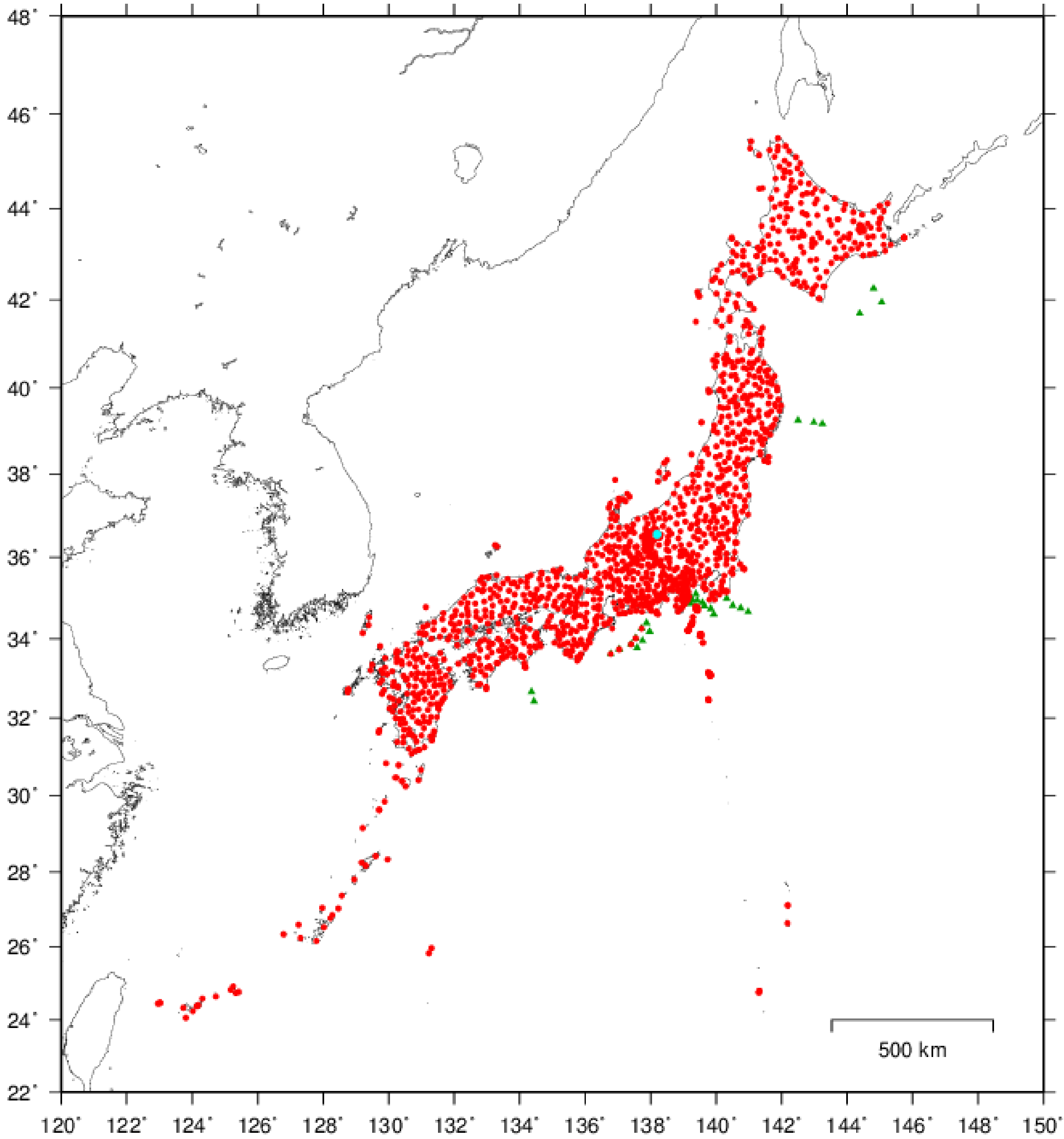

Figure 5.5: *Distribution of seismic stations contributing data shared among JMA, universities and other institutions.*

determinations of location and magnitude for tsunami warnings

Data processing for earthquake early warning occurs first during the sequence of the seismic data analysis when an earthquake is detected, and it is a thoroughly automated operation carried out simultaneously at the JMA Headquarters and at the Osaka Regional Headquarters to estimate a hypocenter and a magnitude based on outputs from multi-function seismic stations for moderate to severe strong motions generated by an earthquake (Kamigaichi *et al.*, 2009).

Waveform data are also processed simultaneously at the JMA Headquarters and at the Osaka Regional Headquarters to identify tsunami-genic earthquakes. Locations and magnitudes calculated on the basis of automatic readings of phase arrival-times and maximum amplitudes from multi-function seismic stations, as well as from seismic stations of other institutions, are presented to analysts on duty. The duty analysts review the results and decide whether to issue a tsunami warning, where appropriate, together with several other kinds of seismic information, including estimates of earthquake location, depth, magnitude and observed seismic intensities.

An initial tsunami warning should be issued within two-to-three minutes after the detection of seismic waves, and the other seismic information should follow not more than 15 minutes later. The duty analysts will also refer to the centroid moment tensor solution, which is automatically computed within 10-30 minutes after the earthquake occurrence using broadband station data, to re-evaluate from the focal mechanism and depth estimates the likelihood that a tsunami was generated. This further review is used to update the information provided by the observations that were required within two-to-three minutes for the initial tsunami warning.

The early warning system continues to be updated in the light of experience gained from recent events such as the 2011 off the Pacific Coast of Tohoku Earthquake (Japan Meteorological Agency, 2013).

ii) Precise analysis - Routine daily review and quality control for the national earthquake catalogue

Seismic events from 0-24 hours in local time are reviewed daily by analysts at six regional operation centers of JMA, each monitoring an area almost 1000 km by 1000 km. The independent analyses are done using different processes from those used for the earthquake and tsunami early warnings.

a) Automatic process

Continuous waveform data, telemetered from seismic stations digitally on a real-time basis, are processed to identify automatically individual seismic events. Phase data at certain groupings of stations are used to locate each earthquake and to estimate the origin time and magnitude. The results are then checked for seismological consistency, such as comparing the differences between observed and computed P-phase and S-phase arrival-times or the consistency of apparent velocity across the grouping of stations. Some identified events remain without hypocenter or magnitude estimations.

b) Review by personnel

Analysts review the results produced by the automatic calculations so as to
• delete false events (noise or artifacts),
• check for consistency with previous seismicity,
• check if the trend in residuals of phase arrival-times shows bias,
• check the azimuth gap of stations included, and so on.

Analysts will re-measure phase arrival-times and maximum amplitudes if necessary.

Reviewed data are relayed to the JMA Headquarters on the afternoon of the next day. Analysts there merge all the reports, checking for duplication of events, and the preliminary results are published on the JMA web-site. After another review, the final determinations are archived and published as the monthly bulletin for Japan a few months later.

iii) Methodology

a) Determination of hypocenters:

Hypocenters are calculated using the arrival-times of P-waves and S-waves, and magnitudes are calculated using the maximum seismic-wave amplitudes. An iterative method (Hamada *et al.*, 1983), an extension of Geiger's method (Geiger, 1910), is used to calculate hypocenters.

The data weight is given by the following formula, where R denotes the hypocentral distance (Ueno *et al.*, 2002):

For P-waves $(W_p) : W_p = {R_{min}}^2/R^2$
For S-waves $(W_s) : W_s = W_p/3$
R_{min}: Hypocentral distance of the station nearest to the hypocenter (km)
(if $R_{min} \leq 50$, then $R_{min} = 50$: if $W_p > 1$, then $W_p = 1$)

The data of any station with large travel-time residuals are not used for the calculations. The depth of focus is calculated first with no restrictions. If the solution is unstable, then the best solution is searched by changing the depth in 1 km steps. In the case that the focus is located in a region where focal depths are considered to be not well determined, such as in the Kurile Islands region, the focal depth is fixed at 30 km.

The JMA2001 travel-time tables (Ueno *et al.*, 2002) are used for the theoretical travel-times. For earthquakes located near the Kurile Islands, the travel-time tables given by Ichikawa (1978) are used. The Jeffreys-Bullen travel-time tables (Jeffreys and Bullen, 1958) are used for earthquakes having an epicentral distance of 2000 km or more from the JMA seismic network.

In principle, the calculation is done only when more than five P or S-wave arrivals have been observed at three or more stations (a criterion used since January 1983). If the number of stations with observations exceeds 40, the nearest 40 stations from the focus are used in the calculation (a criterion used since October 1997). Procedures for the selection of stations are as follows:

A characteristic distance (Δ_{lim}) is defined in terms of the following empirical equation:

$\Delta_{lim} = {\Delta_3}^2/100$ (km) $+H$ (km) +100 (km)

Here Δ_3 denotes the epicentral distance of the third nearest station from the trial hypocenter; H is focal depth: the unit is kilometre.

The 16 stations nearest to the trial hypocenter are selected without regard to station quality. An additional 24 stations within Δ_{lim} are then selected based on the epicentral distance and station quality, where the station quality is given as an attribute constant derived from seven classes regarding the S/N ratio, data-sending capability and average travel-time residual etc. If the number of selected stations is still not enough for robust estimation in the case of an offshore earthquake or a deep earthquake, for example, additional stations outside Δ_{lim} may be selected until the number of stations becomes sufficient.

b) Determination method for magnitudes:

i. Magnitude M_J at the Local Meteorological Observatories

This is calculated only for large and shallow ($H \leq 60$ km) earthquakes using acceleration data from the multi-function seismometers installed at the Local Meteorological Offices. M_J is given by the average of observations of

$$ {M_J}^{OBS} = log\sqrt{({A_N}^2 + {A_E}^2)} + 1.73 log\Delta - 0.83 $$

using the maximum displacement amplitudes at the stations (Tsuboi, 1954). Here the acceleration data are integrated twice to obtain the displacement data, to which a high-pass (6 s) filter is applied to simulate the mechanical strong-motion seismographs. This method will be provisionally used until JMA can confirm the independence of C_D in the next relation (below) for the magnitude of large earthquakes, especially of M7 class or above.

ii. Displacement magnitude M_D

This is calculated as the average of observations of

$$ {M_D}^{ST} = log\sqrt{({A_N}^2 + {A_E}^2)} + \beta_D(\Delta, H) + C_D $$

over stations in the ranges $R \geqslant 30$ km and $\Delta \leq 700$ km for maximum amplitudes of displacement in the horizontal components (Katsumata, 2004). If the number of stations involved in the average is less than three, Δ is extended out to 2000 km. If the number of the stations used to obtain M_D is two, it is denoted as M_d.

iii. Velocity magnitude M_V

This is calculated as the average of observations of

$$M_V^{ST} = \alpha log A_Z + \beta_V(\Delta, H) + C_V$$

over stations in range 5 km $\leq R \leq$ 400 km for maximum amplitude of velocity in the vertical component (Funasaki *et al.*, 2004). If the number of stations involved in the average is less than four, Δ is extended out to 1000 km. If the number of the stations used to obtain M_V is two or three, it is denoted as M_v.

iv. Moment magnitude M_w

A moment magnitude M_w is given as a result of the centroid moment tensor (CMT) solution.

The averaging procedure for *i*, *ii* and *iii* in the above is as follows. First, an initial mean of magnitudes at all the stations is calculated. Then a mean and standard deviation of magnitudes for the stations is calculated, discarding those values deviating more than 0.5 from the initial mean. This mean value is adopted as the magnitude only if the standard deviation is less than 0.35.

The calculated value is adopted as the JMA magnitude according to the priority order $M_J > M_D > M_V > M_d > M_v$, and this is then given as the primary magnitude estimate. The moment magnitude is generally given as the secondary magnitude estimate when CMT solutions are determined; otherwise a secondary magnitude estimate is given according to the priority order.

For reference, the meanings of the symbols used in the above formulas are as follows:

H	Focal depth (km)
Δ	Epicentral distance (km)
R	Hypocentral distance (km)
α	Constant $1/0.85 = 1.176$
β_D, β_V	Terms showing dependence on Δ and H (see Figures 5.6 and 5.7)
C_D	Correction value ($= 0.2$) used for accelerometers
C_V	Correction value depending on types of seismometers (see Table 5.1)
A_N, A_E	Maximum displacement amplitude in the horizontal component of accelerometers. The unit is micrometres (10^{-6} m).
A_Z	Maximum velocity amplitude in the vertical component of velocity meters. The unit is 10^{-5} m/s.

Table 5.1: *Correction value estimated for each type of seismometer (C_V)*

Type of seismometer	Value
Velocity meters	0.00
JMA OBS (velocity)	0.47
JMA velocity type installed in volcanic region	1.13
Other organization, bore-hole installation (velocity)	0.48

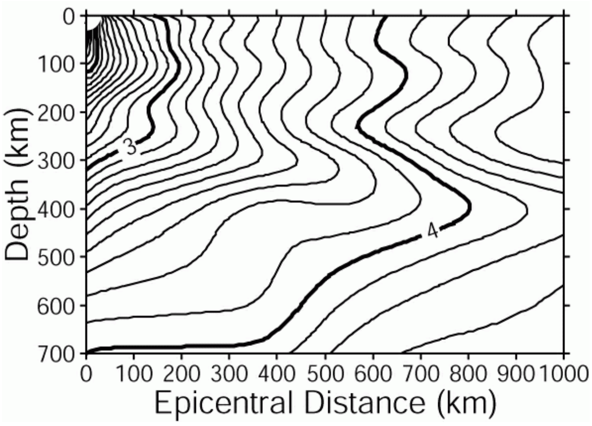

Figure 5.6: Contour representation of β_D.

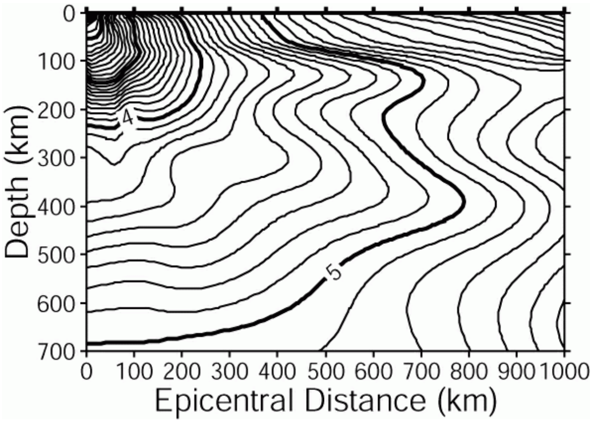

Figure 5.7: Contour representation of β_V.

5.1.5 Data availability

Earthquake locations and magnitudes as a result of data processing by JMA are made public by means of several ways, as follows:

- Prompt information in the case of tsunami warnings and/or felt earthquakes

  If a tsunami is anticipated and/or if a seismic intensity 1 and more is observed when an earthquake occurs, JMA provides prompt information of its location and magnitude in 10-15 minutes after the detection of seismic waves. Warning information will be disseminated as a computer-readable message in a specific format to broadcasting media and to national/local government authorities who have responsibilities for emergency operations. It is also often disseminated through web-sites, including JMA's.

- Preliminary results reviewed by analysts

  Preliminary determinations of earthquake parameters are available on the JMA web-site on the evening of the next day after their origin time.

- Earthquake catalogue of Japan

  Results after a final review process are archived several months later as the earthquake catalogue of Japan, which is also available on the JMA web-site. The catalogue includes locations and magnitudes of earthquakes, as well as phase arrival-times and focal mechanism solutions.

  The publication timeline is summarized in Table 5.2. Waveform data observed not only by JMA but also by the other institutions that have joined in seismic data sharing are available from a data management center operated by the National Institute for Earth Science and Disaster Prevention (NIED).

Table 5.2: Timeline of information and data release by JMA

Timing after an earthquake	Title	Content
Several to tens of seconds	Earthquake Early Warning	Warnings of intensities of ground motions

Table 5.2: *Continued.*

Timing after an earthquake	Title	Content
1.5 to 2 minutes	Seismic Intensity Information	Indicating regions with seismic intensity of 3 or greater
2 to 3 minutes	Tsunami Warning	Fast determinations of the location and magnitude of the earthquake.
5 to 10 minutes	Earthquake and Seismic Intensity Information	Indicating the earthquake location and magnitude, and cities with seismic intensity of 3 or greater
Up to 15 minutes	Seismic Intensity Information	Indicating seismic intensities at observation stations
One day	Preliminary determination of earthquakes	Locations, magnitudes, phase arrivals, after review process by analysts
Beginning of the next month	Monthly report of seismicity of Japan	Overview of seismicity, mostly focused on felt earthquakes
Several months	Monthly Seismological Bulletin of Japan	Locations, magnitudes, phase arrivals, focal mechanisms, seismic intensities, after review process by analysts

5.1.6 History of the seismic network

Before 1994, most of seismic instruments were installed at about 150 of JMA's local offices. Although a computer system for telemetered seismic data processing had been introduced to the six regional tsunami warning centers of JMA late in 1980's, a person in charge there at each local office was still responsible for the reading of phase arrival-times and maximum amplitudes from seismograms and reporting them to the tsunami warning centers. From 1994, the seismic network was renewed, so that seismographic instruments were installed at less noisy sites to detect weaker seismic waves, and all the waveform data were telemetered to regional tsunami warning centers of JMA. In 2004, another renovation was implemented, so as to issue earthquake early warnings following the installation of "multi-function seismic stations," and the tsunami warning centers were centralized to the JMA Headquarters and the Osaka Regional Headquarters after a major data processing system upgrade in 2009. The progressive development of the JMA network is indicated in Figure 5.8. A chronological summary below, after Hamada (2002), has been updated to indicate more recent developments.

1875	The Palmieri seismograph (imported from Italy) was installed and operated by the Weather Section of the Geographical Agency Office of Interior in Tokyo
1892	Seismographs were installed at the 19 weather stations
1926	Deployment of the Wiechert seismograph and Omori's seismograph was promoted for the development of the seismological network after the 1923 Kanto Earthquake
1950	Mechanical strong-motion seismographs (modified type) were manufactured by the Meteorological Instrument Plant. The number of the seismographs installed reached 104 by the end of 1959.

1960	As a successor to the Wiechert seismograph, the JMA59 type electromagnetic seismographs with either an optical recorder (OP) or a visual recorder (VI, $T_0 = 5$s) were developed and deployed. The deployed number of the OP-type was 31 by the end of 1955, and 82 of the VI-type were deployed by the end of 1976.
1978	Ocean-bottom seismometers connected by coaxial cable were deployed off the Tokai coast and data were relayed to the JMA Headquarters
1983	The Seismic Array System became operational at the JMA Seismological Observatory (Matsushiro), performing backup functions of the JMA Headquarters
1985	Another ocean-bottom seismograph observation system was installed off the coast of the Boso Peninsula
1994	Deployment of 180 stations for the Tsunami and Earthquake Observation Network was approved and operation of existing seismic stations was terminated and replaced by the new network
1996	Start of seismic intensity meters in operation, replacing the system of reports sent by observers at meteorological offices of JMA
2003	Installation of multi-function seismic stations began and was completed in 2005
2009	The third ocean-bottom seismograph observation system was deployed in Enshu-nada Sea
2011	Deployment of an additional 50 multi-function seismic stations, coming into operation in 2012-2013

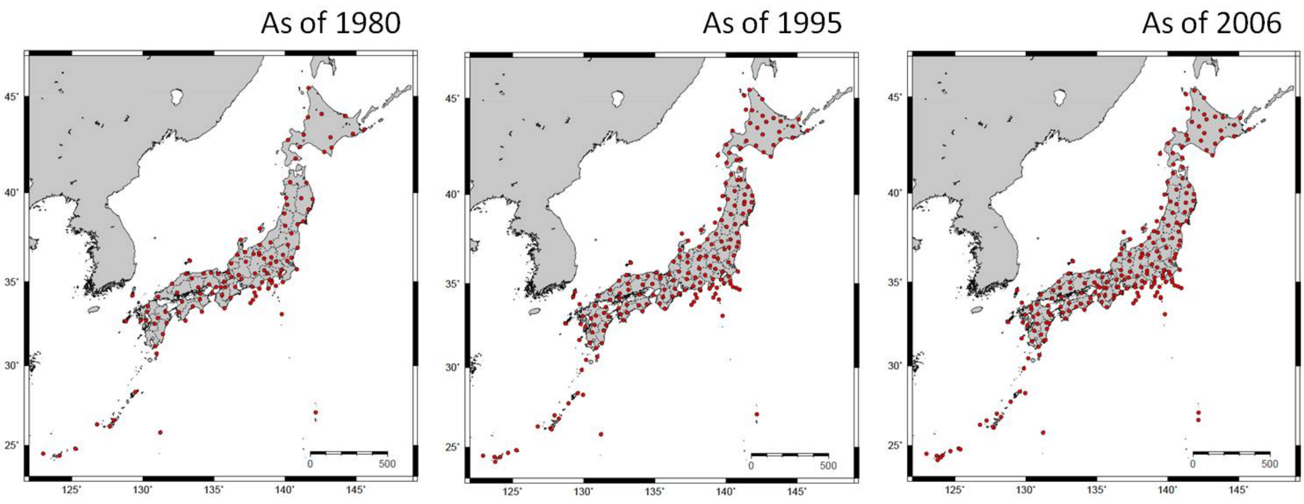

Figure 5.8: *Recent development of the JMA seismic network*

5.1.7 Acknowledgements

The author thanks Messrs S. Tari, K. Moriwaki, and Y. Kawazoe for their drafting of figures for this document, and Mr T. Koizumi for providing the explanation of JMA's instrumental seismic intensity. He also appreciates JMA staff members involved in network maintenance, seismic observation, analysis, and the provision of warning information for their tireless efforts and enthusiasm. Some of the figures were generated using the Generic Mapping Tools (Wessel and Smith, 1998).

5.1.8 References

Doi, K. (2011), The operation and performance of Earthquake Early Warnings by the Japan Meteorological Agency, *Soil Dynam. Earthq. Eng.*, 31, 119-126

Funasaki, J., and Earthquake Prediction Information Division (2004), Revision of the JMA Velocity Magnitude (in Japanese), *Quart. J. Seis.*, 67, 11-20.

Geiger, L. (1910), Herdbestimmung bei Erdbeben aus den Ankunftszeiten, *Nachrichten von der Königlichen Gesellschaft der Wissenschaften zu Göttingen, Mathematisch-Physikalische Klasse*, 331-349.

Hamada, N., A. Yoshida, and H. Hashimoto (1983), Improvement of the Hypocenter Determination Program of the Japan Meteorological Agency (Reanalyses of the Hypocenter Distribution of the 1980 Earthquake Swarm off the east coast of the Izu Peninsula and the Matsushiro Earthquake Swarm) (in Japanese), *Quart. J. Seis.*, 48, 35-55.

Hamada, N. (2002), Centennial Report of Japan – Part5.10 Japan Meteorological Agency (JMA), *International Handbook of Earthquake and Engineering Seismology* Part B, Chap.79-33, Academic Press

Ichikawa, M. (1978), A new subroutine program for determination of earthquake parameters and local travel time tables for events near the southern Kurile trench (in Japanese), *Quart. J. Seis.*, 43, 11-19.

Japan Meteorological Agency (2013), Lessons learned from the tsunami disaster caused by the 2011 Great East Japan Earthquake and improvements in JMA's tsunami warning system, *http://www.seisvol.kishou.go.jp/eq/eng/tsunami/LessonsLearned_Improvements_brochure.pdf*

Jeffreys, H., and K. E. Bullen (1958), *Seismological Tables*, British Association for the Advancement of Science, Gray-Milne Trust.

Kamigaichi, O., M. Saito, K. Doi, T. Matsumori, S. Tsukada, K. Takeda, T. Shimoyama, K. Nakamura, M. Kiyomoto, and Y. Watanabe (2009), Earthquake Early Warning in Japan – Warning the general public and future prospects –, *Seismol. Res. Lett.*, 80, 717-726

Katsumata, A. (2004), Revision of the JMA Displacement Magnitude (in Japanese), *Quart. J. Seis.*, 67, 1-10.

Tsuboi, C. (1954), Determination of the Gutenberg-Richter's magnitude of shallow earthquakes occurring in and near Japan (in Japanese), *Zisin 2* 7, 185-193.

Ueno, H., S. Hatakeyama, T. Aketagawa, J. Funasaki, and N. Hamada (2002), Improvement of hypocenter determination procedures in the Japan Meteorological Agency (in Japanese), *Quart. J. Seis.*, 65, 123-134.

Wessel, P., and W. H. F. Smith (1998), New, improved version of the Generic Mapping Tools released, EOS Trans. AGU, 79, 579, *http://gmt.soest.hawaii.edu/*.

Note: The *Quaternary Journal of Seismology* has been published by Japan Meteorological Agency since 1925. The volumes are available on the JMA web-site.

5.1.9 Appendix: Instrumental seismic intensity

A seismic intensity represents the scale of ground motion at a particular location caused by an earthquake. It varies with the distance from the epicenter and the surface geology as well as the magnitude of the earthquake. The JMA seismic intensity scale has 10 degrees (0 (imperceptible), 1, 2, 3, 4, 5 lower, 5 upper, 6 lower, 6 upper and 7) and is calculated from the acceleration of ground motion.

The process is:

1 Filtering an acceleration seismogram using a band-pass filter providing similar sensitivities to human perceptions in the frequency domain (Figure 5.9)

2 Getting an adjusted maximum acceleration A that satisfies certain criteria with respect to the duration of the ground motion

3 Calculating S by $S = 2.0 * log(A) + 0.94$

4 Rounding S numerically to a whole number for the seismic intensity. If $S = 2.4$, for example, then the seismic intensity becomes 2.

JMA seismic intensity	instrumental seismic intensity (S)	JMA seismic intensity	instrumental seismic intensity (S)
0	$S < 0.5$	5 lower	$4.5 \leq S < 5.0$
1	$0.5 \leq S < 1.5$	5 upper	$5.0 \leq S < 5.5$
2	$1.5 \leq S < 2.5$	6 lower	$5.5 \leq S < 6.0$
3	$2.5 \leq S < 3.5$	6 upper	$6.0 \leq S < 6.5$
4	$3.5 \leq S < 4.5$	7	$S \geqslant 6.5$

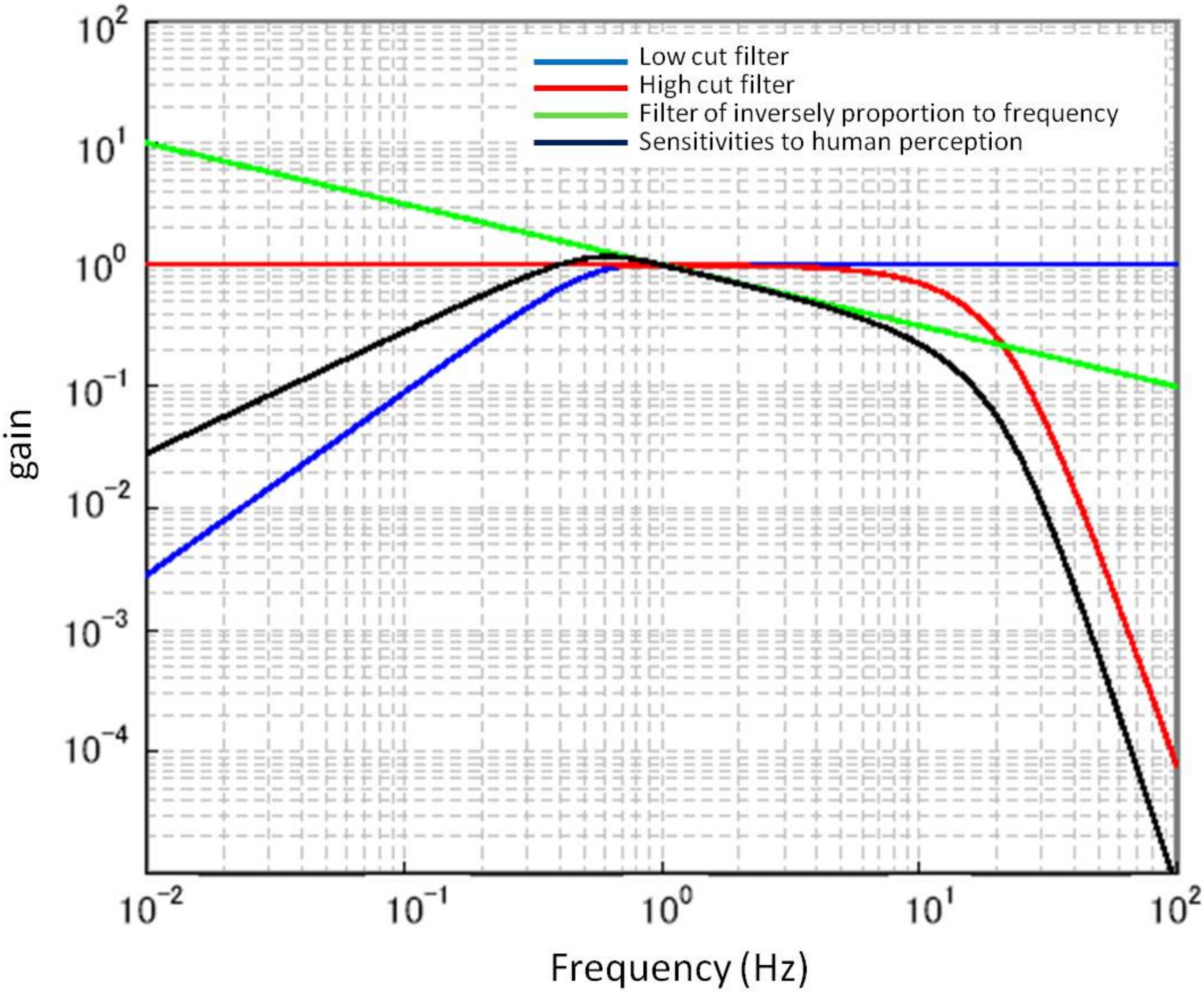

Figure 5.9: *A band-pass filter providing similar sensitivities to human perceptions (black line)*

6

Summary of Seismicity, July - December 2010

The second half of 2010 was less seismically active and less deadly than the first half, though late aftershocks in the Maule and Haiti sequences persisted. A deep cluster of three earthquakes greater than Mw 7.3 within two hours on July 23 and centred about 600 km deep in the Mindanao region, Philippine Islands, were widely felt but without any reported deaths or damage. Similarly, a Mw 7.1 earthquake in August centred about 200 km deep beneath Ecuador was widely felt but with only slight damage reported.

As is usually the case, shallower and much smaller earthquakes were often deadly, with one death in July in southern Iran, three deaths in August in northern Iran, one death in September in southern Iran, one death in October in Pakistan, two deaths in Serbia in November and seven deaths in December in southeastern Iran. In each case there was also considerable damage and numbers of injured. Likewise, considerable damage but without deaths was reported for earthquakes in July in northeastern Iran, in August in the Sichuan region of China, in November in western Iran and in Pakistan, and in December in Ethiopia.

The most deadly event in the second half of 2010 was due to the earthquake in October in the Kepulauan Mentawai region of Indonesia, in which there were at least 445 deaths, 498 injured and 58 missing after the Mw 7.8 earthquake and associated tsunami with a maximum reported height of 7 m. A much smaller tsunami was associated with the Mw 7.3 earthquake in August in the Vanuatu Islands region but it was without any reported deaths, injuries or damage.

The Mw 7.0 Darfield earthquake in September, near the city of Christchurch in New Zealand, was the only other damaging large earthquake in the second half of 2010, but while there were no deaths, and only two reports of serious injuries, there was much damage, including that from landslides and liquefaction. Although the Darfield earthquake initiated an extensive sequence of aftershocks these did not contribute as much to the analysis workload as events in the first half of 2010 had, because here, for example, observations for the US Array fell within the seismic shadow zone.

The number of events in this Bulletin categorised by type are given in Table 6.1.

Figure 6.1 shows the number of moderate and large earthquakes in the second half of 2010. The distribution of the number of earthquakes should follow the Gutenberg-Richter law.

Figures 6.2 to 6.5 show the geographical distribution of moderate and large earthquakes in various magnitude ranges.

The period July to December 2010 produced 12 earthquakes with Mw ≥ 7; these are listed in Table 6.2.

Table 6.1: Summary of events by type between July and December 2010.

damaging earthquake	21
felt earthquake	1843
known earthquake	154341
known chemical explosion	3820
known induced event	2928
known mine explosion	9474
known rockburst	35
suspected earthquake	9550
suspected chemical explosion	82
suspected induced event	9
suspected mine explosion	685
suspected rockburst	209
unknown	100
total	183097

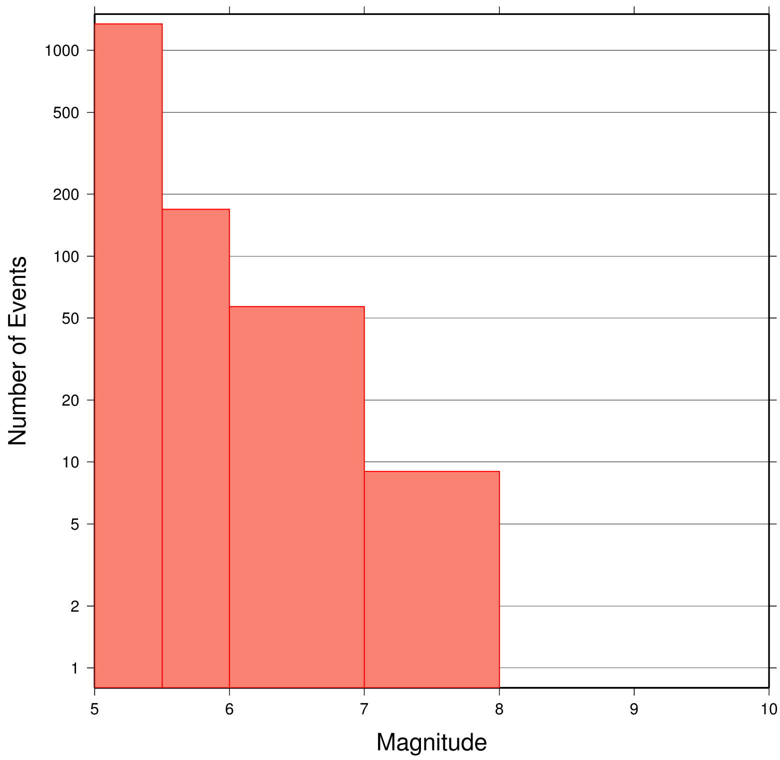

Figure 6.1: *Number of moderate and large earthquakes between July and December 2010. The non-uniform magnitude bias here correspond with the magnitude intervals used in Figures 6.2 to 6.5.*

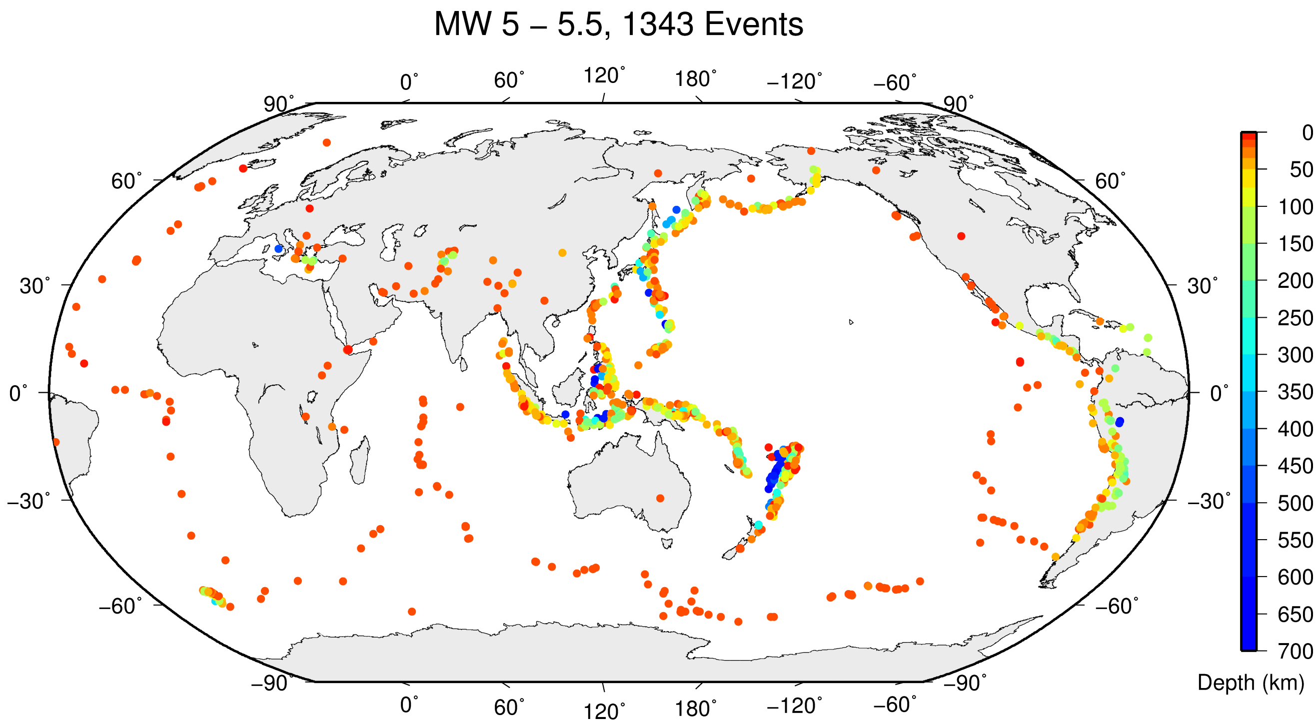

Figure 6.2: Geographic distribution of magnitude 5-5.5 earthquakes between July and December 2010.

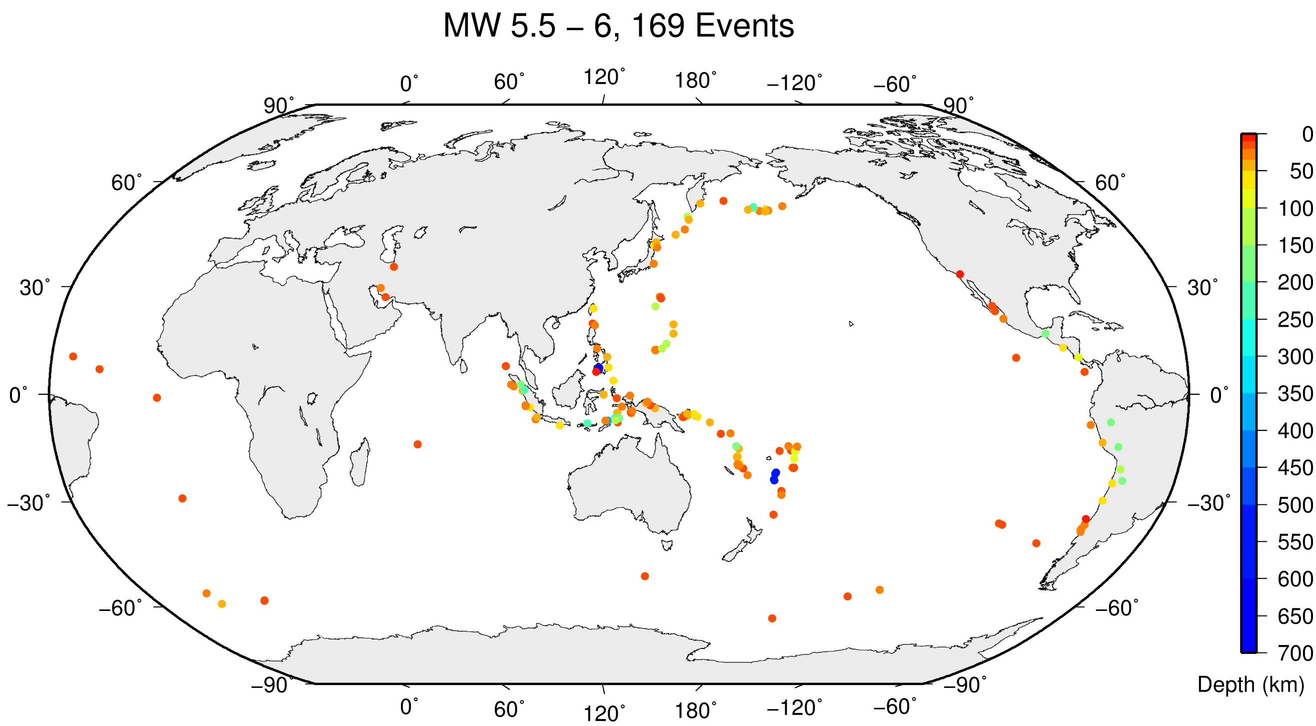

Figure 6.3: Geographic distribution of magnitude 5.5-6 earthquakes between July and December 2010.

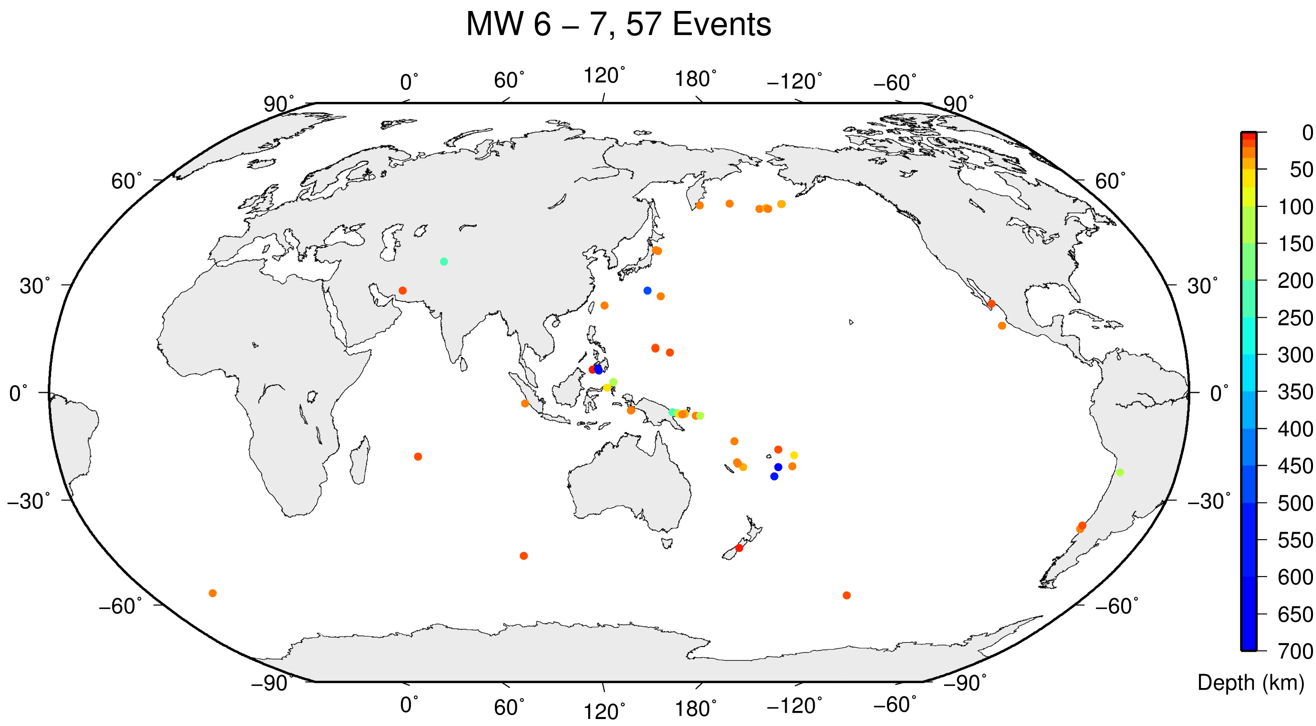

Figure 6.4: *Geographic distribution of magnitude 6-7 earthquakes between July and December 2010.*

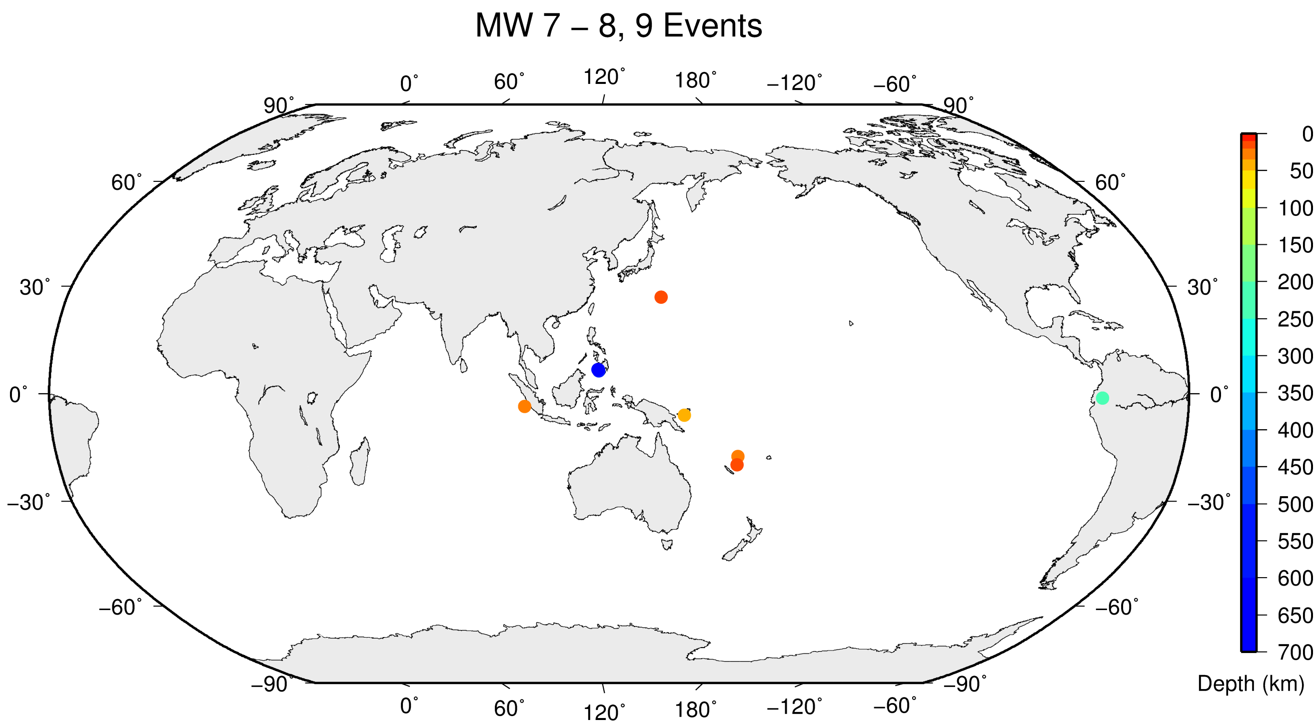

Figure 6.5: *Geographic distribution of magnitude 7-8 earthquakes between July and December 2010.*

Table 6.2: *Summary of the earthquakes of magnitude Mw ≥ 7 between July and December 2010.*

Date	lat	lon	depth	Mw	Flinn-Engdahl Region
2010-10-25 14:42:22	-3.52	100.10	20	7.8	Southern Sumatera
2010-07-23 22:51:13	6.42	123.58	584	7.7	Mindanao
2010-07-23 23:15:09	6.74	123.33	633	7.5	Mindanao
2010-12-21 17:19:41	26.90	143.70	13	7.4	Bonin Islands region
2010-07-18 13:35:00	-6.04	150.66	43	7.4	New Britain region
2010-12-25 13:16:38	-19.84	167.94	15	7.3	Vanuatu Islands region
2010-07-23 22:08:11	6.71	123.49	610	7.3	Mindanao
2010-08-10 05:23:46	-17.53	168.04	33	7.3	Vanuatu Islands
2010-08-12 11:54:15	-1.28	-77.37	206	7.1	Ecuador
2010-09-29 17:11:24	-4.99	133.78	20	7.0	Irian Jaya region
2010-08-04 22:01:43	-5.82	150.77	45	7.0	New Britain region
2010-09-03 16:35:46	-43.36	171.90	4	7.0	South Island

7

Notable event

7.1 The Canterbury, New Zealand Earthquake Sequence I: The M_w 7.1 Darfield Earthquake of 3 September 2010 and Aftershock Sequence

John Ristau
GNS Science
Lower Hutt
New Zealand

7.1.1 Introduction

On 4 September 2010 at 04:35 NZST (3 September 16:35 UTC) the moment magnitude (M_w) 7.1 Darfield earthquake occurred in the Canterbury region of New Zealand, approximately 10 km southeast of the town of Darfield and 40 km west of Christchurch, New Zealand's second largest city with a population of approximately 377 000 (Figure 7.1). The earthquake was widely felt throughout the South Island and the lower North Island, with over 7300 felt reports received, and caused significant damage in Christchurch, with maximum intensity MM 9 in the epicentral region. Extensive liquefaction and lateral spreading contributed significantly to structural damage observed throughout Christchurch. Through a fortunate combination of strict building codes and the earthquake occurring at night, when the streets were largely deserted, there were no deaths and only two serious injuries reported. Most of the damage, including toppled chimneys and parapets, and failure of gables and frames, was confined to unreinforced brick and masonry structures. Modern buildings and light timber frame structures performed well with little structural damage. The Darfield earthquake was the most damaging earthquake in New Zealand since the 3 February 1931 Hawkes Bay earthquake (M_w 7.4 – 7.6).

The Darfield earthquake was recorded (Figure 7.1) by the national GeoNet broadband and strong-motion networks (Petersen *et al.* 2011) and the regional Canterbury CanNet strong-motion network (Avery *et al.* 2004). Of particular interest is the Canterbury network of nearly 40 seismic instruments that provided dense near-field ground-shaking measurements. Immediately following the Darfield earthquake, GNS Science sent teams of technicians to Christchurch and the Canterbury region to install temporary seismometers and accelerometers to better record the aftershocks. In addition, more than 180 low-cost micro-electro-mechanical accelerometers were deployed to a network of volunteer-owned, internet-connected computers as part of the Quake-Catcher Network (QCN) (Lawrence *et al.* 2014; Cochran *et al.* 2011; Cochran *et al.* 2009). As a result the Darfield earthquake sequence is one of the best recorded earthquake sequences anywhere in the world.

New Zealand straddles the boundary of the Pacific and Australian plates, and the Canterbury region,

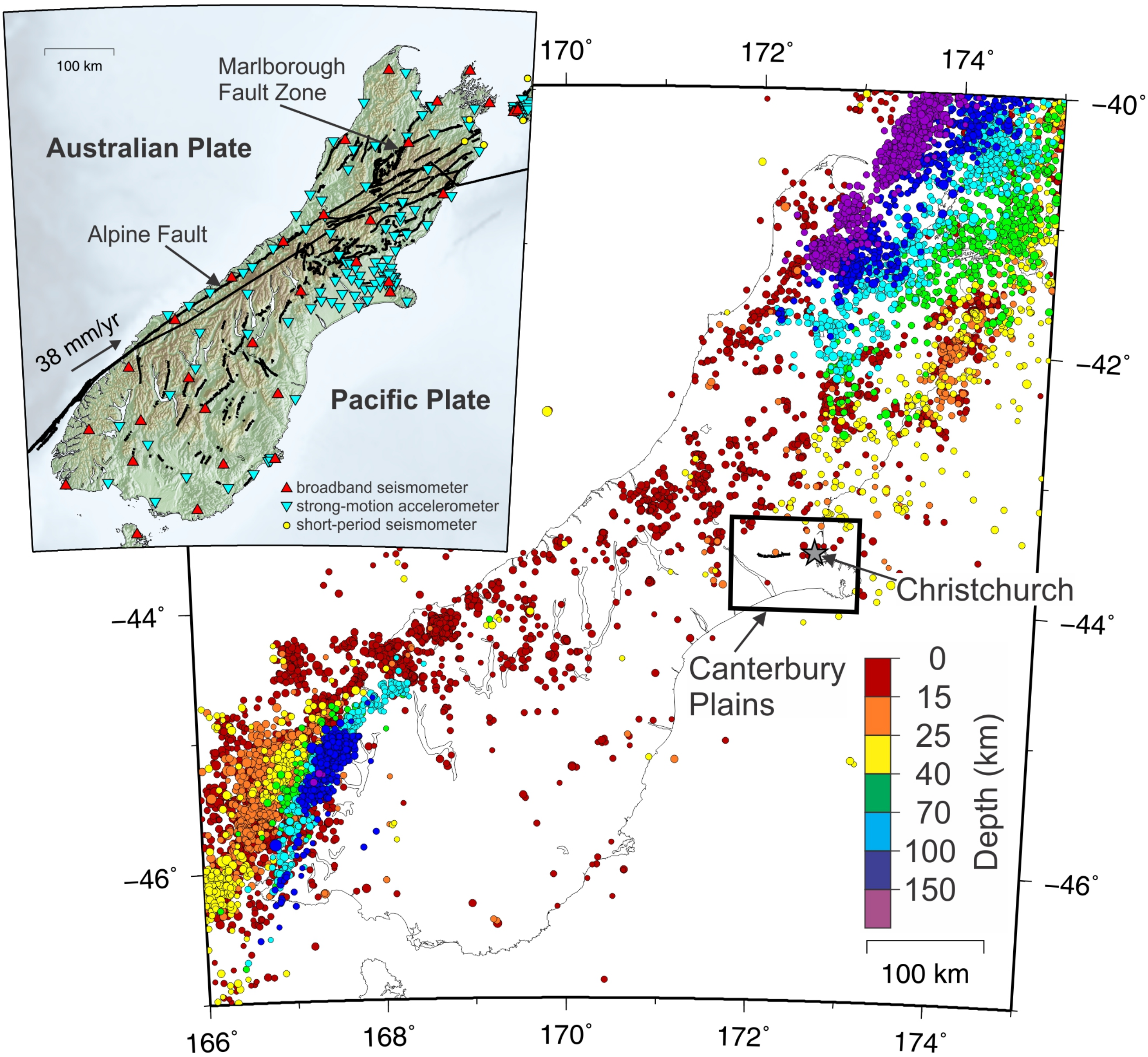

Figure 7.1: *Tectonic setting of the South Island of New Zealand, and recorded seismicity ($M \geq 3$) for the 10-year period until 2 September 2010. Major active faults, including the Alpine Fault and Marlborough Fault Zone, are shown by the black lines. Also shown is the seismograph network of broadband seismometers, strong-motion accelerometers, and short-period seismometers operated by GeoNet. Note the low rate of seismicity in the Canterbury Plains region before September 2010.*

where the earthquake occurred, is a region of continental convergence about 100 km from the Pacific/Australia plate boundary (Figure 7.1). In the South Island, the Alpine Fault runs along the west coast and accommodates the vast majority of the relative plate motion. Palaeoseismic evidence suggests that the Alpine Fault ruptures in major earthquakes ($M > 7.5$) with recurrence intervals of ∽200 – 300 years, with the most recent event in 1717 (e.g. Cooper and Norris 1990; Yetton *et al.* 1998; Rhoades and Van Dissen 2003; Sutherland et al. 2007; Berryman *et al.* 2012). Several $M >$ 6-7 earthquakes have occurred in the foothills of the Southern Alps east of the Alpine Fault and west of Christchurch in the past 150 years. These earthquakes include 1888 North Canterbury M_w 7.1 (Cowan 1991), 1929 Arthur's Pass M_w 7.0 (Doser *et al.* 1999), 1994 Arthur's Pass M_w 6.7 (Abercrombie *et al.* 2000) and 1995 Cass M_w 6.2 (Gledhill *et al.* 2000). There are many mapped active faults in the eastern foothills of the Southern Alps (e.g. Stirling *et al.* 2008); however, no active faults had been previously mapped in the Canterbury plains. Dorn *et al.* (2010) carried out high-resolution reflection seismic studies in the western part of the Canterbury Plains. Unfortunately none of the seismic lines crossed the Greendale Fault. The Darfield earthquake demonstrates that the zone of active deformation in the eastern South Island extends beyond the visible range front.

In this paper I present an overview of the Darfield earthquake and its aftershock sequence before the occurrence of the 21 February (UTC) 2011, M_w 6.2 Christchurch earthquake. I will discuss the source properties of the mainshock, characteristics of the aftershock sequence, and review our current understanding of the sequence including stress studies and aftershock forecasts.

7.1.2 Mainshock Source Properties

Before the Darfield earthquake the Canterbury Plains region had a historically low level of seismic activity compared with many other parts of New Zealand (Figure 7.1). In the mid-2000's Canterbury University and GNS Science established CanNet, a network of strong-motion accelerometers around Christchurch and the Canterbury Plains (Avery *et al.* 2004). CanNet was designed to record a future Alpine Fault earthquake; however, it was ideally positioned to record near-field ground motion and directivity effects from the Darfield earthquake. Several stations were located within a few kilometres of the rupture zone (Figure 7.2a). Supplementary instruments were installed (Figure 7.2b) to better record the aftershocks.

The most obvious physical feature of the Darfield earthquake is a 29.5 km long surface rupture on the previously unknown Greendale Fault (Figure 7.3). The Greendale Fault was buried beneath deposits from the last glacial period 18 000 – 20 000 years ago (Forsyth *et al.* 2008). The fault trace cut across mainly well-cultivated, pastoral farmland, which made it quite visible. Relative movement was predominantly right-lateral strike-slip with an average horizontal displacement of ∽2.5 m, and with maximum displacements of ∽5 m horizontally and 1.5 m vertically (Quigley *et al.* 2010). However, the Darfield earthquake has been shown to be much more complex than a simple strike-slip event, as was similarly shown for the 2010 M_w 7.0 Haiti earthquake (e.g. Hayes *et al.* 2010).

Teleseismic moment tensor solutions calculated by the USGS (http://earthquake.usgs.gov/regional/neic/) and the Global CMT Project (http://www.globalcmt.org/) indicated strike-slip faulting consistent with the surface rupture of the Greendale Fault (Figure 7.2c; Table 7.1). In contrast, the GeoNet regional moment tensor solution and GeoNet first-motion solution indicated reverse faulting on either a shallow

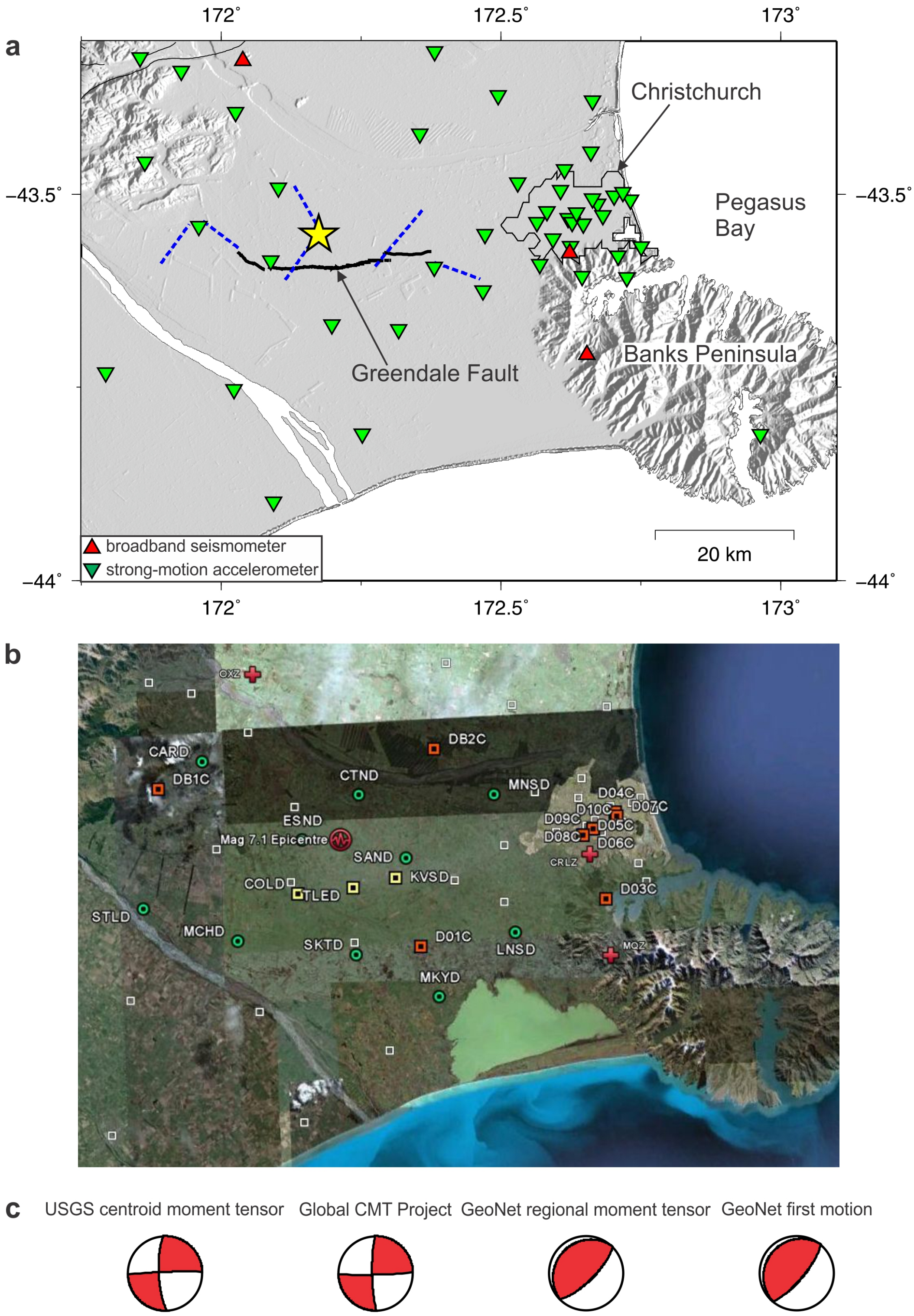

Figure 7.2: *a) Seismograph network in the Canterbury region at the time of the* M_w *7.1 Darfield earthquake (yellow star). Inferred subsurface faults (dashed lines) are those of Beavan et al. (2012), Elliot et al. (2012) and Atzori et al. (2012). Broadband seismometers are indicated by red triangles, and Canterbury University (CanNet) strong-motion accelerometers by inverted green triangles. (b) Temporary short-period seismometer (green circles) and accelerometer (yellow and orange squares) networks installed immediately following the Darfield earthquake. (c) Focal mechanisms for the Darfield earthquake from the USGS centroid moment tensor, Global CMT Project, GeoNet regional moment tensor, and GeoNet first-motion analyses.*

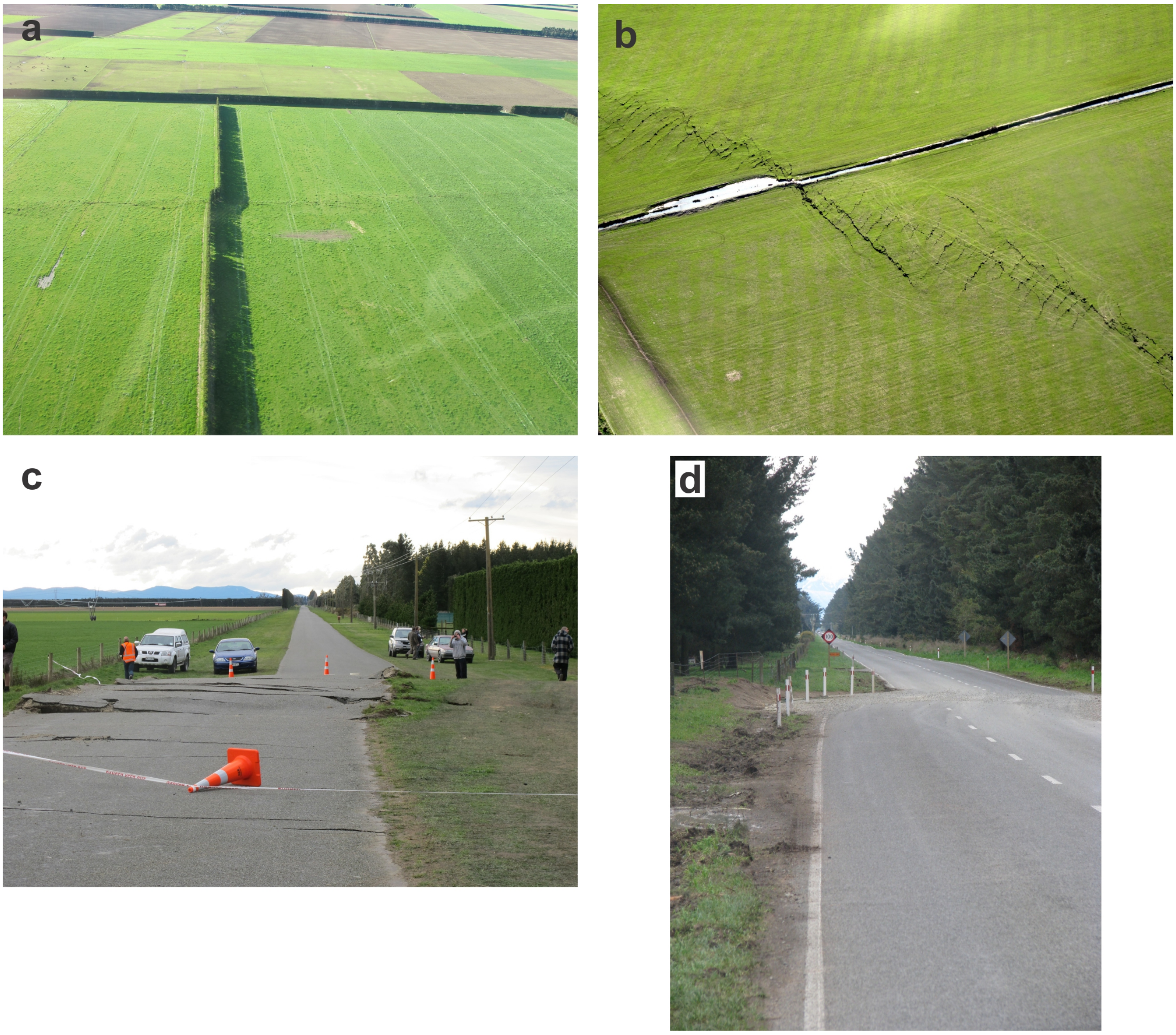

Figure 7.3: *Examples of surface rupture and displacement along the Greendale Fault. (a) Greendale Fault trace, photographer David Barrell, copyright GNS Science/EQC, VML ID 112421. (b) Greendale Fault trace, photographer Richard Jongens, copyright GNS Science/EQC, VML ID 114908. (c) Highfield Road surface rupture and displacement, photographer David Barrell, copyright GNS Science/EQC, VML ID 118544. (d) Road displacement, photographer John Begg, copyright GNS Science/EQC, VML ID 99707.*

NW-dipping plane or a steep SE-dipping plane (Figure 7.2c; Table 7.1). As a result of the high density of strong-motion stations in the vicinity of the mainshock, the hypocentre estimate was well constrained about 4 ± 0.5 km north of the surface trace of the Greendale Fault (Gledhill *et al.* 2011). Due to the well-constrained hypocentre, with an estimated depth of about 11 km, the discrepancy between the hypocentre location and the trace of the Greendale Fault cannot be explained by the location uncertainty. A shallow-dipping fault plane could account for the discrepancy, but there should be near co-incidence of the epicentre with the trace of the Greendale Fault for any near-vertical strike-slip mechanism as indicated in the global moment tensor solutions.

Table 7.1: *Source parameters for the Darfield earthquake.*

Agency/Type	strike/dip/rake	strike/dip/rake	Mo (Nm)	M_w	Depth (km)
USGS centroid moment tensor	268/87/-166	178/77/-3	3.50E+19	7.0	10
Global CMT Project	179/82/3	88/87/172	3.49E+19	7.0	12
GeoNet regional moment tensor	45/73/90	226/17/91	6.10E+19	7.1	8
GeoNet first motion	40/75/90	220/15/90	n/a	n/a	n/a

The teleseismic moment tensor methods may not be able to resolve the distinct mechanisms but instead provide an average over the whole event, which is dominated in this case by slip along the Greendale Fault. The regional moment tensor solution and the first-motion solution used near-source or regional data, making them more sensitive to small-scale features. As a result the GeoNet solutions model the nature of the initial reverse-faulting rupture.

More evidence of a complex rupture comes from strong-motion accelerometer data, which suggest that there were at least three distinct fault ruptures in the sequence (Figure 7.4; Holden and Beavan 2012). The kinematic source model is consistent with an initial rupture on a steeply dipping, blind reverse fault (Charing Cross Fault) with a rupture duration of 3 – 6 s and M_w 6.2. The initial rupture then triggered the Greendale Fault with a rupture duration of 8 – 18 s and a maximum displacement of 5 m at the surface. This Greendale Fault rupture was equivalent to a M_w 6.8 earthquake, making it the largest event of the sequence. After 17 s, a reverse fault at the western end of the Greendale Fault near Hororata was triggered with a M_w 5.7 event. The overall moment release in the kinematic model is equivalent to a M_w 6.9 earthquake.

Geodetic studies of the mainshock using combinations of GPS and InSAR data have been carried out by Beavan *et al.* (2012), Atzori *et al.* (2012) and Elliot *et al.* (2012). All of the geodetic models require multiple fault segments to be active during the earthquake. Beavan *et al.* (2012) used seven individual segments to model the rupture zone (Figure 7.5). The Beavan *et al.* (2012) model requires a steep SE-dipping reverse fault several kilometres north of the Greendale Fault as the initial M_w 6.4 rupture. This is consistent with the hypocentre location, GeoNet focal mechanisms and kinematic results. The M_w 6.8 main rupture was along the Greendale Fault with an average slip of 2.8 m. Several other reverse faulting and strike-slip faulting segments were also active, giving an equivalent M_w 7.1 for the entire sequence. The Elliot *et al.* (2012) and Atzori *et al.* (2012) geodetic models also require multiple ruptures with initial reverse faulting several kilometres to the north of the Greendale Fault.

Peak ground accelerations (PGA) in the Canterbury Plains and Christchurch are shown in Figure 7.6. The largest recorded PGA's were $>$ 1.2 g near the Greendale Fault and to the east of the Greendale

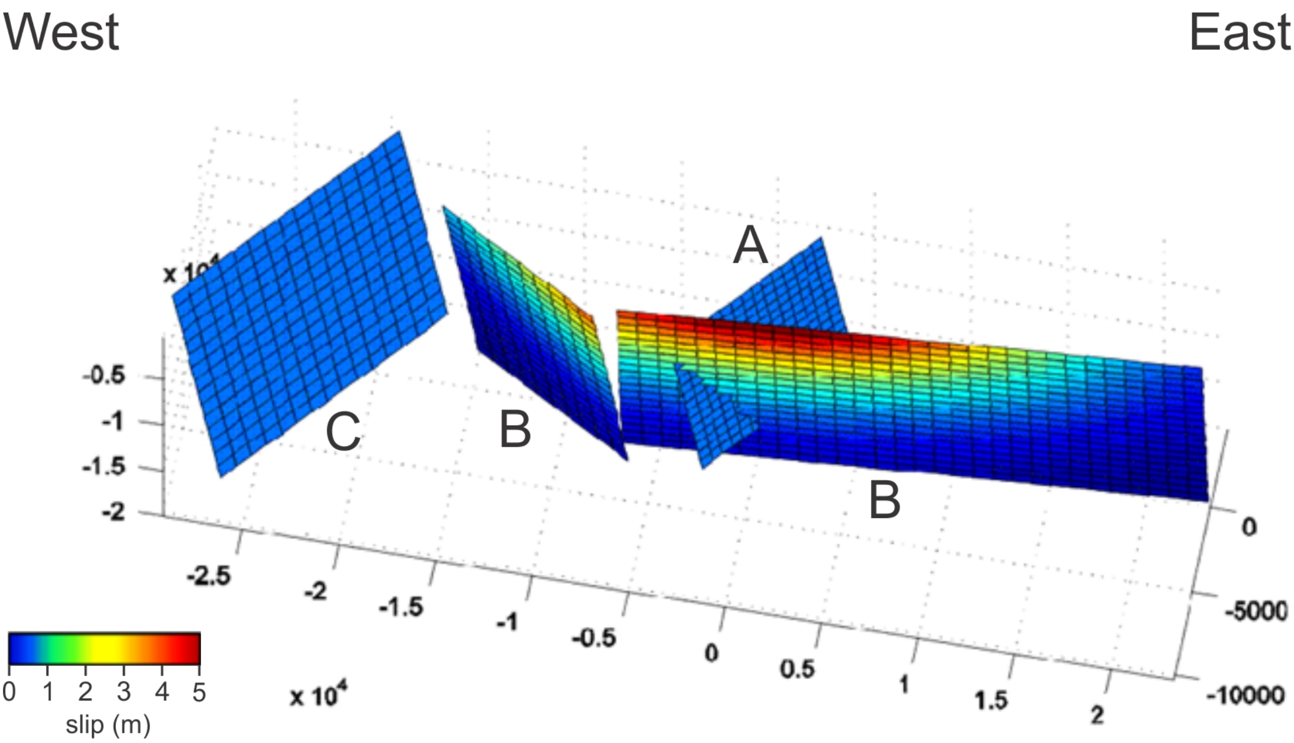

Figure 7.4: *Kinematic source model of the Darfield earthquake showing three distinct fault ruptures. A is the Charing Cross reverse fault where the rupture initiated; B is the Greendale Fault; and C is the reverse fault at the western end of the rupture zone.*

Fault. In Christchurch the observed PGA's were lower, typically ∽0.2 – 0.3 g, although some large horizontal PGA's were recorded SE of the city centre (Figure 7.6). These ground motions were sufficient to generate extensive regions of liquefaction in many areas of Christchurch.

The crustal structure in the Canterbury region is dominated by the Hikurangi Plateau – a large igneous province that was subducted ∽100 million years ago. The Hikurangi Plateau is extremely strong and remains attached to the crust, capped by schist and greywackes containing east-west Cretaceous faults (Reyners *et al.* 2013). As a result of the strength of the crust, the radiated energy (E_S) and apparent stress (τ_a) for the Darfield earthquake were very large. The apparent stress is defined as the product of the rigidity and the E_S per unit moment, which means the apparent stress is greater with stronger crust and larger E_S. Fry and Gerstenberger (2011) calculated τ_a of ∽16 MPa for Darfield, which is significantly greater than global averages for τ_a (e.g. Choy *et al.* 2001; Atkinson and Boore 2006)

The Darfield earthquake involved reactivation of east-west Cretaceous faults that are favourably oriented in the regional stress field. In the region of the Greendale Fault, Reyners *et al.* (2013) found unusually low P- to S-wave velocity ratios of 1.60 compared to 1.71 before the Darfield earthquake. Reyners *et al.* (2013) interpreted this reduced velocity ratio as the signature that the greywackes had been weakened by the rupture front producing widespread cracking around the fault zone. Sibson *et al.* (2011) concluded that the fault system appears to be controlled by the orientation of the tectonic stress field in the upper crust rather than conforming to local plate boundary kinematics. Furthermore, based on anisotropic seismic tomography, Fry *et al.* (2014) suggest that the crust underlying the Canterbury Plains is dominated by faulting parallel to the Greendale Fault. Therefore, the Darfield earthquake can be regarded as an intraplate event, remote from the main Alpine-Marlborough fault system that defines

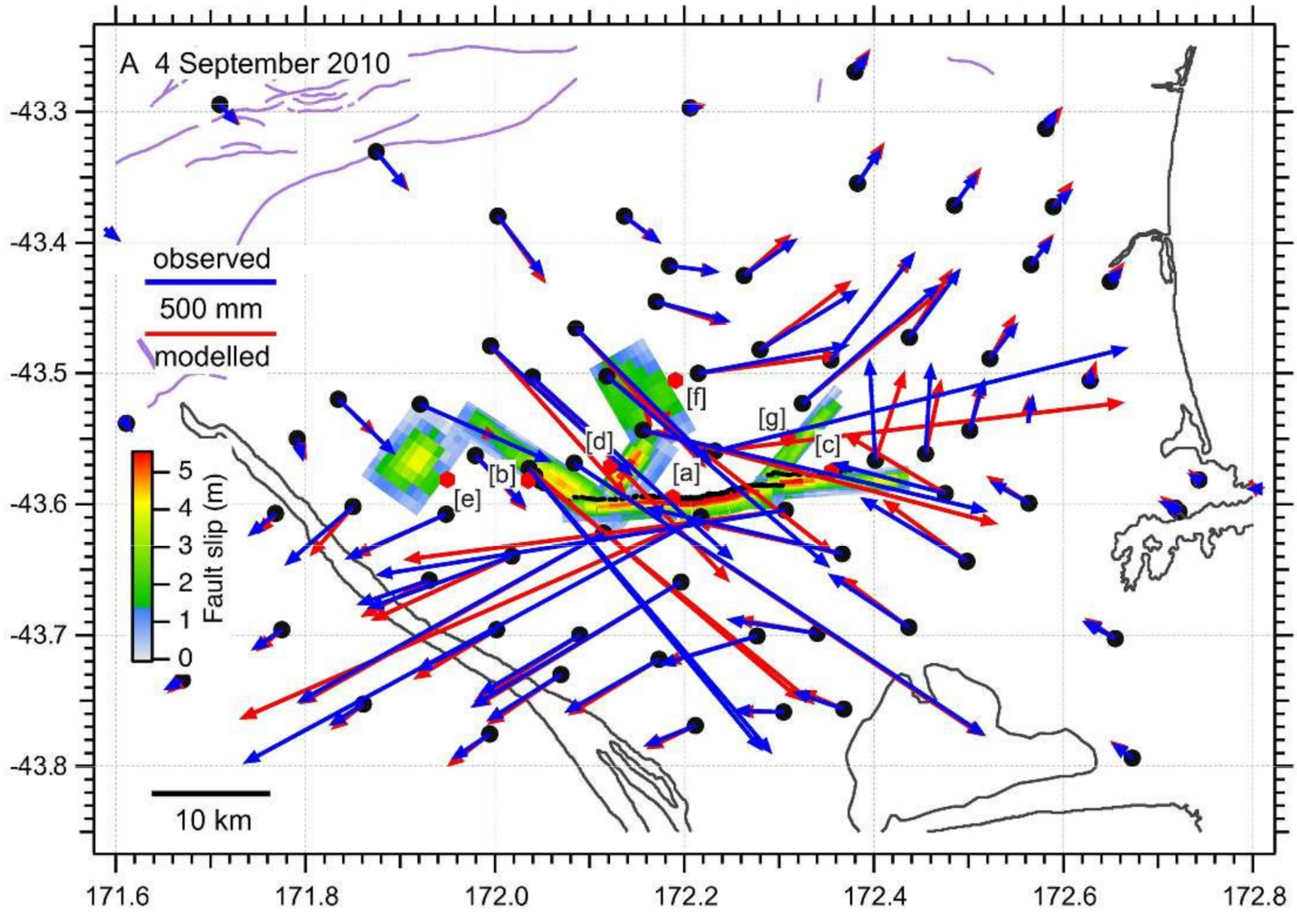

Figure 7.5: *Observed (blue) and modelled (red) displacements at GPS sites, and the slip model derived from GPS and DInSAR for the Darfield earthquake. Red dots with adjacent letters in square brackets (e.g. [a]) are located where the centres of the fault segments would outcrop if extended to the surface (from Beavan et al. 2012).*

the Pacific/Australian plate boundary.

7.1.3 Aftershock Sequence

A well-recorded aftershock sequence followed the Darfield earthquake with over 5000 located events with $M_L \geq 1.7$, and 15 with $M_L \geq 5.0$, in the period from 3 September 2010 – 21 February 2011 (Figure 7.7a). More than 4000 of the aftershocks were relocated using a double-difference tomography method (Bannister *et al.* 2011). The resulting aftershock distribution shows a NNW-SSE oriented trend of aftershocks off the main alignment, consistent with the initial rupture being located to the north of the Greendale Fault. Another cluster of aftershocks is present at the western end of the rupture zone, corresponding to one of the fault segments in the geodetic model. There is also a NE-SW line of aftershocks from the eastern end of the fault zone leading into Christchurch.

Focal mechanisms from 153 regional moment tensor solutions show a variety of faulting styles, providing additional evidence for the complex nature of the rupture process (Figure 7.7b). The initial rupture was a reverse faulting mechanism as discussed earlier. Other focal mechanisms in the immediate area of the initial rupture are for a mixture of reverse and strike-slip faulting. At the western end of the fault

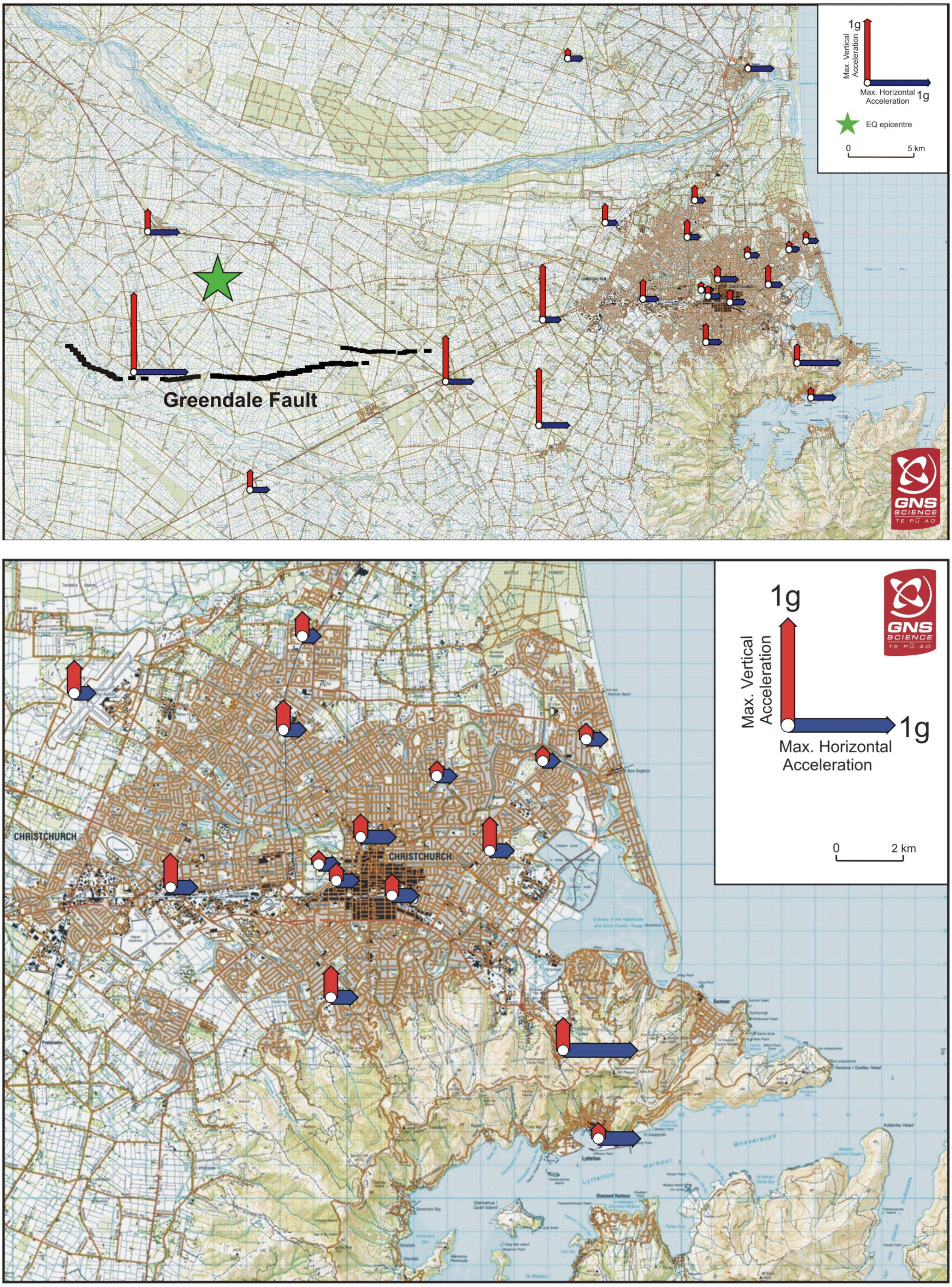

Figure 7.6: *Peak ground accelerations from the Darfield earthquake in the Canterbury Plains and Christchurch. The largest observed PGA's were greater than 1.2 g near the Greendale Fault (black line). In Christchurch PGA's were typically ∽0.2 – 0.3 g, although some larger horizontal accelerations were recorded SE of the city.*

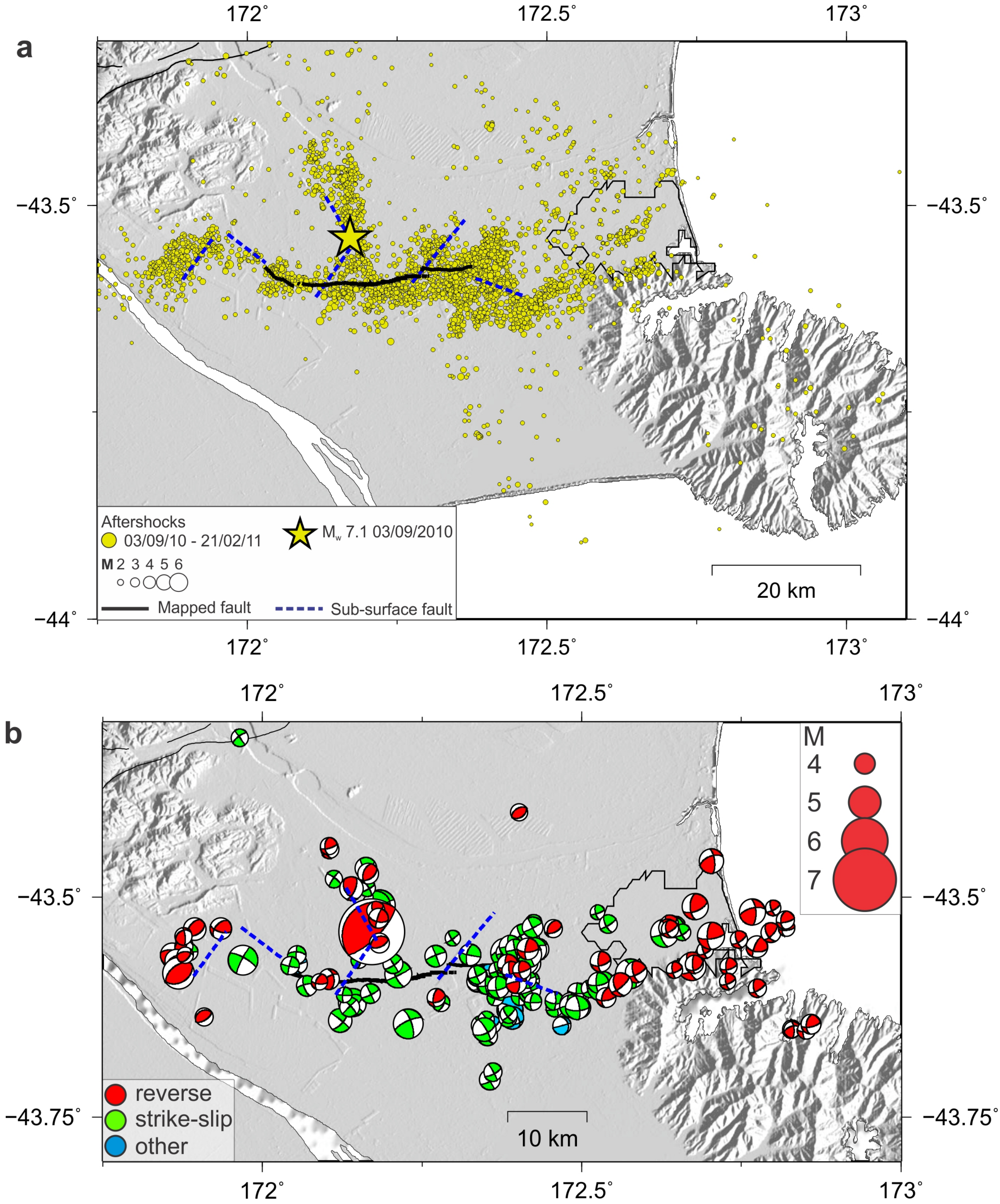

Figure 7.7: *(a) Relocated aftershocks for the period 3 September 2010 – 21 February 2011. The solid black line is the Greendale Fault and the dashed blue lines are inferred subsurface faults. (b) Focal mechanisms derived from 153 regional moment tensor solutions for the period 3 September 2010 – 21 February 2011. Strike-slip faulting is dominant along the Greendale Fault. The focal mechanisms are for predominantly reverse faulting at the western end of the rupture zone and around Christchurch.*

zone the mechanisms are predominantly for reverse faulting, consistent with the geodetic model of the main rupture, which includes a reverse faulting segment at the western end of the rupture zone. East of the main rupture zone, leading into Christchurch, focal mechanisms are mainly for reverse faulting or oblique-reverse faulting.

The aftershock locations mostly coincide with the Greendale Fault trace and the location of inferred subsurface faults (Figure 7.7a,b). However, at the eastern end of the Greendale Fault there is a NE-SW trend of aftershocks that are not associated with any known subsurface fault, and this is particularly noticeable in the plot of focal mechanisms (Figure 7.7b). There is also a NE-SW trend of aftershocks between the Greendale Fault and Christchurch that is also not associated with any known subsurface fault, and in this region the focal mechanisms change from mainly strike-slip faulting in the west to oblique-reverse faulting closer to Christchurch.

On 26 December 2010 NZST (25 December 2010 UTC) a cluster of very shallow aftershocks occurred near the Christchurch city centre. The largest, M_w 4.7, occurred at 12:30 NZST when the city centre was highly populated (Ristau 2011). These aftershocks were widely felt and the M_w 4.7 event caused damage to brick and masonry structures already weakened in the city centre. Three moment tensor solutions were calculated for events in this series of aftershocks, all with strike-slip mechanisms. Ristau (2011) also calculated 16 first-motion focal mechanisms for events in this series, including the three events for which moment tensor solutions had been calculated, and although the first-motion mechanisms were for mainly reverse faulting, the P-axis orientation is consistent with those in the moment tensor solutions.

7.1.4 Stress Studies and Aftershock Forecasts

Steacy *et al.* (2014) studied stress triggering during the Canterbury earthquake sequence by comparing maps of Coulomb stress changes with the location of future events. They investigated whether later large aftershocks were consistent with stress triggering, and whether a simple stress map produced shortly after the Darfield earthquake would have accurately indicated the regions where subsequent activity occurred. Steacy *et al.* (2014) found that all aftershocks with $M > 5.5$ occurred in positive stress areas computed using a slip model for Darfield that was available within 10 days of its occurrence. They also found a stress increase of up to 0.24 MPa on the Porter's Pass fault – an active fault ∽80 km NW of Christchurch capable of generating a M_w 7.5 earthquake. Figure 7.8 shows modelled principal stress ($\sigma 1$) deflections in the region of the Darfield rupture zone, with the thick red line indicating the compressional direction of the regional stress field (S. Ellis, pers. comm.). Along the Greendale Fault $\sigma 1$ is rotated up to 15° counterclockwise, while at the eastern end of the rupture zone and north of the Greendale Fault $\sigma 1$ is rotated up to 15° clockwise.

During the Canterbury earthquake sequence GNS Science provided regular aftershock probability forecasts (e.g. Gerstenberger *et al.* 2014). As the sequence progressed the forecasts varied between daily, weekly and monthly forecasts as required. Figure 7.9 and Table 7.2 show various forecasts for M 4.0 – 4.9 and $M \geq 5.0$. During the first day the observed number of aftershocks in the M 4.0 – 4.9 and $M \geq$ 5.0 ranges were higher than the model predicted. After the first day the observed number of aftershocks fell within the ranges predicted by the models.

Table 7.3 shows 1-week, 1-month and 1-year aftershock probabilities calculated on 13 October 2010 for M

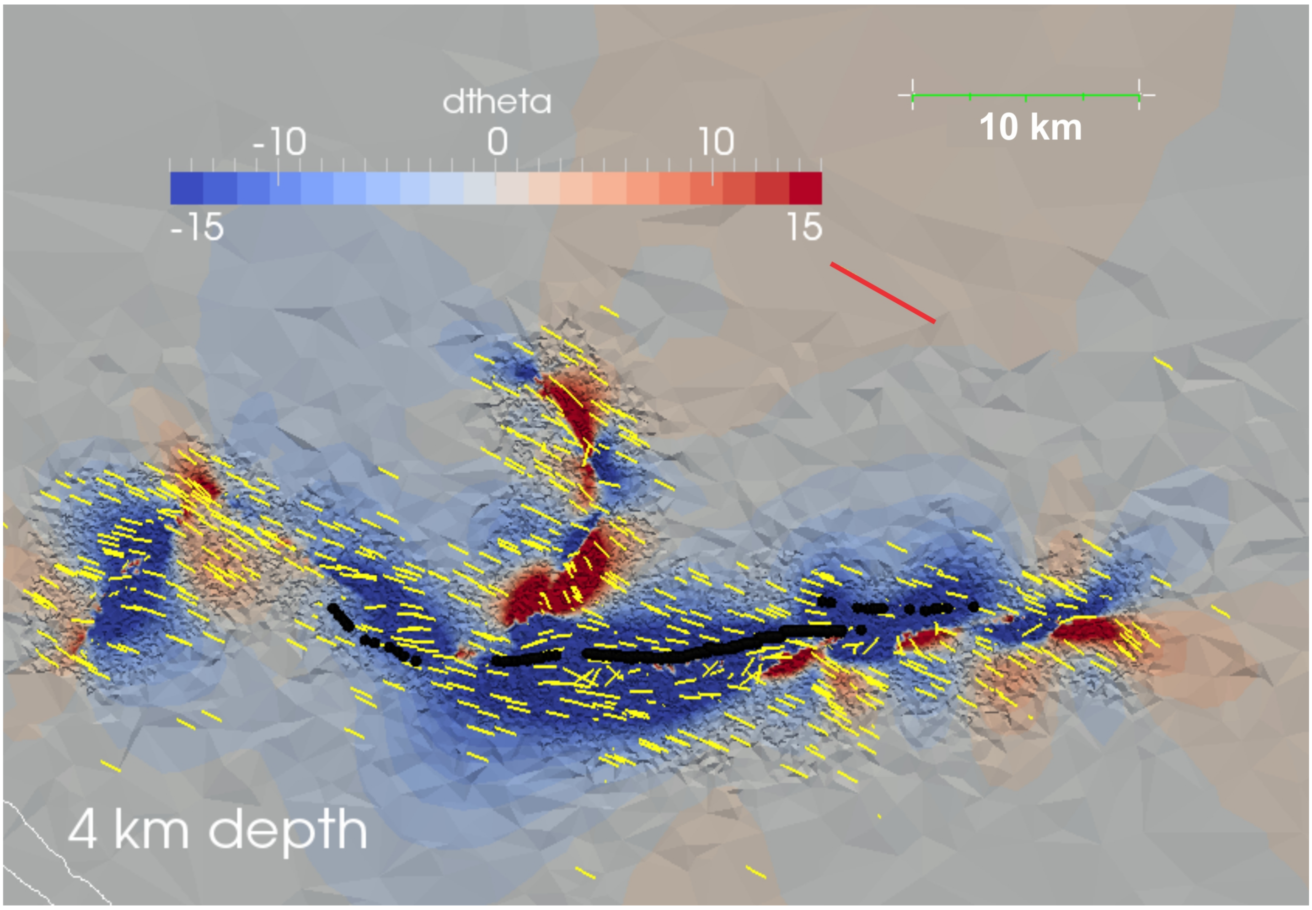

Figure 7.8: *Principal stress (σ1) deflections in the region of the Darfield rupture zone. The thick red line is the compressive direction of the regional stress field, dtheta is the contoured change in degrees from the regional stress field, and the yellow lines are the calculated values. Along the Greendale fault there is a counterclockwise rotation in σ1 with respect to the regional stress field. At the eastern end of the rupture zone and north of the Greendale fault there is a clockwise rotation of σ1.*

Table 7.2: *Expected and observed numbers of aftershocks.*

Date (NZST)	Expected number of aftershocks M 4.0 - 4.9	Observed	Expected number of aftershocks $M >= 5.0$	Observed
4 September 2010 - M_w 7.1	43 - 73	114	2 - 12	18
5 September 2010	11 - 29	19	0 - 5	1
6 - 12 September 2010	28 - 53	37	1 - 9	4
13 - 19 September 2010	8 - 23	20	0 - 5	0
20 - 26 September 2010	4 - 16	9	0 - 3	0
27 September - 3 October 2010	2 - 13	3	0 - 3	0
4 - 31 October 2010	10 - 26	15	0 - 4	3
1 - 28 November 2010	5 - 17	11	0 - 4	0
29 November - 26 December 2010	3 - 13	3	0 - 3	0
27 December 2010 - 23 January 2011	2 - 11	7	0 - 3	1
24 January - 20 February 2011	1 - 9	5	0 - 2	0
21 - 22 February 2011	0 - 2	0	0 - 1	1

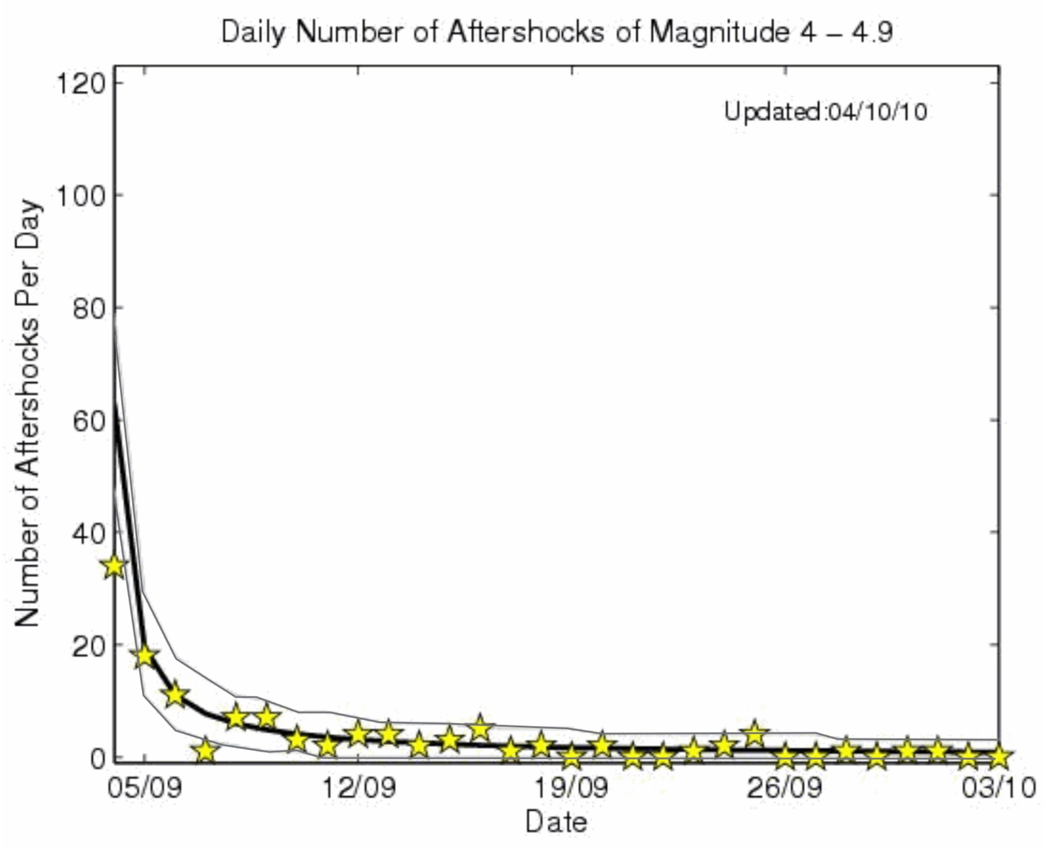

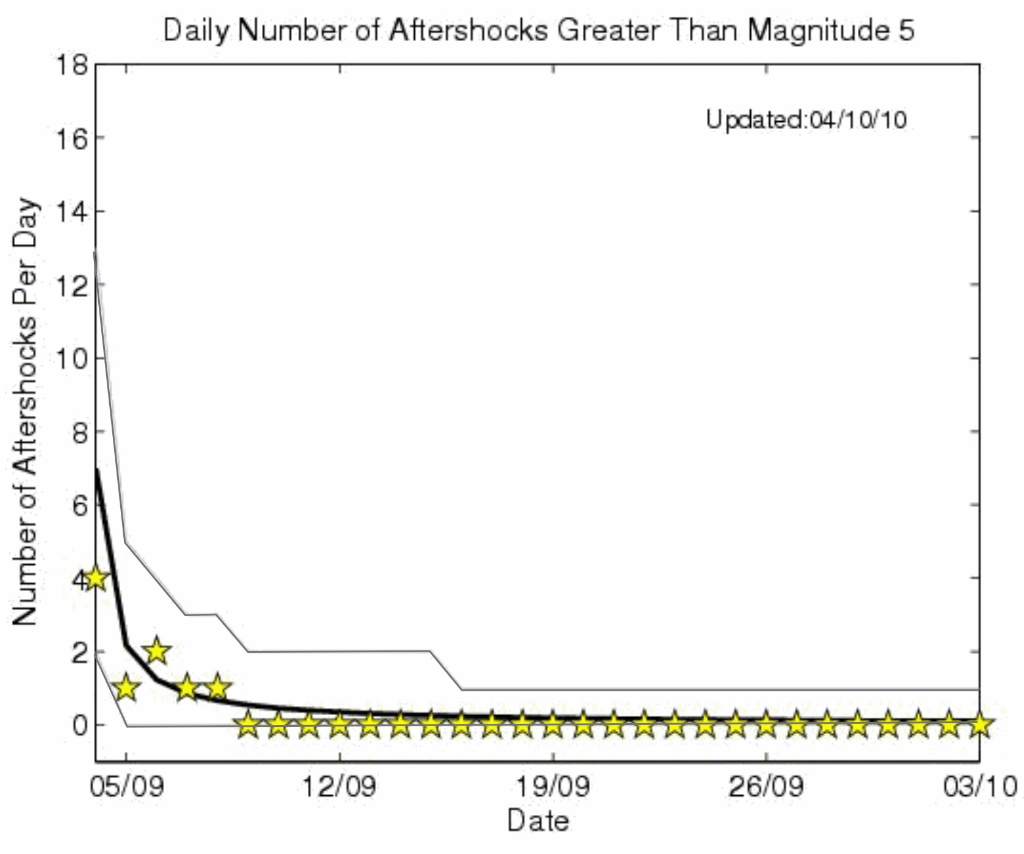

Figure 7.9: *Aftershock probability forecasts for M 4.0 – 4.9 (top) and M $\geq$ 5.0. The black line is the number of aftershocks predicted by the model, grey lines are the confidence limits, and the yellow stars are the observed number of aftershocks. The number of aftershocks predicted by the model fits well with the observed number of aftershocks.*

5.0 – 5.9, M 6.0 – 6.9 and M 7.0+, valid for the entire Canterbury Plains region, including Christchurch. It is important to note that these probabilities were calculated using an incomplete catalogue as only about half the aftershocks had been located at the time, including only about one-half to one-third of those of $M \geq 5$ (A. Christophersen, pers. comm.). Table 7.3 gives a probability 28 – 46% for a M 6.0 – 6.9 aftershock within one year. By 27 January 2011 the one-year probability of a M 6.0 – 6.9 aftershock had dropped by about half to 15 – 28%, and the one-month probability was 2.6 – 4.8%. At this point a 21 February 2011 (UTC) M_w 6.2 Christchurch earthquake could be seen as a lower probability event, although the computed probabilities may have been significantly higher with a more complete dataset.

Table 7.3: *Aftershock probabilities for given magnitude ranges.*

Date	M 5.0 - 5.9			M 6.0 - 6.9			M 7.0+		
	1-week	1-month	1-year	1-week	1-month	1-year	1-week	1-month	1-year
13 Oct 2010	19-35%	51-81%	93-100%	2.5-4.2%	8-14%	28-46%	0.4-0.5%	1.2-1.7%	4.6-6.6%
27 Jan 2011	19-39%	74-96%	74-96%	0.7-1.2%	2.6-4.8%	15-28%	0.09-0.14%	0.37-0.55%	2.3-3.6%

7.1.5 Discussion

In this paper I have summarised some of the major findings from the M_w 7.1 Darfield earthquake and its aftershock sequence. The evidence has shown that the Darfield earthquake initiated several kilometres north of the Greendale Fault and the rupture involved multiple fault segments. Geodetic and kinematic studies have shown that the Darfield sequence began as a steeply dipping reverse-faulting event, continued by triggering the Greendale Fault as a right-lateral strike-slip event that accommodated the majority of the moment release, and also involved several other reverse faulting events at either end of the Greendale Fault.

The located aftershocks show a NNW-SSE oriented trend off the main alignment, consistent with the hypocentre being located north of the Greendale Fault. Regional moment tensor solutions indicate the complexity of the rupture zone, with mainly strike-slip faulting in the vicinity of the Greendale Fault, and with reverse faulting dominant at the western and eastern ends of the Greendale Fault and through to Christchurch.

Stress modelling using a model available within 10 days of the mainshock showed that all the $M > 5.5$ aftershocks occurred in areas of increased stress. Aftershock probability forecasts accurately modelled the number of M 4.0 – 4.9 and $M \geq 5.0$ aftershocks from 3 September 2010 – 21 February 2011. Early in the aftershock sequence (13 October 2011) the one-year probability of a M 6.0 – 6.9 aftershock was 28 – 46%, and on 27 January 2011 it was 15 – 28%. Typically there should have been a large aftershock about one magnitude unit less than that for the mainshock, but none such had occurred early in the sequence.

7.1.6 Conclusions

The M_w 7.1 Darfield earthquake was the most damaging earthquake in New Zealand since the 3 February 1931 Hawkes Bay earthquake (M_w 7.4 – 7.6). As a result of the network of strong-motion instruments operating in the Canterbury Plains and Christchurch before the mainshock, the Darfield earthquake is one of the best recorded major earthquakes anywhere in the world. The near-field strong-motion dataset will be invaluable to future seismic hazard and engineering studies in New Zealand and elsewhere. The complexity of the main rupture further supports the idea that major earthquakes involve multiple rupture segments such as observed for the 2010 Haiti M_w 7.0 (Hayes *et al.* 2010), 2008 Wenchuan M_w 7.9 (Zhang and Ge 2010) and 2002 Denali M_w 7.9 (Eberhart-Phillips *et al.* 2003) events. On 21 February 2011 (UTC) a M_w 6.2 aftershock occurred beneath the outer suburbs of Christchurch and resulted in 185 fatalities and widespread building damage.

7.1.7 Acknowledgements

This paper would not have been possible without many valuable discussions and much input from Stephen Bannister, John Beavan, Anne-Marie Christophersen, Susan Ellis, Bill Fry, Matt Gerstenberger, Caroline Holden, Anna Kaiser, Martin Reyners, Rick Sibson, Sandy Steacy and Charles Williams. Many of the figures were created using Generic Mapping Tools (GMT) (Wessel and Smith 1991). Photographic images are reproduced with the kind permission of GNS Science/EQC.

7.1.8 References

Abercrombie, R.E., T.H. Webb, R. Robinson, P.G. McGinty, J. Mori, and R.J. Beavan (2000). The enigma of the Arthur's Pass, New Zealand earthquake 1. Reconciling a variety of data for an unusual earthquake sequence. *Journal of Geophysical Research* 105, 16119-16137.

Atkinson, G.M., and D.M. Boore (2006). Earthquake ground-motion prediction equations for eastern North America. *Bulletin of the Seismological Society of America* 96, 2181-2205.

Atzori, S., C. Tolomei, A. Antonioli, J. Merryman, S. Bannister, E. Trasatti, P. Pasquiali, and S. Salvi (2012). The 2010-2011 Canterbury, New Zealand, seismic sequence: multiple source analysis from InSAR data and modelling. *Journal of Geophysical Research* 117, B08305, doi:10.1029/2012JB009178.

Avery, H.R., J.B. Berrill, P.F. Coursey, B.L. Deam, M.B. Dewe, C.C. Francois, J.R. Pettinga, and M.D. Yetton (2004). The Canterbury University strong-motion recording project. Proceedings of 13th World Conference on Earthquake Engineering, Vancouver, British Columbia, 1-6 August 2004. *Canadian Association for Earthquake Engineering* paper no. 1335.

Bannister, S., B. Fry, M. Reyners, J. Ristau, and H. Zhang (2011). Fine-scale relocation of aftershocks of the 22 February M_w 6.2 Christchurch earthquake using double-difference tomography. *Seismological Research Letters* 82, 839-845, doi:10.1785/gssrl.82.6.839.

Beavan, J., M. Motagh, E. Fielding, N. Donnelly, and D. Collett (2012). Fault slip models of the 2010-2011 Canterbury, New Zealand, earthquakes from geodetic data, and observations of post-seismic ground deformation. *New Zealand Journal of Geology and Geophysics* 55, 207-221, doi:10.1080/00288306.2012.697472.

Berryman, K.R., U.A. Cochran, K.J. Clark, G.P. Biasi, R.M. Langridge, and P. Villamor (2012). Major earthquakes occur regularly on an isolated plate boundary. *Science* 336, 1690-1693, doi:10.1126/science.1218959.

Choy, G.L., J.L. Boatwright, and S. Kirby (2001). The radiated seismic energy and apparent stress of interplate and intraplate earthquakes at subduction zone environments: implications for seismic hazard estimate. *USGS Open-File Report* 01-005, 10 p.

Cochran, E.S., J.F. Lawrence, C. Christensen, and R.S. Jakka (2009). The Quake-Catcher Network: citizen science expanding seismic horizons. *Seismological Research Letters* 80, 26-30.

Cochran, E.S., J.F. Lawrence, A. Kaiser, B. Fry, A.I. Chung and C. Christensen (2011). Comparison between low-cost and traditional MEMS accelerometers: a case study from the M 7.1 Darfield, New Zealand, aftershock deployment. *Annals of Geophysics* 54, 728-737, doi:10.4401/ag-5268.

Cooper, A.F., and R.J. Norris (1990). Estimates for timing of the last coseismic displacement on the Alpine fault, northern Fiordland, New Zealand. *New Zealand Journal of Geology and Geophysics* 33, 309-307.

Cowan, H.A. (1991). The North Canterbury earthquake of September 1, 1888. *Bulletin of the New Zealand Society for Earthquake Engineering* 43, 222-227.

Dorn, C., A.G. Green, R. Jongens, S. Carpentier, A.E. Kaiser, F. Campbell, H. Horstmeyer, J. Campbell, M. Finnemore, and J. Pettinga (2010). High-resolution seismic images of potentially seismogenic structures beneath the northwest Canterbury Plains, New Zealand. *Journal of Geophysical Research* 115, B11303, doi:10.1029/2010JB007459.

Doser, D.I., T.H. Webb, and D.E. Maunder (1999). Source parameters of large historical (1918-1962) earthquakes, South Island, New Zealand. *Geophysical Journal International* 139, 769-794.

Eberhart-Phillips, D., P.J. Haeussler, J.T. Freymueller, A.D. Frankel, C.M. Rubin, P. Craw, N.A. Ratchkovski, G. Anderson, G.A. Carver, A.J. Crone, T.E. Dawson, H. Fletcher, R. Hansen, E.L. Harp, R.A. Harris, D.P. Hill, S. Hreinsdottir, R.W. Jibson, L.M. Jones, R. Kayen, D.K. Keefer, C.F. Larsen, S.C. Moran, S.F. Personius, G. Plafker, B. Sherrod, K. Sieh, N. Sitar, and W.K. Wallace (2003). The 2002 Denali fault earthquake, Alaska: a large magnitude slip-partitioned event. *Science* 300, 1113-1118.

Elliot, J.R., E.K. Neissen, P.C. England, J.A. Jackson, S. Lamb, Z. Li, M. Oehlers, and B. Parsons (2012). Slip in the 2010-2011 Canterbury earthquakes, New Zealand. *Journal of Geophysical Research* 117, B03401,doi:10.1029/02011jb008868.

Forsyth, P.J., D.J.A. Barrell, and R. Jongens (2008). Geology of the Christchurch Area. Institute of Geological and Nuclear Sciences 1:250 000 geological map 16, 1 sheet + 67 pp. Lower Hutt, NZ: GNS Science.

Fry, B., and M.C. Gerstenberger (2011). Large apparent stresses from the Canterbury earthquakes of 2010 and 2011. *Seismological Research Letters* 82, 833-838, doi:10.1785/gssrl.82.6.833.

Fry, B., F.J. Davey, D. Eberhart-Phillips, and S. Lebedev (2014). Depth variable crustal anisotropy, patterns of crustal weakness, and destructive earthquakes in Canterbury, New Zealand. *Earth and Planetary Science Letters* 392, 50-57, doi:10.1016/j.epsl.2014.02.013.

Gerstenberger, M., G. McVerry, D Rhoades, and M. Stirling (2014). Seismic hazard modelling for the recovery of Christchurch, New Zealand. *Earthquake Spectra* doi:10.1193/021913EQS037M.

Gledhill, K., R., Robinson, R. Abercrombie, T. Webb, J. Beavan, J. Cousins, and D. Eberhart-Phillips (2000). The M_w 6.2 Cass, New Zealand earthquake of 24 November 1995: reverse faulting in a strike-slip regime. *New Zealand Journal of Geology and Geophysics* 43, 255-269.

Gledhill, K., J. Ristau, M. Reyners, B. Fry, and C. Holden (2011). The Darfield (Canterbury, New Zealand) M_w 7.1 earthquake of September 2010: a preliminary seismological report. *Seismological Research Letters* 82, 378-386, doi:10.1785/gssrl.82.3.378.

Hayes, G.P., R.W. Briggs, A. Sladen, E.J. Fielding, C. Prentice, K. Hudnut, P. Mann, F.W. Taylor, A.J. Crone, R. Gold, T. Ito, and M. Simons (2010). Complex rupture during the 12 January 2010 Haiti earthquake. *Nature Geoscience* 3, 800-805, doi:10.1038/NGEO977.

Holden, C., and J. Beavan (2012). Kinematic source studies of the ongoing (2010-2011) sequence of recent large earthquakes in Canterbury. Paper 061 (8 p) *in* Implementing lessons learnt: 2012 Conference, 13-15 April, Christchurch, New Zealand, Christchurch: New Zealand Society for Earthquake Engineering.

Lawrence, J.F., E.S. Cochran, A. Chung, A. Kaiser, C.M. Christensen, R. Allen, J.W. Baker, B. Fry, T. Heaton, D. Kilb, M.D. Kohler and M. Taufer (2014). Rapid earthquake characterization using MEMS accelerometers and volunteer hosts following the M 7.2 Darfield, New Zealand, earthquake. *Bulletin of the Seismological Society of America* 104, 184-192, doi:10.1785/0120120196.

Petersen, T., K. Gledhill, M. Chadwick, N. Gale, and J. Ristau (2011). The New Zealand national seismograph network. *Seismological Research Letters* 82, 9-20, doi:10.1785/gssrl.82.1.9.

Quigley, M., R. Van Dissen, P. Villamor, N. Litchfield, D. Barrell, K. Furlong, T. Stahl, B. Duffy, E. Bilderback, D. Noble, D. Townsend, J. Begg, R. Jongens, W. Ries, J. Claridge, A. Klahn, H. Mackenzie, A. Smith, S. Hornblow, R. Nicol, S. Cox, R. Langridge, and K. Pedley (2010). Surface rupture of the Greendale fault during the M_w 7.1 Darfield (Canterbury) earthquake, New Zealand: initial findings. *Bulletin of the New Zealand Society for Earthquake Engineering* 43, 236-242.

Reyners, M., D. Eberhart-Phillips, and S. Martin (2013). Prolonged Canterbury earthquake sequence linked to widespread weakening of strong crust. *Nature Geoscience* 7, 34-37, doi:10.1038/NGEO2013.

Rhoades, D.A., and R.J. Van Dissen (2003). Estimates of the time varying hazard of rupture of the Alpine fault, New Zealand, allowing for uncertainties. *New Zealand Journal of Geology and Geophysics* 46, 479-488.

Ristau, J. (2011). Focal mechanism analysis of Christchurch boxing day aftershocks. GNS Science Consultancy Report 2011/43, 7 p.

Sibson, R., F. Ghisetti, and J. Ristau (2011). Stress control of an evolving strike-slip fault system during the 2010-2011 Canterbury, New Zealand, earthquake sequence. *Seismological Research Letters* 82, 824-832, doi:10.1785/gssrl.82.6.824.

Steacy, S., A. Jiménez, and C. Holden (2014). Stress triggering and the Canterbury earthquake sequence. *Geophysical Journal International* 196, 473-480, doi:10.1093/gji/ggt380.

Stirling, M., M. Gerstenberger, N. Litchfield, G. McVerry, W. Smith, J. Pettinga, and P. Barnes (2008). Seismic hazard of the Canterbury region, New Zealand: new earthquake source model and methodology. *Bulletin of the New Zealand Society for Earthquake Engineering* 41, 51-67.

Sutherland, R.D. *et al.* (2007). Do great earthquakes occur on the Alpine fault in central South Island, New Zealand?, *in* A Continental Plate Boundary: Tectonics at South Island, New Zealand, p. 235-251, eds. Okaya, D., Stern, T., and Davey, F., Geophysical Monograph 175, American Geophysical Union, Washington, DC.

Wessel, P., and W.H.F. Smith (1991). Free software helps map and display data. EOS Transactions AGU 71, 441.

Yetton, M.D., A. Wells, and N. Traylen (1998). The probability and consequences of the next Alpine fault earthquake, EQC Research Report 95/193,, New Zealand Earthquake Commission, Wellington, New Zealand.

Zhang, H., and Z. Ge (2010). Tracking the rupture of the 2008 Wenchuan earthquake by using the relative back-projection method. *Bulletin of the Seismological Society of America* 100, 2551-2560, doi:10.1785/0120090243.

8

Statistics of Collected Data

8.1 Introduction

The ISC Bulletin is based on the parametric data reports received from seismological agencies around the world. With rare exceptions, these reports include the results of waveform review done by analysts at network data centres and observatories. These reports include combinations of various bulletin elements such as event hypocentre estimates, moment tensors, magnitudes, event type and felt and damaging data as well as observations of the various seismic waves recorded at seismic stations.

Data reports are received in different formats that are often agency specific. Once an authorship is recognised, the data are automatically parsed into the ISC database and the original reports filed away to be accessed when necessary. Any reports not recognised or processed automatically are manually checked, corrected and re-processed. This chapter describes the data that are received at the ISC before the production of the reviewed Bulletin.

Notably, the ISC integrates all newly received data reports into the automatic ISC Bulletin (available on-line) soon after these reports are made available to ISC, provided it is done before the submission deadline that currently stands at 12 months following an event occurrence.

With data constantly being reported to the ISC, even after the ISC has published its review, the total data shown as collected, in this chapter, is limited to two years after the time of the associated reading or event, i.e. any hypocentre data collected two years after the event are not reflected in the figures below.

8.2 Summary of Agency Reports to the ISC

A total of 126 agencies have reported data for July 2010 to December 2010. The parsing of these reports into the ISC database is summarised in Table 8.1.

Table 8.1: *Summary of the parsing of reports received by the ISC from a total of 126 agencies, containing data for this summary period.*

	Number of reports
Total collected	2424
Automatically parsed	1823
Manually parsed	601

Data collected by the ISC consists of multiple data types. These are typically one of:

- Bulletin, hypocentres with associated phase arrival observations.

- Catalogue, hypocentres only.
- Unassociated phase arrival observations.

In Table 8.2, the number of different data types reported to the ISC by each agency is listed. The number of each data type reported by each agency is also listed. Agencies reporting indirectly have their data type additionally listed for the agency that reported it. The agencies reporting indirectly may also have 'hypocentres with associated phases' but with no associated phases listed - this is because the association is being made by the agency reporting directly to the ISC. Summary maps of the agencies and the types of data reported are shown in Figure 8.1 and Figure 8.2.

Table 8.2: *Agencies reporting to the ISC for this summary period. Entries in bold are for new or renewed reporting by agencies since the previous six-month period.*

Agency	Country	Directly or indirectly reporting (D/I)	Hypocentres with associated phases	Hypocentres without associated phases	Associated phases	Unassociated phases	Amplitudes
TIR	Albania	D	250	175	1297	144	0
CRAAG	Algeria	D	555	214	2577	780	0
LPA	Argentina	D	0	0	0	105	6
SJA	Argentina	D	2640	41	40496	38	4533
NSSP	Armenia	D	54	49	313	0	0
AUST	Australia	D	3498	5	45499	0	0
IDC	Austria	D	20347	0	380942	0	351323
VIE	Austria	D	2494	812	15265	0	12185
AZER	Azerbaijan	D	190	95	4409	0	0
BELR	Belarus	D	0	0	0	2931	668
UCC	Belgium	D	0	37	0	3286	799
BDF	Brazil	I NEIC	0	3	0	0	0
VAO	Brazil	D	0	0	0	1737	0
SOF	Bulgaria	D	159	151	1187	2217	0
OTT	Canada	D	1530	37	34969	0	4098
PGC	Canada	I VIE	1035	0	20310	0	0
GUC	Chile	D	3094	34	47634	606	10117
BJI	China	D	2725	35	169927	9347	83709
ASIES	Chinese Taipei	D	0	60	0	0	0
TAP	Chinese Taipei	D	11837	8	251783	0	0
RSNC	Colombia	I NEIC	0	2	0	0	0
CASC	Costa Rica	D	400	22	8652	0	175
HDC	Costa Rica	D	7	1	63	0	0
ICE	**Costa Rica**	**I CASC**	**0**	**1**	**0**	**0**	**0**
UCR	Costa Rica	I NEIC	0	3	0	0	0
ZAG	Croatia	D	0	0	0	2248	0
SSNC	Cuba	D	1	0	13	0	6
NIC	Cyprus	D	195	162	1471	305	0
IPEC	Czech Republic	I CSEM	0	525	0	0	0
PRU	Czech Republic	D	5006	2606	50876	651	12168
WBNET	Czech Republic	D	96	0	1675	354	1975
DNK	Denmark	D	0	121	0	5611	2139
ARO	Djibouti	D	27	0	259	0	0
IGQ	Ecuador	D	0	96	0	3001	0
HLW	Egypt	D	244	124	2024	0	243
SNET	El Salvador	I NEIC	0	6	0	0	0
SSS	El Salvador	I CASC	0	1	0	0	0
EST	Estonia	I HEL	358	38	0	0	0
AAE	Ethiopia	D	0	0	0	739	0
SKO	FYR Macedonia	D	833	502	3856	1698	1844
FIA0	Finland	I HEL	107	15	0	0	0
HEL	Finland	D	7162	5549	109586	81	14735
CSEM	France	D	41551	60379	847193	0	179065
LDG	France	D	1961	1968	39438	0	17481
STR	France	D	501	543	5268	1963	0

Table 8.2: (continued)

Agency	Country	Directly or indirectly reporting (D/I)	Hypocentres with associated phases	Hypocentres without associated phases	Associated phases	Unassociated phases	Amplitudes
PPT	French Polynesia	D	1374	0	9669	445	10086
TIF	Georgia	D	0	1368	0	14524	0
AWI	Germany	D	1744	0	4141	1114	0
BGR	Germany	D	921	433	17276	18	5401
BNS	Germany	I BGR	0	43	0	0	0
BRG	Germany	D	0	0	0	5017	3900
BUG	Germany	I BGR	21	0	0	0	0
CLL	Germany	D	2	0	74	8015	3055
GDNRW	Germany	I BGR	0	22	0	0	0
GFZ	Germany	I BGR	6	0	0	0	0
LEDBW	Germany	I BGR	16	2	0	0	0
SZGRF	Germany	I BGR	318	0	0	0	0
ATH	Greece	D	7810	7615	164650	8190	0
THE	Greece	D	3565	3570	83343	6166	21941
UPSL	Greece	I CSEM	0	203	0	0	0
GCG	Guatemala	I CASC	0	2	0	0	0
HKC	Hong Kong	D	0	1	0	102	0
BUD	Hungary	D	0	48	0	3237	0
REY	Iceland	D	25	16	927	0	0
HYB	India	D	1200	0	15031	16	4308
NDI	India	D	476	318	12124	5503	4242
DJA	Indonesia	D	3594	34	78067	0	89049
TEH	Iran	D	982	360	18488	0	5742
THR	Iran	D	174	331	1819	0	743
ISN	Iraq	D	170	111	1273	0	0
DIAS	Ireland	D	0	0	0	131	0
GII	Israel	D	47	42	1006	0	0
GEN	Italy	I CSEM	0	963	0	0	0
ROM	Italy	D	7252	5861	92211	0	37892
TRI	Italy	D	0	229	0	5180	0
LIC	Ivory Coast	D	633	0	2216	0	1075
JSN	Jamaica	D	94	0	623	2	0
JMA	Japan	D	64519	0	447748	1101	0
MAT	Japan	D	0	0	0	6490	0
NIED	Japan	D	0	851	0	0	0
SYO	Japan	D	0	0	0	3016	0
JSO	Jordan	D	10	5	76	0	0
NNC	Kazakhstan	D	8586	136	65024	0	55857
SIK	Kosovo	I CSEM	0	114	0	0	0
KNET	Kyrgyzstan	D	1342	0	10883	0	1447
KRNET	Kyrgyzstan	D	1604	0	24466	0	0
GRAL	Lebanon	D	231	219	1478	413	0
LIB	**Libya**	**I CSEM**	**0**	**40**	**0**	**0**	**0**
LIT	Lithuania	D	176	244	1286	667	894
KLM	Malaysia	D	537	5	4330	0	0
ECX	Mexico	D	2325	28	48709	0	7119
MEX	Mexico	D	1591	218	12705	0	0
MOLD	Moldova	D	0	0	0	1860	647
PDG	Montenegro	D	686	618	14751	0	7719
CNRM	Morocco	I CSEM	0	147	0	0	0
DMN	Nepal	D	1900	2	18273	0	14527
DBN	Netherlands	D	0	0	0	1661	650
NOU	New Caledonia	D	66	0	505	697	122
WEL	New Zealand	D	8228	8	246438	6813	87835
INET	**Nicaragua**	**I CASC**	**0**	**1**	**0**	**0**	**0**
BER	Norway	D	1641	1859	22669	255	4509
NAO	Norway	D	2761	1505	7176	0	2052
OMAN	Oman	D	403	99	3583	0	0
MSSP	Pakistan	D	0	0	0	838	0
ARE	Peru	I NEIC	0	13	0	0	0
LIM	**Peru**	**I IRIS**	**1**	**0**	**0**	**0**	**0**
MAN	Philippines	D	0	915	0	17554	6602
QCP	Philippines	D	0	0	0	34	0

Table 8.2: *(continued)*

Agency	Country	Directly or indirectly reporting (D/I)	Hypocentres with associated phases	Hypocentres without associated phases	Associated phases	Unassociated phases	Amplitudes
WAR	Poland	D	0	0	0	13235	0
IGIL	Portugal	D	681	0	3506	0	1197
INMG	Portugal	D	1369	685	39767	1839	13980
LIS	**Portugal**	**I NEIC**	**0**	**1**	**0**	**0**	**0**
PDA	Portugal	I SVSA	730	692	0	0	0
SVSA	Portugal	D	798	0	12653	6004	5234
KMA	Republic of Korea	D	983	0	13648	0	0
BUC	Romania	D	698	72	9334	41486	0
ASRS	Russia	D	6	0	61	0	0
BYKL	Russia	D	141	0	10591	0	4099
KOLA	Russia	D	78	0	297	0	0
KRSC	Russia	D	681	0	20793	0	0
MOS	Russia	D	2500	323	404502	0	156674
NERS	Russia	D	34	0	853	0	370
SKHL	Russia	D	421	423	15357	0	6801
YARS	Russia	D	568	676	9657	0	3830
SGS	Saudi Arabia	D	46	39	259	0	0
BEO	Serbia	D	2660	1871	38667	30	0
BRA	Slovakia	D	0	0	0	12327	0
LJU	Slovenia	D	1262	974	15978	4729	5080
HNR	Solomon Islands	D	0	0	0	1088	0
PRE	South Africa	D	1045	1	18029	1982	6879
MDD	Spain	D	2678	6269	81083	0	64474
MRB	Spain	I CSEM	0	20	0	0	0
SFS	Spain	I CSEM	0	213	0	0	0
UPP	Sweden	D	574	2820	6017	0	0
ZUR	Switzerland	D	294	302	3515	0	3078
NSSC	Syria	D	1176	579	23931	122	10661
BKK	Thailand	D	1237	26	13800	0	18864
TRN	Trinidad and Tobago	D	2	543	0	13907	0
TUN	Tunisia	I CSEM	0	17	0	0	0
DDA	Turkey	D	9749	6459	95006	10288	0
ISK	Turkey	D	10	10872	0	74957	0
AEIC	U.S.A.	I IRIS	120	115	0	0	0
ANF	U.S.A.	I IRIS	1732	585	0	0	0
BRK	U.S.A.	I NEIC	0	0	0	0	0
BUT	U.S.A.	I IRIS	4	20	0	0	0
CERI	U.S.A.	I NEIC	60	5	0	0	0
GCMT	U.S.A.	D	0	3537	0	0	0
HON	U.S.A.	I NEIC	0	16	0	0	0
HVO	**U.S.A.**	**I NEIC**	**0**	**2**	**0**	**0**	**0**
IASPEI	U.S.A.	D	0	0	0	12	0
IRIS	U.S.A.	D	3510	4014	319811	0	0
LDO	U.S.A.	I NEIC	0	2	0	0	0
NCEDC	U.S.A.	I IRIS	58	22	0	0	0
NEIC	U.S.A.	D	19628	6143	647145	0	198615
PAS	U.S.A.	I IRIS	94	211	0	0	0
PMR	U.S.A.	I NEIC	0	47	0	0	0
PNSN	U.S.A.	D	5	187	0	0	0
REN	U.S.A.	I IRIS	23	3	0	0	0
RSPR	U.S.A.	D	644	6	8841	0	0
SCEDC	**U.S.A.**	**I IRIS**	**5**	**3**	**0**	**0**	**0**
SEA	U.S.A.	I IRIS	5	48	0	0	0
SIO	U.S.A.	D	1865	0	4796	0	4796
SLC	U.S.A.	I IRIS	3	8	0	0	0
SLM	U.S.A.	I NEIC	0	0	0	0	0
TUL	U.S.A.	I IRIS	96	0	0	0	0
WES	U.S.A.	I NEIC	0	8	0	0	0
SIGU	Ukraine	D	122	122	2556	9	0
DSN	United Arab Emirates	D	573	173	3150	0	0

Table 8.2: (continued)

Agency	Country	Directly or indirectly reporting (D/I)	Hypocentres with associated phases	Hypocentres without associated phases	Associated phases	Unassociated phases	Amplitudes
BGS	United Kingdom	D	219	120	7261	0	2557
MASS	**Unknown**	**I IASPEI**	**0**	**0**	**0**	**11**	**0**
UNK	Unknown	I IRIS	76	785	0	0	0
USP	**Unknown**	**I IASPEI**	**0**	**0**	**0**	**1**	**0**
CAR	Venezuela	I VIE	1	3	0	0	0
FUNV	Venezuela	D	1436	0	19841	0	0
PLV	Vietnam	D	39	0	880	0	160
DHMR	Yemen	D	285	165	2764	3548	1300
BUL	Zimbabwe	D	398	0	1689	597	0

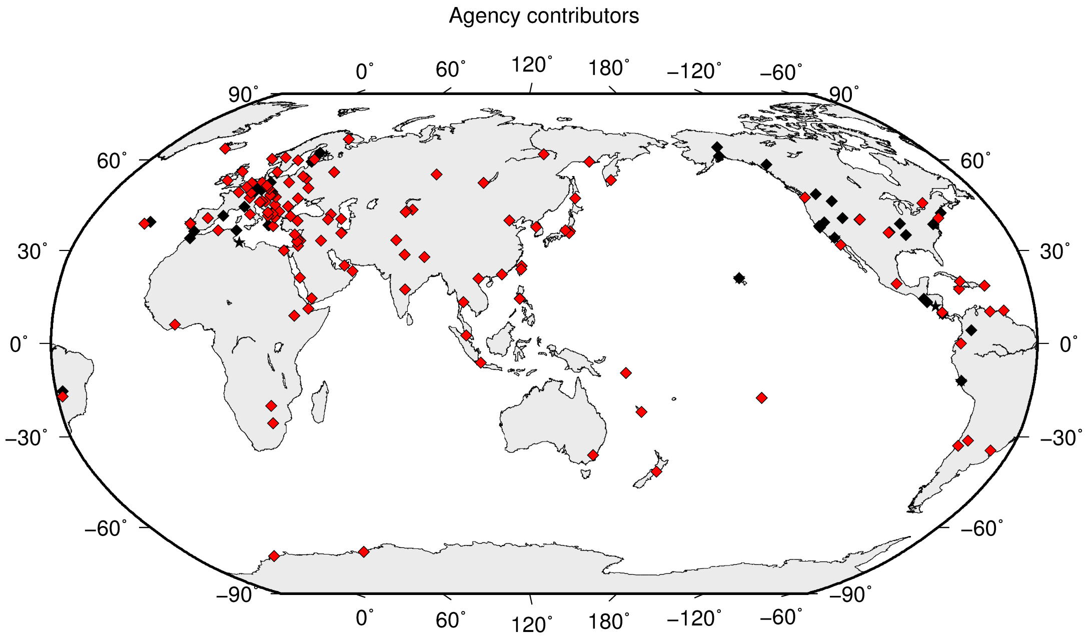

Figure 8.1: *Map of agencies that have contributed data to the ISC for this summary period. Agencies that have reported directly to the ISC are shown in red. Those that have reported indirectly (via another agency) are shown in black. Any new or renewed agencies, since the last six-month period, are shown by a star. Each agency is listed in Table 8.2.*

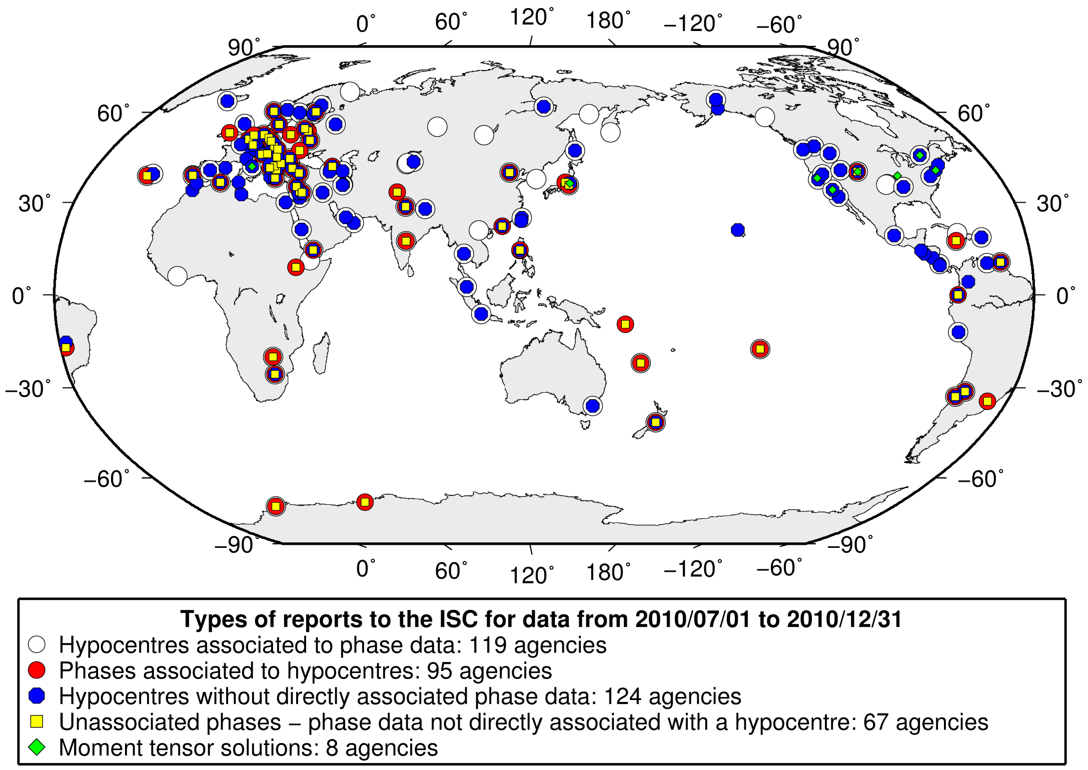

Figure 8.2: *Map of the different data types reported by agencies to the ISC. A full list of the data types reported by each agency is shown in Table 8.2.*

8.3 Arrival Observations

The collection of phase arrival observations at the ISC has increased dramatically with time. The increase in reported phase arrival observations is shown in Figure 8.3.

The reports with phase data are summarised in Table 8.3. This table is split into three sections, providing information on the reports themselves, the phase data, and the stations reporting the phase data. A map of the stations contributing these phase data is shown in Figure 8.4.

The ISC encourages the reporting of phase arrival times together with amplitude and period measurements whenever feasible. Figure 8.5 shows the percentage of events reported by each station was accompanied with amplitude and period measurements.

Figure 8.6 indicates the number of amplitude and period measurement for each station.

Together with the increase in the number of phases (Figure 8.3), there has been an increase in the number of stations reported to the ISC. The increase in the number of stations is shown in Figure 8.7. This increase can also be seen on the maps for stations reported each decade in Figure 8.8.

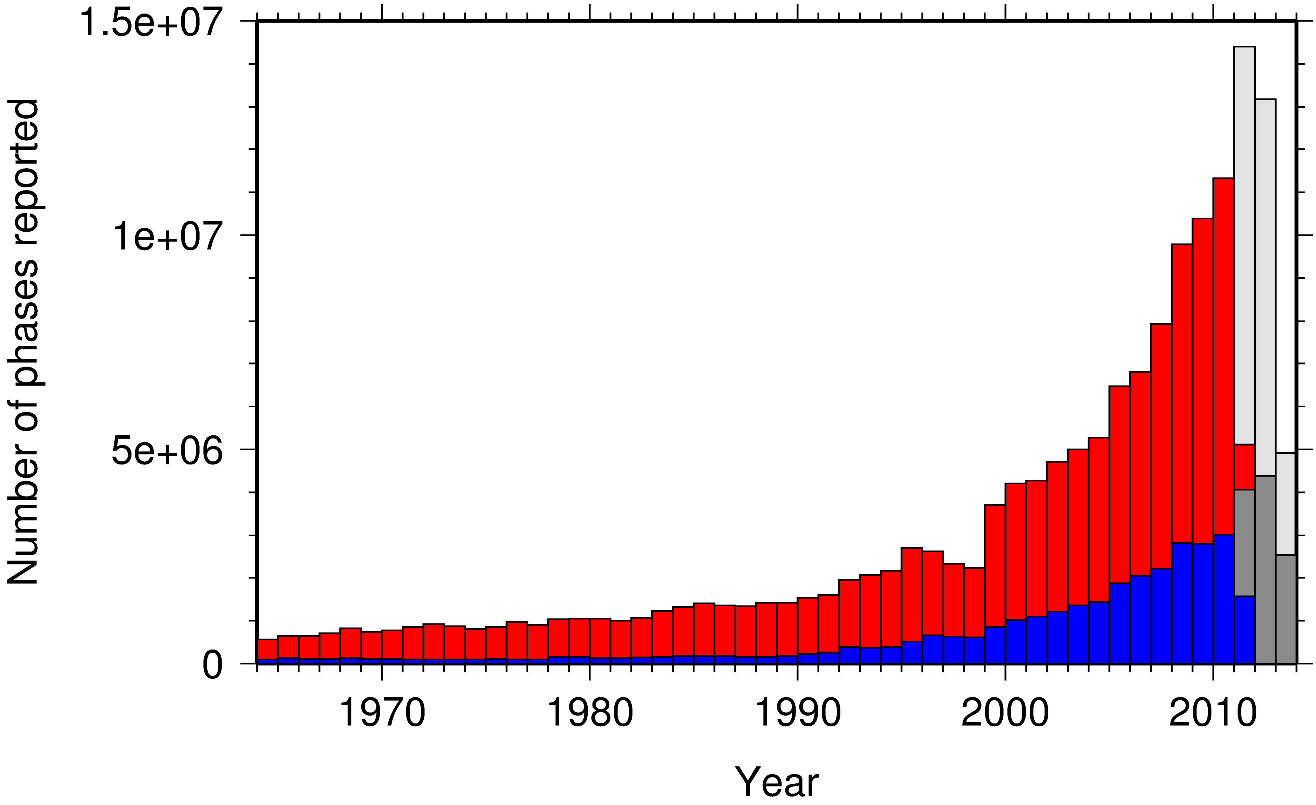

Figure 8.3: *Histogram showing the number of phases (red) and number of amplitudes (blue) collected by the ISC for events each year since 1964. The data in grey covers the current period where data are still being collected before the ISC review takes place and is accurate at the time of publication.*

Table 8.3: *Summary of reports containing phase arrival observations.*

Reports with phase arrivals	1975
Reports with phase arrivals including amplitudes	764
Reports with only phase arrivals (no hypocentres reported)	249
Total phase arrivals received	5678746
Total phase arrival-times received	5390697
Number of duplicate phase arrival-times	1186950 (22.0%)
Number of amplitudes received	1571092
Stations reporting phase arrivals	6342
Stations reporting phase arrivals with amplitude data	2624
Max number of stations per report	1968

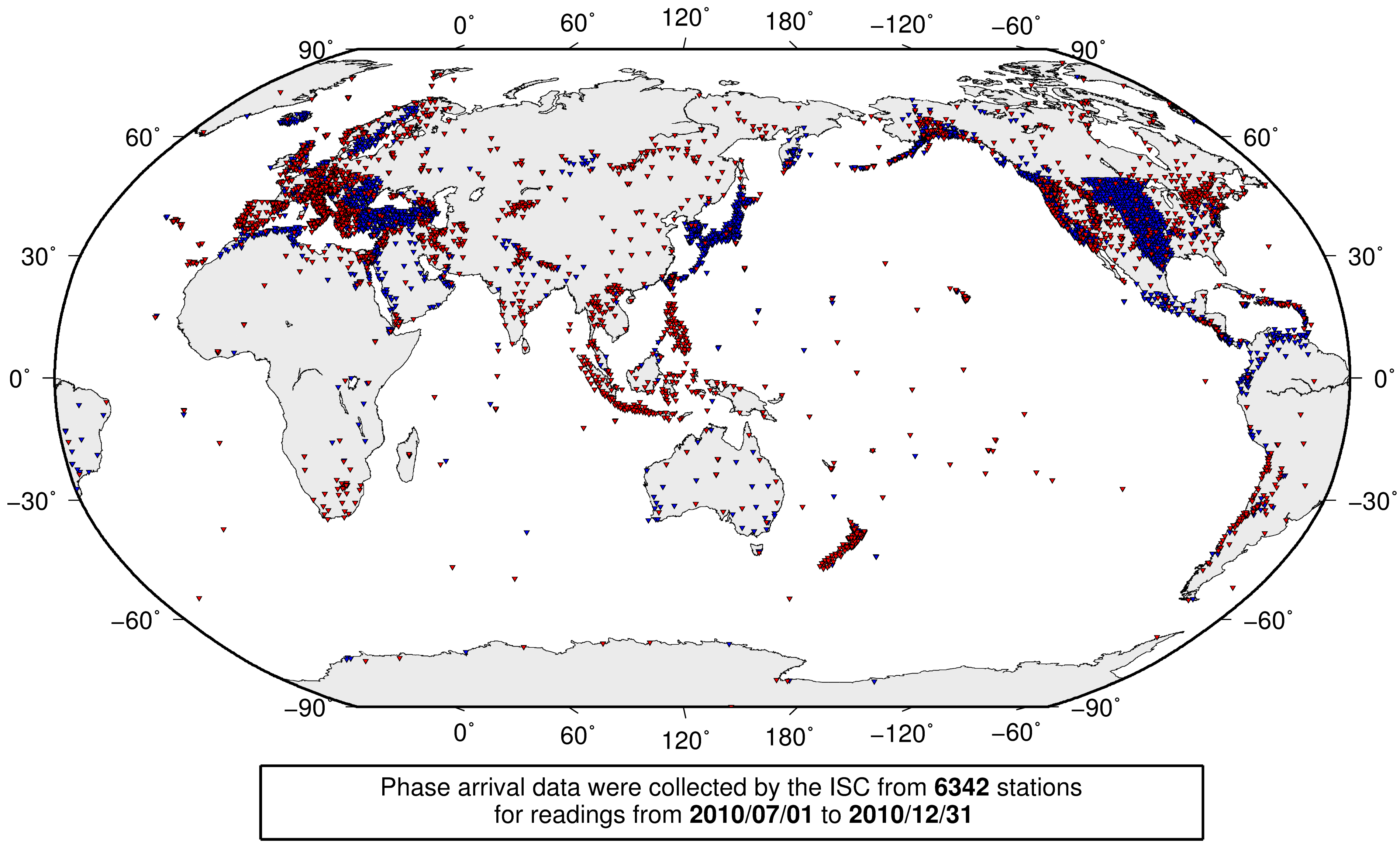

Figure 8.4: *Stations contributing phase data to the ISC for readings from July 2010 to the end of December 2010. Stations in blue provided phase arrival times only; stations in red provided both phase arrival times and amplitude data.*

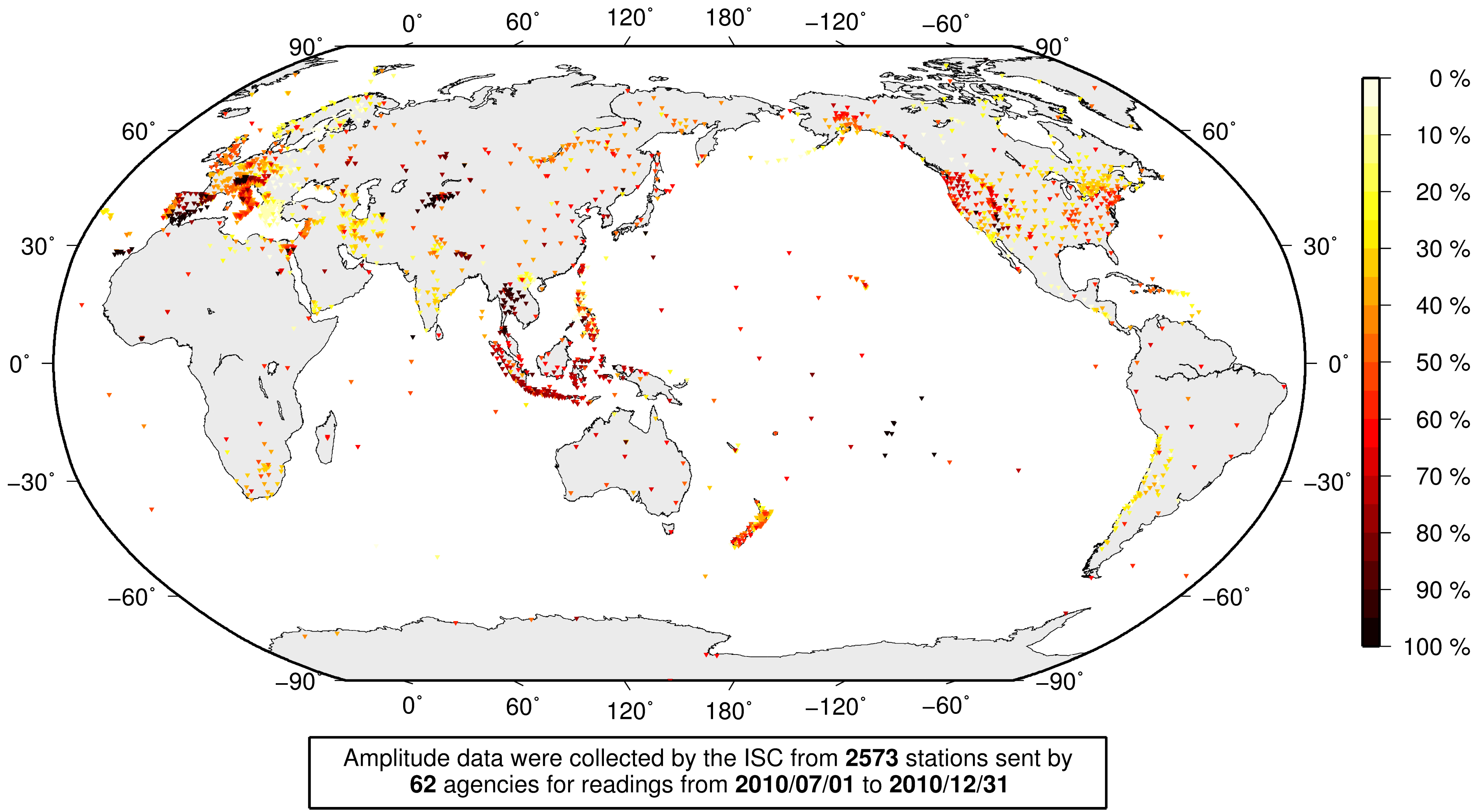

Figure 8.5: *Percentage of events for which phase arrival times from each station are accompanied with amplitude and period measurements.*

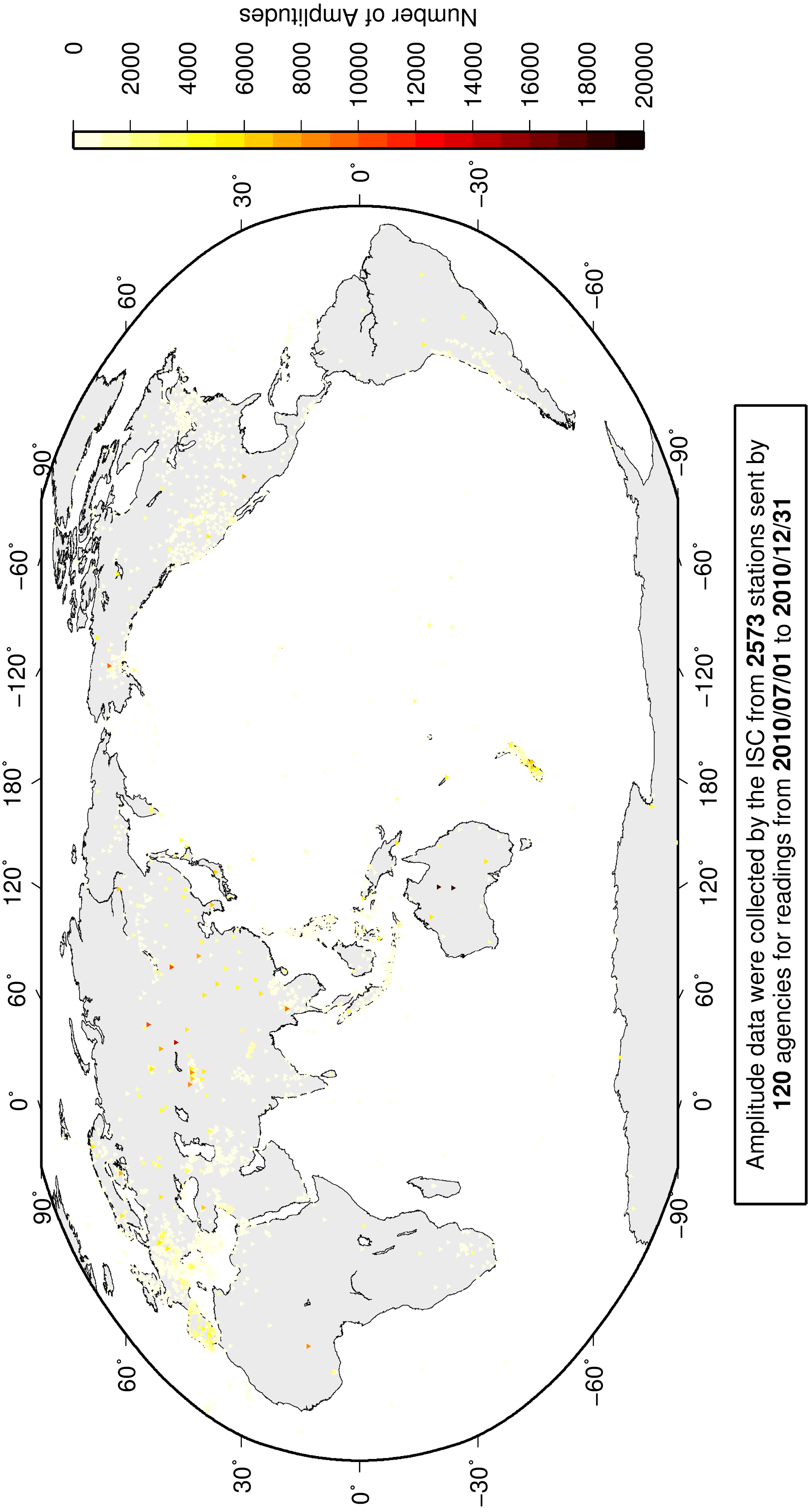

Figure 8.6: *Number of amplitude and period measurements for each station.*

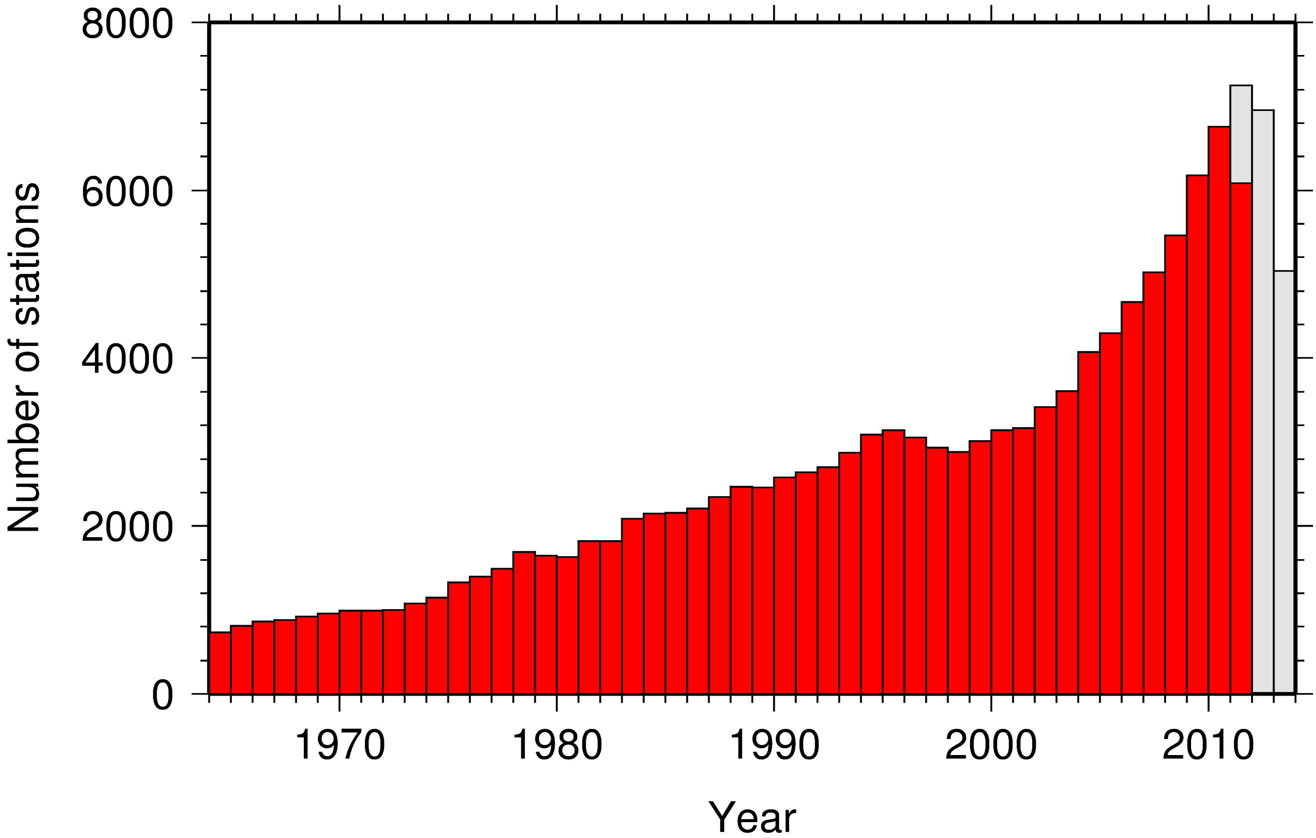

Figure 8.7: *Histogram showing the number of stations reporting to the ISC each year since 1964. The data in grey covers the current period where station information is still being collected before the ISC review of events takes place and is accurate at the time of publication.*

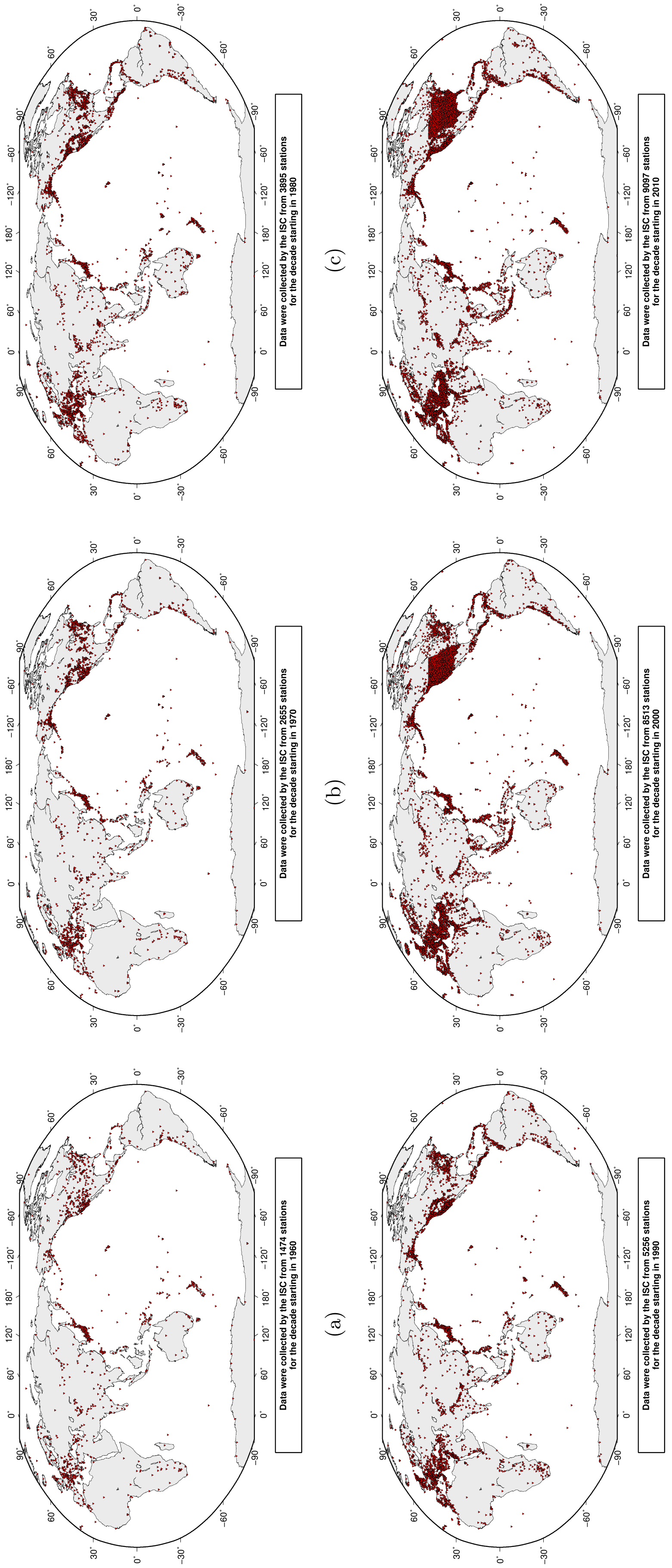

Figure 8.8: *Maps showing the stations reported to the ISC for each decade since 1960. Note that the last map covers a shorter time period.*

8.4 Hypocentres Collected

The ISC Bulletin groups multiple estimates of hypocentres into individual events, with an appropriate prime hypocentre solution selected. The collection of these hypocentre estimates are described in this section.

The reports containing hypocentres are summarised in Table 8.4. The number of hypocentres collected by the ISC has also increased significantly since 1964, as shown in Figure 8.9. A map of all hypocentres reported to the ISC for this summary period is shown in Figure 8.10. Where a network magnitude was reported with the hypocentre, this is also shown on the map, with preference given to reported values, first of M_W followed by M_S, m_b and M_L respectively (where more than one network magnitude was reported).

Table 8.4: *Summary of the reports containing hypocentres.*

Reports with hypocentres	2175
Reports of hypocentres only (no phase readings)	449
Total hypocentres received	366561
Number of duplicate hypocentres	82799 (22.6%)
Agencies determining hypocentres	153

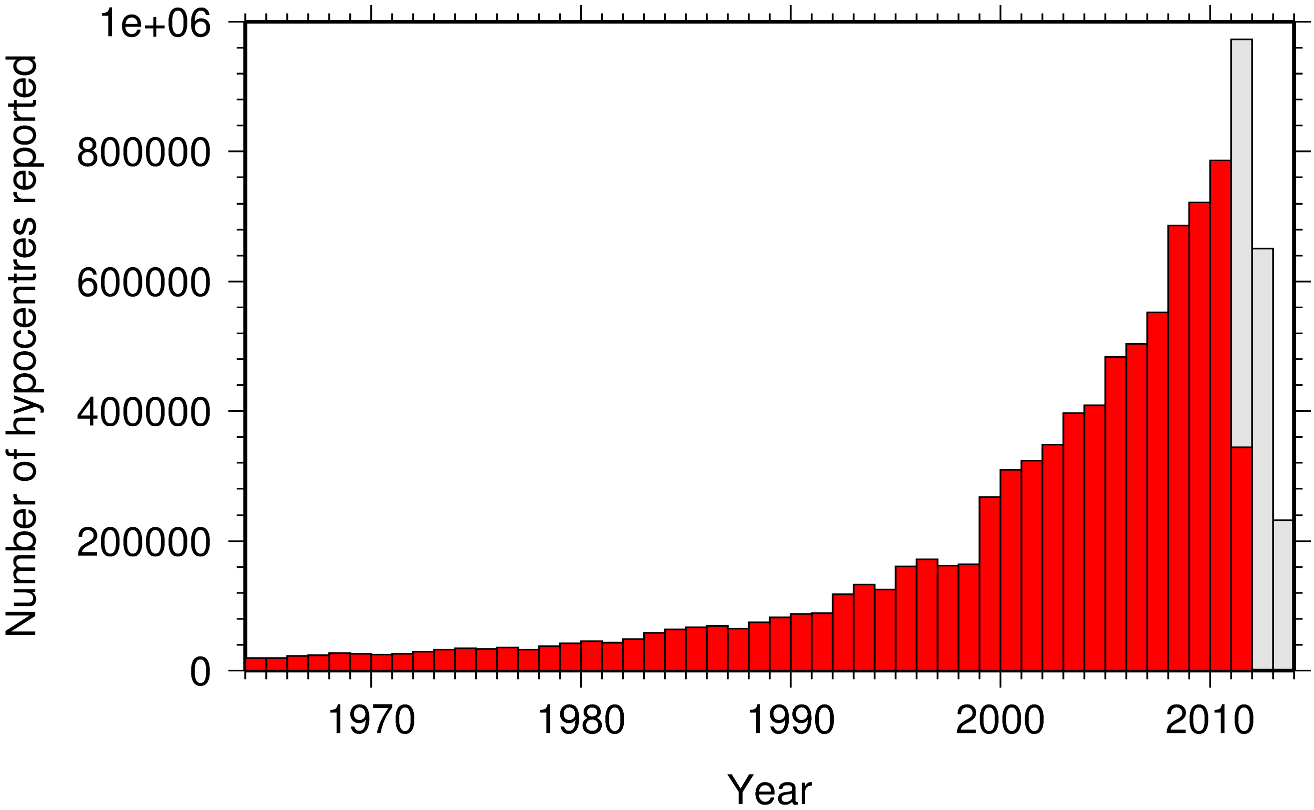

Figure 8.9: *Histogram showing the number of hypocentres collected by the ISC for events each year since 1964. For each event, multiple hypocentres may be reported.*

All the hypocentres that are reported to the ISC are automatically grouped into events, which form the basis of the ISC Bulletin. For this time period 403422 hypocentres (including ISC) were grouped into 192375 events, the largest of these having 81 hypocentres in one event. The total number of events

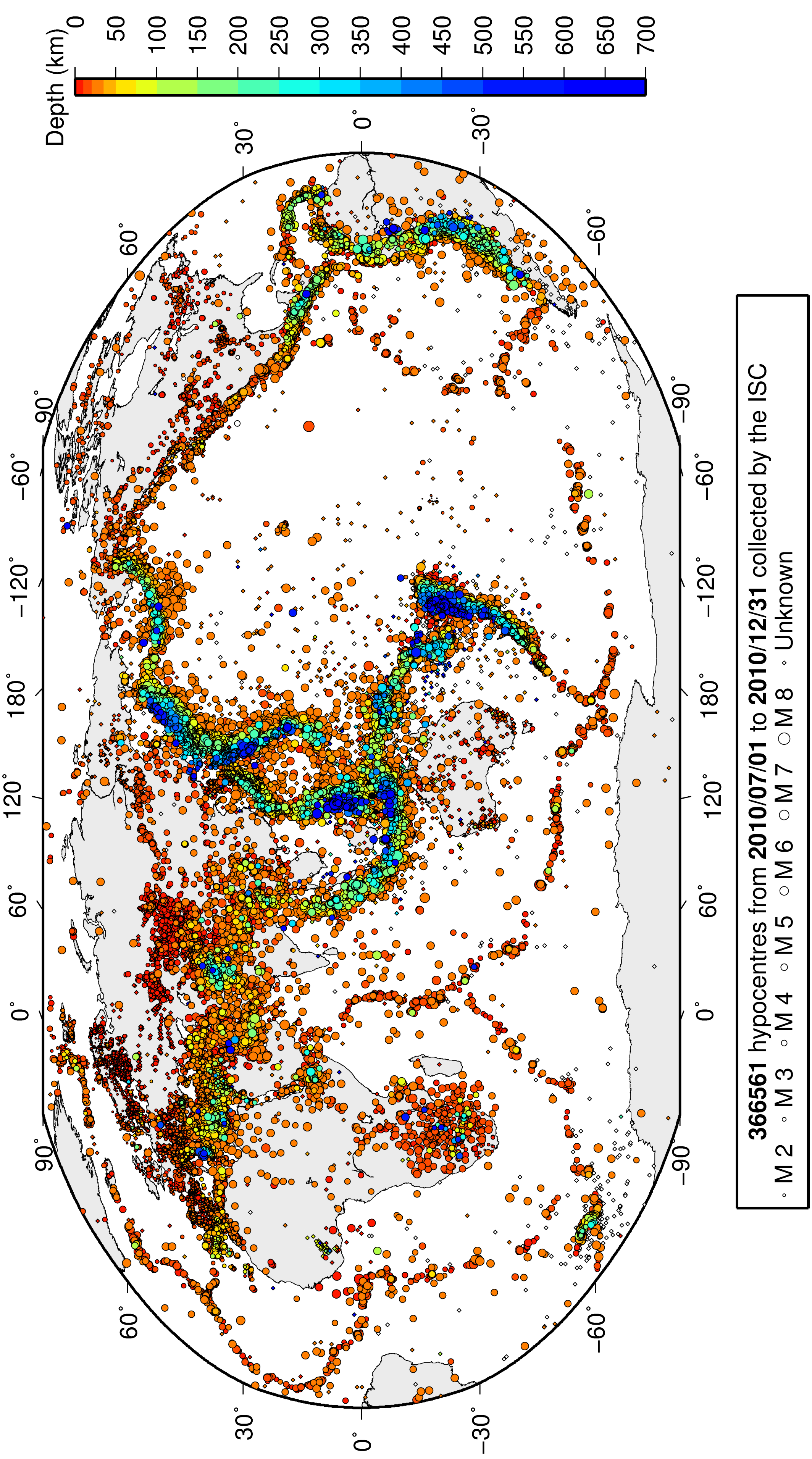

Figure 8.10: *Map of all hypocentres collected by the ISC. The scatter shows the large variation of the multiple hypocentres that are reported for each event. The magnitude corresponds with the reported network magnitude. If more than one network magnitude type was reported, preference was given to values of* M_W, M_S, m_b *and* M_L *respectively. Compare with Figure 9.2*

shown here is the result of an automatic grouping algorithm, and will differ from the total events in the published ISC Bulletin, where both the number of events and the number of hypocentre estimates will have changed due to further analysis. Figure 9.2 on page 92 shows a map of all prime hypocentres.

8.5 Collection of Network Magnitude Data

Data contributing agencies normally report earthquake hypocentre solutions along with magnitude estimates. For each seismic event, each agency may report one or more magnitudes of the same or different types. This stems from variability in observational practices at regional, national and global level in computing magnitudes based on a multitude of wave types. Differences in the amplitude measurement algorithm, seismogram component(s) used, frequency range, station distance range as well as the instrument type contribute to the diversity of magnitude types. Table 8.5 provides an overview of the complexity of reported network magnitudes reported for seismic events during the current period.

Table 8.5: *Statistics of magnitude reports to the ISC; M – average magnitude of estimates reported for each event.*

	M<3.0	3.0≤M<5.0	M≥5.0
Number of seismic events	140304	35001	456
Average number of magnitude estimates per event	1.9	5.3	30.6
Average number of magnitudes (by the same agency) per event	1.4	2.8	4.5
Average number of magnitude types per event	1.2	4.1	10.9
Number of magnitude types	21	27	23

Table 8.6 gives the basic description, main features and scientific paper references for the most commonly reported magnitude types.

Table 8.6: *Description of the most common magnitude types reported to the ISC.*

Magnitude type	Description	References	Comments
M	Unspecified		Often used in real or near-real time magnitude estimations
mB	Medium-period and Broad-band body-wave magnitude	*Gutenberg* (1945a); *Gutenberg* (1945b); *IASPEI* (2005); *IASPEI* (2013); *Bormann et al.* (2009); *Bormann and Dewey* (2012)	
mb	Short-period body-wave magnitude	*IASPEI* (2005); *IASPEI* (2013); *Bormann et al.* (2009); *Bormann and Dewey* (2012)	Classical mb based on stations between 21°-100° distance

Table 8.6: *continued*

Magnitude type	Description	References	Comments
mb1	Short-period body-wave magnitude	*IDC* (1999) and references therein	Reported only by the IDC; also includes stations at distances less than 21°
mb1mx	Maximum likelihood short-period body-wave magnitude	*Ringdal* (1976); *IDC* (1999) and references therein	Reported only by the IDC
mbtmp	short-period body-wave magnitude with depth fixed at the surface	*IDC* (1999) and references therein	Reported only by the IDC
mbLg	Lg-wave magnitude	*Nuttli* (1973); *IASPEI* (2005); *IASPEI* (2013); *Bormann and Dewey* (2012)	Also reported as MN
Mc	Coda magnitude		
MD (Md)	Duration magnitude	*Bisztricsany* (1958); *Lee et al.* (1972)	
ME (Me)	Energy magnitude	*Choy and Boatwright* (1995)	Reported only by NEIC
MJMA	JMA magnitude	*Tsuboi* (1954)	Reported only by JMA
ML (Ml)	Local (Richter) magnitude	*Richter* (1935); *Hutton and Boore* (1987); *IASPEI* (2005); *IASPEI* (2013)	
MLSn	Local magnitude calculated for Sn phases	*Balfour et al.* (2008)	Reported by PGC only for earthquakes west of the Cascadia subduction zone
MLv	Local (Richter) magnitude computed from the vertical component		Reported only by DJA and BKK
MN (Mn)	Lg-wave magnitude	*Nuttli* (1973); *IASPEI* (2005)	Also reported as mbLg
MS (Ms)	Surface-wave magnitude	*Gutenberg* (1945c); *Vaněk et al.* (1962); *IASPEI* (2005)	Classical surface-wave magnitude computed from station between 20°-160° distance
Ms1	Surface-wave magnitude	*IDC* (1999) and references therein	Reported only by the IDC; also includes stations at distances less than 20°
ms1mx	Maximum likelihood surface-wave magnitude	*Ringdal* (1976); *IDC* (1999) and references therein	Reported only by the IDC

Table 8.6: *continued*

Magnitude type	Description	References	Comments
Ms7	Surface-wave magnitude	*Bormann et al.* (2007)	Reported only by BJI and computed from records of a Chinese-made long-period seismograph in the distance range 3°-177°
MW (Mw)	Moment magnitude	*Kanamori* (1977); *Dziewonski et al.* (1981)	Computed according to the *IASPEI* (2005) and *IASPEI* (2013) standard formula
Mw(mB)	Proxy Mw based on mB	*Bormann and Saul* (2008)	Reported only by DJA and BKK
Mwp	Moment magnitude from P-waves	*Tsuboi et al.* (1995)	Reported only by DJA and BKK and used in rapid response
mbh	Unknown		
mbv	Unknown		
MG	Unspecified type		Contact contributor
Mm	Unknown		
msh	Unknown		
MSV	Unknown		

Table 8.7 lists all magnitude types reported, the corresponding number of events in the ISC Bulletin and the agency codes along with the number of earthquakes.

Table 8.7: *Summary of magnitude types in the ISC Bulletin for this summary period. The number of events with values for each magnitude type is listed. The agencies reporting these magnitude types are listed, together with the total number of values reported.*

Magnitude type	Events	Agencies reporting magnitude type (number of values)
M	4003	DJA (2961), SKO (670), FDF (213), BKK (170), PRU (18)
mB	3136	BJI (2412), DJA (1295), BKK (74), NEIC (1)
MB	7	BGR (7)
mb	24968	IDC (18257), NEIC (6110), NNC (4006), MOS (2468), BJI (2225), DJA (1643), KRNET (1592), MAN (864), VIE (798), CSEM (678), SKHL (406), KLM (276), MDD (229), DSN (199), SZGRF (189), BGR (166), SIGU (102), IGQ (82), BKK (78), NIC (62), IASPEI (10), CRAAG (5), PDA (5), DMN (4), NDI (4), IGIL (3), GII (3), THR (2), CASC (1), DHMR (1), PDG (1), BGS (1)
mb1	18722	IDC (18722)
mb1mx	18722	IDC (18722)
mbh	17	SKHL (17)
mbLg	2448	MDD (2448)
mbtmp	18722	IDC (18722)
Mc	3	CSEM (3)

Table 8.7: Continued.

Magnitude type	Events	Agencies reporting magnitude type (number of values)
MD	35483	CSEM (17631), DDA (9586), ATH (7574), ROM (6723), ISK (5225), ECX (2220), MEX (1812), LDG (1601), RSPR (896), BER (863), BUC (699), PDA (612), SJA (457), PDG (412), TRN (394), CASC (385), NSSC (283), GRAL (231), HLW (168), SOF (155), CNRM (147), PNSN (131), NCEDC (121), TUL (72), INMG (61), CERI (61), JSN (50), GII (46), NOU (43), BUL (42), SEA (22), SNET (22), TUN (17), IGQ (15), PLV (14), DHMR (9), BUT (6), HVO (6), UCR (5), LDO (4), TIR (3), HDC (3), WES (2), GCG (2), SSS (1), JSO (1), NEIC (1), SLC (1), BDF (1)
ME	85	NEIC (85)
MG	344	AEIC (277), WEL (48), GUC (15), ARE (3), DJA (1)
MJMA	62557	JMA (62557)
ML	78718	CSEM (20905), TAP (11859), IDC (10460), WEL (7949), ROM (6984), HEL (6788), AEIC (3695), THE (3546), GUC (3166), BEO (2650), UPP (2640), ECX (2501), LDG (1919), SJA (1828), LJU (1225), VIE (1099), BER (998), PRE (996), GEN (963), ATH (957), PGC (944), INMG (915), NAO (902), MAN (865), NSSC (851), PDA (684), KRSC (680), SKO (648), PDG (620), IPEC (524), STR (501), CRAAG (461), IGIL (454), PAS (409), ISK (376), BJI (339), ZUR (293), DHMR (263), TEH (252), SFS (210), HLW (205), THR (204), TIR (200), NIC (195), KLM (169), DDA (159), BGR (156), DSN (134), CASC (131), KNET (124), FIA0 (122), ISN (106), NEIC (100), PPT (94), WBNET (94), NDI (93), OTT (90), BGS (57), REN (52), BNS (43), PLV (39), UCC (37), NOU (37), NCEDC (29), ARO (27), SLC (25), HVO (22), BUG (21), MRB (20), DMN (19), BUT (17), ARE (14), HYB (6), RSNC (4), AUST (4), RSPR (3), BUC (3), REY (2), LDO (2), HON (2), SZGRF (1), LEDBW (1), SEA (1), AZER (1), INET (1), BDF (1), CLL (1), NSSP (1)
MLSn	84	PGC (84)
MLv	3033	DJA (3017), BKK (145)
Mm	17	GII (17)
MN	585	OTT (483), NEIC (52), TEH (47), TUL (24), WES (11), MDD (4), OGSO (1), BDF (1)
MPV	1	NERS (1)
mpv	4337	NNC (4337)
MS	9235	IDC (8250), BJI (1945), MAN (885), MOS (544), KLM (204), NEIC (199), CSEM (119), DSN (78), BGR (59), NSSP (55), SZGRF (53), SKHL (49), VIE (28), NOU (7), ASRS (6), IASPEI (5), LDG (5), WEL (1), PDA (1)
Ms1	8250	IDC (8250)
ms1mx	8250	IDC (8250)
Ms7	1920	BJI (1920)
msh	85	SKHL (85)
MSV	676	YARS (676)

Table 8.7: *Continued.*

Magnitude type	Events	Agencies reporting magnitude type (number of values)
MW	4813	FUNV (1435), SJA (1153), NIED (1127), GCMT (958), NEIC (402), PGC (376), BRK (43), CSEM (36), OTT (22), CAR (14), SLM (8), BER (5), NCEDC (3), PAS (3), CRAAG (2), UCR (2), DDA (1), WEL (1), THR (1), ROM (1), PDA (1), NSSC (1)
Mw(mB)	1338	DJA (1295), BKK (75)
Mwp	170	DJA (164), BKK (7)

The most commonly reported magnitude types are short-period body-wave, surface-wave, local (or Richter), moment, duration and JMA magnitude type. For a given earthquake, the number and type of reported magnitudes greatly vary depending on its size and location. The large earthquake of October 25, 2010 gives an example of the multitude of reported magnitude types for large earthquakes (Listing 8.1). Different magnitude estimates come from global monitoring agencies such as the IDC, NEIC and GCMT, a local agency (GUC) and other agencies, such as MOS and BJI, providing estimates based on the analysis of their networks. The same agency may report different magnitude types as well as several estimates of the same magnitude type, such as NEIC estimates of Mw obtained from W-phase, centroid and body-wave inversions.

Listing 8.1: *Example of reported magnitudes for a large event*

```
Event   15264887 Southern Sumatera
   Date       Time        Err   RMS Latitude Longitude  Smaj  Smin  Az Depth   Err Ndef Nsta Gap  mdist  Mdist Qual   Author      OrigID
2010/10/25 14:42:22.18   0.27 1.813  -3.5248  100.1042 4.045 3.327  54  20.0  1.37 2102 2149  23   0.76 176.43 m i de ISC        01346132
 (#PRIME)

Magnitude  Err Nsta Author      OrigID
mb      6.1       61 BJI       15548963
mB      6.9       68 BJI       15548963
Ms      7.7       85 BJI       15548963
Ms7     7.5       86 BJI       15548963
mb      5.3 0.1   48 IDC       16686694
mb1     5.3 0.1   51 IDC       16686694
mb1mx   5.3 0.0   52 IDC       16686694
mbtmp   5.3 0.1   51 IDC       16686694
ML      5.1 0.2    2 IDC       16686694
MS      7.1 0.0   31 IDC       16686694
Ms1     7.1 0.0   31 IDC       16686694
ms1mx   6.9 0.1   44 IDC       16686694
mb      6.1      243 ISCJB     01677901
MS      7.3      228 ISCJB     01677901
M       7.1      117 DJA       01268475
mb      6.1 0.2  115 DJA       01268475
mB      7.1 0.1  117 DJA       01268475
MLv     7.0 0.2   26 DJA       01268475
        7.1 0.4  117 DJA       01268475
Mwp     6.9 0.2  102 DJA       01268475
mb      6.4       49 MOS       16742129
MS      7.2       70 MOS       16742129
mb      6.5      110 NEIC      01288303
ME      7.3          NEIC      01288303
MS      7.3      143 NEIC      01288303
MW      7.7          NEIC      01288303
MW      7.8      130 GCMT      00125427
mb      5.9          KLM       00255772
ML      6.7          KLM       00255772
MS      7.6          KLM       00255772
mb      6.4       20 BGR       16815854
Ms      7.2        2 BGR       16815854
mb      6.3 0.3  250 ISC       01346132
MS      7.3 0.1  237 ISC       01346132
```

An example of a relatively small earthquake that occurred in northern Italy for which we received magnitude reports of mostly local and duration type from six agencies in Italy, France and Austria is given in Listing 8.2.

Listing 8.2: *Example of reported magnitudes for a small event*

```
Event 15089710 Northern Italy
   Date       Time        Err   RMS Latitude Longitude  Smaj  Smin  Az Depth   Err Ndef Nsta Gap  mdist  Mdist Qual   Author      OrigID
2010/08/08 15:20:46.22   0.94 0.778  45.4846    8.3212 2.900 2.539 110  28.6  9.22  172  110  82   0.41   5.35 m i ke ISC        01249414
 (#PRIME)

Magnitude  Err Nsta Author      OrigID
ML      2.4       10 ZUR       15925566
Md      2.6 0.2   19 ROM       16861451
Ml      2.2 0.2    9 ROM       16861451
ML      2.5          GEN       00554757
```

```
ML      2.6 0.3    28 CSEM        00554756
Md      2.3 0.0     3 LDG         14797570
Ml      2.6 0.3    32 LDG         14797570
```

Figure 8.11 shows a distribution of the number of agencies reporting magnitude estimates to the ISC according to the magnitude value. The peak of the distribution corresponds to small earthquakes where many local agencies report local and/or duration magnitudes. The number of contributing agencies rapidly decreases for earthquakes of approximately magnitude 5.5 and above, where magnitudes are mostly given by global monitoring agencies.

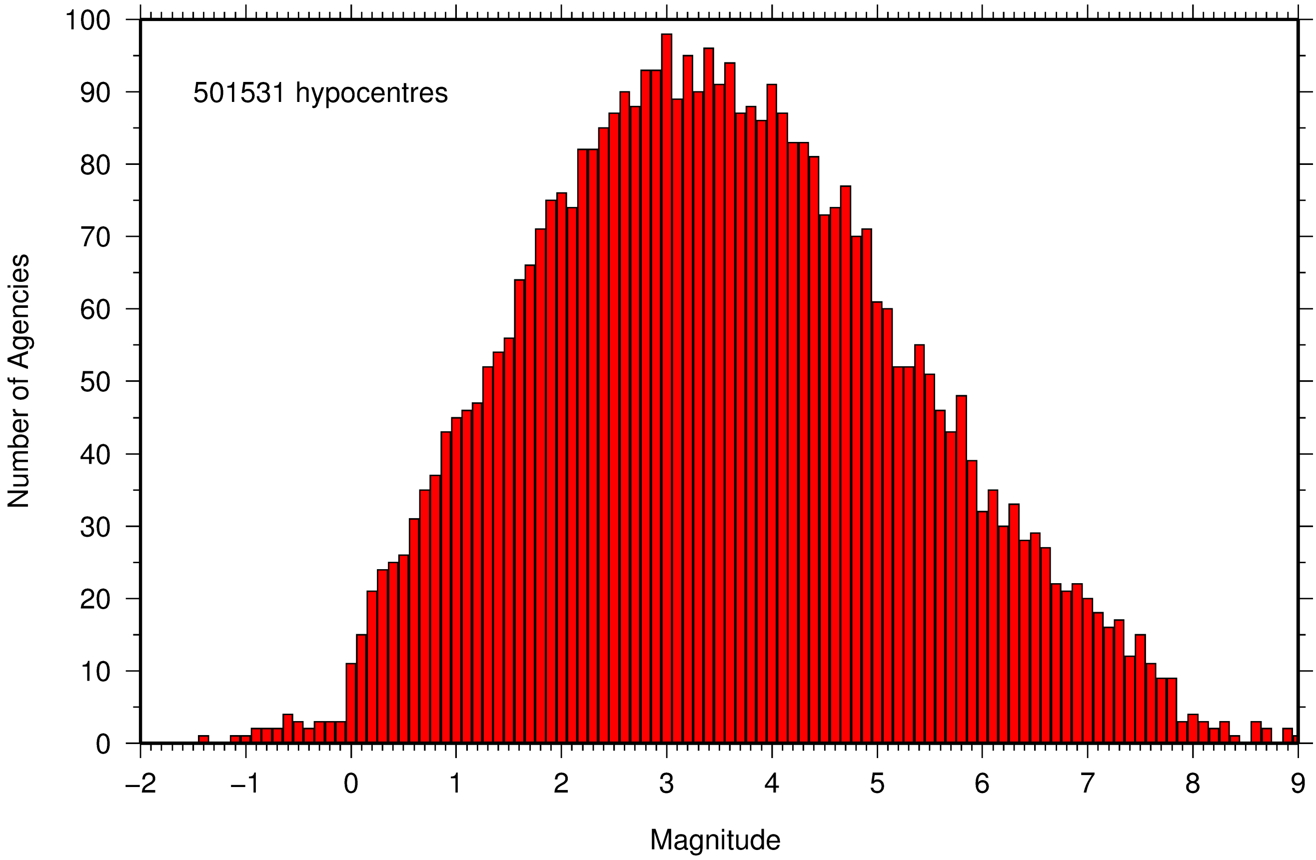

Figure 8.11: *Histogram showing the number of agencies that reported network magnitude values. All magnitude types are included.*

8.6 Moment Tensor Solutions

The ISC Bulletin publishes moment tensor solutions, which are reported to the ISC by other agencies. The collection of moment tensor solutions is summarised in Table 8.8. A histogram showing all moment tensor solutions collected throughout the ISC history is shown in Figure 8.12. Several moment tensor solutions from different authors and different moment tensor solutions calculated by different methods from the same agency may be present for the same event.

The number of moment tensors for this summary period, reported by each agency, is shown in Table 8.9. The moment tensor solutions are plotted in Figure 8.13.

Table 8.8: Summary of reports containing moment tensor solutions.

Reports with Moment Tensors	12
Total moment tensors received	5042
Agencies reporting moment tensors	8

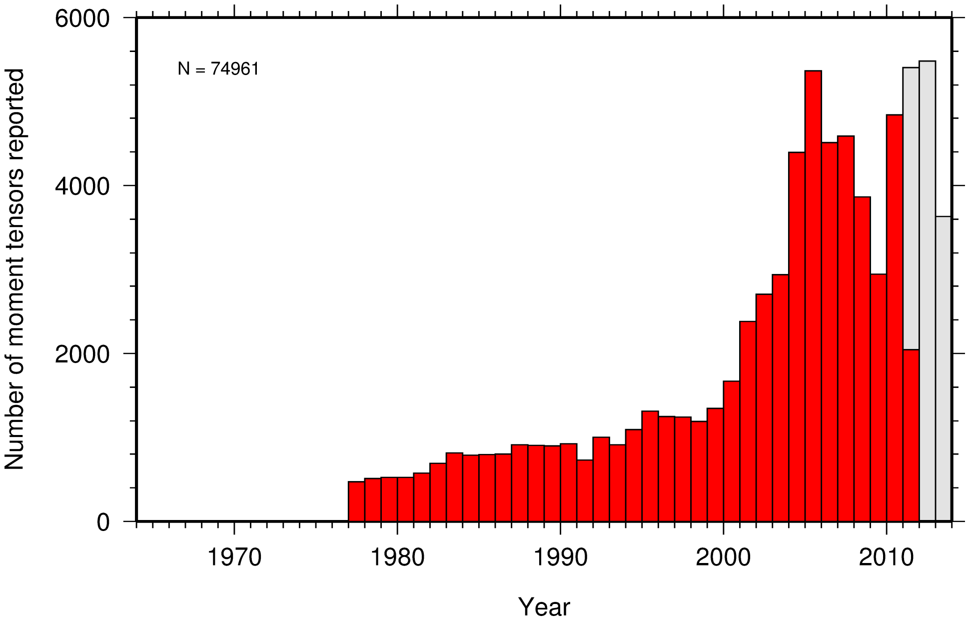

Figure 8.12: Histogram showing the number of moment tensors reported to the ISC since 1964. The regions in grey represent data that are still being actively collected.

Table 8.9: Summary of moment tensor solutions in the ISC Bulletin reported by each agency.

Agency	Number of moment tensor solutions
GCMT	957
NEIC	364
NIED	253
BRK	38
OTT	12
SLM	8
PAS	1
ROM	1

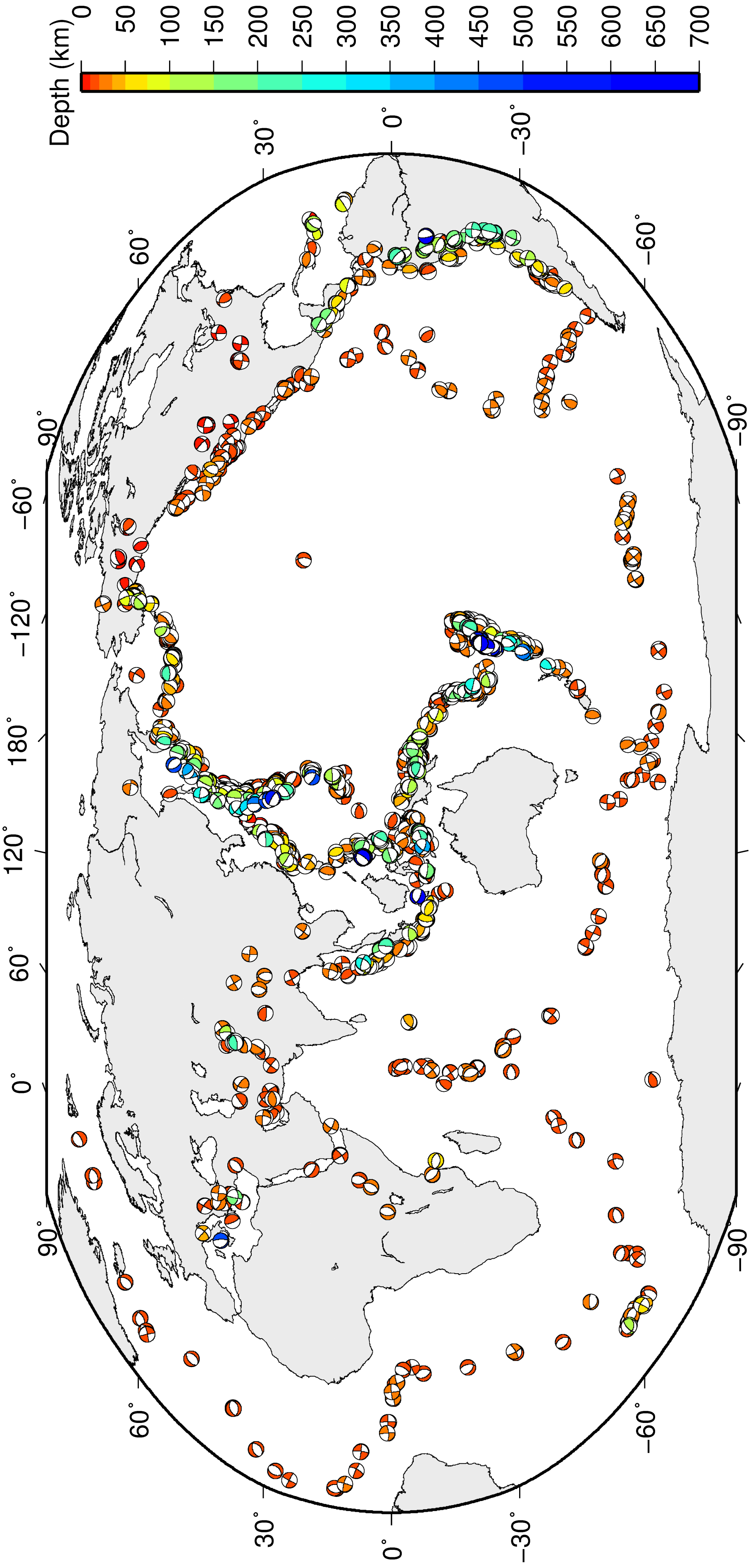

ISC Bulletin: **1634** focal mechanism solutions for **1257** events from **2010/07/01** to **2010/12/31**

Figure 8.13: *Map of all moment tensor solutions in the ISC Bulletin for this summary period.*

8.7 Timing of Data Collection

Here we present the timing of reports to the ISC. Please note, this does not include provisional alerts, which are replaced at a later stage. Instead, it reflects the final data sent to the ISC. The absolute timing of all hypocentre reports, regardless of magnitude, is shown in Figure 8.14. In Figure 8.15 the reports are grouped into one of six categories - from within three days of an event origin time, to over one year. The histogram shows the distribution with magnitude (for hypocentres where a network magnitude was reported) for each category, whilst the map shows the geographic distribution of the reported hypocentres.

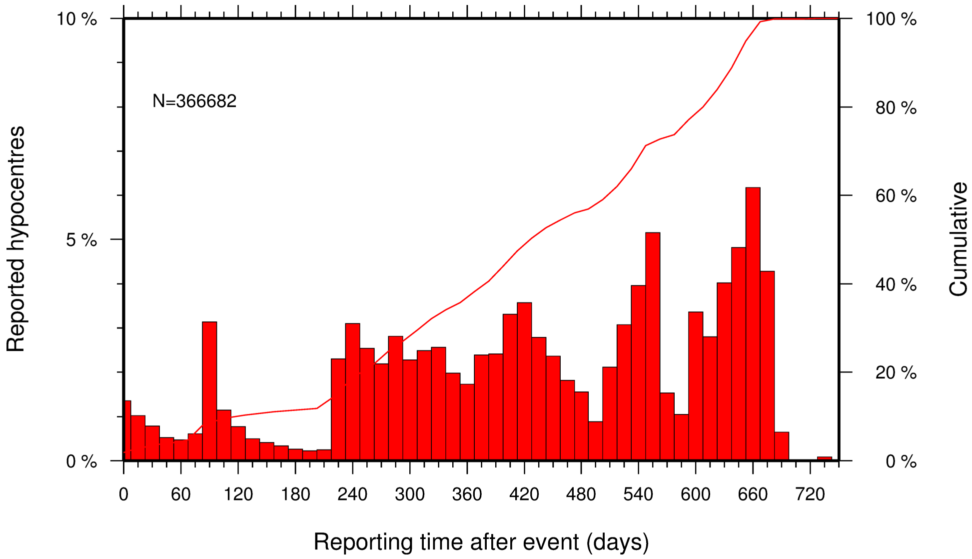

Figure 8.14: *Histogram showing the timing of final reports of the hypocentres (total of N) to the ISC. The cumulative frequency is shown by the solid line.*

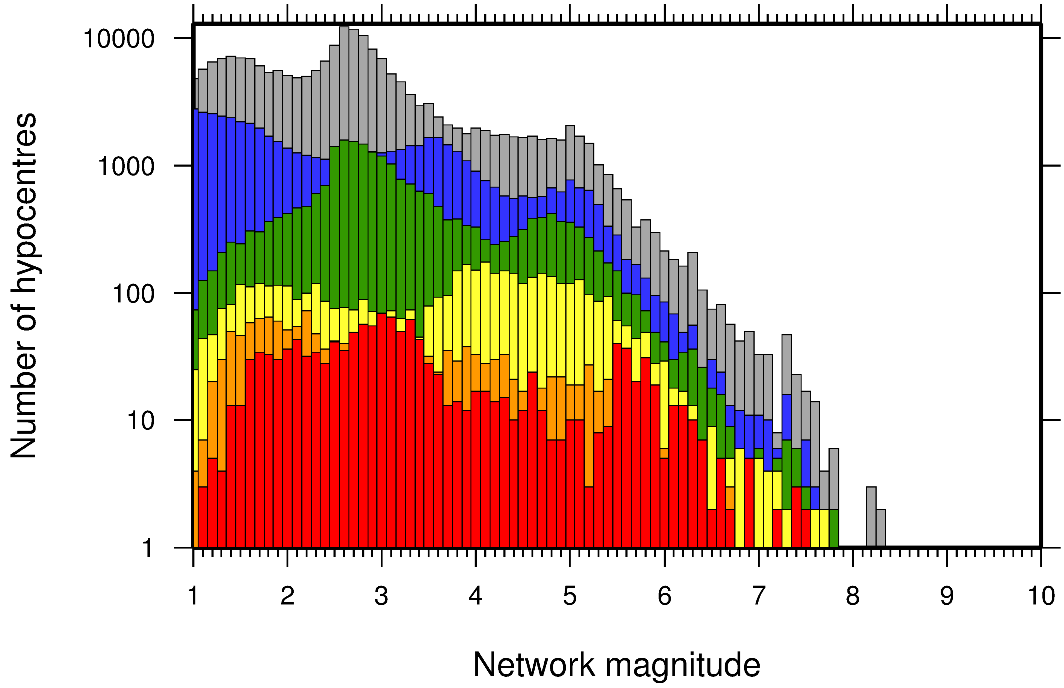

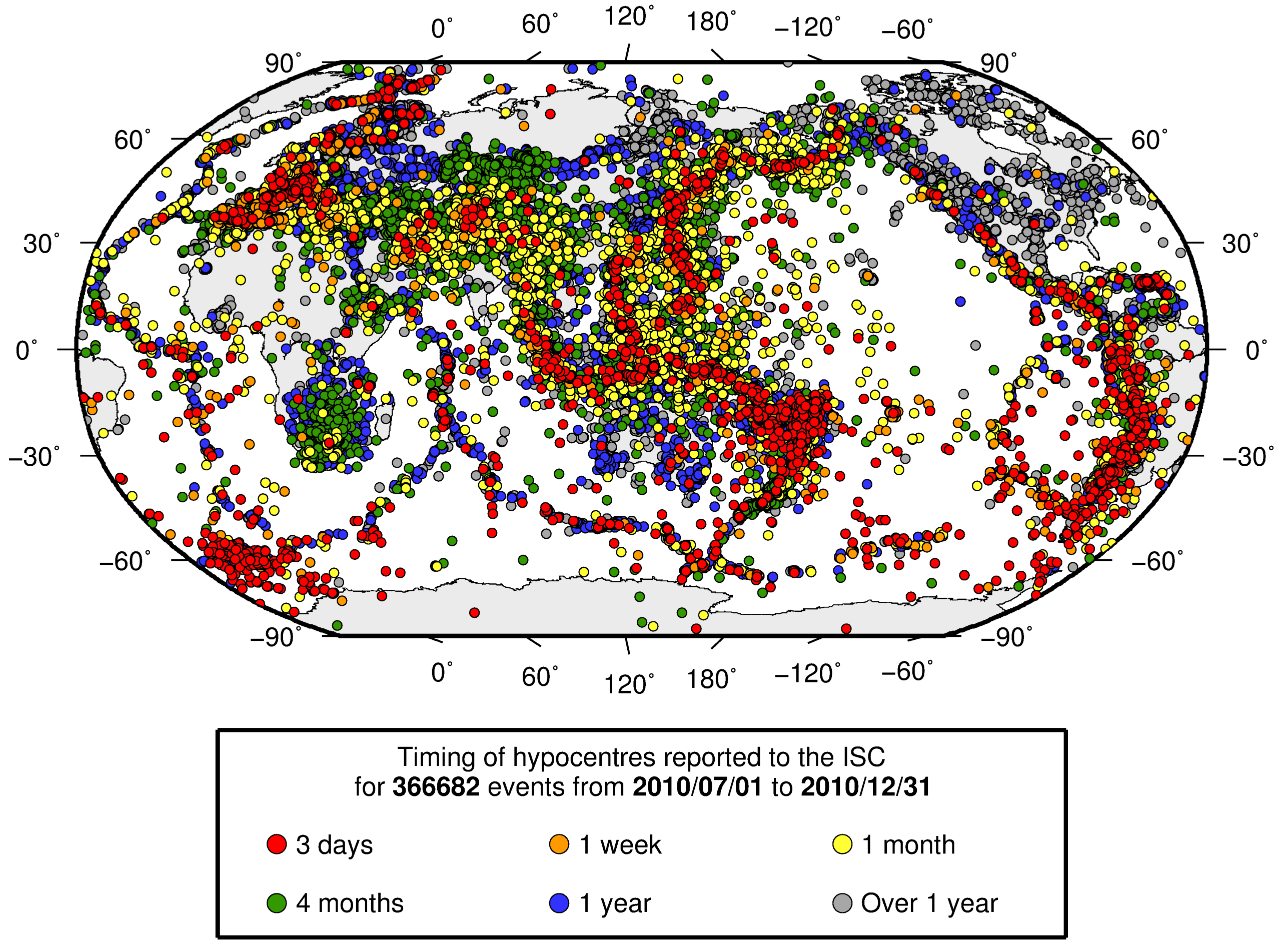

Figure 8.15: *Timing of hypocentres reported to the ISC. The colours show the time after the origin time that the corresponding hypocentre was reported. The histogram shows the distribution with magnitude. If more than one network magnitude was reported, preference was given to a value of M_W followed by M_S, m_b and M_L respectively; all reported hypocentres are included on the map. Note: early reported hypocentres are plotted over later reported hypocentres, on both the map and histogram.*

9

Overview of the ISC Bulletin

This section provides an overview of the seismic event data in the ISC Bulletin. We indicate the differences between all ISC events and those ISC events that are reviewed or located. We describe the wealth of phase arrivals and phase amplitudes and periods observed at seismic stations worldwide, reported in the ISC Bulletin and often used in the ISC location and magnitude determination. Finally, we make some comparisons of the ISC magnitudes with those reported by other agencies, and discuss magnitude completeness of the ISC Bulletin.

9.1 Events

Altogether 183,103 events occurred during the summary period between 2010/07/01 and 2010/12/31. Some 90% (165,755) of the events were identified as earthquakes, the rest (17,348) were of anthropogenic (rockbursts, induced events, mine and other chemical explosions) origin. As discussed in Section 3.3.3 of the January-June 2010 Bulletin Summary, typically about 20% of the events are selected for ISC review, and about half of the events selected for review are located by the ISC. In this summary period 17% of the events were reviewed and 10% of the events were located by the ISC. For events that are not located by the ISC, the prime hypocentre is identified according to the rules described in Section 3.3.1 of the January-June 2010 Bulletin Summary.

Out of the 5,200,000 reported seismic phase arrivals as many as 54% correspond to ISC-reviewed events, and 50% of the reported observations are associated to events selected for ISC location. Note that all large events are reviewed and located by the ISC. Since large events are globally recorded and thus reported by stations worldwide, they will provide the bulk of observations. This explains why only about one-fifth of the events in any given month is reviewed although the number of phases associated to reviewed events has increased nearly exponentially in the past decades.

Figure 9.1 shows the daily number of events throughout the summary period. Figure 9.2 shows the locations of the events in the ISC Bulletin; the locations of ISC-reviewed and ISC-located events are shown in Figures 9.3 and 9.4, respectively.

Figure 9.5 shows the hypocentral depth distributions of events in the ISC Bulletin for the summary period. The vast majority of events occur in the Earth's crust. Note that the peaks at 0, 10, 35 km, and at every 50 km intervals deeper than 100 km are artifacts of analyst practices of fixing the depth to a nominal value when the depth cannot be reliably resolved.

Figure 9.6 shows the depth distribution of free-depth solutions in the ISC Bulletin. The depth of a hypocentre reported to the ISC is assumed to be determined as a free parameter, unless it is explicitly labelled as a fixed-depth solution. On the other hand, as described in Section 3.4 of the January-June

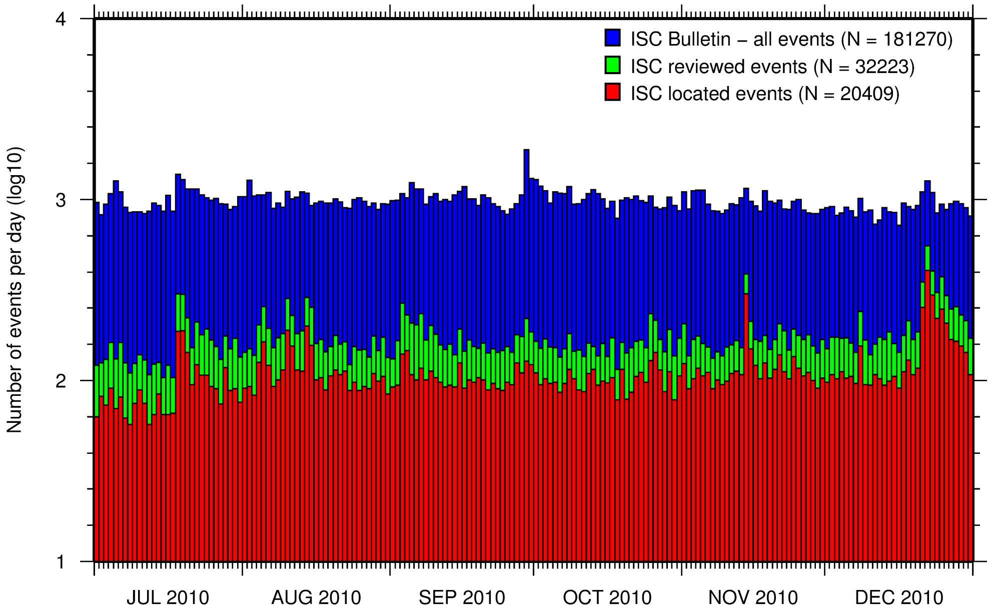

Figure 9.1: *Histogram showing the number of events in the ISC Bulletin for the current summary period. The vertical scale is logarithmic.*

2010 Bulletin Summary, the ISC locator attempts to get a free-depth solution if, and only if, there is resolution for the depth in the data, i.e. if there is a local network and/or sufficient depth-sensitive phases are reported.

Figure 9.7 shows the depth distribution of fixed-depth solutions in the ISC Bulletin. Except for a fraction of events whose depth is fixed to a shallow depth, this set constitutes mostly ISC-located events. If there is no resolution for depth in the data, the ISC locator fixes the depth to a value obtained from the ISC default depth grid file, or if no default depth exists for that location, to a nominal default depth assigned to each Flinn-Engdahl region (see details in Section 3.4 of the January-June 2010 Bulletin Summary). During the ISC review editors are inclined to accept the depth obtained from the default depth grid, but they typically change the depth of those solutions that have a nominal (10 or 35 km) depth. When doing so, they usually fix the depth to a round number, preferably divisible by 50.

For events selected for ISC location, the number of stations typically increases as arrival data reported by several agencies are grouped together and associated to the prime hypocentre. Consequently, the network geometry, characterised by the secondary azimuthal gap (the largest azimuthal gap a single station closes), is typically improved. Figure 9.8 illustrates that the secondary azimuthal gap is indeed generally smaller for ISC-located events than that for all events in the ISC Bulletin. Figure 9.9 shows the distribution of the number of associated stations. For large events the number of associated stations is usually larger for ISC-located events than for any of the reported event bulletins. On the other hand, events with just a few reporting stations are rarely selected for ISC location. The same is true for the number of defining stations (stations with at least one defining phase that were used in the location). Figure 9.10 indicates that because the reported observations from multiple agencies are associated to the prime, large ISC-located events typically have a larger number of defining stations than any of the reported event bulletins.

The formal uncertainty estimates are also typically smaller for ISC-located events. Figure 9.11 shows the

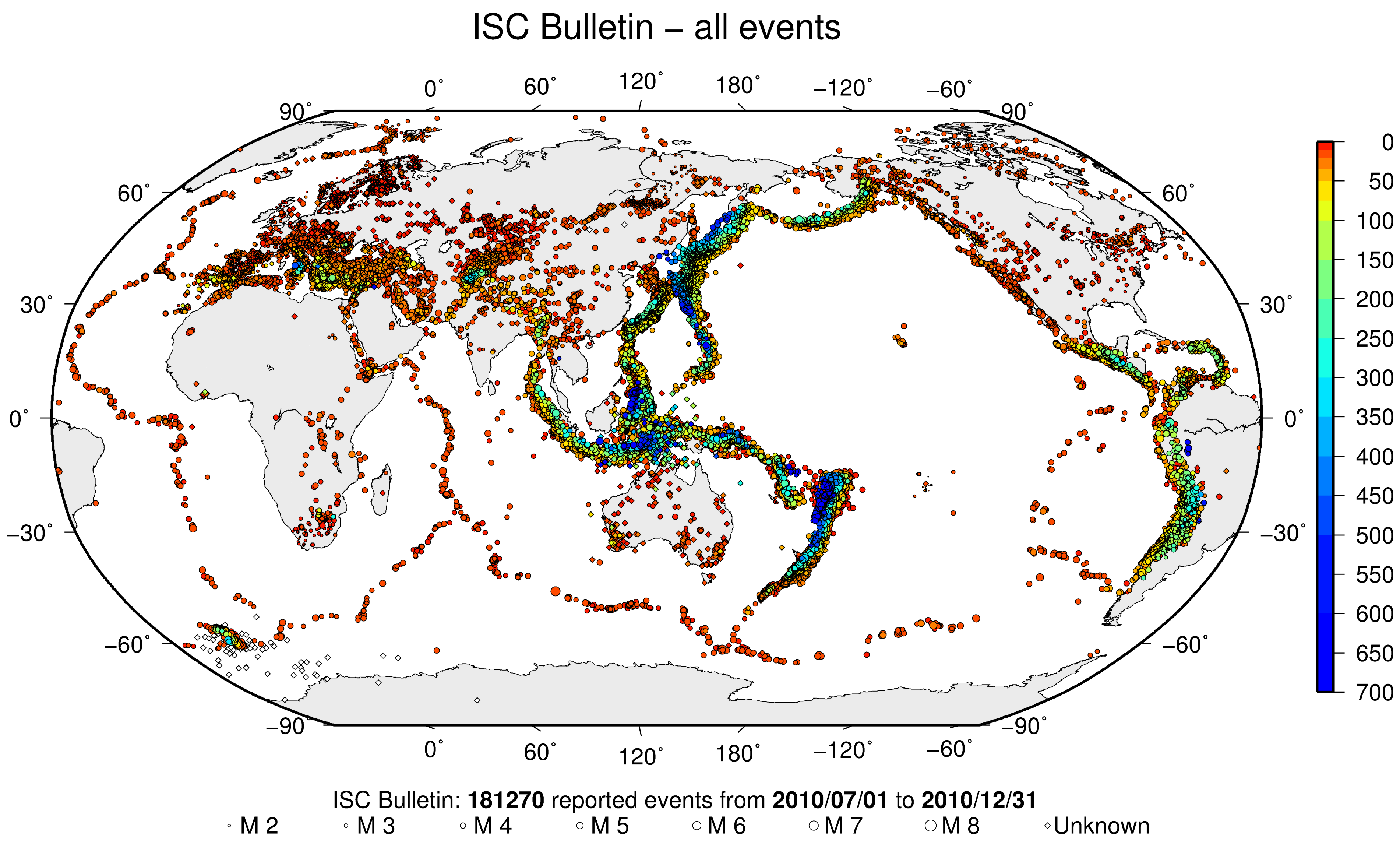

Figure 9.2: *Map of all events in the ISC Bulletin. Prime hypocentre locations are shown. Compare with Figure 8.10.*

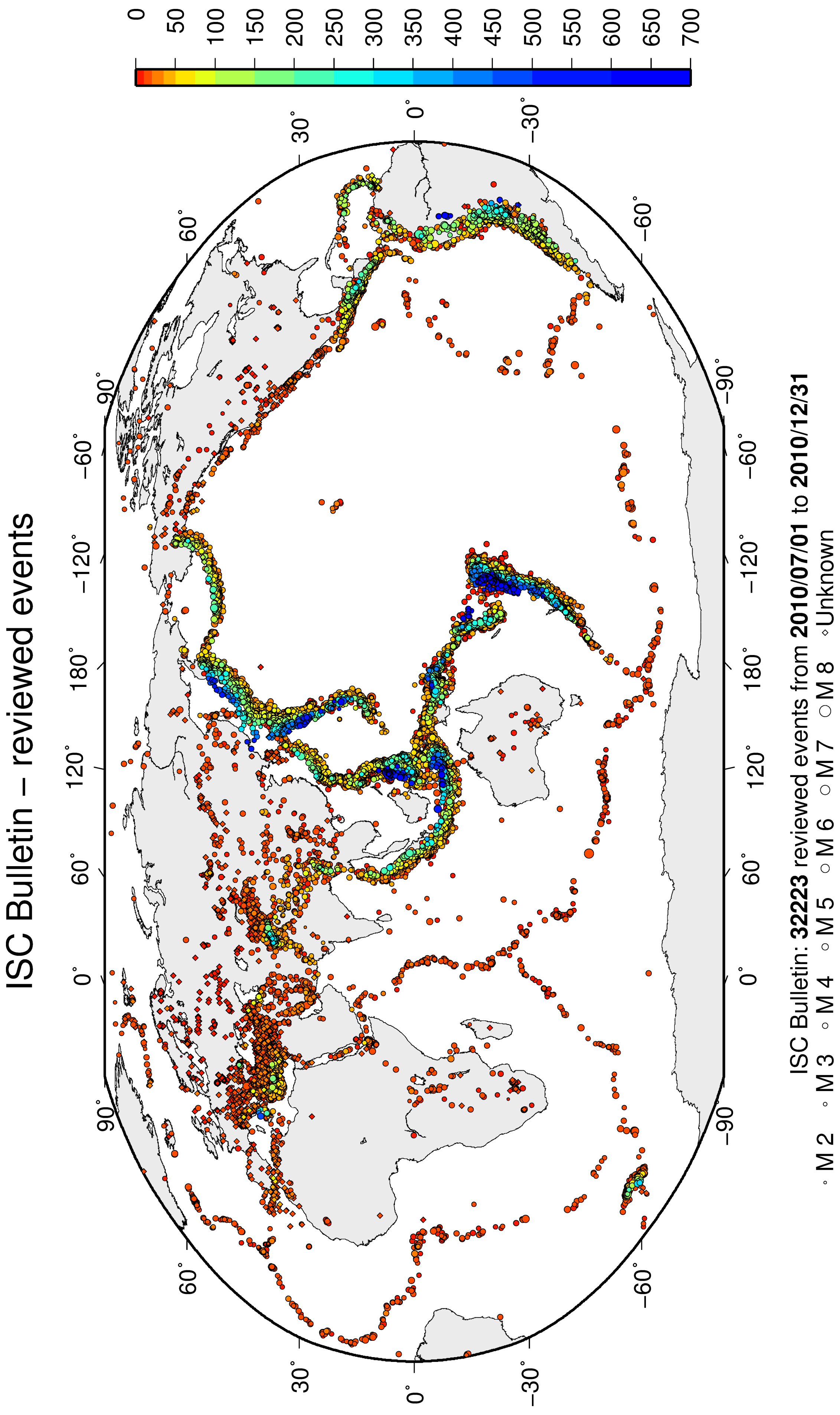

Figure 9.3: *Map of all events reviewed by the ISC for this time period. Prime hypocentre locations are shown.*

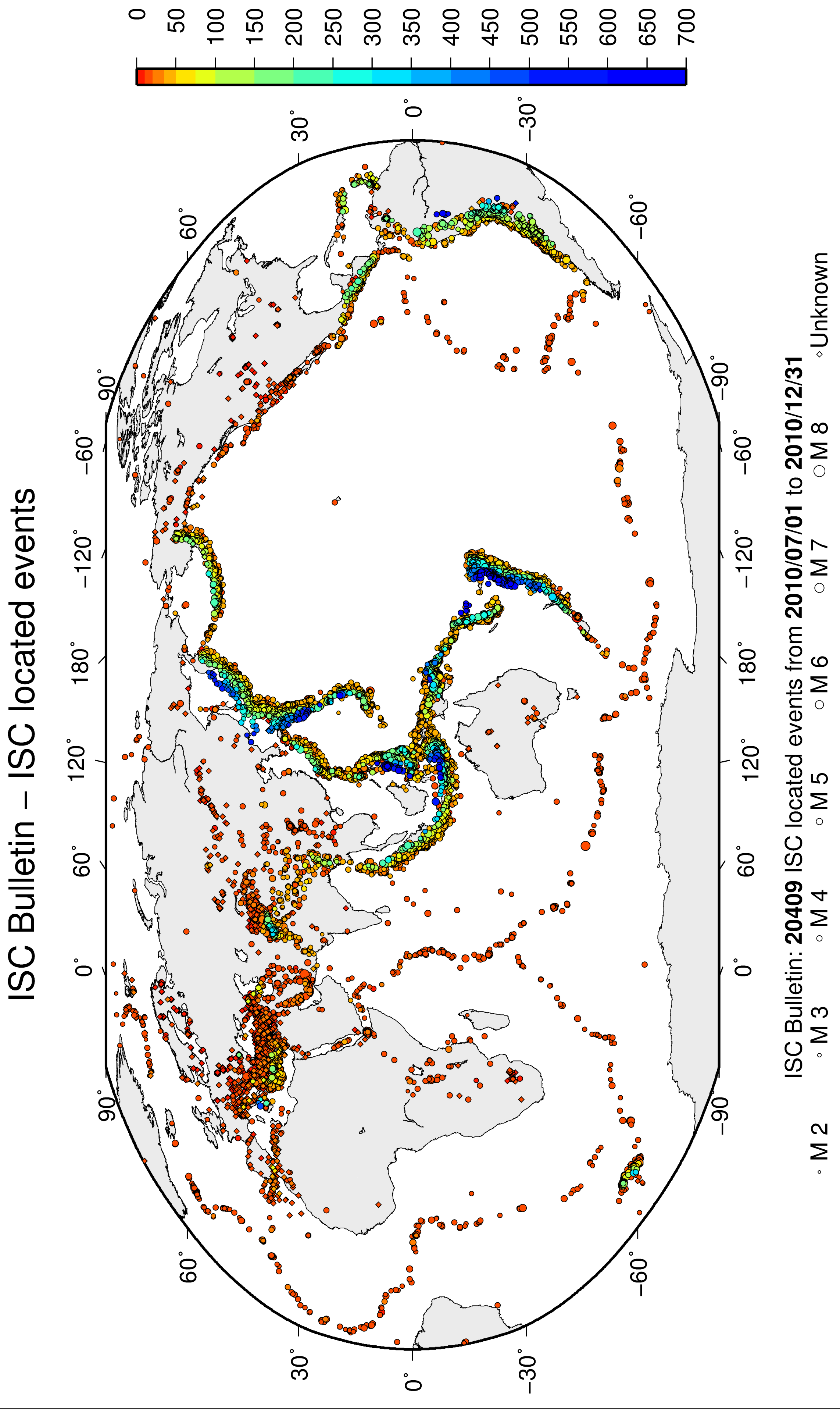

Figure 9.4: *Map of all events located by the ISC for this time period. ISC determined hypocentre locations are shown.*

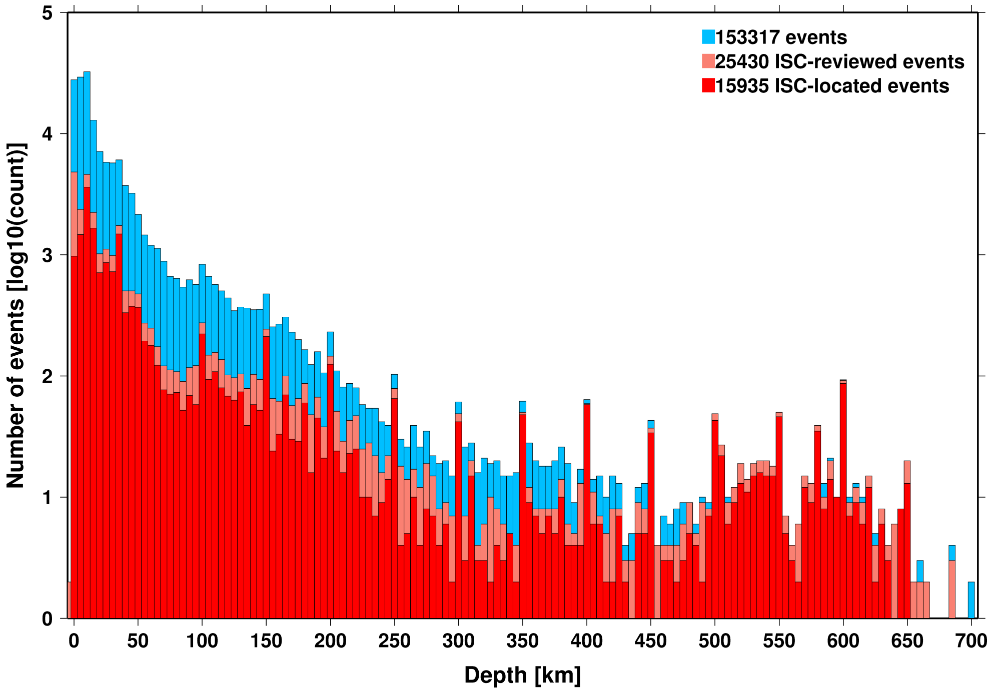

Figure 9.5: *Distribution of event depths in the ISC Bulletin (blue) and for the ISC-reviewed (pink) and the ISC-located (red) events during the summary period. All ISC-located events are reviewed, but not all reviewed events are located by the ISC. The vertical scale is logarithmic.*

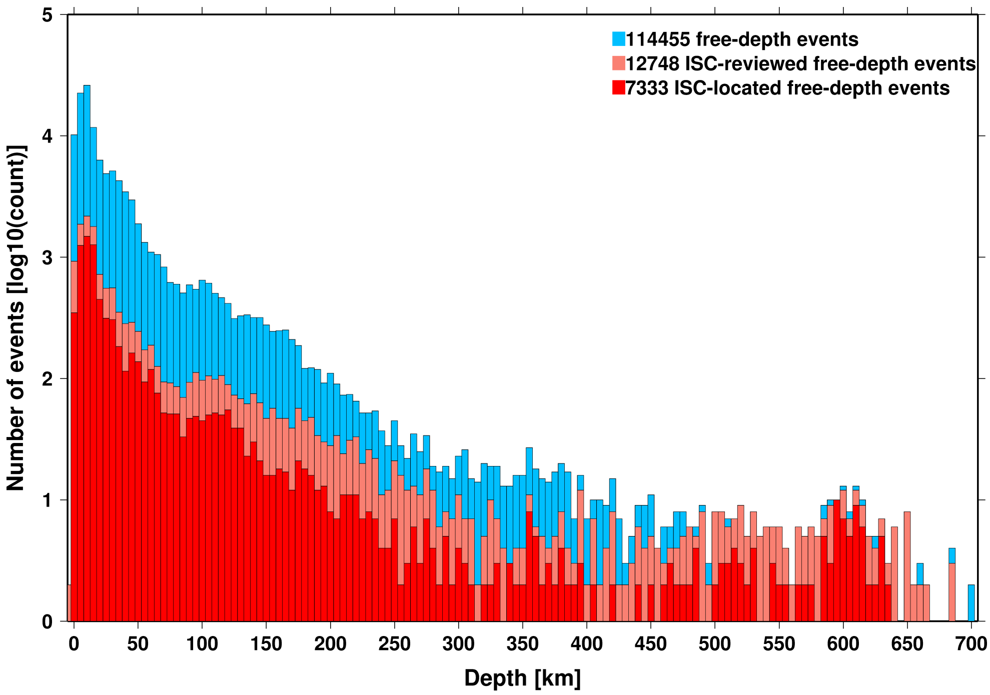

Figure 9.6: *Hypocentral depth distribution of events where the prime hypocentres are reported/located with a free-depth solution in the ISC Bulletin. The vertical scale is logarithmic.*

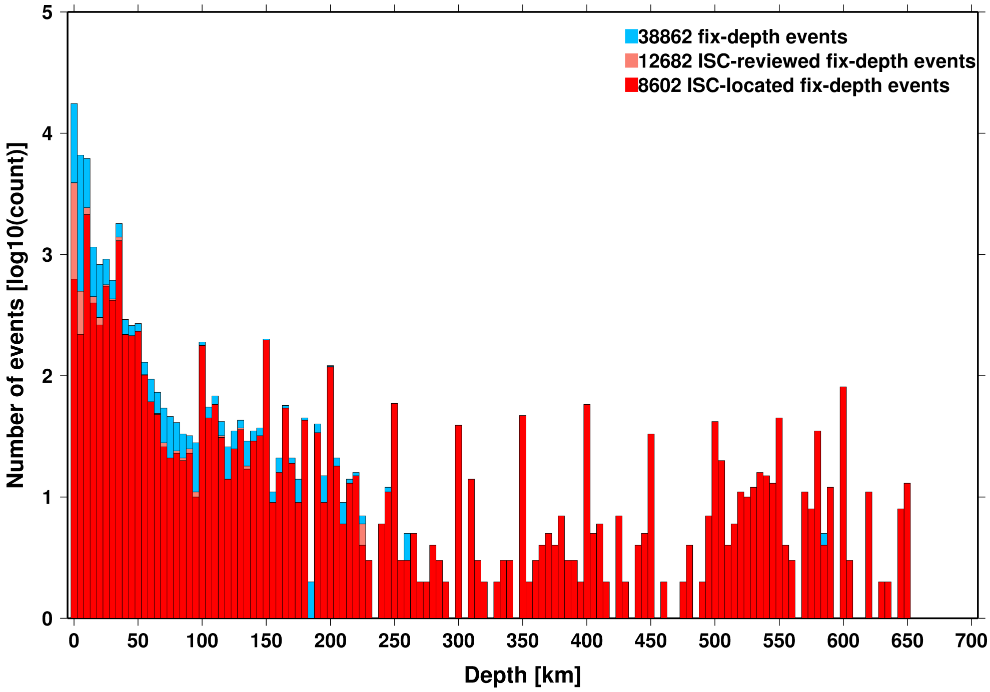

Figure 9.7: *Hypocentral depth distribution of events where the prime hypocentres are reported/located with a fixed-depth solution in the ISC Bulletin. The vertical scale is logarithmic.*

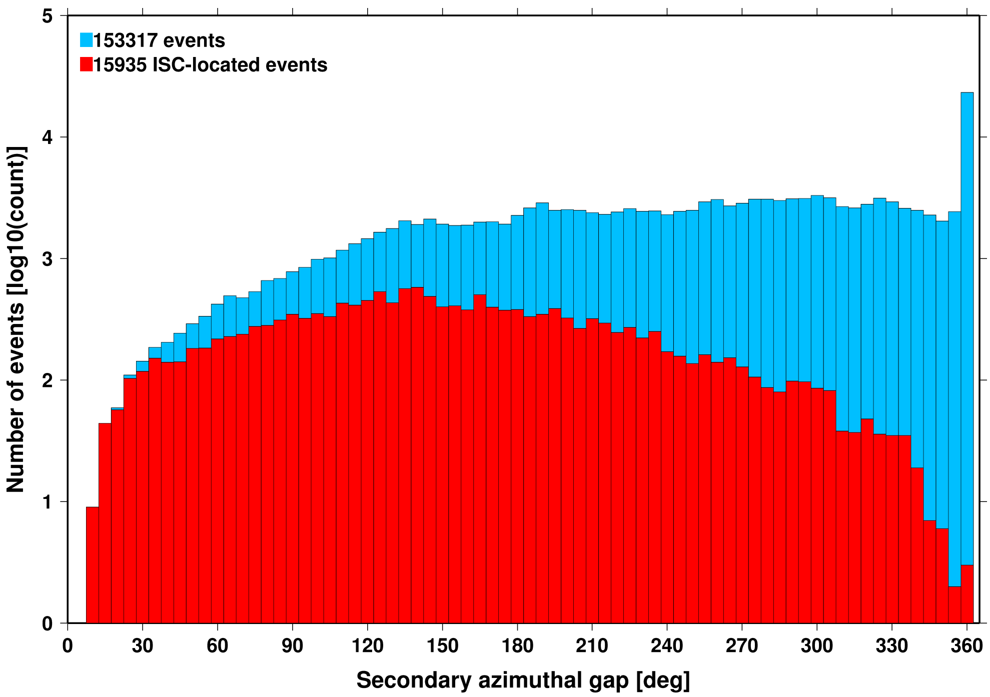

Figure 9.8: *Distribution of secondary azimuthal gap for events in the ISC Bulletin (blue) and those selected for ISC location (red). The vertical scale is logarithmic.*

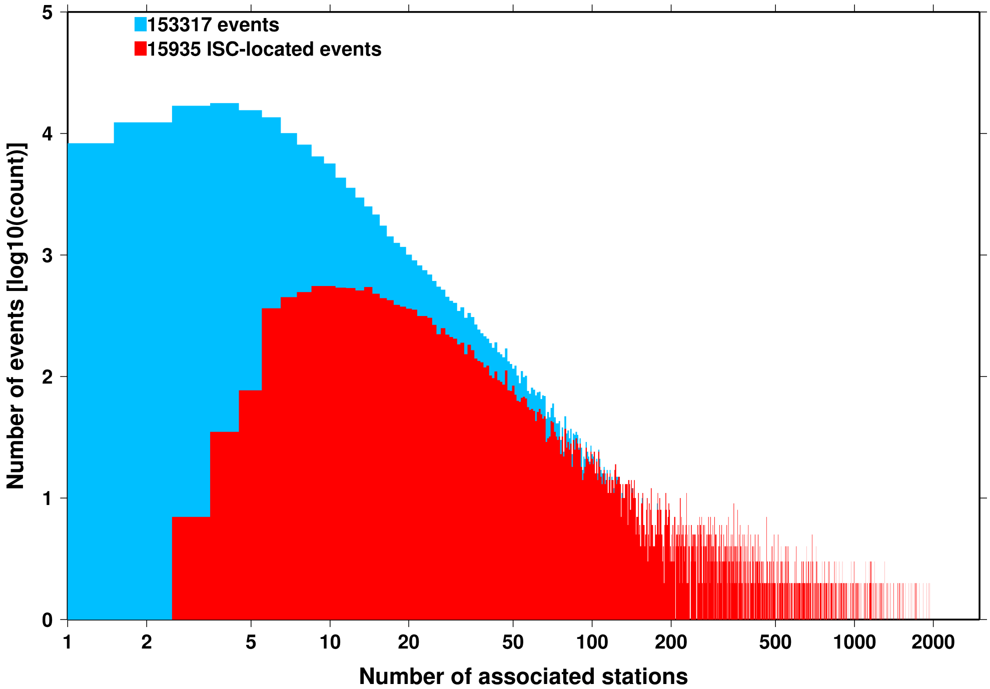

Figure 9.9: *Distribution of the number of associated stations for events in the ISC Bulletin (blue) and those selected for ISC location (red). The vertical scale is logarithmic.*

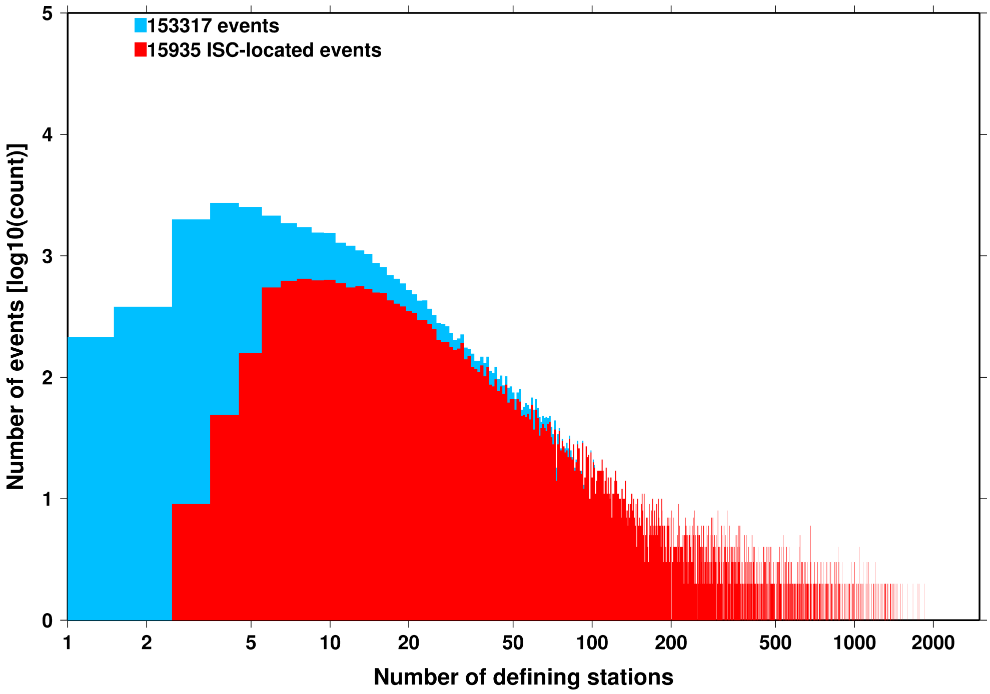

Figure 9.10: *Distribution of the number of defining stations for events in the ISC Bulletin (blue) and those selected for ISC location (red). The vertical scale is logarithmic.*

distribution of the area of the 90% confidence error ellipse for ISC-located events during the summary period. The distribution suffers from a long tail indicating a few poorly constrained event locations. Nevertheless, half of the events are characterised by an error ellipse with an area less than 203 km^2, 90% of the events have an error ellipse area less than 1,460 km^2, and 95% of the events have an error ellipse area less than 2,412 km^2.

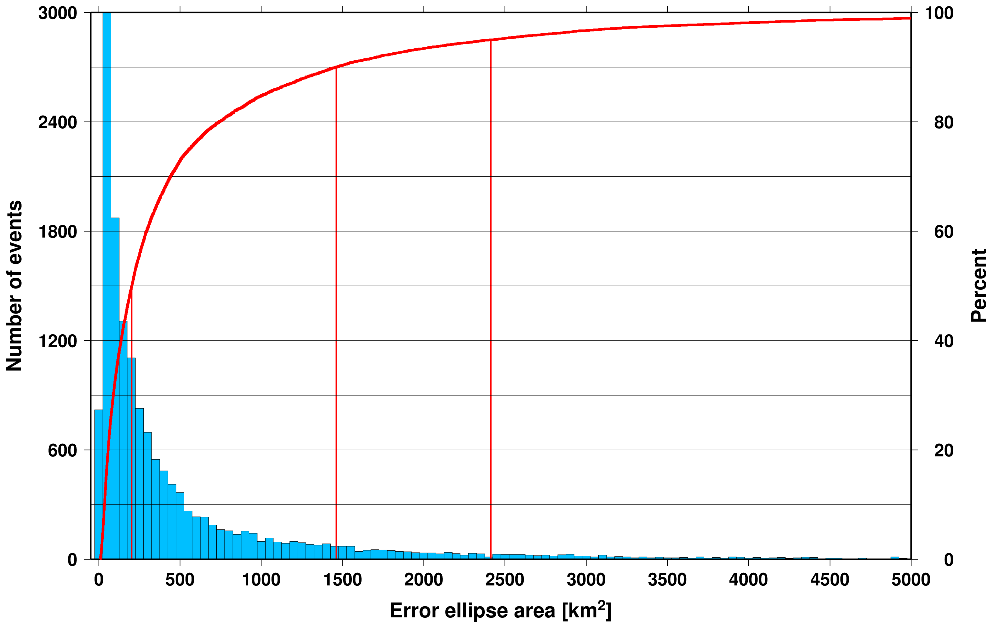

Figure 9.11: *Distribution of the area of the 90% confidence error ellipse of the ISC-located events. Vertical red lines indicate the 50th, 90th and 95th percentile values.*

Figure 9.12 shows one of the major characteristic features of the ISC location algorithm (Bondár and Storchak, 2011). Because the ISC locator accounts for correlated travel-time prediction errors due to unmodelled velocity heterogeneities along similar ray paths, the area of the 90% confidence error ellipse does not decrease indefinitely with increasing number of stations, but levels off once the information carried by the network geometry is exhausted, thus providing more realistic uncertainty estimates.

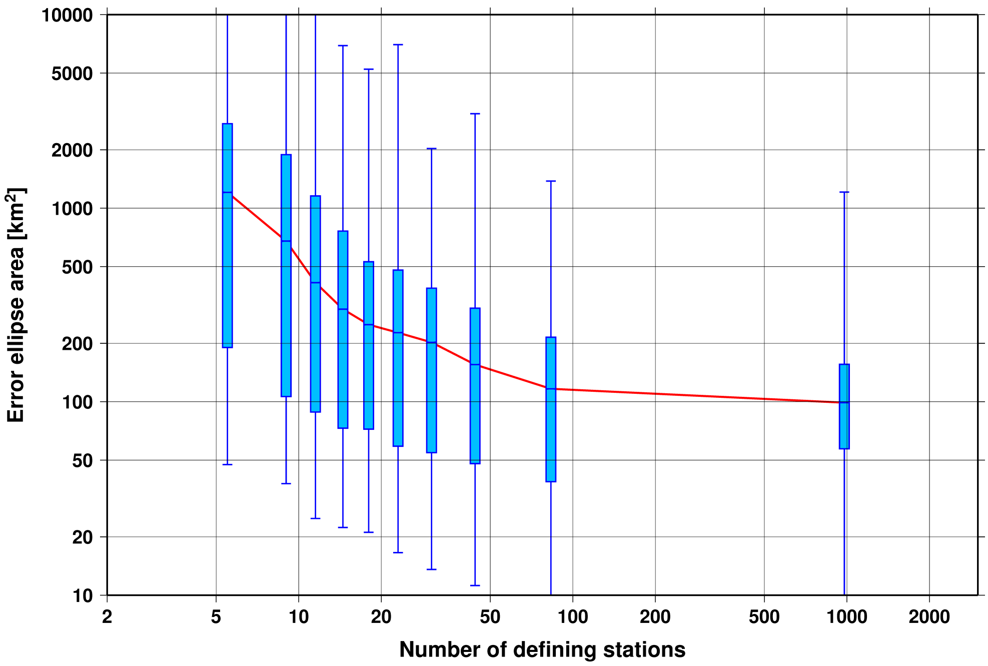

Figure 9.12: *Box-and-whisker plot of the area of the 90% confidence error ellipse of the ISC-located events as a function of the number of defining stations. Each box represents one-tenth-worth of the total number of data. The red line indicates the median 90% confidence error ellipse area.*

9.2 Seismic Phases and Travel-Time Residuals

The number of phases that are associated to events over the summary period in the ISC Bulletin is shown in Figure 9.13. Phase types and their total number in the ISC Bulletin is shown in the Appendix, Table 11.2. A summary of phase types is indicated in Figure 9.14.

In computing ISC locations, the current (for events since 2009) ISC location algorithm (*Bondár and Storchak*, 2011) uses all *ak135* phases where possible. Within the Bulletin, the phases that contribute to an ISC location are labelled as *time defining*. In this section, we summarise these time defining phases.

In Figure 9.15, the number of defining phases is shown in a histogram over the summary period. Each defining phase is listed in Table 9.1, which also provides a summary of the number of defining phases per event. A pie chart showing the proportion of defining phases is shown in Figure 9.16. Figure 9.17 shows travel times of seismic waves. The distribution of residuals for these defining phases is shown for the top five phases in Figures 9.18 through 9.22.

Table 9.1: *Numbers of 'time defining' phases (N) within the ISC Bulletin for 20409 ISC located events.*

Phase	Number of 'defining' phases	Number of events	Max per event	Median per event
P	868802	13853	2301	10
Pn	410904	18202	862	10
Sn	125785	15622	203	4
Pg	86299	7665	193	8
PKPdf	81047	5233	877	2
Pb	74192	8894	132	5
Sg	64837	7337	134	6
Sb	53942	8857	87	4
S	36378	3557	240	4
PKPbc	34527	4924	310	2
pP	22174	2357	242	4
PKPab	18900	3390	389	1

Table 9.1: *(continued)*

Phase	Number of 'defining' phases	Number of events	Max per event	Median per event
PcP	15872	3865	88	2
Pdif	15738	1136	590	2
PKiKP	13726	1123	501	2
PP	11908	1934	222	3
sP	7764	1521	148	4
ScP	7467	1510	425	2
SS	6490	1684	45	2
sS	3579	1089	17	2
PKKPbc	3096	445	186	2
SKSac	2813	702	87	2
ScS	2022	956	55	1
PnPn	1830	846	13	2
pPKPdf	1821	469	64	2
SnSn	1514	746	10	1
SKPbc	1302	313	81	2
PKKPab	997	235	119	1
PcS	728	518	5	1
SKKSac	695	401	17	1
SKiKP	693	339	85	1
P'P'df	632	132	49	2
SKSdf	624	320	17	1
PKKPdf	575	214	33	1
PKSdf	513	303	15	1
PS	501	166	26	1
pPKPbc	381	196	14	1
SKPab	375	168	46	1
SP	313	84	24	2
Sdif	247	114	23	1
PnS	237	140	11	1
pPKPab	201	93	16	1
SKPdf	188	63	38	1
SKKPbc	85	32	10	2
pPKiKP	58	26	10	1
SPn	37	25	6	1
sPKPdf	28	19	3	1
pPdif	26	8	8	3
pwP	26	20	4	1
P'P'bc	24	16	3	1
PKSbc	18	9	9	1
SKKSdf	17	15	2	1
S'S'ac	16	4	9	3
SKKPab	15	9	4	1
PbPb	15	14	2	1
P'P'ab	12	8	3	1
SbSb	12	10	2	1
SKKPdf	10	6	4	1
sPKPbc	9	9	1	1
sPKPab	9	6	4	1
pPn	7	6	2	1
PKSab	7	3	5	1
sPKiKP	4	4	1	1
pS	4	4	1	1
sPn	2	2	1	1
sSdif	2	2	1	1
PKKSdf	1	1	1	1
PgPg	1	1	1	1

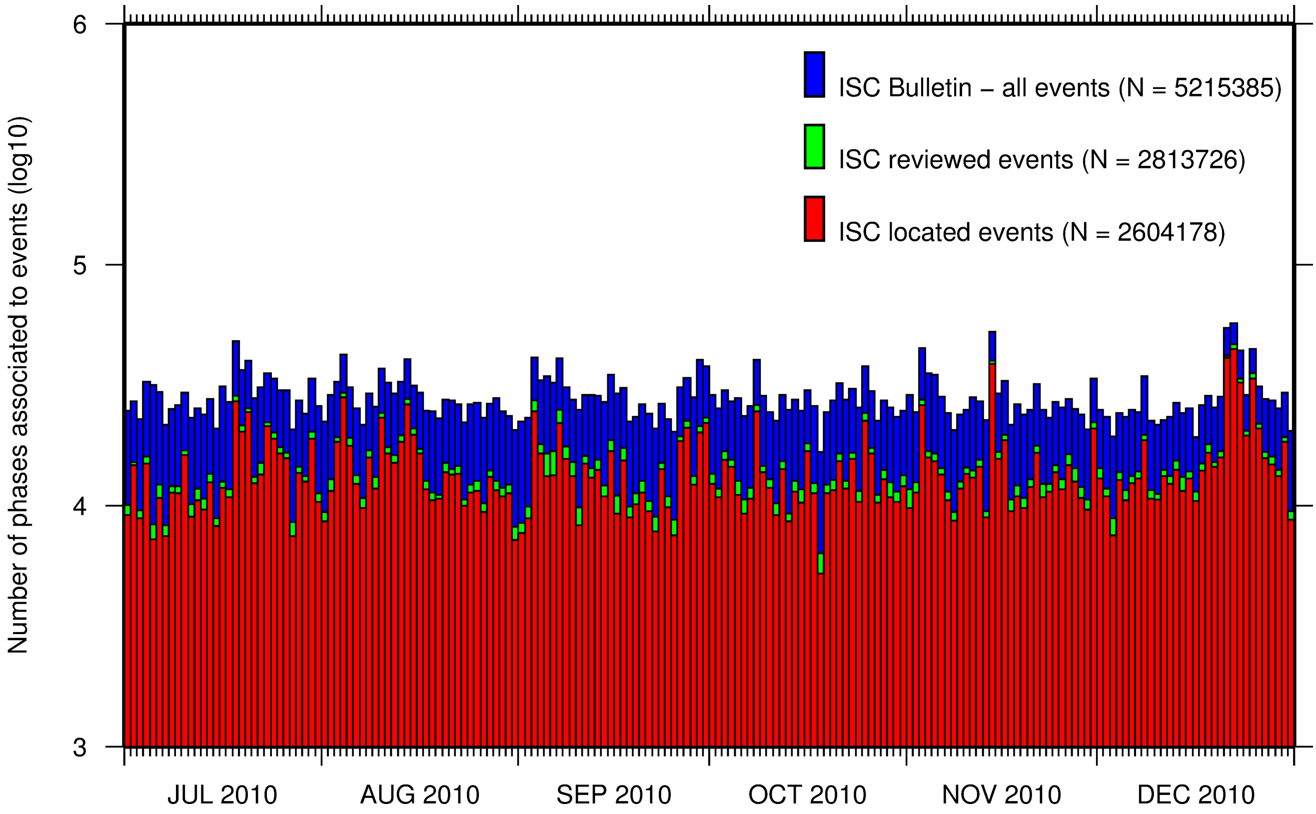

Figure 9.13: *Histogram showing the number of phases (N) that the ISC has associated to events within the ISC Bulletin for the current summary period.*

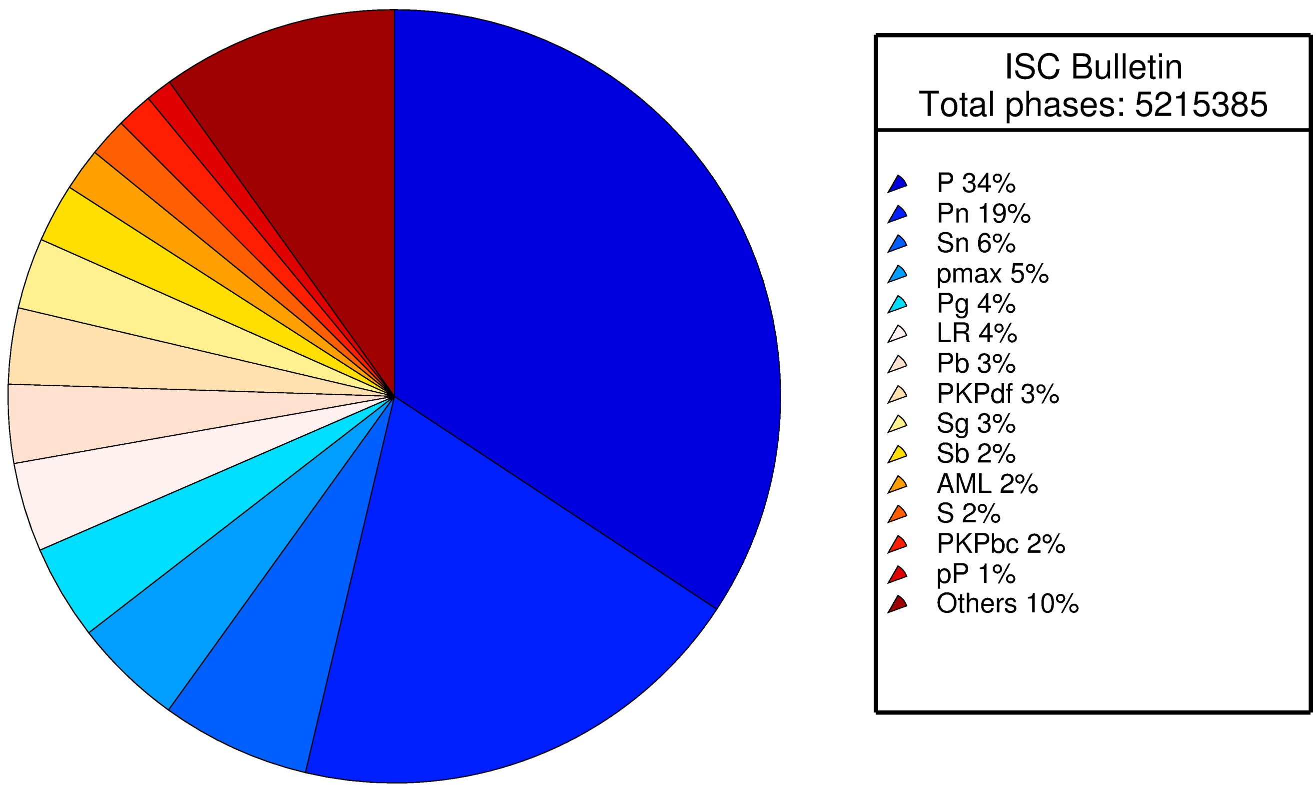

Figure 9.14: *Pie chart showing the fraction of various phase types in the ISC Bulletin for this summary period.*

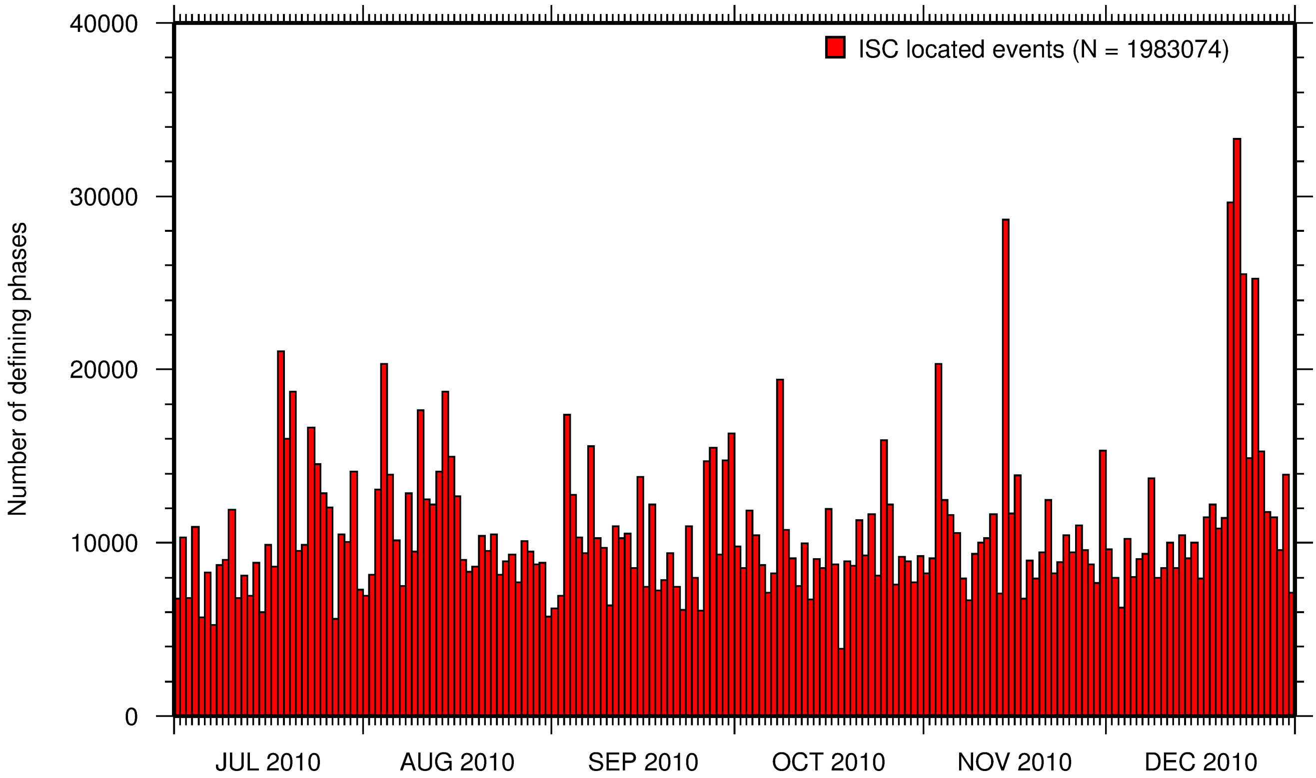

Figure 9.15: *Histogram showing the number of defining phases in the ISC Bulletin, for events located by the ISC.*

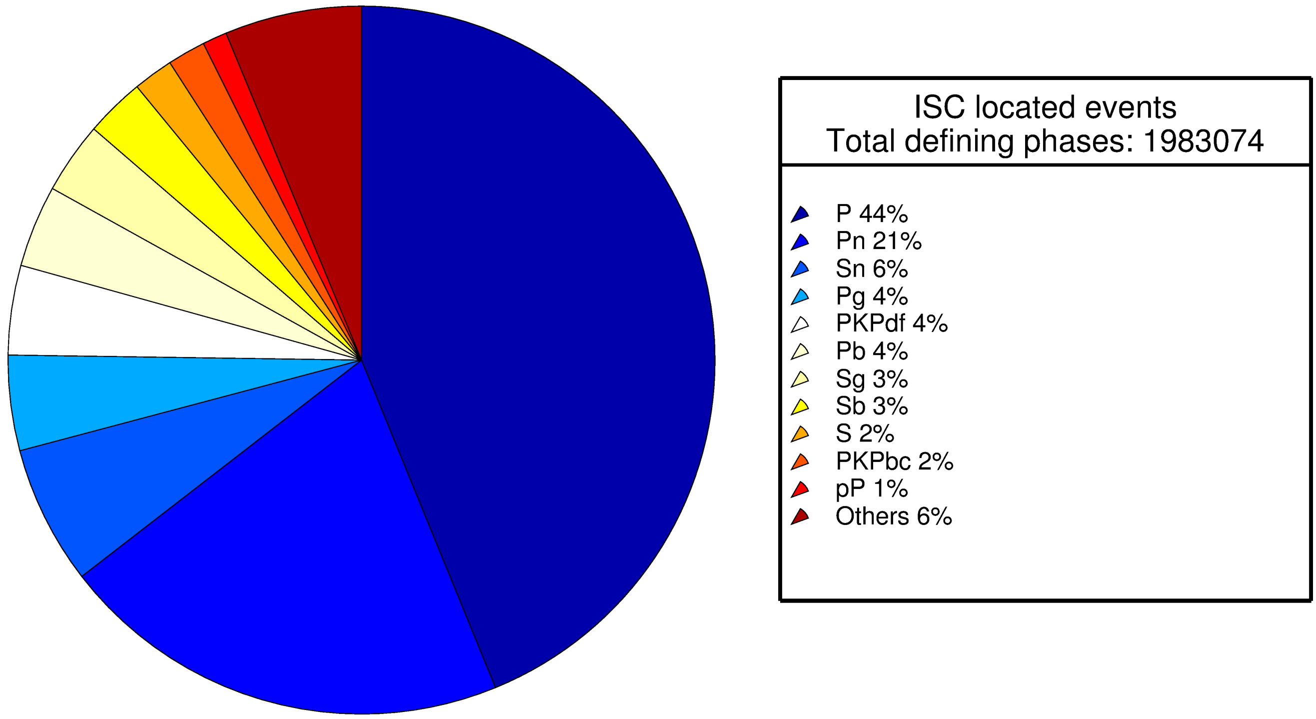

Figure 9.16: *Pie chart showing the defining phases in the ISC Bulletin, for events located by the ISC. A complete list of defining phases is shown in Table 9.1.*

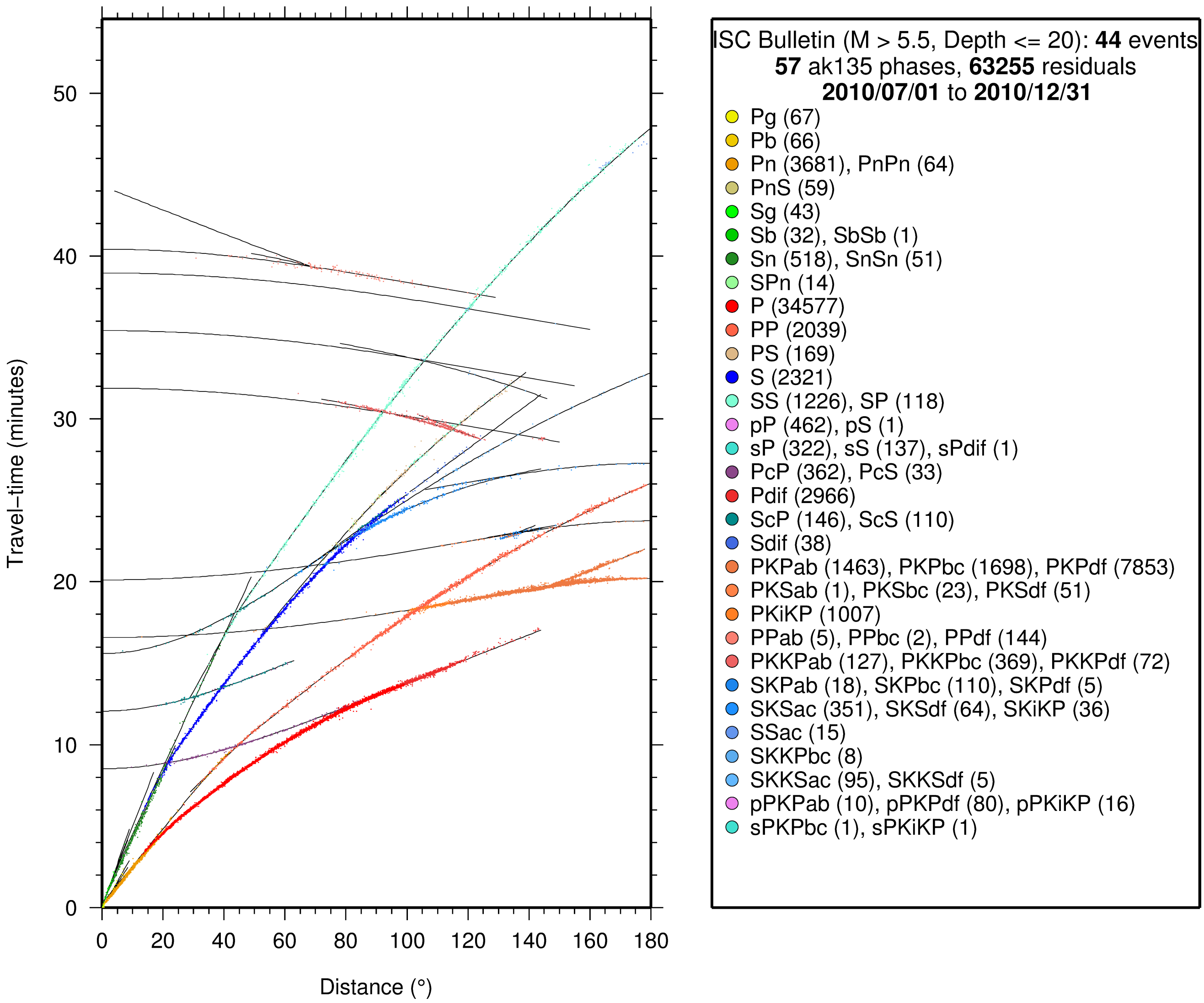

Figure 9.17: *Distribution of travel-time observations in the ISC Bulletin for events with M > 5.5 and depth less than 20 km. The travel-time observations are shown relative to a 0 km source and compared with the theoretical ak135 travel-time curves (solid lines). The legend lists the number of each phase plotted.*

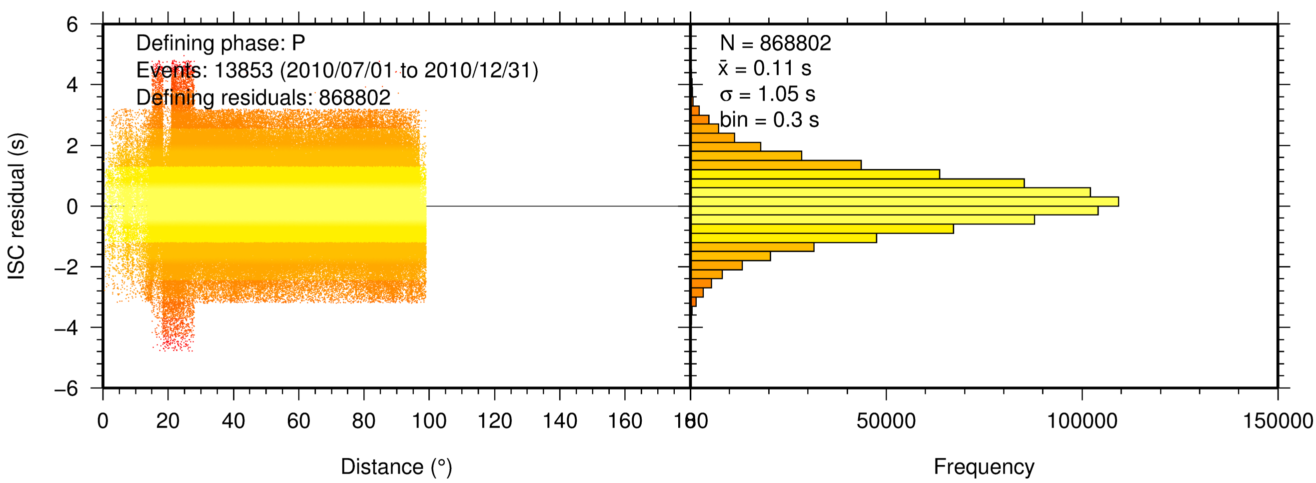

Figure 9.18: *Distribution of travel-time residuals for the defining P phases used in the computation of ISC located events in the Bulletin.*

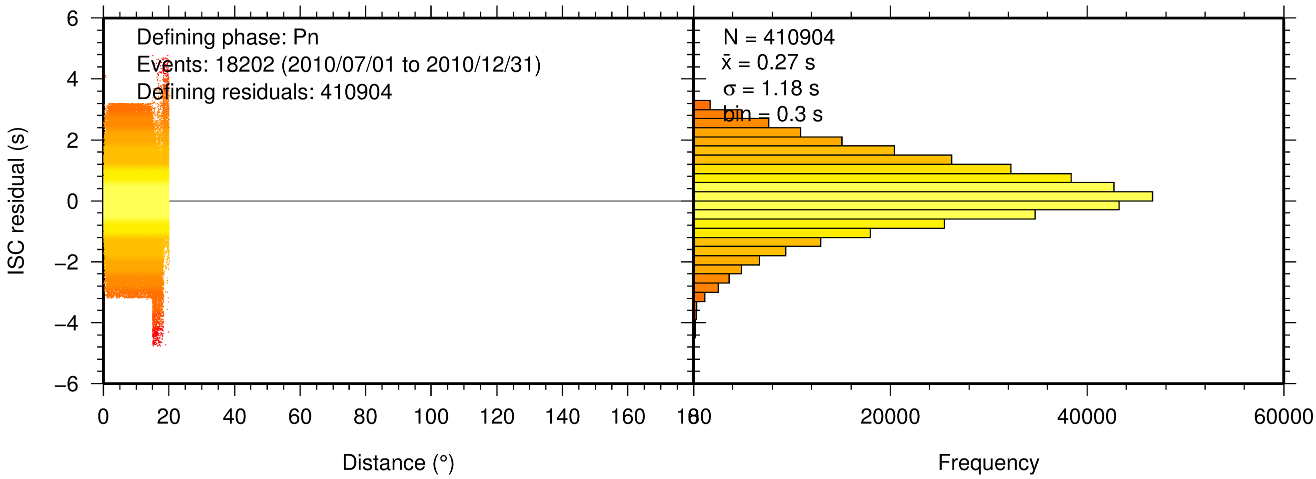

Figure 9.19: *Distribution of travel-time residuals for the defining Pn phases used in the computation of ISC located events in the Bulletin.*

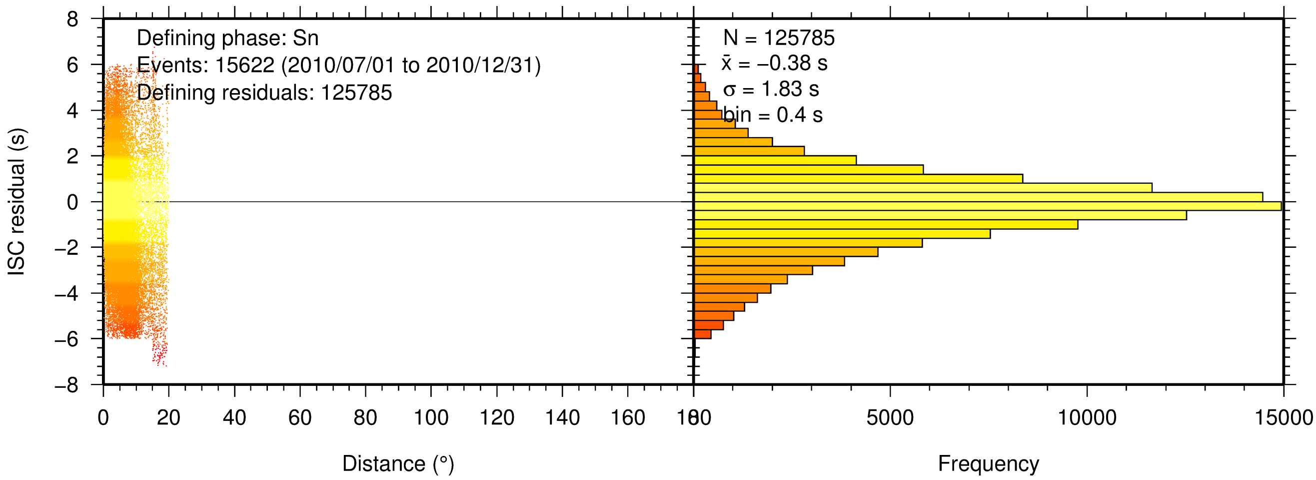

Figure 9.20: *Distribution of travel-time residuals for the defining Sn phases used in the computation of ISC located events in the Bulletin.*

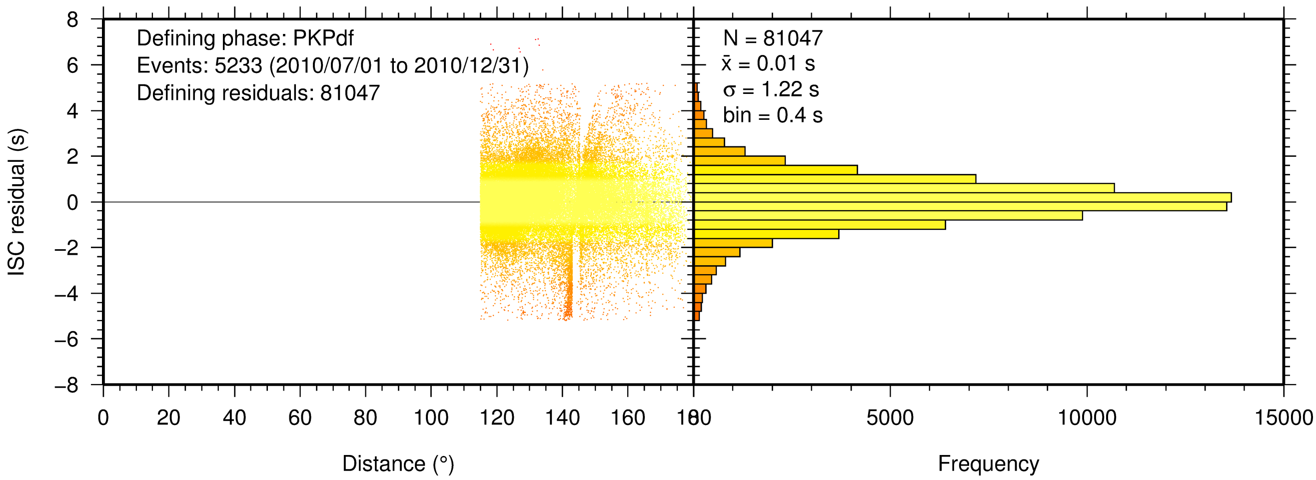

Figure 9.21: *Distribution of travel-time residuals for the defining PKPdf phases used in the computation of ISC located events in the Bulletin.*

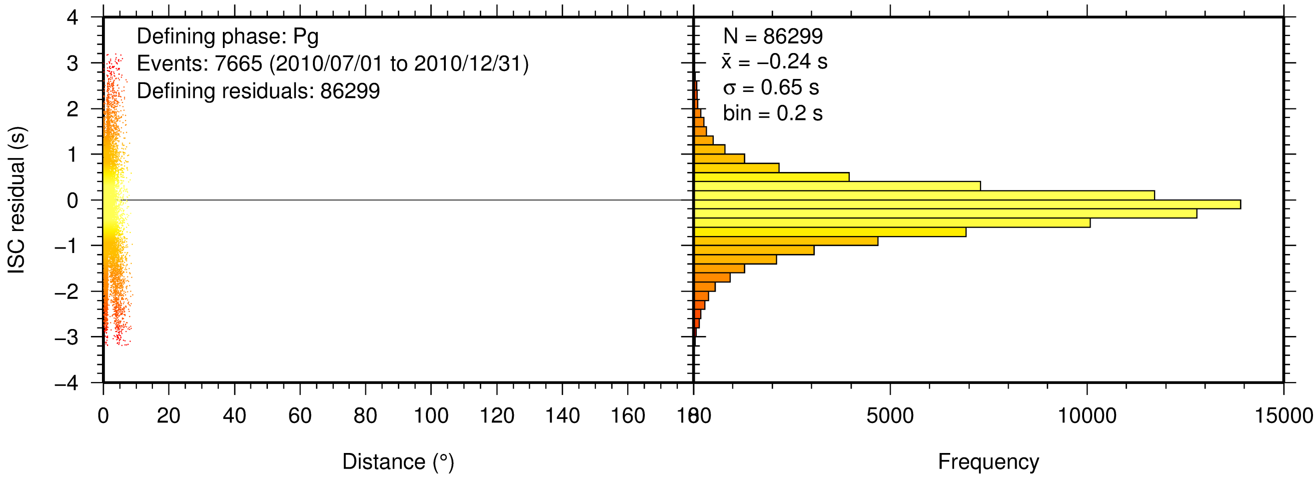

Figure 9.22: *Distribution of travel-time residuals for the defining Pg phases used in the computation of ISC located events in the Bulletin.*

9.3 Seismic Wave Amplitudes and Periods

The ISC Bulletin contains a variety of seismic wave amplitudes and periods measured by reporting agencies. For this Bulletin Summary, the total of collected amplitudes and periods is 1,571,092 (see Section 8.3). For the determination of the ISC magnitudes MS and mb, only a fraction of such data can be used. Indeed, the ISC network magnitudes are computed only for ISC located events. Here we recall the main features of the ISC procedure for MS and mb computation (see detailed description in Section 3.4 of the January-June 2010 Bulletin Summary). For each amplitude-period pair in a reading the ISC algorithm computes the magnitude (a reading can include several amplitude-period measurements) and the reading magnitude is assigned to the maximum A/T in the reading. If more than one reading magnitude is available for a station, the station magnitude is the median of the reading magnitudes. The network magnitude is computed then as the 20% alpha-trimmed median of the station magnitudes (at least three required). MS is computed for shallow earthquakes (depth $\leq$ 60 km) only and using amplitudes and periods on all three components (when available) if the period is within 10-60 s and the epicentral distance is between 20° and 160°. mb is computed also for deep earthquakes (depth down to 700 km) but only with amplitudes on the vertical component measured at periods $\leq$ 3 s in the distance range 21°-100°.

Table 9.2 is a summary of the amplitude and period data that contributed to the computation of station and ISC MS and mb network magnitudes for this Bulletin Summary.

Table 9.2: *Summary of the amplitude-period data used by the ISC Locator to compute MS and mb.*

	MS	mb
Number of amplitude-period data	97321	408278
Number of readings	93542	406882
Percentage of readings in the ISC located events with qualifying data for magnitude computation	11.7	45.0
Number of station magnitudes	85602	339933
Number of network magnitudes	3334	12495

A small percentage of the readings with qualifying data for MS and mb calculation have more than one amplitude-period pair. Notably, only 11.7% of the readings for the ISC located (shallow) events included qualifying data for MS computation, whereas for mb the percentage is much higher. This is due to the seismological practice of reporting agencies. Agencies contributing systematic reports of amplitude and period data are listed in Appendix Table 11.3. Obviously the ISC Bulletin would benefit if more agencies included surface wave amplitude-period data in their reports.

Figure 9.23 shows the distribution of the number of station magnitudes versus distance. For mb there is a significant increase in the distance range 70°-90°, whereas for MS most of the contributing stations are below 100°. The increase in number of station magnitude between 70°-90° for mb is partly due to the very dense distribution of seismic stations in North America and Europe with respect to earthquake occurring in various subduction zones around the Pacific Ocean.

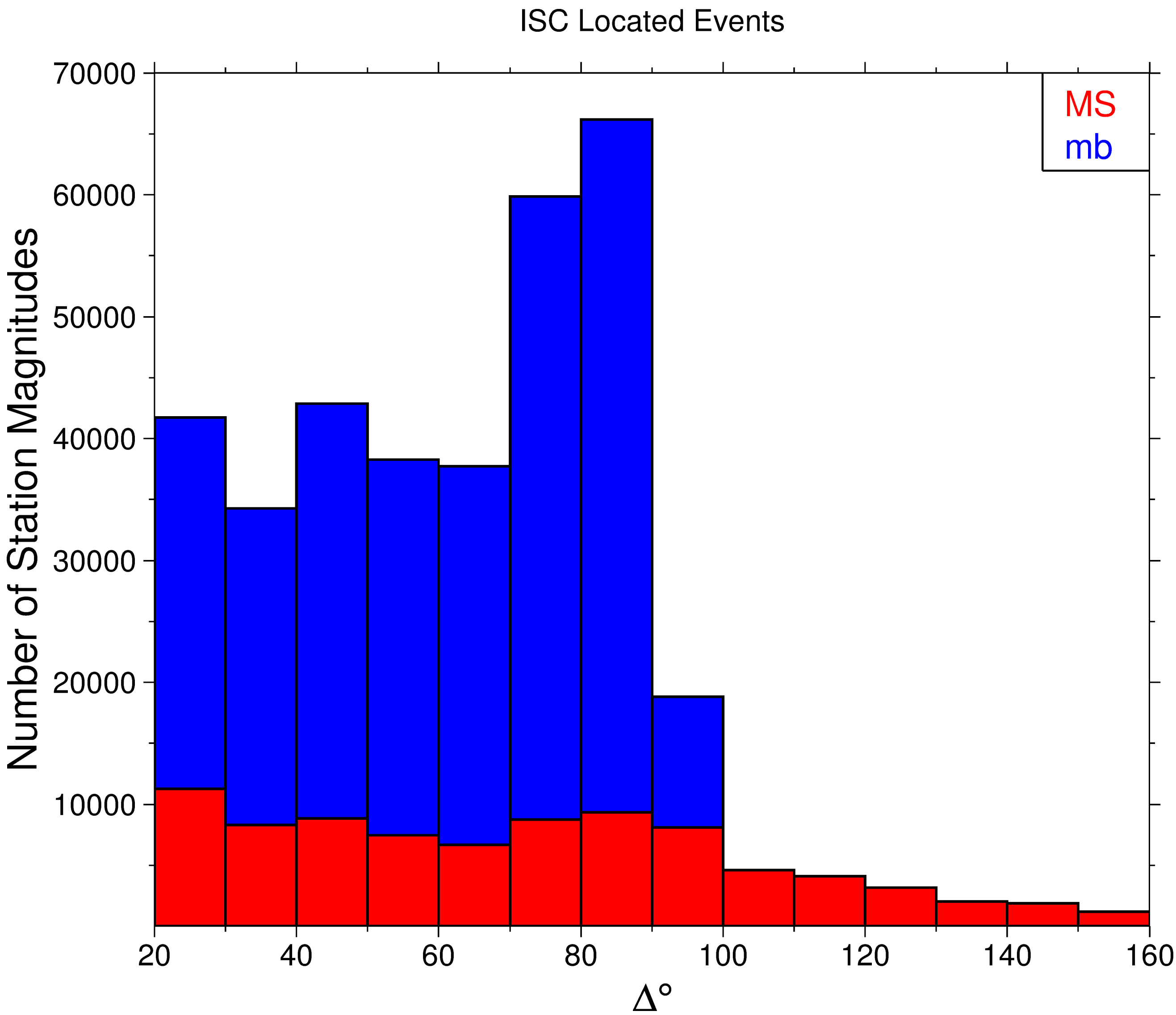

Figure 9.23: *Distribution of the number of station magnitudes computed by the ISC Locator for mb (blue) and MS (red) versus distance.*

Finally, Figure 9.24 shows the distribution of network MS and mb as well as the median number of stations for magnitude bins of 0.2. Clearly with increasing magnitude the number of events is smaller but with a general tendency of having more stations contributing to the network magnitude.

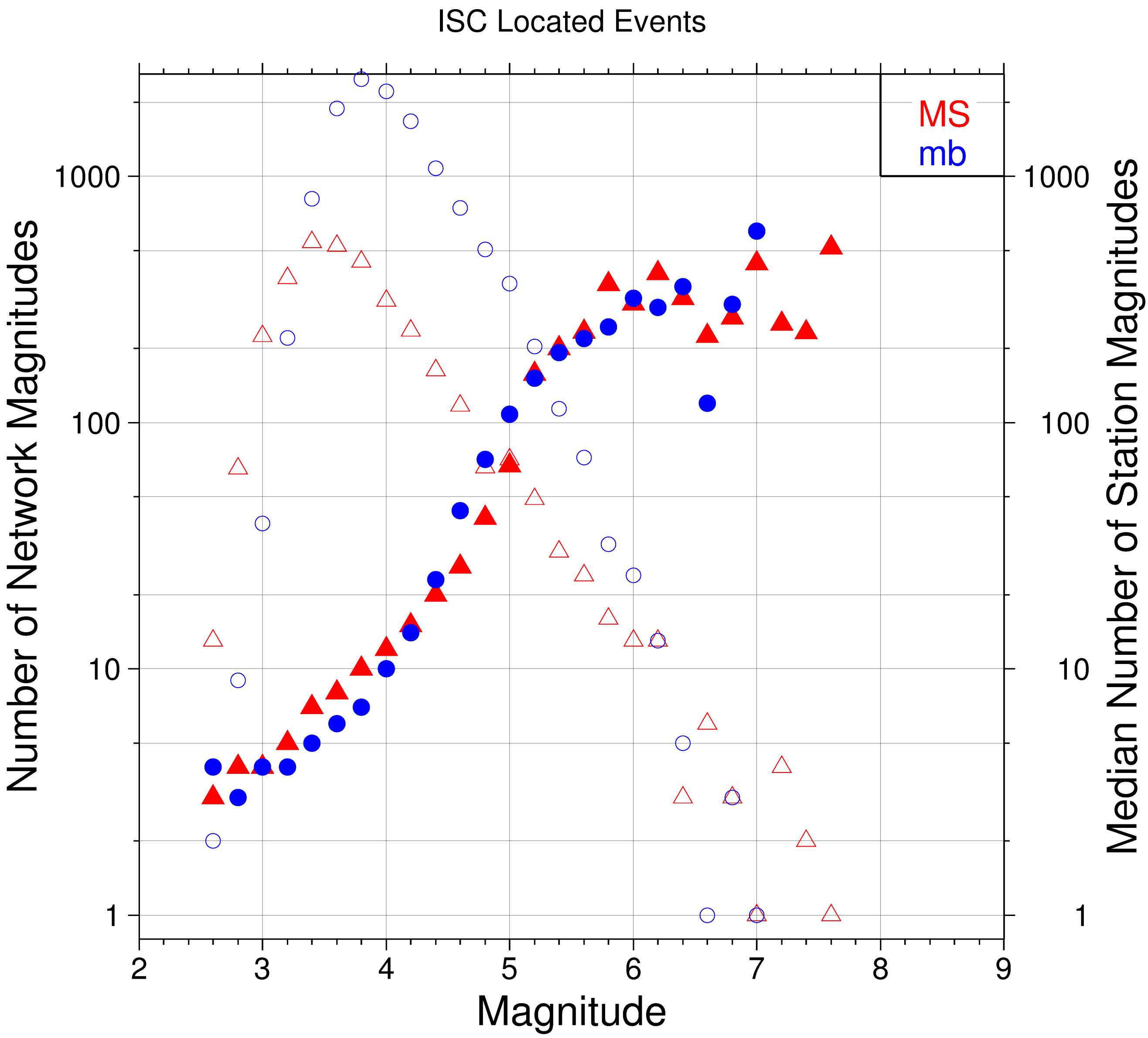

Figure 9.24: *Number of network magnitudes (open symbols) and median number of stations magnitudes (filled symbols). Blue circles refer to mb and red triangles to MS. The width of the magnitude interval δM is 0.2, and each symbol includes data with magnitude in $M \pm \delta M/2$.*

9.4 Completeness of the ISC Bulletin

The completeness of the ISC Bulletin can be expressed as a magnitude value, above which we expect the Bulletin to contain 100% of events. This magnitude of completeness, M_C can be measured as the point where the seismicity no longer follows the Gutenberg-Richter relationship. We compute an estimate of M_C using the maximum curvature technique of *Woessner and Wiemer* (2005).

The completeness of the ISC Bulletin for this summary period is shown in Figure 9.25. A history of completeness for the ISC Bulletin is shown in Figure 9.26. The step change in 1996 corresponds with the inclusion of the Prototype IDC (EIDC) Bulletin, followed by the Reviewed Event Bulletin (REB) of the IDC.

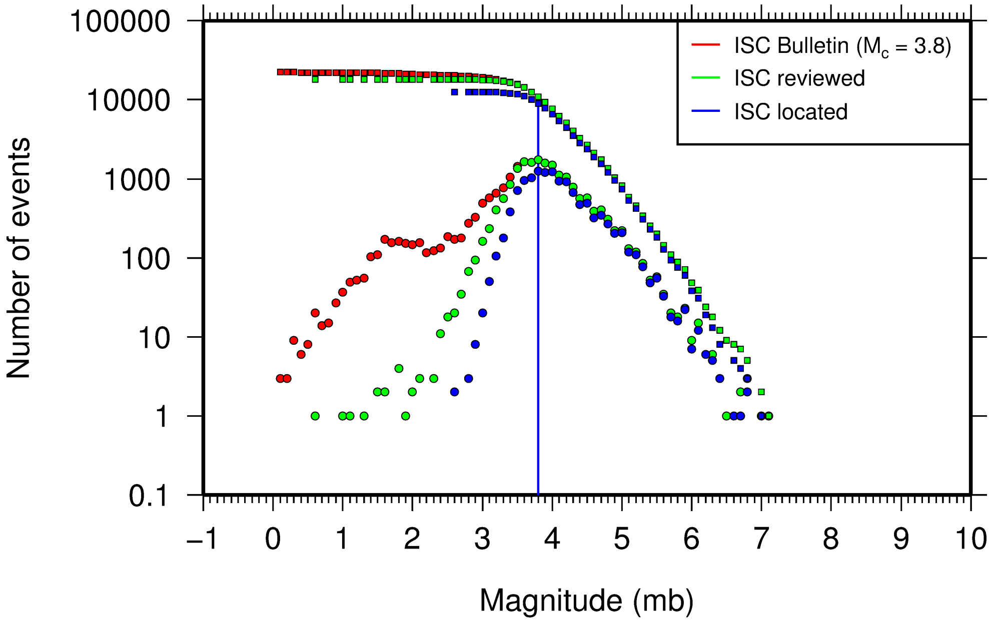

Figure 9.25: *Frequency and cumulative frequency magnitude distribution for all events in the ISC Bulletin, ISC reviewed events and events located by the ISC. The magnitude of completeness (M_C) is shown for the ISC Bulletin. Note: only events with values of mb are represented in the figure.*

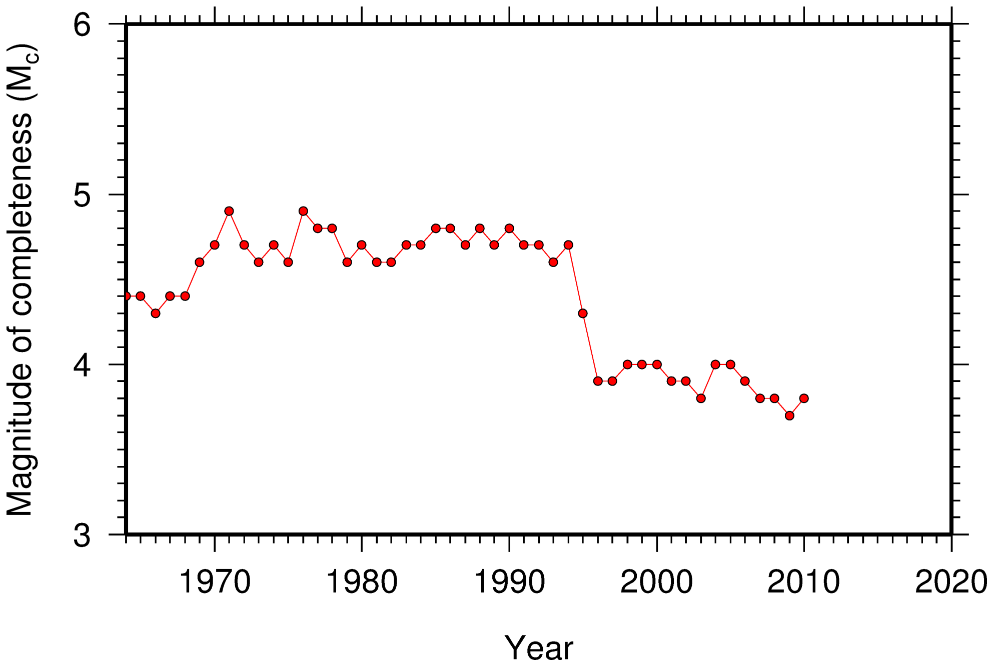

Figure 9.26: *Variation of magnitude of completeness (M_C) for each year in the ISC Bulletin. Note: M_C is calculated only using those events with values of mb.*

9.5 Magnitude Comparisons

The ISC Bulletin publishes network magnitudes reported by multiple agencies to the ISC. For events that have been located by the ISC, where enough amplitude data has been collected, the MS and mb magnitudes are calculated by the ISC (MS is computed only for depths $\leq$ 60 km). In this section, ISC magnitudes and some other reported magnitudes in the ISC Bulletin are compared.

The comparison between MS and mb computed by the ISC locator for events in this summary period is shown in Figure 9.27, where the large number of data pairs allows a colour coding of the data density. The scatter in the data reflects the fundamental differences between these magnitude scales.

Similar plots are shown in Figure 9.28 and 9.29, respectively, for comparisons of ISC mb and ISC MS with Mw from the GCMT catalogue. Since Mw is not often available below magnitude 5, these distributions are mostly for larger, global events. Not surprisingly, the scatter between mb and Mw is larger than the scatter between MS and Mw. Also, the saturation effect of mb is clearly visible for earthquakes with Mw $>$ 6.5. In contrast, MS scales well with Mw $>$ 6, whereas for smaller magnitudes MS appears to be systematically smaller than Mw.

In Figure 9.30 ISC values of mb are compared with all reported values of mb, values of mb reported by NEIC and values of mb reported by IDC. Similarly in Figure 9.31, ISC values of MS are compared with all reported values of MS, values of MS reported by NEIC and values of MS reported by IDC. There is a large scatter between the ISC magnitudes and the mb and MS reported by all other agencies.

The scatter decreases both for mb and MS when ISC magnitudes are compared just with NEIC and IDC magnitudes. This is not surprising as the latter two agencies provide most of the amplitudes and periods used by the ISC locator to compute MS and mb. However, ISC mb appears to be smaller than NEIC mb for mb $<$ 4 and larger than IDC mb for mb $>$ 4. Since NEIC does not include IDC amplitudes, it seems these features originate from observations at the high-gain, low-noise sites reported by the IDC. For the MS comparisons between ISC and NEIC a similar but smaller effect is observed for MS $<$ 4.5, whereas a good scaling is generally observed for the MS comparisons between ISC and IDC.

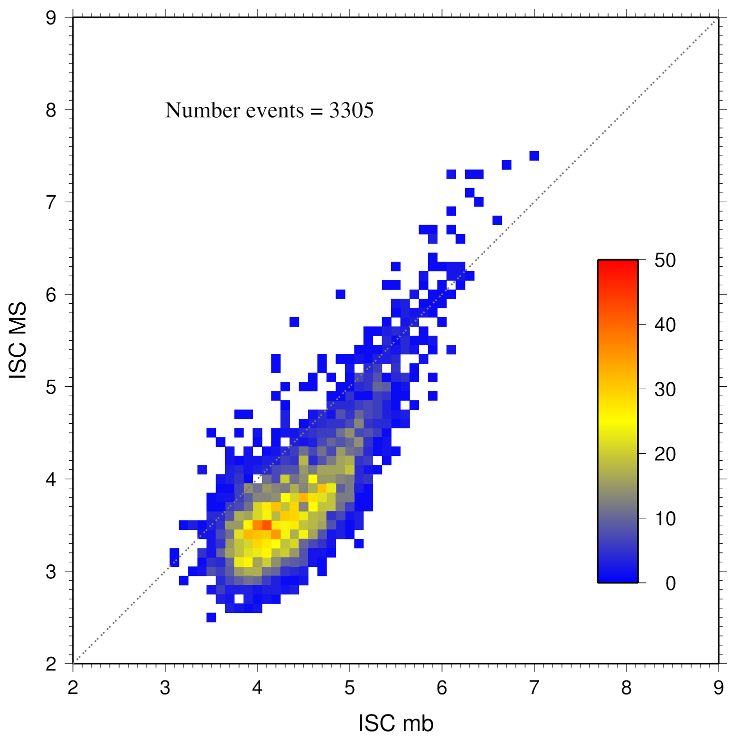

***Figure 9.27:** Comparison of ISC values of MS with mb for common event pairs.*

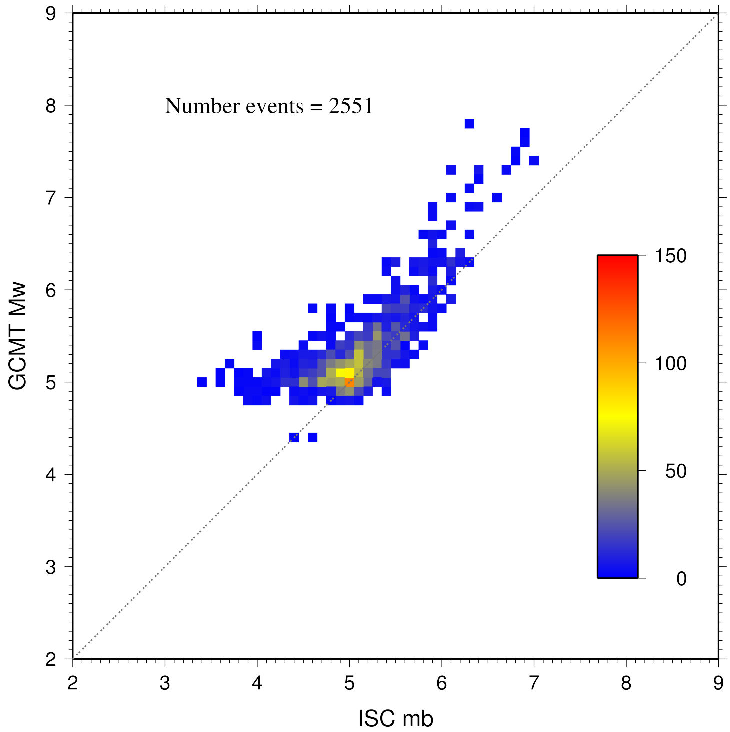

Figure 9.28: *Comparison of ISC values of mb with GCMT Mw for common event pairs.*

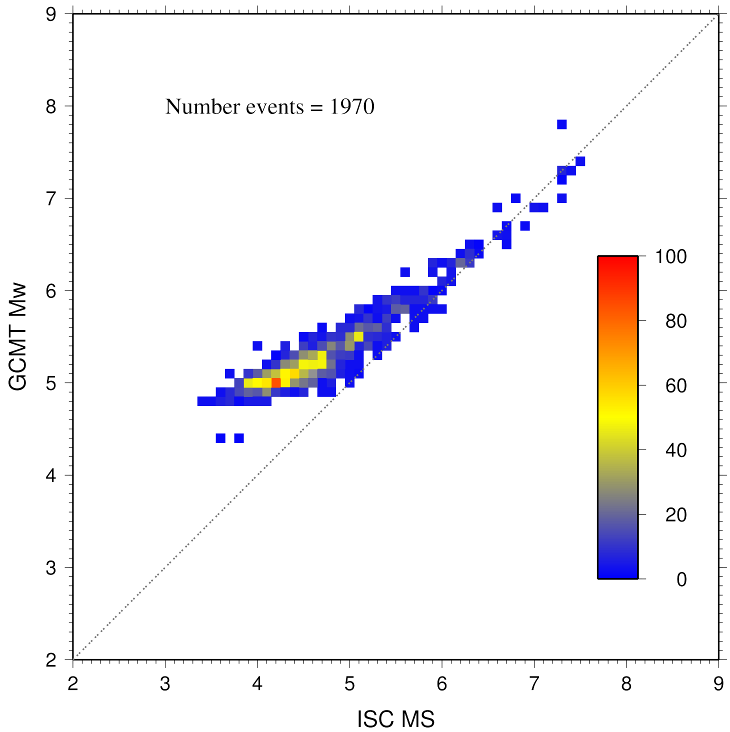

Figure 9.29: *Comparison of ISC values of MS with GCMT Mw for common event pairs.*

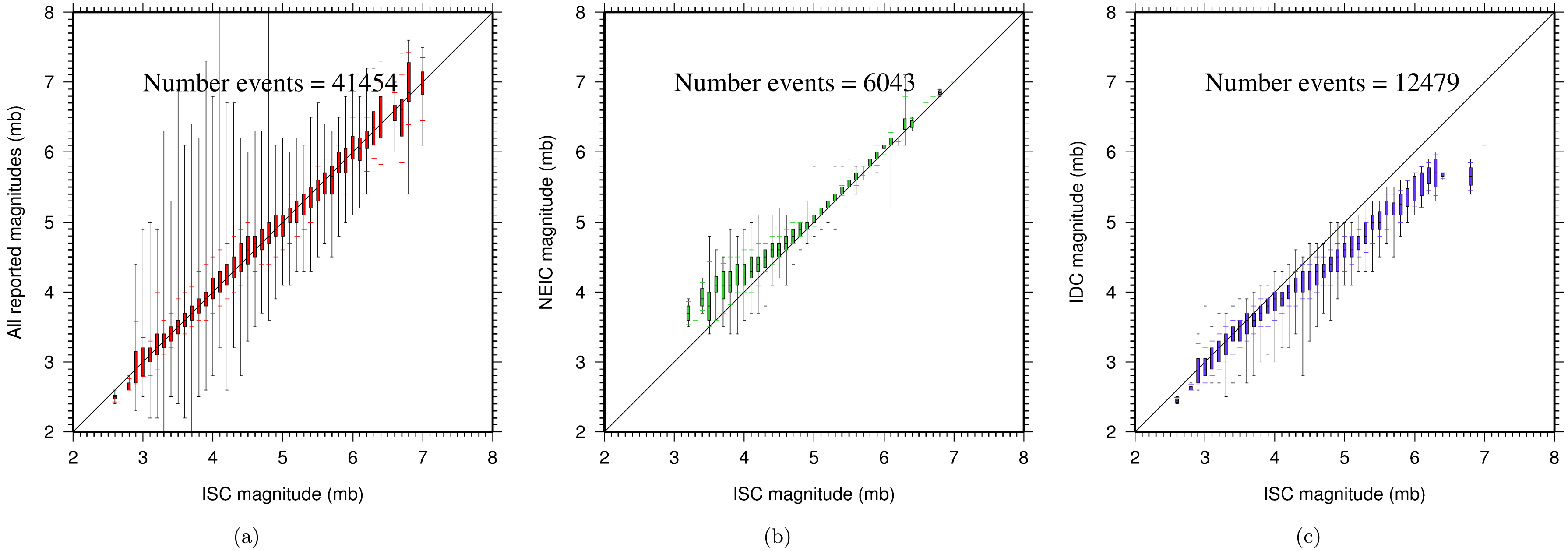

Figure 9.30: *Comparison of ISC magnitude data (mb) with additional agency magnitudes (mb). The statistical summary is shown in box-and-whisker plots where the 10th and 90th percentiles are shown in addition to the max and min values. (a): All magnitudes reported; (b): NEIC magnitudes; (c): IDC magnitudes.*

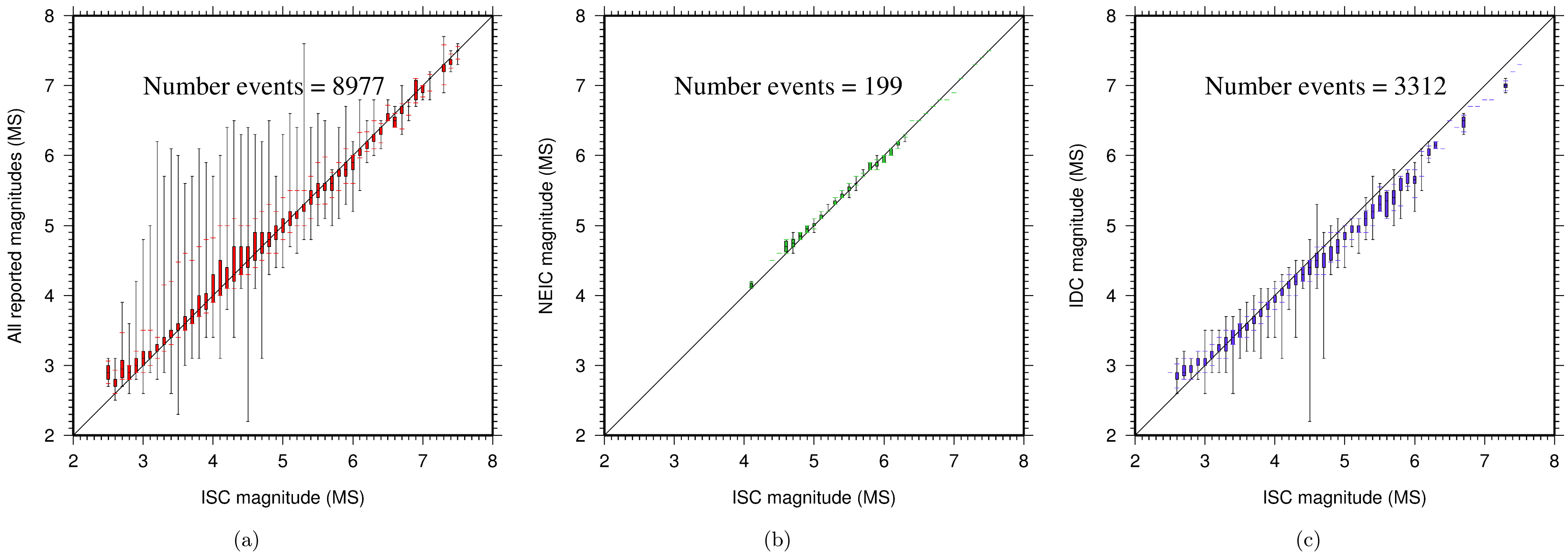

Figure 9.31: *Comparison of ISC magnitude data (MS) with additional agency magnitudes (MS). The statistical summary is shown in the box-and-whisker plots where the 10th and 90th percentiles are shown in addition to the max and min values. (a): All magnitudes reported; (b): NEIC magnitudes; (c): IDC magnitudes.*

10

The Leading Data Contributors

As many as 126 agencies reported bulletin data related to the current six month period. Although we are grateful for every report, we nevertheless would like to acknowledge those agencies that made the most useful or distinct contributions to the contents of the ISC Bulletin. Here we note those agencies that:

- provided a comparatively large volume of parametric data (see Section 10.1),
- reported data that helped quite considerably to improve the quality of the ISC locations or magnitude determinations (see Section 10.2),
- helped the ISC by consistently reporting data in one of the standard recognised formats and in-line with the ISC data collection schedule (see Section 10.3).

We do not aim to discourage those numerous small networks who provide comparatively smaller yet still most essential volumes of regional data regularly, consistently and accurately. Without these reports the ISC Bulletin would not be as comprehensive and complete as it is today.

10.1 The Largest Data Contributors

We commend the contribution of those agencies that submitted information for a large portion of seismic events. We acknowledge the contribution of IDC, NEIC, MOS, BJI, USArray and a few others (Figure 10.1) that reported the majority of moderate to large events recorded at teleseismic distances. The contributions of JMA, NEIC, IDC, CSEM, and a number of others are also acknowledged with respect to small seismic events. Note that the NEIC bulletin accumulates a contribution of all regional networks in the USA. Similarly, the CSEM communicates contributions of many tens of European and Mediterranean networks a few of which the ISC does not always receive directly. Several agencies monitoring highly seismic regions routinely report large volumes of small to moderate magnitude events, such as those in Japan, Chinese Taipei, Turkey, Chile, Italy, Indonesia, Greece, New Zealand and southern Kazakhstan. Contributions of small magnitude events by agencies in regions of low seismicity, such as Finland, Czech Republic, Australia and central and northern Kazakhstan are also gratefully received.

We also would like to acknowledge contributions of those agencies that report a large portion of arrival time and amplitude data (Figure 10.2). For small magnitude events, these are local agencies in charge of monitoring local and regional seismicity. For moderate to large events, contributions of NEIC, IDC, USArray and MOS are especially acknowledged. Notably, three agencies (IDC, NEIC and MOS) reported together over 70% of all amplitude measurements made for teleseismically recorded events. We hope

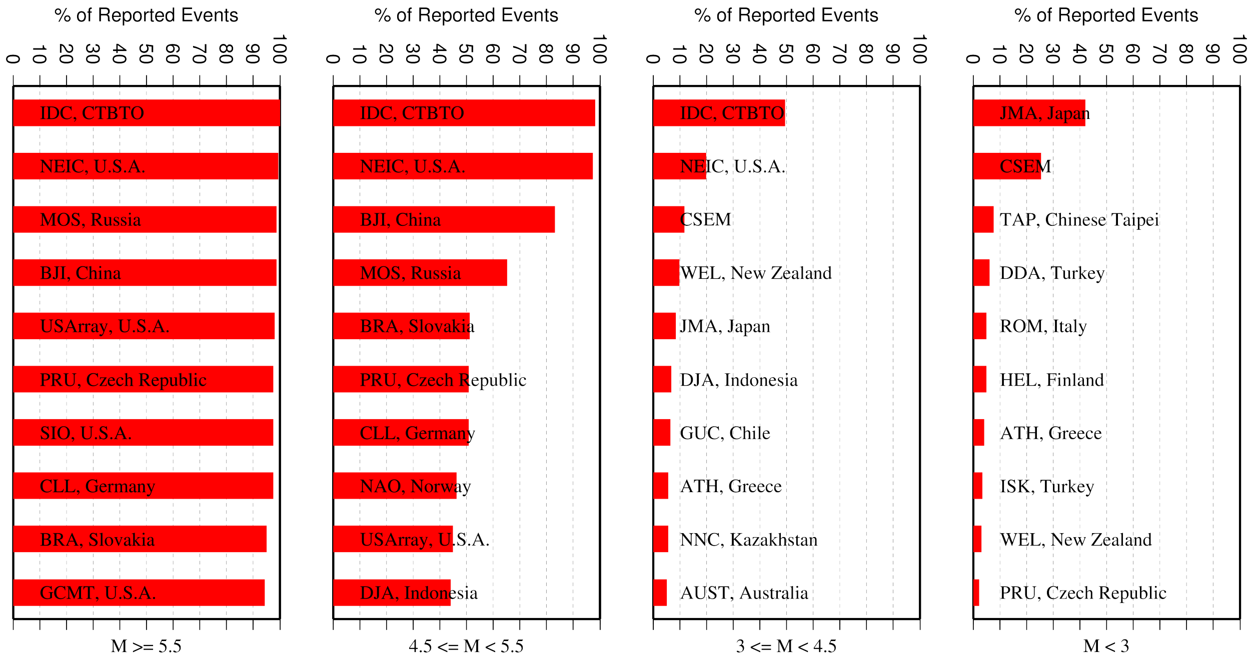

Figure 10.1: *Frequency of events in the ISC Bulletin for which an agency reported at least one item of data: a moment tensor, a hypocentre, a station arrival time or an amplitude. The top ten agencies are shown for four magnitude intervals.*

that other agencies would also be able to update their monitoring routines in the future to include the amplitude reports for teleseismic events compliant with the IASPEI standards.

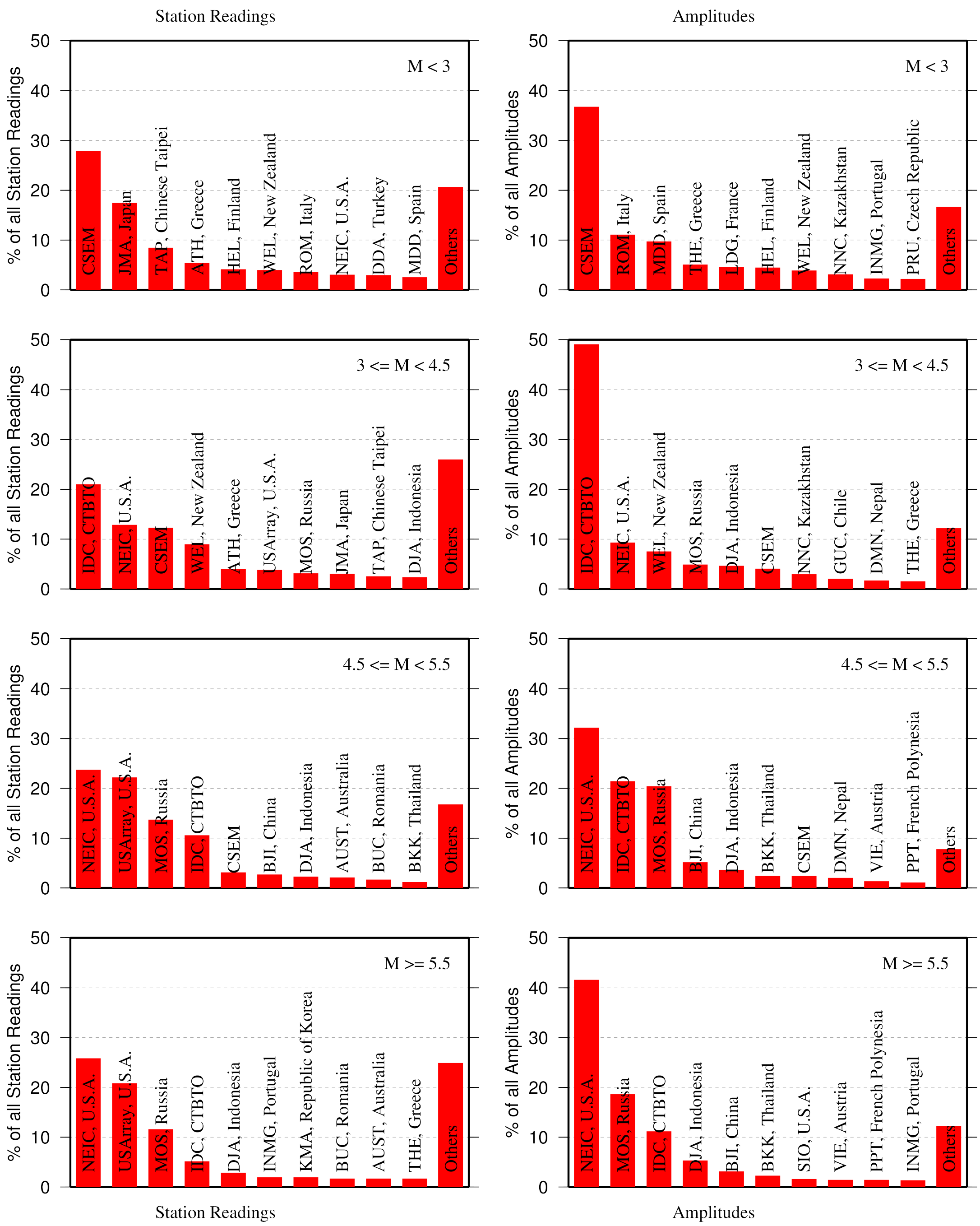

Figure 10.2: *Contributions of station arrival time readings (left) and amplitudes (right) of agencies to the ISC Bulletin. Top ten agencies are shown for four magnitude intervals.*

10.2 Contributors Reporting the Most Valuable Parameters

One of the main ISC duties is to re-calculate hypocentre estimates for those seismic events where a collective wealth of all station reports received from all agencies is likely to improve either the event location or depth compared to the hypocentre solution from each single agency. For areas with a sparse local seismic network or an unfavourable station configuration, readings made by other networks at teleseismic distances are very important. All events near mid-oceanic ridges as well as those in the majority of subduction zones around the world fall into this category. Hence we greatly appreciate the effort made by many agencies that report data for remote earthquakes (Figure 10.3). For some agencies, such as the IDC and the NEIC, it is part of their mission. For instance, the IDC reports almost every seismic event that is large enough to be recorded at teleseismic distance (20 degrees and beyond). This is largely because the International Monitoring System of primary arrays and broadband instruments is distributed at quiet sites around the world in order to be able to detect possible violations of the Comprehensive Test Ban Treaty. The NEIC reported over 30% of those events as their mission requires them to report events above magnitude 4.5 outside the United States of America. For other agencies reporting distant events it is an extra effort that they undertake to notify their governments and relief agencies as well as to help the ISC and academic research in general. Hence these agencies usually report on the larger magnitude events. BJI, MOS, AUST, NAO, CLL, PRU, DMN and AWI each reported manually picked individual station arrivals for several percent of all relevant events. We encourage other agencies to report distant events to us.

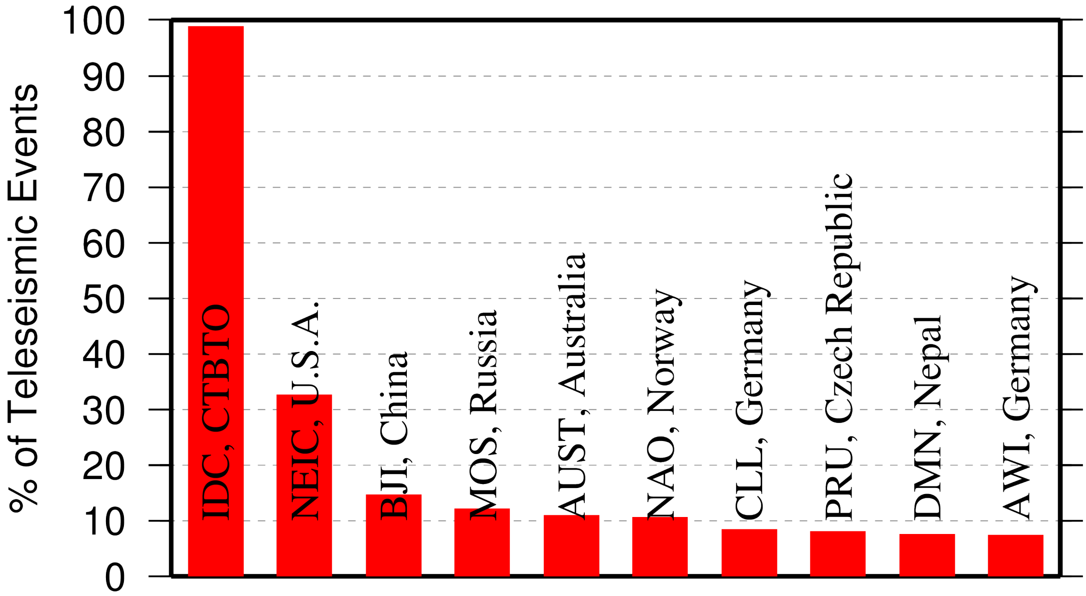

Figure 10.3: *Top ten agencies that reported teleseismic phase arrivals for a large portion of ISC events.*

In addition to the first arriving phase we encourage reporters to contribute observations of secondary seismic phases that help constrain the event location and depth: S, Sn, Sg and pP, sP, PcP (Figure 10.4). We expect though that these observations are actually made from waveforms, rather than just predicted by standard velocity models and modern software programs. It is especially important that these arrivals are manually reviewed by an operator (as we know takes place at the IDC and NEIC), as opposed to some lesser attempts to provide automatic phase readings that are later rejected by the ISC due to a generally poor quality of unreviewed picking.

Another important long-term task that the ISC performs is to compute the most definitive values of MS and mb network magnitudes that are considered reliable due to removal of outliers and consequent averaging (using alpha-trimmed median) across the largest network of stations, generally not feasible for a single agency. Despite concern over the bias at the lower end of mb introduced by the body wave amplitude data from the IDC, other agencies are also known to bias the results. This topic is further discussed in Section 9.5.

Notably, the IDC reports almost 100% of all events for which MS and mb are estimated. This is due to the standard routine that requires determination of body and surface wave magnitudes useful for

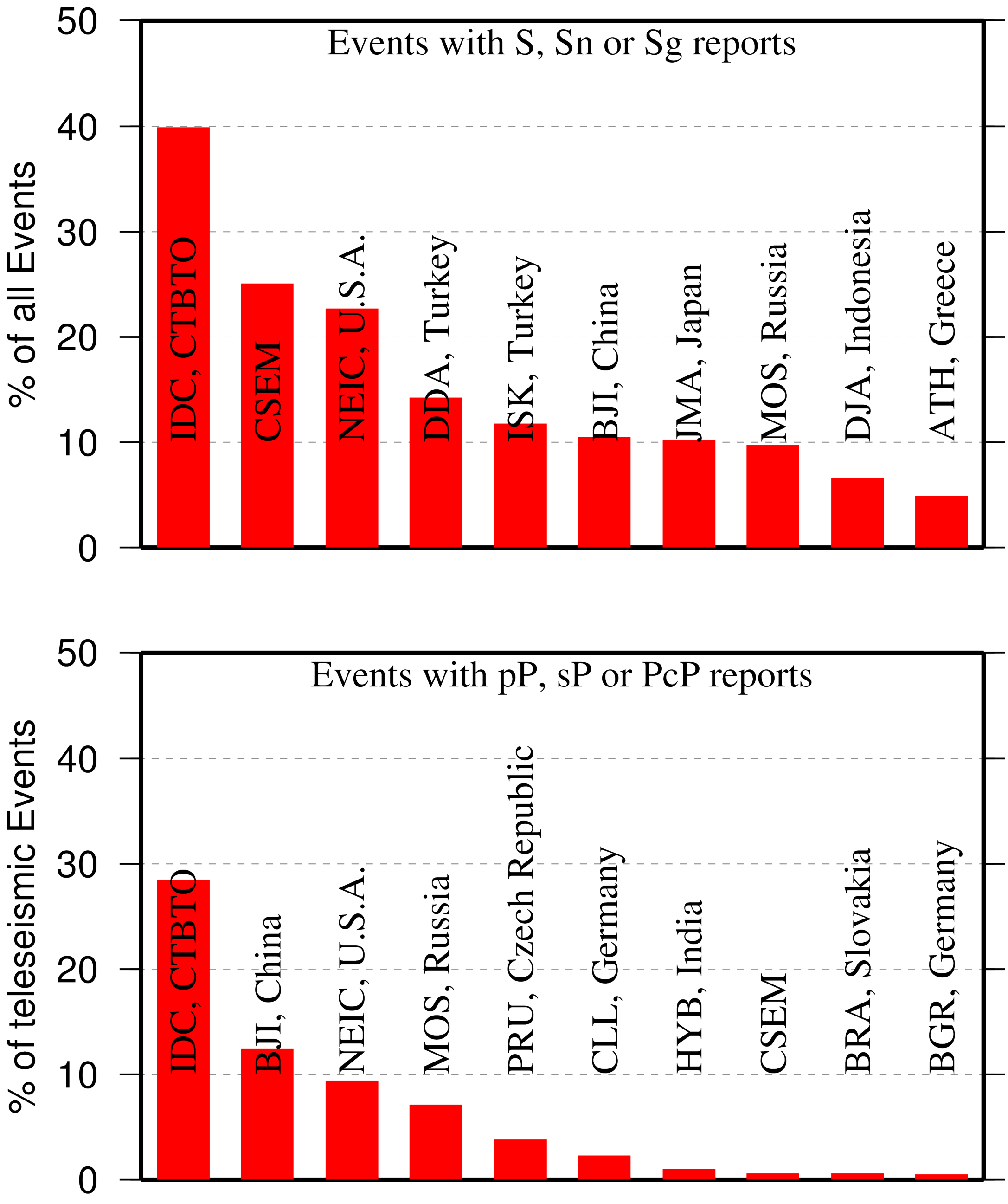

Figure 10.4: *Top ten agencies that reported secondary phases important for an accurate epicentre location (top) and focal depth determination (bottom).*

discrimination purposes. NEIC, MOS, BJI, NAO, PRU and a few other agencies (Figure 10.5) are also responsible for the majority of the amplitude and period reports that contribute towards the ISC magnitudes.

Since the ISC does not routinely process waveforms, we rely on other agencies to report moment magnitudes as well as moment tensor determinations (Figure 10.6).

Among other event parameters the ISC Bulletin also contains information on event type. We cannot independently verify the type of each event in the Bulletin and thus rely on other agencies to report the event type to us. Practices of reporting non-tectonic events vary greatly from country to country. Many agencies do not include anthropogenic events in their reports. Suppression of such events from

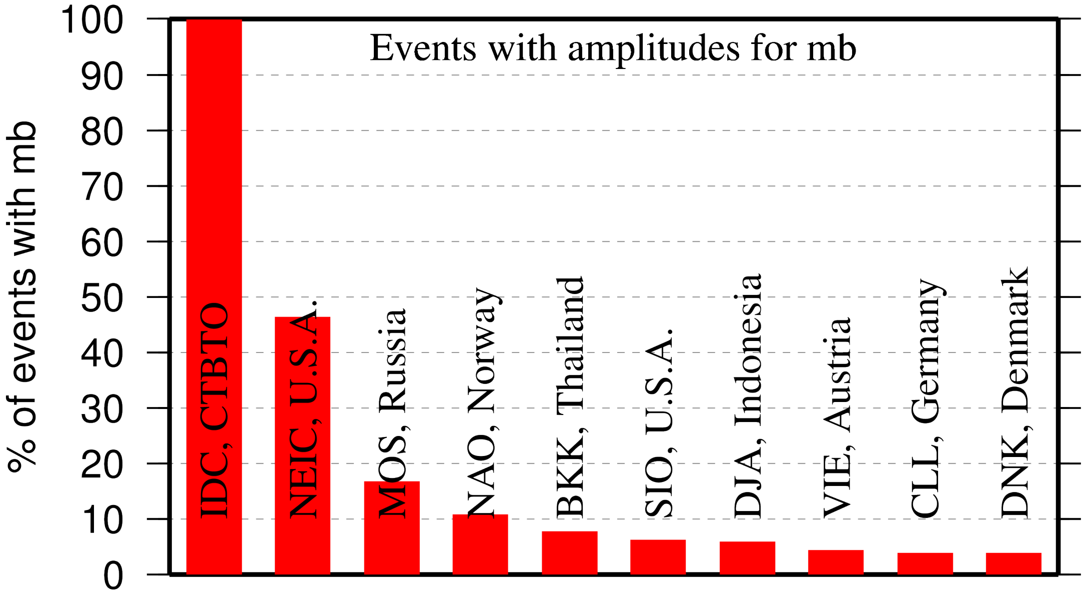

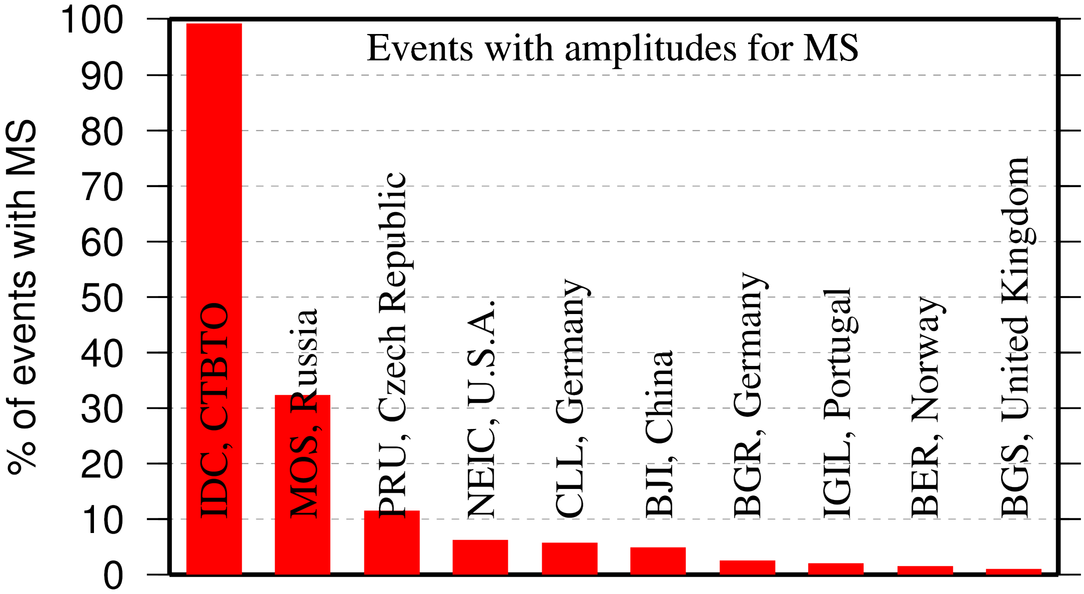

Figure 10.5: *Agencies that report defining body (top) and surface (bottom) wave amplitudes and periods for the largest fraction of those ISC Bulletin events with MS/mb determinations.*

reports to the ISC may lead to a situation where a neighbouring agency reports the anthropogenic event as an earthquake for which expected data are missing. This in turn is detrimental to ISC Bulletin users studying natural seismic hazard. Hence we encourage all agencies to join the agencies listed on Figure 10.7 and several others in reporting both natural and anthropogenic events to the ISC.

The ISC Bulletin also contains felt and damaging information when local agencies have reported it to us. Agencies listed on Figure 10.8 provide such information for the majority of all felt or damaging events in the ISC Bulletin.

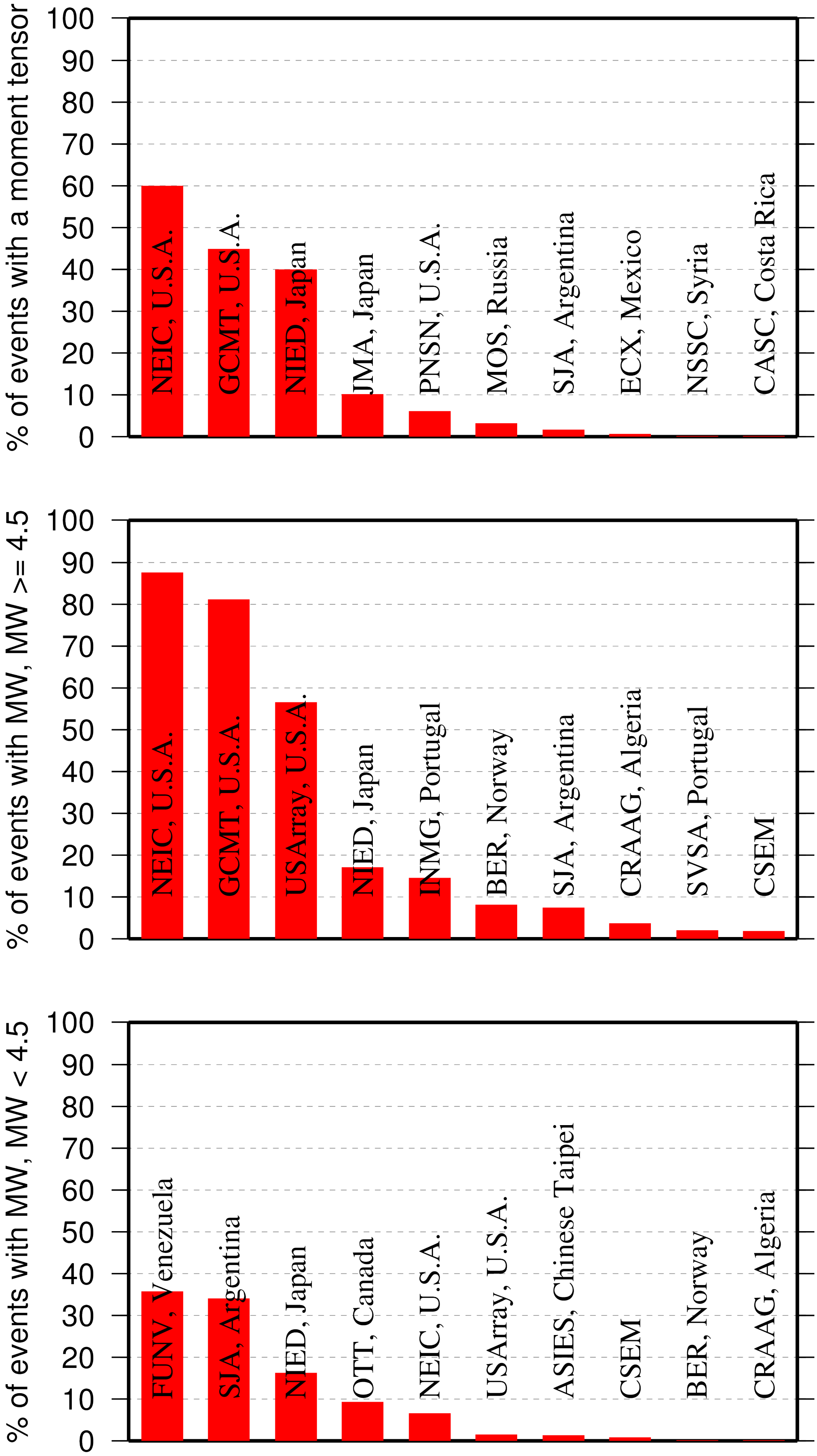

Figure 10.6: *Top ten agencies that most frequently report determinations of seismic moment tensor (top) and moment magnitude (middle/bottom for M greater/smaller than 4.5).*

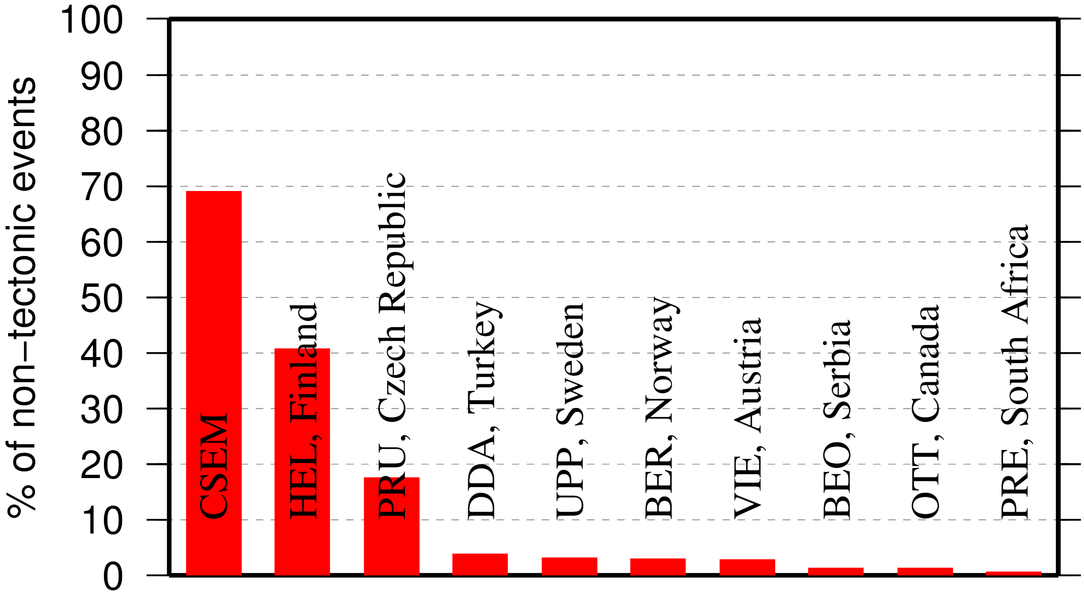

Figure 10.7: *Top ten agencies that most frequently report non-tectonic seismic events to the ISC.*

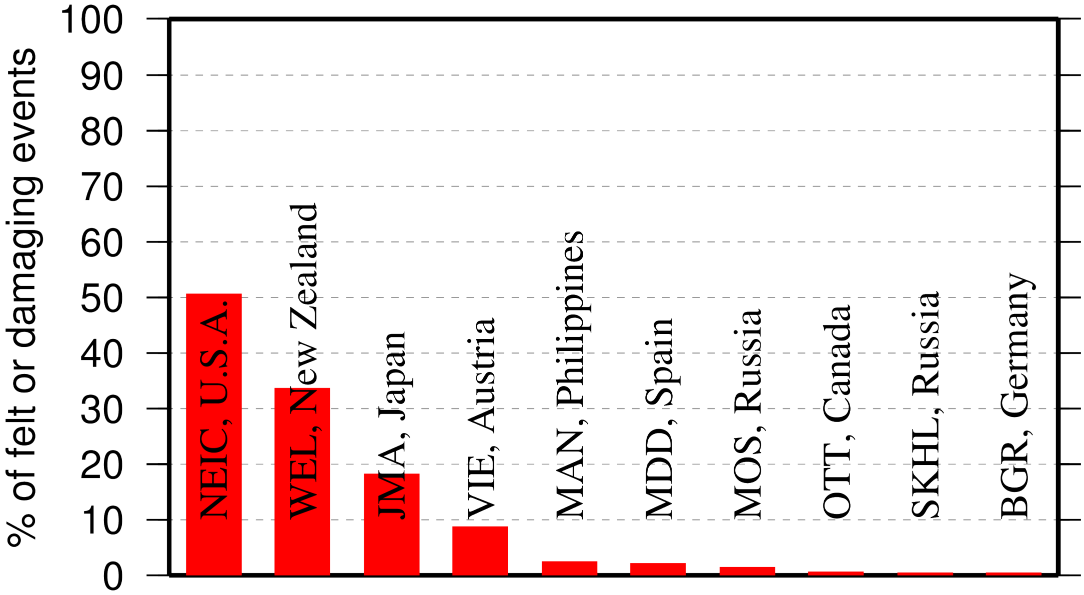

Figure 10.8: *Top ten agencies that most frequently report macroseismic information to the ISC.*

10.3 The Most Consistent and Punctual Contributors

During this six month period, 33 agencies reported their bulletin data in one of the standard seismic formats (ISF, IMS, GSE or Nordic) and within the current 12 month deadline. Here we must reiterate that the ISC accepts reviewed bulletin data after a final analysis as soon as they are ready. These data, even if they arrive before the deadline, are immediately parsed into the ISC database, grouped with other data and become available to the ISC users on-line as part of the preliminary ISC Bulletin. There is no reason to wait until the deadline to send the data to the ISC. Table 10.1 lists all agencies that have been helpful to the ISC in this respect during the six month period.

Table 10.1: *Agencies that contributed reviewed bulletin data to the ISC in one of the standard international formats before the submission deadline.*

Agency Code	Country	Average Delay from real time (days)
SSNC	Cuba	20
LDG	France	23
NAO	Norway	24
PPT	French Polynesia	25
LIC	Ivory Coast	30
IGIL	Portugal	32
PDG	Montenegro	33
TIR	Albania	44
UCC	Belgium	49
SVSA	Portugal	51
DMN	Nepal	56
PRE	South Africa	62
IDC	Austria	69
INMG	Portugal	76
KRSC	Russia	78
ISN	Iraq	109
BJI	China	116
ASRS	Russia	135
THE	Greece	142
BGR	Germany	171
AUST	Australia	194
AZER	Azerbaijan	200
LIT	Lithuania	202
BER	Norway	204
GRAL	Lebanon	236
MOLD	Moldova	246
ZUR	Switzerland	249
DBN	Netherlands	249
OMAN	Oman	250
NERS	Russia	251
BGS	United Kingdom	271
BEO	Serbia	272
BYKL	Russia	300

11

Appendix

Table 11.1: *Listing of all 306 agencies that have directly reported to the ISC. The 126 agencies highlighted in bold have reported data to the ISC Bulletin for the period of this Bulletin Summary.*

Agency Code	Agency Name
AAA	Alma-ata, Kazakhstan
AAE	**University of Addis Ababa, Ethiopia**
AAM	University of Michigan, USA
ADE	Primary Industries and Resources SA, Australia
ADH	Observatorio Afonso Chaves, Portugal
AEIC	Alaska Earthquake Information Center, USA
AFAR	Afar Depression: Interpretation of the 1960-2000 Earthquakes, Israel
ALG	Algiers University, Algeria
ANF	USArray Array Network Facility, USA
ANT	Antofagasta, Chile
ARE	Instituto Geofisico del Peru, Peru
ARO	**Observatoire Géophysique d'Arta, Djibouti**
ASIES	**Institute of Earth Sciences, Academia Sinica, Chinese Taipei**
ASL	Albuquerque Seismological Laboratory, USA
ASM	University of Asmara, Eritrea
ASRS	**Altai-Sayan Seismological Centre, GS SB RAS, Russia**
ATA	The Earthquake Research Center Ataturk University, Turkey
ATH	**National Observatory of Athens, Greece**
AUST	**Geoscience Australia, Australia**
AWI	**Alfred Wegener Institute for Polar and Marine Research, Germany**
AZER	**Republic Center of Seismic Survey, Azerbaijan**
BCIS	Bureau Central International de Sismologie, France
BDF	Observatório Sismológico da Universidade de Brasília, Brazil
BELR	**Centre of Geophysical Monitoring, Belarus**
BEO	**Seismological Survey of Serbia, Serbia**
BER	**University of Bergen, Norway**
BERK	Berkheimer H, Germany
BGR	**Bundesanstalt für Geowissenschaften und Rohstoffe, Germany**
BGS	**British Geological Survey, United Kingdom**
BHUJ2	Study of Aftershocks of the Bhuj Earthquake by Japanese Research Team, Japan
BIAK	Biak earthquake aftershocks (17-Feb-1996), USA
BJI	**China Earthquake Networks Center, China**
BKK	**Thai Meteorological Department, Thailand**
BNS	Erdbebenstation, Geologisches Institut der Universität, Köl, Germany
BOG	Universidad Javeriana, Colombia
BRA	**Geophysical Institute, Slovak Academy of Sciences, Slovakia**

Table 11.1: Continued.

Agency Code	Agency Name
BRG	**Seismological Observatory Berggießhübel, TU Bergakademie Freiberg, Germany**
BRK	Berkeley Seismological Laboratory, USA
BRS	Brisbane Seismograph Station, Australia
BUC	**National Institute for Earth Physics, Romania**
BUD	**Geodetic and Geophysical Research Institute, Hungary**
BUG	Institute of Geology, Mineralogy & Geophysics, Germany
BUL	**Goetz Observatory, Zimbabwe**
BUT	Montana Bureau of Mines and Geology, USA
BYKL	**Baykal Regional Seismological Centre, GS SB RAS, Russia**
CADCG	Central America Data Centre, Costa Rica
CAN	Australian National University, Australia
CANSK	Canadian and Scandinavian Networks, Sweden
CAR	Instituto Sismologico de Caracas, Venezuela
CASC	**Central American Seismic Center, Costa Rica**
CERI	Center for Earthquake Research and Information, USA
CLL	**Geophysikalisches Observatorium Collm, Germany**
CNG	Seismographic Station Changalane, Mozambique
CNRM	Centre National de Recherche, Morocco
COSMOS	Consortium of Organizations for Strong Motion Observations, USA
CRAAG	**Centre de Recherche en Astronomie, Astrophysique et Géophysique, Algeria**
CSC	University of South Carolina, USA
CSEM	**Centre Sismologique Euro-Méditerranéen (CSEM/EMSC), France**
DASA	Defense Atomic Support Agency, USA
DBN	**Koninklijk Nederlands Meteorologisch Instituut, Netherlands**
DDA	**Disaster and Emergency Management Presidency, Turkey**
DHMR	**Yemen National Seismological Center, Yemen**
DIAS	**Dublin Institute for Advanced Studies, Ireland**
DJA	**Badan Meteorologi, Klimatologi dan Geofisika, Indonesia**
DMN	**Department of Mines and Geology, Ministry of Industry of Nepal, Nepal**
DNK	**Geological Survey of Denmark and Greenland, Denmark**
DSN	**Dubai Seismic Network, United Arab Emirates**
DUSS	Damascus University, Syria, Syria
EAF	East African Network, Unknown
EAGLE	Ethiopia-Afar Geoscientific Lithospheric Experiment, Unknown
EBR	Observatori de l'Ebre, Spain
EBSE	Ethiopian Broadband Seismic Experiment, Unknown
ECX	**Red Sismica del Noroeste de Mexico (RESOM), Mexico**
EFATE	OBS Experiment near Efate, Vanuatu, USA
EHB	Engdahl, van der Hilst and Buland, USA
EIDC	Experimental (GSETT3) International Data Center, USA
EKA	Eskdalemuir Array Station, United Kingdom
ENT	Geological Survey and Mines Department, Uganda
EPSI	Reference events computed by the ISC for EPSI project, United Kingdom

Table 11.1: Continued.

Agency Code	Agency Name
ERDA	Energy Research and Development Administration, USA
EST	Geological Survey of Estonia, Estonia
FBR	Fabra Observatory, Spain
FDF	Fort de France, Martinique
FIA0	Finessa Array, Finland
FOR	Unknown Historical Agency, Unknown - historical agency
FUNV	**Fundación Venezolana de Investigaciones Sismológicas**, **Venezuela**
FUR	Geophysikalisches Observatorium der Universität München, Germany
GBZT	Marmara Research Center, Turkey
GCG	INSIVUMEH, Guatemala
GCMT	**The Global CMT Project**, **USA**
GDNRW	Geologischer Dienst Nordrhein-Westfalen, Germany
GEN	Dipartimento per lo Studio del Territorio e delle sue Risorse (RSNI), Italy
GFZ	Helmholtz Centre Potsdam GFZ German Research Centre For Geosciences, Germany
GII	**The Geophysical Institute of Israel**, **Israel**
GOM	Observatoire Volcanologique de Goma, Democratic Republic of the Congo
GRAL	**National Council for Scientific Research**, **Lebanon**
GSDM	Geological Survey Department Malawi, Malawi
GTFE	German Task Force for Earthquakes, Germany
GUC	**Departamento de Geofísica, Universidad de Chile**, **Chile**
HAN	Hannover, Germany
HDC	**Observatorio Vulcanológico y Sismológico de Costa Rica**, **Costa Rica**
HEL	**Institute of Seismology, University of Helsinki**, **Finland**
HFS	Hagfors Observatory, Sweden
HFS1	Hagfors Observatory, Sweden
HFS2	Hagfors Observatory, Sweden
HKC	**Hong Kong Observatory**, **Hong Kong**
HLUG	Hessisches Landesamt für Umwelt und Geologie, Germany
HLW	**National Research Institute of Astronomy and Geophysics**, **Egypt**
HNR	**Ministry of Mines, Energy and Rural Electrification**, **Solomon Islands**
HON	Pacific Tsunami Warning Center - NOAA, USA
HRVD	Harvard University, USA
HRVD_LR	Department of Geological Sciences, Harvard University, USA
HVO	Hawaiian Volcano Observatory, USA
HYB	**National Geophysical Research Institute**, **India**
HYD	National Geophysical Research Institute, India
IAG	Instituto Andaluz de Geofisica, Spain
IASPEI	**IASPEI Working Group on Reference Events**, **USA**
ICE	Instituto Costarricense de Electricidad, Costa Rica
IDC	**International Data Centre, CTBTO**, **Austria**

Table 11.1: *Continued.*

Agency Code	Agency Name
IGIL	**Instituto Geofisico do Infante Dom Luiz**, **Portugal**
IGQ	**Servicio Nacional de Sismología y Vulcanología**, **Ecuador**
IGS	Institute of Geological Sciences, United Kingdom
INDEPTH3	International Deep Profiling of Tibet and the Himalayas, USA
INET	Instituto Nicaragüense de Estudios Territoriales, Nicaragua
INMG	**Instituto Português do Mar e da Atmosfera, I.P.**, **Portugal**
IPEC	Ústav fyziky Země, Czech Republic
IPRG	Institute for Petroleum Research and Geophysics, Israel
IRIS	**IRIS Data Management Center**, **USA**
IRSM	Institute of Rock Structure and Mechanics, Czech Republic
ISK	**Kandilli Observatory and Research Institute**, **Turkey**
ISN	**Iraqi Meteorological and Seismology Organisation**, **Iraq**
ISS	International Seismological Summary, United Kingdom
IST	Institute of Physics of the Earth, Technical University of Istanbul, Turkey
JEN	Geodynamisches Observatorium Moxa, Germany
JMA	**Japan Meteorological Agency**, **Japan**
JOH	Bernard Price Institute of Geophysics, South Africa
JSN	**Jamaica Seismic Network**, **Jamaica**
JSO	**Jordan Seismological Observatory**, **Jordan**
KBC	Institut de Recherches Géologiques et Minières, Cameroon
KEW	Kew Observatory, United Kingdom
KHC	Geofysikalni Ustav, Ceske Akademie Ved, Czech Republic
KISR	Kuwait Institute for Scientific Research, Kuwait
KLM	**Malaysian Meteorological Service**, **Malaysia**
KMA	**Korea Meteorological Administration**, **Republic of Korea**
KNET	**Kyrgyz Seismic Network**, **Kyrgyzstan**
KOLA	**Kola Regional Seismic Centre, GS RAS**, **Russia**
KRL	Geodätisches Institut der Universität Karlsruhe, Germany
KRNET	**Institute of Seismology, Academy of Sciences of Kyrgyz Republic**, **Kyrgyzstan**
KRSC	**Kamchatkan Experimental and Methodical Seismological Department, GS RAS**, **Russia**
KSA	Observatoire de Ksara, Lebanon
KUK	Geological Survey Department of Ghana, Ghana
LAO	Large Aperture Seismic Array, USA
LDG	**Laboratoire de Détection et de Géophysique/CEA**, **France**
LDN	University of Western Ontario, Canada
LDO	Lamont-Doherty Earth Observatory, USA
LED	Landeserdbebendienst Baden-Württemberg, Germany
LEDBW	Landeserdbebendienst Baden-Württemberg, Germany
LER	Besucherbergwerk Binweide Station, Germany
LIB	Tripoli, Libya
LIC	**Station Géophysique de Lamto**, **Ivory Coast**
LIM	Lima, Peru
LIS	Instituto de Meteorologia, Portugal
LIT	**Geological Survey of Lithuania**, **Lithuania**
LJU	**Environmental Agency of the Republic of Slovenia**, **Slovenia**

Table 11.1: Continued.

Agency Code	Agency Name
LPA	**Universidad Nacional de La Plata**, **Argentina**
LSZ	Geological Survey Department of Zambia, Zambia
LVSN	Latvian Seismic Network, Latvia
MAN	**Philippine Institute of Volcanology and Seismology**, **Philippines**
MAT	**The Matsushiro Seismological Observatory**, **Japan**
MCO	Macao Meteorological and Geophysical Bureau, Macao, China
MDD	**Instituto Geográfico Nacional**, **Spain**
MED_RCMT	MedNet Regional Centroid - Moment Tensors, Italy
MES	Messina Seismological Observatory, Italy
MEX	**Instituto de Geofísica de la UNAM**, **Mexico**
MOLD	**Institute of Geophysics and Geology**, **Moldova**
MOS	**Geophysical Survey of Russian Academy of Sciences**, **Russia**
MOZ	Direccao Nacional de Geologia, Mozambique
MRB	Institut Cartogràfic de Catalunya, Spain
MSI	Messina Seismological Observatory, Italy
MSSP	**Micro Seismic Studies Programme, PINSTECH**, **Pakistan**
MUN	Mundaring Observatory, Australia
NAI	University of Nairobi, Kenya
NAM	The Geological Survey of Namibia, Namibia
NAO	**Stiftelsen NORSAR**, **Norway**
NCEDC	Northern California Earthquake Data Center, USA
NDI	**India Meteorological Department**, **India**
NEIC	**National Earthquake Information Center**, **USA**
NEIS	National Earthquake Information Service, USA
NERS	**North Eastern Regional Seismological Centre, GS RAS**, **Russia**
NIC	**Cyprus Geological Survey Department**, **Cyprus**
NIED	**National Research Institute for Earth Science and Disaster Prevention**, **Japan**
NNC	**National Nuclear Center**, **Kazakhstan**
NOU	**IRD Centre de Nouméa**, **New Caledonia**
NSSC	**National Syrian Seismological Center**, **Syria**
NSSP	**National Survey of Seismic Protection**, **Armenia**
OBM	Research Centre of Astronomy and Geophysics, Mongolia
OGSO	Ohio Geological Survey, USA
OMAN	**Sultan Qaboos University**, **Oman**
ORF	Orfeus Data Center, Netherlands
OTT	**Canadian Hazards Information Service, Natural Resources Canada**, **Canada**
PAL	Palisades, USA
PAS	California Institute of Technology, USA
PDA	Universidade dos Açores, Portugal
PDG	**Seismological Institute of Montenegro**, **Montenegro**
PEK	Peking, China
PGC	Pacific Geoscience Centre, Canada
PLV	**National Center for Scientific Research**, **Vietnam**
PMEL	Pacific seismicity from hydrophones, USA
PMR	Alaska Tsunami Warning Center,, USA

Table 11.1: Continued.

Agency Code	Agency Name
PNSN	**Pacific Northwest Seismic Network**, **USA**
PPT	**Laboratoire de Géophysique/CEA**, **French Polynesia**
PRE	**Council for Geoscience**, **South Africa**
PRU	**Geophysical Institute, Academy of Sciences of the Czech Republic**, **Czech Republic**
PTO	Instituto Geofísico da Universidade do Porto, Portugal
PTWC	Pacific Tsunami Warning Center, USA
QCP	**Manila Observatory**, **Philippines**
QUE	Pakistan Meteorological Department, Pakistan
QUI	Escuela Politécnica Nacional, Ecuador
RAB	Rabaul Volcanological Observatory, Papua New Guinea
RBA	Université Mohammed V, Morocco
REN	MacKay School of Mines, USA
REY	**Icelandic Meteorological Office**, **Iceland**
RMIT	Royal Melbourne Institute of Technology, Australia
ROC	Odenbach Seismic Observatory, USA
ROM	**Istituto Nazionale di Geofisica e Vulcanologia**, **Italy**
RRLJ	Regional Research Laboratory Jorhat, India
RSMAC	Red Sísmica Mexicana de Apertura Continental, Mexico
RSNC	Red Sismológica Nacional de Colombia, Colombia
RSPR	**Red Sísmica de Puerto Rico**, **USA**
RYD	King Saud University, Saudi Arabia
SAPSE	Southern Alps Passive Seismic Experiment, New Zealand
SAR	Sarajevo Seismological Station, Bosnia and Herzegovina
SCB	Observatorio San Calixto, Bolivia
SCEDC	Southern California Earthquake Data Center, USA
SDD	Universidad Autonoma de Santo Domingo, Dominican Republic
SEA	Geophysics Program AK-50, USA
SEPA	Seismic Experiment in Patagonia and Antarctica, USA
SET	Setif Observatory, Algeria
SFS	Real Instituto y Observatorio de la Armada, Spain
SGS	**Saudi Geological Survey**, **Saudi Arabia**
SHL	Central Seismological Observatory, India
SIGU	**Subbotin Institute of Geophysics, National Academy of Sciences**, **Ukraine**
SIK	Seismic Institute of Kosovo, Kosovo
SIO	**Scripps Institution of Oceanography**, **USA**
SJA	**Instituto Nacional de Prevención Sísmica**, **Argentina**
SJS	Instituto Costarricense de Electricidad, Costa Rica
SKHL	**Sakhalin Experimental and Methodological Seismological Expedition, GS RAS**, **Russia**
SKL	Sakhalin Complex Scientific Research Institute, Russia
SKO	**Seismological Observatory Skopje**, **FYR Macedonia**
SLC	Salt Lake City, USA
SLM	Saint Louis University, USA
SNET	Servicio Nacional de Estudios Territoriales, El Salvador
SNM	New Mexico Institute of Mining and Technology, USA

Table 11.1: Continued.

Agency Code	Agency Name
SNSN	Saudi National Seismic Network, Saudi Arabia
SOF	**Geophysical Institute, Bulgarian Academy of Sciences, Bulgaria**
SOME	Seismological Experimental Methodological Expedition, Kazakhstan
SPA	USGS - South Pole, Antarctica
SPGM	Service de Physique du Globe, Morocco
SRI	Stanford Research Institute, USA
SSN	Sudan Seismic Network, Sudan
SSNC	**Servicio Sismológico Nacional Cubano, Cuba**
SSS	Centro de Estudios y Investigaciones Geotecnicas del San Salvador, El Salvador
STK	Stockholm Seismological Station, Sweden
STR	**Institut de Physique du Globe, France**
STU	Stuttgart Seismological Station, Germany
SVSA	**Sistema de Vigilância Sismológica dos Açores, Portugal**
SYO	**National Institute of Polar Research, Japan**
SZGRF	Seismologisches Zentralobservatorium Gräfenberg, Germany
TAC	Estación Central de Tacubaya, Mexico
TAN	Antananarivo, Madagascar
TANZANIA	Tanzania Broadband Seismic Experiment, USA
TAP	**CWB, Chinese Taipei**
TAU	University of Tasmania, Australia
TEH	**Tehran University, Iran**
TEIC	Center for Earthquake Research and Information, USA
THE	**Department of Geophysics, Aristotle University of Thessaloniki, Greece**
THR	**International Institute of Earthquake Engineering and Seismology (IIEES), Iran**
TIF	**Seismic Monitoring Centre of Georgia, Georgia**
TIR	**The Institute of Seismology, Academy of Sciences of Albania, Albania**
TRI	**Osservatorio Geofisico Sperimentale, Italy**
TRN	**University of the West Indies, Trinidad and Tobago**
TTG	Titograd Seismological Station, Montenegro
TUL	Oklahoma Geological Survey, USA
TUN	Institut National de la Météorologie, Tunisia
TVA	Tennessee Valley Authority, USA
TZN	University of Dar Es Salaam, Tanzania
UAV	Red Sismológica de Los Andes Venezolanos, Venezuela
UCC	**Royal Observatory of Belgium, Belgium**
UCR	Universidad de Costa Rica, Costa Rica
UGN	Institute of Geonics AS CR, Czech Republic
ULE	University of Leeds, United Kingdom
UNAH	Universidad Nacional Autonoma de Honduras, Honduras
UPA	Universidad de Panama, Panama
UPP	**University of Uppsala, Sweden**
UPSL	University of Patras, Department of Geology, Greece
USAEC	United States Atomic Energy Commission, USA

Table 11.1: *Continued.*

Agency Code	Agency Name
USCGS	United States Coast and Geodetic Survey, USA
USGS	**United States Geological Survey**, **USA**
UVC	Universidad del Valle, Colombia
VAO	**Instituto Astronomico e Geofísico**, **Brazil**
VIE	**Österreichischer Geophysikalischer Dienst**, **Austria**
VSI	University of Athens, Greece
WAR	**Institute of Geophysics, Polish Academy of Sciences**, **Poland**
WBNET	**West Bohemia Seismic Network**, **Czech Republic**
WEL	**Institute of Geological and Nuclear Sciences**, **New Zealand**
WES	Weston Observatory, USA
YARS	**Yakutiya Regional Seismological Center, GS SB RAS**, **Russia**
ZAG	**Seismological Survey of the Republic of Croatia**, **Croatia**
ZUR	**Swiss Seismological Sevice (SED)**, **Switzerland**
ZUR_RMT	Zurich Moment Tensors, Switzerland

Table 11.2: *Phases reported to the ISC. These include phases that could not be matched to an appropriate* ak135 *phases. Those agencies that reported at least 10% of a particular phase are also shown.*

Reported Phase	Total	Agencies reporting
P	2221849	NEIC (17%), IRIS (12%)
S	841223	JMA (26%), TAP (14%), CSEM (12%)
Pg	341836	CSEM (55%), ROM (15%)
Pn	265610	CSEM (41%), NEIC (24%)
Sg	238207	CSEM (51%), ROM (17%)
PN	200259	WEL (49%), ATH (25%), ISK (15%)
pmax	125377	MOS (99%)
AML	110571	WEL (68%)
Sn	106970	CSEM (36%), NEIC (13%), IDC (12%)
LR	101026	IDC (55%), NEIC (38%)
Lg	98173	CSEM (51%), MDD (26%), NNC (11%)
PG	85909	ISK (28%), ATH (21%), HEL (18%), WEL (14%), PRU (11%)
SG	67757	HEL (26%), PRU (21%), ISK (17%), WEL (16%), ATH (11%)
NULL	62106	MOS (50%), ECX (11%)
SN	50002	ATH (36%), WEL (34%), HEL (15%)
PB	43533	ATH (86%), HEL (14%)
Pb	43000	CSEM (78%), IRIS (21%)
Sb	39316	CSEM (67%), IRIS (32%)
PKP	37294	IDC (43%), NEIC (31%)
PMZ	34909	BJI (100%)
SB	32803	ATH (79%), HEL (21%)
PKPbc	29721	NEIC (41%), IDC (40%)
P*	29005	WEL (96%)
pP	28070	BJI (38%), NEIC (30%), IDC (15%)
MLR	26105	MOS (100%)
T	25860	IDC (92%)
PKPdf	25435	NEIC (72%)
PcP	21233	NEIC (42%), IDC (41%)
PP	20084	BJI (40%), NEIC (21%), IDC (12%)
PKIKP	19790	MOS (96%)
PFAKE	19746	NEIC (100%)
A	17240	INMG (55%), SVSA (29%), SKHL (16%)
PKiKP	15000	IRIS (67%), NEIC (14%)
LZ	14440	BJI (100%)
MSG	14392	HEL (100%)
LN	14133	BJI (100%)
LE	13277	BJI (100%)
IAML	12577	ECX (54%), BER (24%), SJA (20%)
S*	11820	WEL (97%)
SS	11814	BJI (50%), MOS (29%)
PKPab	11672	NEIC (41%), IDC (31%)
sP	11490	BJI (82%)
ScP	9409	NEIC (42%), IDC (37%), BJI (13%)
x	8309	PRU (55%), NDI (44%)
Pdiff	7647	IRIS (84%)
smax	7556	MOS (93%)

Table 11.2: (continued)

Reported Phase	Total	Agencies reporting
AMB	6567	SKHL (52%), NDI (30%), BGS (14%)
AMS	5896	PRU (71%), BGS (11%)
sS	5503	BJI (99%)
IAmb	5004	HYB (59%), BER (17%), LIT (17%)
*PP	4851	MOS (100%)
PKKPbc	4806	NEIC (55%), IDC (44%)
Trac	4071	OTT (100%)
PKP2	3756	MOS (97%)
Pdif	2862	NEIC (84%)
Sm	2682	YARS (95%)
SKS	2466	BJI (66%), PRU (13%), INMG (12%)
SKPbc	2376	NEIC (53%), IDC (45%)
pPKP	2340	PRU (37%), BJI (24%), IDC (21%), NEIC (16%)
PKPpre	2172	NEIC (97%)
ScS	1922	BJI (86%)
Smax	1916	BYKL (100%)
PKHKP	1802	MOS (100%)
PPP	1801	MOS (83%)
PKhKP	1558	IDC (98%)
LG	1525	OTT (69%), BRA (26%)
Pmax	1497	BYKL (97%)
Rg	1430	NNC (69%), NAO (12%), BER (12%)
PPMZ	1395	BJI (100%)
LQ	1387	PPT (58%), INMG (23%), BELR (14%)
IVMs_BB	1350	HYB (84%), BER (16%)
Pm	1345	YARS (93%)
SSS	1228	MOS (71%), CLL (16%)
PS	1109	MOS (48%), CLL (16%), PRU (12%)
sPKP	1076	BJI (81%), PRU (17%)
pPKPbc	997	IDC (42%), NEIC (30%), BGR (21%)
L	921	BGR (43%), STR (31%)
*SP	915	MOS (100%)
SKKS	880	BJI (79%)
PKKP	868	IDC (45%), NEIC (34%), PRU (16%)
PKKPab	857	NEIC (56%), IDC (37%)
PcS	801	BJI (99%)
SP	794	PRU (40%), MOS (30%)
LRM	759	MOLD (57%), BELR (43%)
SKP	734	NEIC (42%), IDC (41%)
PKPAB	732	PRU (99%)
SKSac	729	HYB (39%), BER (16%)
pPKPdf	723	NEIC (53%), VIE (19%)
PKPPKP	715	IDC (90%)
X	704	JMA (70%), SYO (26%)
SMN	613	BJI (100%)
SME	612	BJI (100%)
PKS	579	BJI (88%)

Table 11.2: *(continued)*

Reported Phase	Total	Agencies reporting
P'P'	535	NEIC (99%)
max	522	BYKL (100%)
R	518	STR (96%)
*SS	515	MOS (100%)
SKKPbc	448	IDC (52%), NEIC (45%)
PCP	436	PRU (72%), BRA (23%)
AMP	399	HLW (61%), NOU (31%)
PDIFF	397	PRU (73%), BRA (25%)
Lm	383	CLL (100%)
LmV	332	CLL (100%)
(P)	313	BRG (63%), VAO (20%), CLL (16%)
LMZ	303	WAR (100%)
IAMs_20	297	BER (66%), PRE (34%)
PKKPdf	296	NEIC (81%), BUD (15%)
Sgm	294	SIGU (100%)
PKP1	291	LIC (99%)
PKP2bc	273	IDC (100%)
PPS	273	CLL (60%), MOS (23%), MOLD (12%)
pPKPab	263	NEIC (39%), IDC (27%), CLL (15%)
PM	256	BELR (100%)
Sgmax	238	NERS (100%)
PKPDF	232	PRU (100%)
mb	232	OMAN (88%), OTT (12%)
SKPdf	214	NEIC (68%)
P'P'df	203	NEIC (100%)
PDIF	179	BRA (88%), BRG (12%)
pg	175	BUD (100%)
sg	173	BUD (100%)
AMb	172	IGIL (80%), DHMR (16%)
pPcP	171	IDC (58%), NEIC (39%)
P3KPbc	166	IDC (100%)
LmH	165	CLL (100%)
pPP	131	BGR (73%), CLL (18%)
SKPab	123	NEIC (48%), IDC (46%)
S	122	YARS (100%)
Snm	121	SIGU (100%)
Pgm	120	SIGU (100%)
Pgmax	117	NERS (100%)
rx	117	SKHL (100%)
P	114	YARS (100%)
SDIF	97	PRU (99%)
pn	92	BUD (100%)
Pu	89	NEIC (100%)
PmP	86	BGR (100%)
sn	84	BUD (100%)
Sdif	83	CLL (58%), PPT (18%), HYB (14%)
P4KPbc	80	IDC (100%)

Table 11.2: (continued)

Reported Phase	Total	Agencies reporting
sPKPdf	80	VIE (68%), CLL (14%), NEIC (12%)
SSSS	79	CLL (99%)
APKP	77	UCC (100%)
pPKiKP	75	VIE (24%), CLL (19%), HYB (17%), IDC (16%), BUD (15%)
PKP2ab	75	IDC (100%)
SmS	73	BGR (100%)
H	72	IDC (100%)
SKKP	70	IDC (37%), NEIC (33%), PRU (24%)
ml	66	OMAN (100%)
Sg	62	SIGU (100%)
SH	61	SYO (100%)
SKKSac	61	CLL (49%), BGR (31%)
Pnm	60	SIGU (100%)
AP	60	UCC (100%)
XS	59	PRU (100%)
RG	58	HEL (100%)
(sP)	55	CLL (100%)
PKPPKPdf	54	BUD (80%), CLL (20%)
IVMsBB	53	HYB (100%)
E	49	UCC (76%), WAR (22%)
P'P'ab	49	NEIC (100%)
PgPg	47	BYKL (98%)
SKSdf	46	HYB (35%), WAR (35%), BUD (26%)
Lmax	46	CLL (100%)
LQM	42	BELR (100%)
AMSG	41	BER (54%), BGS (44%)
pPdiff	40	BGR (50%), VIE (18%), SYO (15%)
P3KP	39	IDC (100%)
pPn	39	BUD (49%), NEIC (21%), SKHL (21%)
sPP	38	CLL (95%)
Pg	37	SIGU (100%)
MSN	35	HEL (91%)
SKKPdf	34	BUD (76%), VIE (12%)
PKKKP	33	NEIC (100%)
sPKiKP	31	BUD (42%), VIE (35%), CLL (13%)
PKSbc	31	BGR (74%), CLL (26%)
PPPP	29	CLL (100%)
SCS	29	PRU (62%), NDI (21%), LPA (14%)
pScP	28	IDC (54%), NEIC (46%)
Sdiff	28	LJU (36%), IDC (36%), VIE (11%)
SgSg	28	BYKL (100%)
LV	27	CLL (100%)
AMPG	27	BER (67%), BGS (30%)
PSKS	27	CLL (96%)
XP	27	UCC (93%)
SCP	25	PRU (84%), BRG (16%)
PN5	25	THR (64%), HYB (36%)

Table 11.2: *(continued)*

Reported Phase	Total	Agencies reporting
SN5	24	HYB (96%)
SKSP	23	DBN (39%), CLL (30%), BELR (22%)
sPdif	23	HYB (57%), CLL (43%)
i-	23	INMG (100%)
sSS	22	CLL (100%)
TT	22	NEIC (100%)
SPP	22	CLL (50%), HYB (14%), WAR (14%), MOS (14%)
pPdif	22	HYB (73%), CLL (27%)
M	21	MOLD (62%), NDI (38%)
SKKKS	20	BELR (100%)
Plp	20	CLL (100%)
SM	20	BELR (100%)
PPlp	19	CLL (100%)
IVmB_BB	19	HYB (100%)
PKPdif	19	NEIC (89%), CLL (11%)
(pP)	19	CLL (100%)
sPKPbc	18	VIE (33%), CLL (28%), HYB (17%), IDC (11%)
PPM	18	BELR (100%)
SKiKP	17	IDC (100%)
m	17	YARS (100%)
PKPc	16	WAR (100%)
pPg	16	SKHL (100%)
PA	16	JSN (100%)
SDIFF	16	BRG (100%)
(PP)	15	CLL (100%)
sPKPab	14	HYB (36%), CLL (36%), BUD (14%), SYO (14%)
PKPM	14	BELR (100%)
P4KP	14	IDC (57%), NEIC (43%)
pPKKP	14	BGR (100%)
PsP	13	MOLD (92%)
(SS)	13	CLL (100%)
(PKiKP)	13	CLL (100%)
Li	13	MOLD (100%)
Smn	12	SIGU (100%)
SKSSKS	12	PRU (100%)
PCS	12	NDI (58%), PRU (42%)
PKPdiff	12	CLL (100%)
Smg	12	SIGU (100%)
(S)	12	CLL (100%)
PK	12	LIC (100%)
PPPrev	11	CLL (100%)
sPn	11	SKHL (64%), NEIC (18%), BUD (18%)
(Pg)	10	CLL (100%)
Pmn	9	SIGU (100%)
Pmg	9	SIGU (100%)
(PcP)	9	CLL (100%)
PnPn	9	HYB (67%), BUD (33%)

Table 11.2: (continued)

Reported Phase	Total	Agencies reporting
(SSS)	8	CLL (100%)
PX	8	WAR (100%)
PKKS	8	PRU (100%)
Lg2	8	MOLD (100%)
PKPBC	8	PRU (100%)
pwP	8	NEIC (100%)
sPg	8	SKHL (100%)
Y	8	BGR (100%)
PKSdf	8	CLL (100%)
Sm	8	SIGU (100%)
(SSSS)	7	CLL (100%)
SKPa	7	NAO (100%)
PSPS	7	CLL (100%)
P(2)	7	CLL (100%)
XM	7	MOLD (100%)
(PKPab)	7	CLL (100%)
SMZ	7	BJI (100%)
(PPP)	6	CLL (100%)
XSKS	6	PRU (100%)
MPN	6	HEL (100%)
sSSS	6	CLL (100%)
PKPlp	6	CLL (100%)
Pm	6	SIGU (100%)
SKKSacre	6	CLL (100%)
PSS	6	CLL (67%), WAR (33%)
sPPS	6	CLL (100%)
PKKSdf	6	NEIC (50%), CLL (50%)
PcPPKPre	5	CLL (100%)
Lg1	5	MOLD (100%)
PPPPrev	5	CLL (100%)
(pPKiKP)	5	CLL (100%)
(Pdif)	5	CLL (100%)
pPKKPbc	5	CLL (100%)
sPPP	5	CLL (100%)
Sgd	5	WAR (100%)
sPS	5	CLL (100%)
pPPS	5	CLL (100%)
Sn	5	SIGU (100%)
Lm(360	4	CLL (100%)
PSP	4	LPA (50%), MOLD (50%)
sSKKSac	4	CLL (100%)
SKKSdf	4	CLL (100%)
pPmax	4	CLL (100%)
sSSSS	4	CLL (100%)
AS	4	PRU (100%)
PKKPDF	4	BRA (100%)
(PPS)	4	CLL (100%)

Table 11.2: *(continued)*

Reported Phase	Total	Agencies reporting
(PKPdf)	4	CLL (100%)
SKPB	4	BRA (100%)
(pPKPdf)	4	CLL (100%)
(Pn)	4	CLL (100%)
Pn	4	SIGU (100%)
PDN	3	NDI (100%)
APKPab	3	UCC (100%)
APKPbc	3	UCC (100%)
(PS)	3	CLL (100%)
PP(2)	3	CLL (100%)
PGS	3	NDI (100%)
SKIKS	3	LPA (100%)
I	3	BER (67%), ECX (33%)
PKIKS	3	LPA (100%)
p	3	BUD (67%), NDI (33%)
Pdiffmax	3	CLL (100%)
pPPP	3	CLL (100%)
s	3	INMG (67%), NDI (33%)
SKPDF	3	BRA (100%)
(pPKPab)	3	CLL (100%)
PSSrev	3	CLL (100%)
PPmax	3	CLL (100%)
Ec	3	WAR (100%)
ES	3	YARS (100%)
sSdiff	3	CLL (100%)
sPb	3	BUD (100%)
SG4	3	HEL (100%)
(SP)	3	CLL (100%)
(Sg)	2	CLL (100%)
Px	2	WAR (100%)
PCN	2	NDI (100%)
(Sdif)	2	CLL (100%)
LH	2	CLL (100%)
AMSN	2	SJA (50%), GUC (50%)
PNDS	2	NDI (100%)
pP(2)	2	CLL (100%)
(PSPS)	2	CLL (100%)
LRM1	2	BELR (100%)
SKKPab	2	IDC (100%)
(PKP)	2	CLL (100%)
(pPdif)	2	CLL (100%)
pPS	2	CLL (100%)
PDS	2	NDI (100%)
(PG)	2	BRG (100%)
pSKKPbc	2	CLL (100%)
S	2	YARS (100%)
pSKKSac	2	CLL (100%)

Table 11.2: *(continued)*

Reported Phase	Total	Agencies reporting
IVmBBB	2	HYB (100%)
SKIKP	2	LPA (100%)
eSm	2	SKHL (100%)
N	2	AWI (100%)
pPPmax	2	CLL (100%)
PKPdf(2)	2	CLL (100%)
Slp	2	CLL (100%)
(PPPrev)	2	CLL (100%)
Sglp	2	CLL (100%)
Sgc	2	WAR (100%)
PC	2	BER (100%)
PKKSbc	2	CLL (100%)
(sPKPbc)	2	CLL (100%)
(Sn)	2	CLL (100%)
PPk	2	CLL (100%)
PKHKPM	2	BELR (100%)
PD	2	BER (100%)
PNCN	2	NDI (100%)
pPKPdf2	2	CLL (100%)
pPKS	2	LPA (100%)
PGCS	2	NDI (100%)
(Sb)	2	CLL (100%)
PKIKPM	1	BELR (100%)
(SKPbc)	1	CLL (100%)
PKPdfr	1	NEIC (100%)
X1	1	BGR (100%)
pPcPPKPr	1	CLL (100%)
(pPKPbc)	1	CLL (100%)
EP	1	YARS (100%)
PN3	1	SJA (100%)
(sPKiKP)	1	CLL (100%)
pPKPPKPd	1	CLL (100%)
PKPmax	1	CLL (100%)
EA	1	WAR (100%)
sPSPS	1	CLL (100%)
Ap	1	GUC (100%)
sPKKPbc	1	CLL (100%)
EB	1	WAR (100%)
(sSdiff)	1	CLL (100%)
sPKPdf2	1	CLL (100%)
SM2	1	MOLD (100%)
pPP(2)	1	CLL (100%)
pSKSP	1	CLL (100%)
pSKSac	1	CLL (100%)
PKPDf	1	SYO (100%)
d	1	WAR (100%)
pPKPmax	1	CLL (100%)

Table 11.2: *(continued)*

Reported Phase	Total	Agencies reporting
SSP	1	CLL (100%)
PFIF	1	BRG (100%)
ScSP	1	DBN (100%)
(sSSS)	1	CLL (100%)
(SPS)	1	CLL (100%)
(PPPP)	1	CLL (100%)
PNDN	1	NDI (100%)
PGCN	1	NDI (100%)
SKPPKPdf	1	CLL (100%)
PGDN	1	NDI (100%)
(sSS)	1	CLL (100%)
PKKPbc2	1	CLL (100%)
P(3)	1	CLL (100%)
PKiK	1	NAO (100%)
PKPab(2)	1	CLL (100%)
sSKSac	1	CLL (100%)
sSKPbc	1	CLL (100%)
MB	1	NDI (100%)
LmV(360	1	CLL (100%)
PE	1	NDI (100%)
sPcP	1	CLL (100%)
QM	1	MOLD (100%)
sSKS	1	DBN (100%)
sPmax	1	CLL (100%)
xP	1	BGR (100%)
sSP	1	CLL (100%)
g	1	BUD (100%)
sPdiff	1	SYO (100%)
P1C	1	ECX (100%)
SKSp	1	BRA (100%)
SKSSKSac	1	CLL (100%)
PPPS	1	DBN (100%)
(sPP)	1	CLL (100%)
(PcS)	1	CLL (100%)
sPPPPrev	1	CLL (100%)
(PKKPdf)	1	CLL (100%)
SSrev	1	CLL (100%)
SM1	1	MOLD (100%)
og	1	BUD (100%)
P'P'P'	1	BRG (100%)
IP	1	BELR (100%)
(sPPS)	1	CLL (100%)
PcPPKPr	1	CLL (100%)
(PKSdf)	1	CLL (100%)
S(2)	1	CLL (100%)
lg	1	MDD (100%)
(sPdif)	1	CLL (100%)

Table 11.2: *(continued)*

Reported Phase	Total	Agencies reporting
(L)	1	CLL (100%)
3PKPbc	1	CLL (100%)
PGN	1	NDI (100%)
(SKPdf)	1	CLL (100%)
P2	1	ECX (100%)
PKPbc(2)	1	CLL (100%)
sSKSP	1	CLL (100%)
X2	1	BGR (100%)
PNCS	1	NDI (100%)
LgX	1	CSEM (100%)
PKIK	1	BELR (100%)
PcP(2)	1	CLL (100%)
Pp	1	BUD (100%)
SKPPKP	1	CLL (100%)
(SKKSac)	1	CLL (100%)
pSKPbc	1	CLL (100%)
p3PKPbc	1	CLL (100%)
Pdiff(2)	1	CLL (100%)
-ML	1	INMG (100%)
(sPKSdf)	1	CLL (100%)
PKPdfc	1	WAR (100%)
(SKSP)	1	CLL (100%)
PPKdf	1	BER (100%)
cpg	1	BUD (100%)
f	1	BUD (100%)
PgP	1	BUD (100%)
O	1	SYO (100%)
pN	1	ISN (100%)
P	1	YARS (100%)
SPS	1	CLL (100%)
pPKSbc	1	CLL (100%)

Table 11.3: Reporters of amplitude data

Agency	Number of reported amplitudes	Number of amplitudes in ISC located events	Number used for ISC mb	Number used for ISC MS
IDC	351325	317079	140057	35573
NEIC	198615	198073	132062	36885
CSEM	179065	32267	9377	0
MOS	156674	153089	61612	16850
DJA	89049	55301	9094	0
WEL	87835	11912	0	0
BJI	83709	81450	462	506
MDD	64474	10128	0	0
NNC	55857	12680	71	0
ROM	37892	2442	0	0
THE	21941	5498	0	0
BKK	18864	18110	9182	0
LDG	17481	3912	3	0
HEL	14735	449	0	0
DMN	14527	13862	0	0
INMG	13980	6618	3253	0
VIE	12185	8629	3542	0
PRU	12168	6589	0	2424
NSSC	10661	3483	0	0
GUC	10117	3182	0	0
PPT	10086	8367	923	0
PDG	7719	3555	0	0
ECX	7119	1069	0	0
PRE	6879	1133	410	129
SKHL	6801	6164	4	0
MAN	6602	3028	0	0
TEH	5742	3963	0	0
BGR	5401	5307	4199	167
SVSA	5234	411	165	0
LJU	5080	530	2	0
SIO	4796	4785	3566	0
SJA	4533	1741	0	0
BER	4509	1921	702	175
HYB	4308	4274	2481	0
NDI	4242	3515	1318	91
BYKL	4099	2359	0	0
OTT	4098	202	0	0
BRG	3900	2800	388	0
YARS	3830	119	0	0
ZUR	3078	494	19	0
CLL	3055	2817	497	317
BGS	2557	1757	771	479
DNK	2139	1896	1174	0
NAO	2052	1998	1357	0

Table 11.3: Continued.

Agency	Number of reported amplitudes	Number of amplitudes in ISC located events	Number used for ISC mb	Number used for ISC MS
WBNET	1975	12	0	0
SKO	1844	586	0	0
KNET	1447	419	0	0
DHMR	1300	71	14	0
IGIL	1197	554	96	180
LIC	1075	1006	536	0
LIT	894	868	607	0
UCC	799	697	432	0
THR	743	732	0	0
BELR	668	132	0	49
DBN	650	383	178	0
MOLD	647	388	62	0
NERS	370	131	0	0
HLW	243	126	0	0
CASC	175	135	0	0
PLV	160	69	0	0
NOU	122	71	0	0
LPA	6	4	0	0
SSNC	6	6	0	2

12

Glossary of ISC Terminology

- Agency/ISC data contributor

  An academic or government institute, seismological organisation or company, geological/meteorological survey, station operator or author that reports or contributed data in the past to the ISC or one of its predecessors. Agencies may contribute data to the ISC directly, or indirectly through other ISC data contributors.

- Agency code

  A unique, maximum eight-character code for a data reporting agency (e.g. NEIC, GFZ, BUD) or author (e.g. ISC, EHB, IASPEI). Often the agency code is the commonly used acronym of the reporting institute.

- Arrival

  A phase pick at a station is characterised by a phase name and an arrival time.

- Associated phase

  Associated phase arrival or amplitude measurements represent a collection of observations belonging to (i.e. generated by) an event. The complete set of observations are associated to the prime hypocentre.

- Azimuthal gap/Secondary azimuthal gap

  The azimuthal gap for an event is defined as the largest angle between two stations with defining phases when the stations are ordered by their event-to-station azimuths. The secondary azimuthal gap is the largest azimuthal gap a single station closes.

- BAAS

  Seismological bulletins published by the British Association for the Advancement of Science (1913-1917) under the leadership of H.H. Turner. These bulletins are the predecessors of the ISS Bulletins and include reports from stations distributed worldwide.

- Bulletin

  An ordered list of event hypocentres, uncertainties, focal mechanisms, network magnitudes, as well as phase arrival and amplitude observations associated to each event. An event bulletin may list all the reported hypocentres for an event. The convention in the ISC Bulletin is that the preferred (prime) hypocentre appears last in the list of reported hypocentres for an event.

- Catalogue

  An ordered list of event hypocentres, uncertainties and magnitudes. An event catalogue typically lists only the preferred (prime) hypocentres and network magnitudes.

- CoSOI/IASPEI

  Commission on Seismological Observation and Interpretation, a commission of IASPEI that prepares and discusses international standards and procedures in seismological observation and interpretation.

- Defining/Non-defining phase

  A defining phase is used in the location of the event (time-defining) or in the calculation of the network magnitude (magnitude-defining). Non-defining phases are not used in the calculations because they suffer from large residuals or could not be identified.

- Direct/Indirect report

  A data report sent (e-mailed) directly to the ISC, or indirectly through another ISC data contributor.

- Duplicates

  Nearly identical phase arrival time data reported by one or more agencies for the same station. Duplicates may be created by agencies reporting observations from other agencies, or several agencies independently analysing the waveforms from the same station.

- Event

  A natural (e.g. earthquake, landslide, asteroid impact) or anthropogenic (e.g. explosion) phenomenon that generates seismic waves and its source can be identified by an event location algorithm.

- Grouping

  The ISC algorithm that organises reported hypocentres into groups of events. Phases associated to any of the reported hypocentres will also be associated to the preferred (prime) hypocentre. The grouping algorithm also attempts to associate phases that were reported without an accompanying hypocentre to events.

- Ground Truth

  An event with a hypocentre known to certain accuracy at a high confidence level. For instance, GT0 stands for events with exactly known location, depth and origin time (typically explosions); GT5 stands for events with their epicentre known to 5 km accuracy at the 95% confidence level, while their depth and origin time may be known with less accuracy.

- Ground Truth database

  On behalf of IASPEI, the ISC hosts and maintains the IASPEI Reference Event List, a bulletin of ground truth events.

- IASPEI

  International Association of Seismology and Physics of the Earth Interior, www.iaspei.org.

- International Registry of Seismograph Stations (IR)

  Registry of seismographic stations, jointly run by the ISC and the World Data Center for Seismology, Denver (NEIC). The registry provides and maintains unique five-letter codes for stations participating in the international parametric and waveform data exchange.

- ISC Bulletin

  The comprehensive bulletin of the seismicity of the Earth stored in the ISC database and accessible through the ISC website. The bulletin contains both natural and anthropogenic events. Currently the ISC Bulletin spans more than 50 years (1960-to date) and it is constantly extended by adding both recent and past data. Eventually the ISC Bulletin will contain all instrumentally recorded events since 1900.

- ISC Governing Council

  According to the ISC Working Statutes the Governing Council is the governing body of the ISC, comprising one representative for each ISC Member.

- ISC-located events

  A subset of the events selected for ISC review are located by the ISC. The rules for selecting an event for location are described in Section 3.4 of the January-June 2010 Bulletin Summary; ISC-located events are denoted by the author ISC.

- ISC Member

  An academic or government institute, seismological organisation or company, geological/meteorological survey, station operator, national/international scientific organisation that contribute to the ISC budget by paying membership fees. ISC members have voting rights in the ISC Governing Council.

- ISC-reviewed events

  A subset of the events reported to the ISC are selected for ISC analyst review. These events may or may not be located by the ISC. The rules for selecting an event for review are described in Section 3.3.3 of the January-June 2010 Bulletin Summary. Non-reviewed events are explicitly marked in the ISC Bulletin by the comment following the prime hypocentre "Event not reviewed by the ISC".

- ISF

  International Seismic Format (www.isc.ac.uk/standards/isf). A standard bulletin format approved by IASPEI. The ISC Bulletin is presented in this format at the ISC website.

- ISS

  International Seismological Summary (1918-1963). These bulletins are the predecessors of the ISC Bulletin and represent the major source of instrumental seismological data before the digital era. The ISS contains regionally and teleseismically recorded events from several hundreds of globally distributed stations.

- Network magnitude

  The event magnitude reported by an agency or computed by the ISC locator. An agency can report several network magnitudes for the same event and also several values for the same magnitude type. The network magnitude obtained with the ISC locator is defined as the median of station magnitudes of the same magnitude type.

- Phase

  A maximum eight-character code for a seismic, infrasonic, or hydroacoustic phase. During the ISC processing, reported phases are mapped to standard IASPEI phase names. Amplitude measurements are identified by specific phase names to facilitate the computation of body-wave and surface-wave magnitudes.

- Prime hypocentre

  The preferred hypocentre solution for an event from a list of hypocentres reported by various agencies or calculated by the ISC.

- Reading

  Parametric data that are associated to a single event and reported by a single agency from a single station. A reading typically includes one or more phase names, arrival time and/or amplitude/period measurements.

- Report/Data report

  All data that are reported to the ISC are parsed and stored in the ISC database. These may include event bulletins, focal mechanisms, moment tensor solutions, macroseismic descriptions and other event comments, as well as phase arrival data that are not associated to events. Every single report sent to the ISC can be traced back in the ISC database via its unique report identifier.

- Shide Circulars

  Collections of station reports for large earthquakes occurring in the period 1899-1912. These reports were compiled through the efforts of J. Milne. The reports are mainly for stations of the British Empire equipped with Milne seismographs. After Milne's death, the Shide Circulars were replaced by the Seismological Bulletins of the BAAS.

- Station code

  A unique, maximum six-character code for a station. The ISC Bulletin contains data exclusively from stations registered in the International Registry of Seismograph Stations.

13

Acknowledgements

We thank John Ristau of GNS, New Zealand, and Keiji Doi of JMA, Japan, for kindly accepting our invitation and submitting articles for this issue of the Summary.

We are also grateful to all the developers of the Generic Mapping Tools (GMT) suite of software (Wessel and Smith, 1998), used extensively here in producing the graphical figures.

Finally, we thank the ISC Member Institutions, Data Contributors, Funding Agencies (including NSF Award 0949072) and Sponsors for supporting the ISC long-term operations.

References

Balfour, N., R. Baldwin, and A. Bird (2008), Magnitude calculations in Antelope 4.10, *Analysis Group Note of Geological Survey of Canada*, pp. 1–13.

Bisztricsany, E. A. (1958), A new method for the determination of the magnitude of earthquakes, *Geofiz. Kozl*, pp. 69–76.

Bondár, I., and D. Storchak (2011), Improved location procedures at the International Seismological Centre, *Geophysical Journal International*, *186*, 1220–1244.

Bormann, P., and J. W. Dewey (2012), The new iaspei standards for determining magnitudes from digital data and their relation to classical magnitudes, is 3.3, *New Manual of Seismological Observatory Practice 2 (NMSOP-2), P. Bormann (Ed.)*, pp. 1–44, doi:10.2312/GFZ.NMSOP-2_IS_3.3,10.2312/GFZ.NMSOP-2, `http://nmsop.gfz-postsdam.de`.

Bormann, P., and J. Saul (2008), The new IASPEI standard broadband magnitude mB, *Seism. Res. Lett*, *79*(5), 698–705.

Bormann, P., R. Liu, X. Ren, R. Gutdeutsch, D. Kaiser, and S. Castellaro (2007), Chinese national network magnitudes, their relation to NEIC magnitudes and recommendations for new IASPEI magnitude standards, *Bulletin of the Seismological Society of America*, *97*(1B), 114–127, doi:10.1785/012006007835.

Bormann, P., R. Liu, Z. Xu, R. Ren, and S. Wendt (2009), First application of the new IASPEI teleseismic magnitude standards to data of the China National Seismographic Network, *Bulletin of the Seismological Society of America*, *99*, 1868–1891, doi:10.1785/0120080010.

Choy, G. L., and J. L. Boatwright (1995), Global patterns of readiated seismic energy and apparent stress, *J. Geophys. Res.*, *100*(B9), 18,205–18,228.

Dziewonski, A. M., T.-A. Chou, and J. H. Woodhouse (1981), Determination of earthquake source parameters from waveform data for studies of global and regional seismicity, *J. Geophys. Res.*, *86*, 2825–2852.

Engdahl, E. R., and A. Villaseñor (2002), Global seismicity: 1900-1999, *International Handbook of Earthquake Engineering and Seismology, International Geophysics series*, *81A*, 665–690.

Engdahl, E. R., R. van der Hilst, and R. Buland (1998), Global teleseismic earthquake relocation with improved travel times and procedures for depth determination, *Bulletin of the Seismological Society of America*, *88*, 722–743.

Gutenberg, B. (1945a), Amplitudes of P, PP and S and magnitude of shallow earthquakes, *Bulletin of the Seismological Society of America*, *35*, 57–69.

Gutenberg, B. (1945b), Magnitude determination of deep-focus earthquakes, *Bulletin of the Seismological Society of America*, *35*, 117–130.

Gutenberg, B. (1945c), Amplitudes of surface waves and magnitudes of shallow earthquakes, *Bulletin of the Seismological Society of America*, *35*, 3–12.

Hutton, L. K., and D. M. Boore (1987), The ML scale in southern California, *Bulletin of the Seismological Society of America*, *77*, 2074–2094.

IASPEI (2005), Summary of magnitude working group recommendations on standard procedures for determining earthquake magnitudes from digital data, `http://www.iaspei.org/commissions/CSOI.html#wgmm,http://www.iaspei.org/commissions/CSOI/summary_of_WG_recommendations_2005.pdf`.

IASPEI (2013), Summary of magnitude working group recommendations on standard procedures for determining earthquake magnitudes from digital data, http://www.iaspei.org/commissions/CSOI/Summary_of_WG_recommendations_20130327.pdf.

IDC (1999), IDC processing of seismic, hydroacoustic and infrasonic data, *IDC Documentation*.

Kanamori, H. (1977), The energy release in great earthquakes, *J. Geophys. Res.*, *82*, 2981–2987.

Lee, W. H. K., R. Bennet, and K. Meagher (1972), A method of estimating magnitude of local earthquakes from signal duration, *U.S. Geol. Surv.*, Open-File Rep.

Nuttli, O. W. (1973), Seismic wave attenuation and magnitude relations for eastern North America, *J. Geophys. Res.*, *78*, 876–885.

Richter, C. F. (1935), An instrumental earthquake magnitude scale, *Bulletin of the Seismological Society of America*, *25*, 1–32.

Ringdal, F. (1976), Maximum-likelihood estimation of seismic magnitude, *Bulletin of the Seismological Society of America*, *66*(3), 789–802.

Tsuboi, C. (1954), Determination of the Gutenberg-Richter's magnitude of earthquakes occurring in and near Japan, *Zisin (J. Seism. Soc. Japan), Ser. II*(7), 185–193.

Tsuboi, S., K. Abe, K. Takano, and Y. Yamanaka (1995), Rapid determination of Mw from broadband P waveforms, *Bulletin of the Seismological Society of America*, *85*(2), 606–613.

Vaněk, J., A. Zapotek, V. Karnik, N. V. Kondorskaya, Y. V. Riznichenko, E. F. Savarensky, S. L. Solov'yov, and N. V. Shebalin (1962), Standardization of magnitude scales, *Izvestiya Akad. SSSR., Ser. Geofiz.*(2), 153–158, pages 108–111 in the English translation.

Woessner, J., and S. Wiemer (2005), Assessing the quality of earthquake catalogues: estimating the magnitude of completeness and its uncertainty, *Bulletin of the Seismological Society of America*, *95*(2), doi:10/1785/012040,007.

WHITE PAPER

COMPLETE INTEGRATED AFTERSHOCK SYSTEM PROVIDES QUICK AND EASY SOLUTION FOR RAPID AFTERSHOCK DEPLOYMENT

LEONID ZIMAKOV

TRIMBLE INFRASTRUCTURE, PLANO, TEXAS, USA

INTRODUCTION

Rapid aftershock mobilization plays an essential role in the understanding of both focal mechanism and rupture propagation caused by strong earthquakes. A quick assessment of the data provides a unique opportunity to study the dynamics of the entire earthquake process in-situ. Aftershock study also provides practical information for local authorities regarding post-earthquake activity, which is very important in order to conduct the necessary actions for public safety in the area affected by a strong earthquake.

Due to a relatively short aftershock activity period (several weeks to several months), it is critical to rapidly deploy emergency personnel to the affected area in order to minimize the time required to estimate the extent and amplitude of strong shaking from aftershock events.

A dense array of seismic stations consisting of high resolution seismic recorders with short period seismometers and accelerometers is required in order to reduce the time needed to detect an event and provide high resolution maps of ground accelerations across the affected earthquake region. Therefore, the rapid aftershock mobilization of seismic equipment should comply with the following critical requirements:

- Lightweight and small in size
- Integrated design with minimal or no external peripheral equipment
- Very low power consumption
- Minimal or no field programming
- Easy and quick data download in the field
- Low maintenance

WHAT DOES THE 160-03 OFFER?

The REF TEK High Resolution Aftershock System, Model 160-03, is a self-contained, fully integrated Aftershock System providing the customer with simple and quick deployment during aftershock emergency mobilization. The 160-03, six channel recorder, contains three major components integrated in one case:

- 24-bit resolution low power ADC with CPU and lid interconnect boards;
- power source; and
- three component 2 Hz sensors (two horizontals and one vertical and a triaxial +/-4g MEMS accelerometer.

Figure 1: REF TEK 160-03 High Resolution Aftershock System

Figure 2: Inside the case of the REF TEK 160-03 High Resolution Aftershock System

The self-contained rechargeable battery pack provides power autonomy for up to 7 days during continuous data acquisition at 200 sps on three weak motion and three triggered strong motion recording channels. For longer power autonomy, the 160-03 Aftershock System battery pack can be charged from an external source (solar power system). To download recorded data the customer has two options:

- Connect a laptop to the 160-03 and the data is then automatically uploaded; or
- Connect the REF TEK Wi-Fi Serial Adaptor to upload data to the REF TEK iFSC Controller.

The 160-03 configuration is fixed based on a configuration file stored in the system, so no external command/control interface is required for parameter setup in the field. For visual control of the system performance in the field, the 160-03 has a built-in LED display which indicates the system's recording status, as well as a hot swappable USB drive and battery status. As an added customer convenience, four 160-03 systems can be housed in a small, lightweight, watertight rolling case that will keep the recorders safe during transport. The ease of having an all-in-one aftershock system also provides the customer flexibility in sending the equipment to the affected region via a more cost effective way as the equipment/carrying case can easily be checked on both domestic and international commercial flights.

160-03 SPECIFICATIONS

Model	160-03 (Part No. 97124-00)
Mechanical	
Size: Weight: Watertight Integrity:	6” (15.2cm) high x 8.63” (21.9cm) diameter 11.7 lbs. (5.3 kg) IP67
Environmental	
Operating Temp.:	-30°C to +60°C
Storage Temp.:	-40°C to +70°C
Power	
Average Power:	<400 mW
A/D Convertor	
Type:	Delta-Sigma Modulation, 24-bit output resolution
Dynamic Range:	>138 dB@100 sps
Channels:	6
Input Impedance:	Matched to sensors
Sample Rates:	200 sps default; 100, 250, 500 sps optional
Seismometer	
Type:	Moving coil / mass
Natural Frequency:	2 Hz
Accelerometer	
Type:	± 4g
Frequency Response:	DC – 45 Hz
Damping:	0.7 to critical
Data Storage	
Type:	USB Flash
User Interface	
Type:	LED array consisting of 16 LED display recording status, USB drive status, battery voltage, etc.
Power Control:	Magnetic switch to turn on both power and acquisition

Table 1: 160-03 Specifications

CONTACT US

Phone: +1 (214) 440 1265

Email: sales@reftek.com